# The role of neutrophils in MASLD associated hepatocellular carcinoma

**Daniel Geh**

**Doctor of Philosophy**

**Newcastle University**

**Biosciences Institute**

**September 2024**



## Abstract

### Background

Neutrophils are key drivers of hepatocellular carcinoma (HCC) progression and immunotherapy resistance in the context of metabolic dysfunction-associated steatotic liver disease (MASLD). I aimed to investigate neutrophil heterogeneity and phenotype in both patients and pre-clinical models. I also aimed to investigate mechanisms of immune checkpoint inhibitor resistance in a pre-clinical model of MASLD-HCC.

### Methods

I isolated neutrophils from HCC and chronic liver disease (CLD) patients, healthy volunteers and mice with MASLD and orthotopically implanted HCCs. I characterised neutrophils using flow cytometry and functional assays. To investigate immune checkpoint inhibitor effectiveness in MASLD-HCC I implanted MASLD or lean mice with intrahepatic or subcutaneous tumours then treated with anti-PDL1/anti-VEGF therapy.

### Results

There was an increased frequency of circulating neutrophils in HCC and CLD patients as well as HCC-bearing mice with a preferential increase in low density (LD) neutrophils with an activated, degranulated and aged phenotype. Tumour neutrophils had a similar phenotype. These neutrophil populations had high reactive oxygen species (ROS) production and high PDL1 expression which may indicate immunosuppressive functions. Phosphorylated STAT3 expression was increased in tumour neutrophils, suggesting this as a driving pathway. Treatment with a JAK2 inhibitor reduced tumour burden and ameliorated neutrophil ageing, degranulation and activation. In MASLD mice anti-PDL1/anti-VEGF therapy had a poor treatment effect in intrahepatic tumours but a good treatment effect in subcutaneous tumours. This was likely due to an expansion of $PD1^{+}CXCR6^{+}EOMES^{+}$ CD8 T cells, which were expanded in the MASLD liver.

### Conclusion

My data demonstrates neutrophil heterogeneity in HCC with an expansion of circulating LD neutrophils. LD neutrophils and tumour neutrophils have an activated,

degranulated and aged phenotype which may be therapeutically manipulated by inhibiting the JAK2-STAT3 pathway. In pre-clinical models of MASLD-HCC anti-PDL1/anti-VEGF therapy resistance was driven by the intrahepatic microenvironment of MASLD. Specifically due to the expansion of $PD1^{+}CXCR6^{+}EOMES^{+}$ CD8 T cells with an exhausted and auto-aggressive phenotype.

## Acknowledgements

I would like to acknowledge my supervisors, Prof Derek Mann, Dr Jack Leslie and Prof Helen Reeves for their guidance, mentorship and support throughout my ACF and PhD. I would also like to acknowledge Prof Steve Clifford and Prof Sophie Hambleton for their advice and guidance as part of my progress panel during my PhD.

I would like to thank members of the Newcastle Fibrosis Research Group who have helped and supported me. I would like to acknowledge Prof Fiona Oakley and Dr Lee Borthwick who advised on specific parts of my work. I would also like to acknowledge Erik Ramon-Gil, Niall Wilson, Maja Laszczewska, Rainie Cameron, Dr Saimir Luli and Dr Amy Collins who helped with the laboratory work. I would like to acknowledge Dr Shoba Amarnath for her guidance on designing a T cell flow cytometry panel.

I would like to thank those working as part of the HUNTER study who helped me in acquiring patient samples and data. I would like to thank Robyn Watson and Misti McCain in helping me with the logistics of obtaining these patient samples. I would like to thank the research nurses who assisted me in recruiting patients. I would also like to thank Prof Tom Bird and his group at the Cancer Research UK Scotland Institute for their guidance and for supplying the *Cxcr2*$^{DNeut}$ mice.

I would like to thank my NHS colleagues at the Newcastle upon Tyne Hospitals NHS Foundation Trust who helped me in recruiting patients and taught me to be a better clinician; Dr Steve Masson, Dr Stuart McPherson, Dr Preya Patel and Dr Louise Macdougall. I would like to thank the pathology team for helping me acquire HCC resection tissue; Dr Sam Cook, Dr Julian Pulle, Dr Jonathan Lye, Dr Beate Haugk, Louise Thew and Louise Hall.

I would like to thank the Flow Cytometry Core Facility staff for their guidance and support in experiment design; Prof Andy Filby, Dr David MacDonald, Dr Gill Hulme and Carly Knill.

I would like to thank the staff of the Comparative Biology Centre for their support in running the in vivo studies.

This work was supported by the Cancer Research UK Clinical Academic Training programme. I would like to acknowledge Prof Ruth Plummer in her role in obtaining this funding and her belief in me as its first candidate.

Finally, I would like to thank my family for their unfailing love and support during my PhD. I would like to thank my wife Isobel for her constant practical and emotional support and putting up with my busy workloads and hectic schedule. Thank you for always believing in me and journeying with me in the challenges of the past few years. I would also like to thank my newly adopted son, Isaiah, for making me a more resilient, loving, compassionate and humble person during this time.

## Table of Contents

Table of Contents ..... i

List of Abbreviations ..... ix

Table of Figures ..... xv

Table of Tables ..... xviii

**1. Introduction** ..... **1**

1.1. Hepatocellular carcinoma: clinical aspects ..... 1

1.1.1. Epidemiology ..... 1

1.1.2. Chronic liver disease ..... 2

1.1.3. The pre-cancerous niche ..... 4

1.1.4. HCC classification ..... 5

1.1.5. HCC diagnosis, staging and management ..... 6

1.1.6. Systemic therapies for the treatment of HCC ..... 9

1.1.7. Underlying CLD and response to systemic therapies ..... 10

1.2. Neutrophils in health ..... 13

1.2.1. Granulopoiesis ..... 13

1.2.2. Neutrophil aging, circadian rhythm and clearance ..... 14

1.2.3. Neutrophil trafficking ..... 17

1.2.4. Antimicrobial and inflammatory actions of neutrophils ..... 17

1.2.5. Neutrophil heterogeneity in health ..... 20

1.3. Neutrophils in cancer ..... 20

1.3.1. The N1 and N2 spectrum ..... 20

1.3.2. Low density neutrophils ..... 22

1.3.3. Myeloid derived suppressor cells ..... 23

1.3.4. Problems with current classification ..... 25

1.4. Neutrophils in HCC ..... 25

1.4.1. Circulating neutrophils ..... 25

1.4.2. Tumour associated neutrophils ..... 26
1.4.3. Neutrophil heterogeneity in HCC ..... 27
1.4.4. Tumour associated neutrophil recruitment and induction to a pro-tumour phenotype ..... 27
1.4.5. Role of neutrophils in tumour development ..... 31
1.4.6. Role of neutrophils in local tumour progression ..... 31
1.4.7. Role of neutrophils in tumour metastasis ..... 33
1.4.8. Potential anti-tumour functions of neutrophils ..... 35
1.5. Neutrophils as therapeutic targets in HCC ..... 35
1.5.1. Effect of conventional HCC therapies on neutrophils ..... 36
1.5.2. Chemokine inhibitors ..... 36
1.5.3. Cytokine inhibitors ..... 37
1.5.4. Oligonucleotide based therapies ..... 38
1.5.5. Phosphodiesterase type 5 inhibition ..... 38
1.5.6. Histone deacetylase inhibitors ..... 38
1.5.7. STAT3 inhibitors ..... 39
1.5.8. CD47-SIRPα checkpoint inhibitors ..... 39
1.5.9. TRAIL receptor 2 agonists ..... 39
1.5.10. S100A9 inhibition ..... 40
1.5.11. Other novel therapeutic approaches ..... 40
1.6. Areas of future development ..... 45
1.6.1. Improving murine and humanised pre-clinical models ..... 45
1.6.2. Understanding the role of neutrophils in chronic liver disease ..... 47
1.6.3. Better characterisation of neutrophil heterogeneity ..... 47
1.7. Conclusion ..... 47

**2. Aims and Objectives** ..... **49**

**3. Materials and Methods** ..... **51**
3.1. Human blood characterisation ..... 51
3.1.1. Human blood sample collection ..... 51
3.1.2. General immune cell isolation ..... 51
3.1.3. Neutrophil isolation ..... 51
3.2. HCC liver and tumour immune cell and neutrophil characterisation ..... 52

3.2.1. Human HCC and liver tissue collection ..... 52
3.2.2. Surgical resection HCC liver and tumour immune cell isolation ..... 52
3.2.3. Liver and tumour biopsy immune cell isolation ..... 53
3.3. Human flow cytometry ..... 53
3.3.1. Flow cytometry surface marker cell staining ..... 53
3.3.2. Flow cytometry intracellular phosphoflow staining ..... 54
3.3.3. Flow cytometry acquisition ..... 54
3.3.4. Human neutrophil cell sorting ..... 54
3.3.5. Flow cytometry data analysis ..... 55
3.3.6. Human flow cytometry panels ..... 56
3.4. Human neutrophil functional assays ..... 58
3.4.1. Human neutrophil ROS assay ..... 58
3.4.2. Human neutrophil phagocytosis assay ..... 59
3.4.3. Human neutrophil migration assay ..... 60
3.5. ImageStream ..... 60
3.5.1. ImageStream cell staining and preparation ..... 60
3.5.2. ImageStream experiment set up and acquisition ..... 61
3.5.3. ImageStream analysis ..... 61
3.6. LEGENDScreen ..... 62
3.6.1. LEGENDScreen cell preparation and staining ..... 62
3.6.2. LEGENDScreen sample acquisition ..... 63
3.6.3. LEGENDScreen analysis ..... 63
3.7. Cytospin ..... 65
3.7.1. Cytospin preparation ..... 65
3.7.2. Cytospin nuclear cell staining ..... 65
3.7.3. Cytospin nuclear staining image analysis ..... 65
3.7.4. Cytospin immunofluorescence cell staining and microscopy ..... 65
3.8. In vivo models ..... 66
3.8.1 Ethical statement and animal husbandry ..... 66
3.8.2. Mouse strains ..... 66
3.8.3. Dietary induced MASH model – modified western diet model ..... 67
3.8.4. Intrahepatic HCC model ..... 67
3.8.5. Subcutaneous HCC model ..... 67
3.8.6. Cancer therapies ..... 67

3.8.7. Mouse tail vein blood collection....68
3.8.8. Mouse harvests....69
3.9. Mouse immune cell isolations....69
3.9.1. Bone marrow isolation....69
3.9.2. Whole blood immune cell isolation....70
3.9.3. Tail vein blood immune cell isolation....70
3.9.4. Blood neutrophil isolation....70
3.9.5. Spleen immune cell isolation....71
3.9.6. Liver and tumour immune cell isolation....71
3.10. Mouse flow cytometry....72
3.10.1. Flow cytometry surface marker cell staining....72
3.10.2. Flow cytometry intracellular marker cell staining....72
3.10.3. Flow cytometry intracellular phosphoflow staining....72
3.10.4. Flow cytometry acquisition....73
3.10.5. Flow cytometry data analysis....73
3.10.6. Mouse flow cytometry panels....73
3.11. Mouse neutrophil functional assays....77
3.11.1. Mouse neutrophil ROS assay....77
3.11.2. Mouse neutrophil phagocytosis assay....78
3.11.3. Mouse neutrophil migration assay....78
3.12. BrdU neutrophil tracking experiment....79
3.12.1. BrdU administration....79
3.12.2. BrdU flow cytometry staining....79
3.12.3. BrdU flow cytometry acquisition and data analysis....80
3.13. Histology....80
3.13.1. Tissue processing and slide preparation....80
3.13.2. Haematoxylin and Eosin stain....81
3.13.3. Immunohistochemistry....81
3.13.4. Image analysis....82
3.14. Cell culture....83
3.15. In vitro AZD1480 experiments....83
3.15.1. In vitro effect of AZD1480 on leukocytes....83
3.15.2. In vitro effect of AZD1480 on Hep 53.4 proliferation....83
3.16. Statistics....84

**4. Neutrophil heterogeneity and phenotype in hepatocellular carcinoma and chronic liver disease ..... 85**
4.1. Introduction ..... 85
4.2. Circulating immune cell characterisation ..... 85
4.2.1. Patient clinical characterisation ..... 85
4.2.2. Gating strategy ..... 87
4.2.3. Circulating immune cell frequencies ..... 89
4.3. Circulating neutrophil population frequencies ..... 90
4.3.1. Gating strategy ..... 90
4.3.2. Frequencies of circulating neutrophil populations ..... 90
4.4. Focused characterisation of circulating neutrophil populations ..... 91
4.4.1. Nuclear morphology and immunofluorescence analysis ..... 92
4.4.2. Phenotype ..... 93
4.4.3. Functional assays ..... 95
4.5. Unbiased characterisation of circulating neutrophil populations ..... 97
4.5.1. LEGENDScreen LD CD16$^{high}$ vs ND comparison ..... 97
4.5.2. Neutrophils expressing CD41 and CD36 are neutrophil-platelets aggregates ..... 99
4.5.3. LEGENDScreen LD CD16$^{high}$ vs LD CD16$^{low}$ comparison ..... 100
4.6. Dynamic characterisation of circulating neutrophil populations ..... 103
4.6.1. Effects of PMA stimulation on neutrophil density and phenotype ..... 103
4.6.2. Effects of time and ageing on neutrophil density and phenotype ..... 105
4.7. Neutrophil phenotype and function in healthy controls versus CLD and HCC patients ..... 107
4.7.1. Neutrophil phenotype ..... 107
4.7.2. Neutrophil functional assays ..... 109
4.8. Tumour, liver and blood immune cell frequencies in HCC patients undergoing surgical resection ..... 111
4.9. Tumour, liver and blood neutrophil phenotype in HCC ..... 113
4.10. Conclusion ..... 115

**5. Neutrophil heterogeneity and phenotype in a pre-clinical model of MASH-HCC ..... 117**
5.1. Introduction ..... 117
5.2. Clinical characterisation of model ..... 117
5.2.1. MASH model characterisation – clinical phenotype ..... 117
5.2.2. MASH model characterisation – liver immune infiltrate ..... 119
5.2.2.1. Flow cytometry gating strategy – tissue ..... 119
5.2.2.2. MASH model – liver immune infiltrate ..... 121
5.2.3. Orthotopic HCC model characterisation – clinical phenotype ..... 123
5.2.4. Orthotopic HCC model characterisation – immune infiltrate ..... 125
5.3. Blood immune cell frequencies in the western diet and western diet – orthotopic HCC models ..... 126
5.3.1. Flow cytometry gating strategy – blood ..... 126
5.3.2. Blood immune cell frequencies ..... 127
5.4. Pre-clinical model circulating neutrophil heterogeneity and phenotype ..... 129
5.4.1. Circulating ND and LD gating strategy ..... 129
5.4.2. Frequency and phenotype of circulating neutrophil populations ..... 129
5.4.3. Circulating neutrophil platelet marker expression ..... 132
5.4.4. Circulating neutrophil functional assays ..... 132
5.4.5. Comparison of mouse and human circuiting neutrophil populations ..... 133
5.5. Experimental manipulation of neutrophil ageing and the effect on LD neutrophils ..... 135
5.5.1. The effect of neutrophil specific CXCR2 deletion on circulating neutrophil populations ..... 135
5.5.2. BrdU neutrophil tracking experiment to establish the origin of circulating LD neutrophils ..... 137
5.5.2.1. BrdU tracking validation and flow cytometry gating strategy. 137
5.5.2.2. BrdU tracking of ND and LD neutrophils ..... 138
5.6. Neutrophil dynamics across biological compartments ..... 141
5.6.1. Frequency of bone marrow, spleen, liver and tumour neutrophils in HCC ..... 141
5.6.2. Dynamic changes in granulopoiesis associated with HCC ..... 143
5.7. Neutrophil phenotype and function across biological compartments ..... 145
5.7.1. Neutrophil phenotype across biological compartments ..... 145

5.7.2. Neutrophil functional assays across biological compartments ..... 147
5.8. Effect of HCC on neutrophil phenotype and function..... 148
5.8.1. Effect of HCC on neutrophil phenotype ..... 148
5.8.2. Effect of HCC on neutrophil function ..... 149
5.9. Conclusion ..... 151

**6. Testing neutrophil targeted therapies in a pre-clinical model of MASH-HCC ..... 153**
6.1. Introduction ..... 153
6.2. Targeting the JAK2-STAT3 pathway ..... 153
6.2.1. Neutrophil p-STAT3 expression in HCC ..... 154
6.2.2. Effect of JAK2 inhibition on neutrophils ex vivo ..... 157
6.2.3. Effect of JAK2 inhibition on Hep 53.4 cells in vitro..... 158
6.2.4. JAK2 inhibition in a lean HCC pre-clinical model..... 159
6.2.5. JAK2 inhibition in a MASH-HCC pre-clinical model ..... 161
6.2.6. JAK2 inhibitor study conclusion ..... 163
6.3. Targeting S100A8 and S100A9 in a HCC pre-clinical model ..... 164
6.4. ALK5 inhibition in pre-clinical models ..... 166
6.4.1. ALK5 inhibition in a lean HCC pre-clinical model ..... 166
6.4.2. ALK5 inhibition in a MASH-HCC pre-clinical model..... 168
6.5 Conclusion ..... 170

**7. Exploring mechanisms behind primary immune checkpoint inhibitor resistance in MASH-HCC ..... 171**
7.1. Introduction ..... 171
7.2. Therapy response to anti-PDL1/anti-VEGF in lean vs MASH intrahepatic HCC..... 171
7.3. Immunological effects of anti-PDL1/anti-VEGF therapy in lean vs MASH intrahepatic HCC ..... 174
7.4. Effects of anti-PDL1/anti-VEGF therapy on CD8 subpopulations in lean vs MASH intrahepatic HCC..... 176
7.5. CD8 T cell subpopulations in the MASH..... 177
7.6. Therapy response to anti-PDL1/anti-VEGF in lean vs MASH subcutaneous HCC..... 179

7.7. Immunological effects of anti-PDL1/anti-VEGF therapy in lean vs MASH subcutaneous HCC ..... 181
7.8. Effects of anti-PDL1/anti-VEGF therapy on T cell subpopulations in lean vs MASH subcutaneous HCC ..... 183
7.9. Conclusion ..... 184

**8. Discussion** ..... **186**
8.1. Neutrophil heterogeneity in health, CLD and HCC ..... 186
8.1.1. Circulating neutrophil heterogeneity ..... 186
8.1.1.1. LD CD16$^{low}$ neutrophil characterisation ..... 187
8.1.1.2. LD CD16$^{high}$ neutrophil characterisation ..... 188
8.1.1.3. LD CD16$^{high}$ neutrophil expansion in CLD and HCC ..... 189
8.1.1.4. Technical limitations ..... 190
8.1.1.5. Differences between mouse and human LD neutrophils ..... 191
8.1.1.6. Disease specific changes in neutrophil phenotype ..... 192
8.1.1.7. Role of neutrophil ageing in MASH and HCC ..... 193
8.1.2. Origins of low density circulating neutrophils ..... 194
8.1.3. Low density neutrophil-platelet aggregates ..... 196
8.1.4. Neutrophil heterogeneity across biological compartments ..... 198
8.2. Experimental neutrophil therapeutics ..... 199
8.2.1. ALK5 inhibition ..... 199
8.2.2. S100A8/9 inhibition ..... 201
8.2.3. JAK2-STAT3 inhibition ..... 202
8.3 The hepatic microenvironment of MASH makes HCC resistant to immune checkpoint inhibition ..... 205
8.4 Conclusion ..... 208

**9. Bibliography** ..... **210**

## List of Abbreviations

| | |
|---|---|
| °C | degrees celsius |
| ADCC | antibody dependent cell mediated cytotoxicity |
| AFP | alpha-fetoprotein |
| AIH | autoimmune hepatitis |
| ALD | alcohol associated liver disease |
| ALIOS | American lifestyle-induced obesity syndrome |
| ALK5 | activin receptor-like kinase 5 |
| ANOVA | analysis of variance |
| APC | allophycocyanin |
| ArC | Amine Reactive Compensation |
| ARG1 | arginase 1 |
| ATP | adenosine triphosphate |
| BCLC | Barcelona Clinic for Liver Cancer |
| BM | bone marrow |
| BrdU | bromodeoxyuridine |
| BSC | best supportive care |
| BSG | British Society of Gastroenterology |
| BUV | brilliant ultra violet |
| C/EBP-α | CCAAT/enhancer binding protein alpha |
| CAF | cancer associated fibroblast |
| CAR | chimeric antigen receptor |
| CCL | C-C motif ligand |
| CCR | C-C chemokine receptor |
| CD | control diet |
| cDC1 | conventional dendritic cell type 1 |
| cDC2 | conventional dendritic cell type 2 |
| cGVHD | chronic graft versus host disease |
| CIK | cytokine induced killer cell |
| CLD | chronic liver disease |
| COX2 | cyclooxygenase-2 |
| CT | computed tomography |
| CTLA4 | anti-cytotoxic T-lymphocyte associated protein 4 |

| | |
|---|---|
| CX3CR | CX3C chemokine receptor |
| CXCL | C-X-C Motif Chemokine Ligand |
| CXCR | C-X-C chemokine receptor |
| Cy7 | cyanine 7 |
| DAB | 3,3'-diaminobenzidine |
| DC | dendritic cell |
| DEN | diethylnitrosamine |
| DHR | 123 dihydrorhodamine 123 |
| DMEM | Dulbecco's modified eagle medium |
| DMSO | dimethylsulfoxide |
| DNA | deoxyribonucleic acid |
| DPBS- | Dulbecco's phosphate-buffered saline modified without magnesium and calcium |
| ECOG | Eastern Cooperative Oncology Group |
| EDTA | ethylenediaminetetraacetic acid |
| EHS | extrahepatic disease spread |
| EMT | epithelial-mesenchymal transition |
| ENTPD2 | ectonucleotide triphosphate diphosphohydrolase 2 |
| EOMES | eomesodermin |
| FACS | fluorescence-activated cell sorting |
| FBS | fetal bovine serum |
| FFPE | formalin fixed paraffin embedded |
| FITC | fluorescein isothiocyanate |
| fMLP | N-formylmethionine-leucyl-phenylalanine |
| FSC-A | forward scatter area |
| FSC-H | forward scatter hight |
| g | gram |
| G-CSF | granulocyte colony-stimulating factor |
| GLP-1 | glucagon-like peptide 1 |
| GM-CSF | granulocyte-macrophage colony stimulating factor |
| GMP | granulocyte-monocyte |
| GPIbα | glycoprotein Ibα |
| GSEA | gene set enrichment analysis |
| H&E | Haematoxylin and Eosin |

| | |
|---|---|
| HBSS- | Hank's Balanced Salt Solution modified without magnesium and calcium |
| HBV | hepatitis B virus |
| HCC | hepatocellular carcinoma |
| HCON | healthy control |
| HCV | hepatitis C virus |
| HD | high density |
| HDAC | histone deacetylase |
| HGF | hepatocyte growth factor |
| HIF | hypoxia inducible factor |
| HLA | human leukocyte antigens |
| HMGB1 | high mobility group box 1 |
| HPMC | hydroxypropyl methylcellulose |
| HSC | hepatic stellate cell |
| HTS | high throughput screening |
| ICC | intrahepatic cholangiocarcinoma |
| IDO | indoleamine 2,3-dioxygenase |
| IHC | immunohistochemistry |
| IL | interleukin |
| iNOS | inducible nitric oxide synthase |
| IP | intraperitoneal |
| IQR | interquartile range |
| JAK | Janus kinase |
| kg | kilogram |
| L | litre |
| LASA | laboratory animal science association |
| LD | low density |
| LFA-1 | lymphocyte function-associated antigen 1 |
| LMPP | lymphoid-primed multipotent progenitor |
| LOX-1 | lectin-like low-density lipoprotein receptor-1 |
| LPS | lipopolysaccharide |
| M-MDSCs | monocytic myeloid derived suppressor cell |
| mAb | monoclonal antibody |
| Mac-1 | macrophage-1 antigen |

| | |
|---|---|
| MASH | metabolic dysfunction-associated steatohepatitis |
| MASLD | metabolic dysfunction-associated steatotic liver disease |
| MDSC | myeloid derived suppressor cell |
| MetALD | MASLD with increased alcohol intake |
| MFI | mean fluorescent intensity |
| mg | milligram |
| MHCII | major histocompatibility complex class II |
| ml | millilitre |
| mm | millimetre |
| MMP9 | matrix metallopeptidase 9 |
| moDC | monocytic dendritic cell |
| MPO | myeloperoxidase |
| MPP | multipotent progenitor |
| MRI | magnetic resonance imaging |
| mTOR | mammalian target of rapamycin |
| MVI | microvascular tumour infiltration |
| NADPH | nicotinamide adenine dinucleotide phosphate |
| NAFLD | non-alcoholic fatty liver disease |
| NASH | non-alcoholic steatohepatitis |
| ND | normal density |
| NE | neutrophil elastase |
| NET | neutrophil extracellular trap |
| ng | nanogram |
| NK | natural killer |
| NLR | neutrophil-lymphocyte ratio |
| nm | nanometre |
| nM | nanomolar |
| NO | nitric oxide |
| NPA | neutrophil platelet aggregate |
| OG | oral gavage |
| OSM | oncostatin M |
| p-STAT3 | phosphorylated STAT3 |
| pAb | polyclonal antibody. |
| PAMP | pathogen-associated molecular pattern |

| | |
|---|---|
| PBC | primary biliary cholangitis |
| PBS | phosphate buffered saline |
| PD1 | programmed cell death protein 1 |
| PDAC | pancreatic ductal adenocarcinoma |
| pDC | plasmacytoid dendritic cell |
| PDE5 | phosphodiesterase type 5 |
| PDL1 | programmed cell death ligand 1 |
| PE | phycoerythrin |
| PerCP | peridinin-chlorophyll-protein |
| PGE-2 | prostaglandin E2 |
| PMA | phorbol 12-myristate 13-acetate |
| PMN-MDSC | polymorphonuclear myeloid derived suppressor cell |
| PS | performance status |
| PSC | primary sclerosing cholangitis |
| PSGL-1 | P-selectin glycoprotein ligand-1 |
| PVT | portal vein thrombosis |
| RAGE | receptor for advanced glycan end-products |
| RFU | relative florescence unit |
| RNA | ribonucleic acid |
| ROS | reactive oxygen species |
| rpm | revolutions per minute |
| RPMI | Roswell park memorial institute |
| RT-PCR | reverse transcription polymerase chain reaction |
| SABR | stereotactic ablative radiotherapy |
| scRNA-seq | single cell RNA sequencing |
| SEM | standard error of the mean |
| SIRPα | signal-regulatory protein alpha |
| SIRT | selective internal radiation therapy |
| SLD | steatotic liver disease |
| SLE | systemic lupus erythematosus |
| SSC-A | side scatter area |
| STAM | streptozotocin and high-fat diet treated mouse |
| STAT | signal transducer and activator of transcription |
| TACE | transarterial chemoembolization |

| | |
|---|---|
| TAN | tumour associated neutrophil |
| TBS | tris-buffered saline |
| TBST | tris-buffered saline with tween 20 |
| TGF | transforming growth factor |
| TLR | toll-like receptor |
| TME | tumour microenvironment |
| TMN | tumour node metastasis |
| TNF | tumour necrosis factor |
| TRAIL-R2 | TNF-related apoptosis inducing ligand receptor 2 |
| Treg | T regulatory cell |
| tSNE | t-distributed stochastic neighbour embedding |
| UMAP | uniform manifold approximation and projection |
| US | ultrasound |
| VEGF | vascular endothelial growth factor |
| VEGFR2 | vascular endothelial growth factor receptor 2 |
| vs | versus |
| WD | western diet |
| xg | centrifugal force |
| µg | microgram |
| µl | microlitre |
| µm | micrometre |
| µM | micromolar |

**Table of Figures**

Figure 1.1 – Natural history of chronic liver disease ..... 3
Figure 1.2 – Hepatocellular carcinoma staging and management ..... 7
Figure 1.3 – Hepatocellular carcinoma treatment decision strategy in the UK ..... 8
Figure 1.4 – The immunosuppressive microenvironment of MASH-HCC and therapeutic response to PD1 therapy ..... 12
Figure 1.5 – Neutrophil granulopoiesis ..... 14
Figure 1.6 – Neutrophil ageing and circadian clock ..... 16
Figure 1.7 – Recruitment and anti-microbial functions of neutrophils ..... 19
Figure 1.8 – Neutrophil phenotypes in cancer ..... 24
Figure 1.9 – Neutrophil tumour recruitment and polarisation to a pro-tumour phenotype ..... 30
Figure 1.10 – Neutrophil tumour promoting mechanisms in HCC ..... 34
Figure 1.11 – Neutrophil therapeutic targets in HCC ..... 41
Figure 3.1 – Human neutrophil density gradient separation ..... 52
Figure 3.2 – Flow cytometry neutrophil sorting gating strategy ..... 55
Figure 3.3 – ImageStream gating strategy and image acquisition ..... 62
Figure 3.4 – LegendScreen experiment set up and analysis ..... 64
Figure 3.5 – Mouse peripheral blood LD and ND neutrophil isolation ..... 71
Figure 3.6 – BrdU tracking experiment design and flow cytometry gating ..... 80
Figure 4.1 – Gating strategy used for leukocyte populations in human whole blood ..... 88
Figure 4.2 – Frequency of circulating leukocyte populations in HCC patients, CLD patients and healthy controls ..... 89
Figure 4.3 – Neutrophil density separation gating strategy ..... 90
Figure 4.4 – Neutrophil populations following density separation ..... 91
Figure 4.5 – LD CD16$^{low}$, LD C16$^{high}$ and ND neutrophil morphology and MPO expression ..... 92
Figure 4.6 – Phenotypical analysis of circulating neutrophil populations ..... 94
Figure 4.7 – Circulating neutrophil population functional assays ..... 96
Figure 4.8 – LEGENDScreen comparison LD CD16$^{high}$ vs ND neutrophils ..... 98
Figure 4.9 – Confirmation of neutrophil-platelet aggregates in LD CD16$^{high}$ neutrophils ..... 100
Figure 4.10 – LEGENDScreen comparison LD CD16$^{low}$ vs LD CD16$^{high}$ ..... 102

Figure 4.11 – Effects of PMA stimulation on neutrophil density and phenotype .....104
Figure 4.12 – Effects of time and ageing on neutrophil density and phenotype.....106
Figure 4.13 – Neutrophil phenotype in HCC patients, CLD patients and healthy controls .....108
Figure 4.14 – Neutrophil function in HCC patients, CLD patients and healthy controls .....110
Figure 4.15 – Tumour, liver and blood immune cell frequencies in HCC patients undergoing surgical resection .....112
Figure 4.16 – Tumour, liver and blood neutrophil phenotype in HCC patients undergoing surgical resection .....114
Figure 5.1 – MASH model – clinical phenotype.....118
Figure 5.2 – Mouse general immune cell panel gating strategy for tissue .....120
Figure 5.3 – MASH model – liver immune infiltrate .....122
Figure 5.4 – Orthotopic HCC model – clinical phenotype .....124
Figure 5.5 – Orthotopic HCC model – immune infiltrate.....126
Figure 5.6 – Mouse general immune cell panel gating strategy for blood .....127
Figure 5.7 – Circulating immune cell frequencies in the pre-clinical model.....128
Figure 5.8 – Mouse blood neutrophil density gating strategy .....129
Figure 5.9 – Pre-clinical model - frequency and phenotype of circulating neutrophil populations.....131
Figure 5.10 – Pre-clinical model - circulating neutrophil CD36 and CD41 expression.....132
Figure 5.11 – Pre-clinical model - circulating neutrophil functional assays .....133
Figure 5.12 – Mouse LD vs human LD CD16$^{high}$ neutrophil comparison.....134
Figure 5.13 – The effect of neutrophil specific CXCR2 deletion on circulating neutrophil populations.....136
Figure 5.14 – BrdU tracking validation and flow gating strategy .....138
Figure 5.15 – BrdU tracking of ND and LD neutrophils in WD-HCC mice.....140
Figure 5.16 – Frequency of bone marrow, spleen, liver and tumour neutrophils in WD-HCC vs WD-Sham mice .....142
Figure 5.17 – Altered granulopoiesis associated with HCC .....144
Figure 5.18 – Neutrophil phenotype across biological compartments.....146
Figure 5.19 – Neutrophil functional assays across biological compartments.....148
Figure 5.20 – Effect of HCC on neutrophil phenotype.....149

Figure 5.21 – Effect of HCC on neutrophil function ..... 150
Figure 6.1 – JAK2-STAT3 signalling pathway and its relation to IL-6 and CXCR2 in neutrophils ..... 154
Figure 6.2 – Neutrophil p-STAT3 expression in HCC patients and pre-clinical models ..... 156
Figure 6.3 – Ex vivo effect of AZD1480 on neutrophils ..... 157
Figure 6.4 – In vitro effect of AZD1480 on the Hep 53.4 cell line ..... 159
Figure 6.5 – In vivo effect of AZD1480 in lean HCC-bearing mice ..... 160
Figure 6.6 – In vivo effect of AZD1480 in MASH HCC-bearing mice ..... 162
Figure 6.7 – In vivo effect of targeting S100A8 and S100A9 in HCC-bearing mice 165
Figure 6.8 – In vivo effect of AZ12601011 in lean HCC-bearing mice ..... 167
Figure 6.9 – In vivo effect of AZ12601011 in MASH HCC-bearing mice ..... 169
Figure 7.1 – Therapy response to anti-PDL1/anti-VEGF in lean vs MASH intrahepatic HCC ..... 173
Figure 7.2 – Immunological effects of anti-PDL1/anti-VEGF therapy in lean vs MASH intrahepatic HCC ..... 175
Figure 7.3 – Effects of anti-PDL1/anti-VEGF therapy on CD8 subpopulations in lean vs MASH intrahepatic HCC ..... 177
Figure 7.4 – CD8 T cell subpopulations in MASH ..... 178
Figure 7.5 – Therapy response to anti-PDL1/anti-VEGF in lean vs MASH subcutaneous HCC ..... 180
Figure 7.6 – Immunological effects of anti-PDL1/anti-VEGF therapy in lean vs MASH subcutaneous HCC ..... 182
Figure 7.7 – Effects of anti-PDL1/anti-VEGF therapy on T cell subpopulations in lean vs MASH subcutaneous HCC ..... 184
Figure 8.1 – Possible origins of circulating LD neutrophil populations ..... 196
Figure 8.2 – Neutrophil platelet interactions ..... 198

**Table of Tables**

Table 1.1 – Aetiologies of chronic liver disease .....4
Table 1.2 – Neutrophil therapies for HCC in clinical trials .....43
Table 1.3 – Neutrophil therapies for other cancers in clinical trials .....44
Table 3.1 – Human flow cytometry antibodies and dilutions .....57
Table 3.2 – Laser configuration on ImageStream Mk II imaging flow cytometer and channel set up.....61
Table 3.3 – Antibodies used for immunofluorescence staining .....66
Table 3.4 – Monoclonal antibody therapies.....68
Table 3.5 – Small molecule inhibitor therapies.....68
Table 3.6 – Mouse flow cytometry antibodies and dilutions .....76
Table 3.7 – Antibodies used for immunohistochemistry along with corresponding antigen retrieval and dilutions .....82
Table 4.1 – Demographics and clinical characteristics of patients.....86
Table 8.1 – Circulating neutrophil heterogeneity in humans and mice.....193

# 1. Introduction

## 1.1. Hepatocellular carcinoma: clinical aspects

### 1.1.1. Epidemiology

Primary liver cancer is the sixth most common cancer by incidence and the third leading cause of cancer-related mortality worldwide, with 906,000 newly diagnosed cases and 830,000 deaths in 2020.[1] Hepatocellular carcinoma (HCC) is the most common form of primary liver cancer accounting for around 80% of cases. Other causes of primary liver cancer include intrahepatic cholangiocarcinoma (ICC) (accounting for around 10%), combined HCC-ICC (accounting for around 5%) and rare cancers such as fibrolamellar HCC, hepatic angiosarcoma and hepatoblastoma (together accounting for around 5% of primary liver cancer cases in adults, although hepatoblastoma is more common in children).[1-4] HCC almost always develops on the background of chronic liver disease of various aetiologies. Risk factors for the development of HCC include chronic hepatitis B virus (HBV) and hepatitis C virus (HCV) infection, aflatoxin exposure, metabolic syndrome (characterised by the presence of; insulin resistance, obesity, hyperlipidaemia, hypertension and non-alcoholic fatty liver disease) and excessive alcohol intake (table 1.1).[1] In addition there is sexual dimorphism for HCC risk, with HCC being three times more common in men compared to women.[5] The underlying aetiology of HCC varies greatly according to geographic location. Chronic HBV infection with or without aflatoxin exposure is common in East Asia and Sub-Saharan Africa, whereas chronic HCV infection is common in Japan, North Africa and Western Europe.[1] Excess alcohol intake is also an important risk factor in many developed countries.[1] The advent of highly effective direct acting antiviral therapies for HCV and the implementation of public health and vaccination programmes for HBV eradication, together with an increase in the prevalence of the metabolic syndrome of epidemic proportions, has resulted in metabolic dysfunction-associated steatotic liver disease (MASLD) becoming a major cause of HCC worldwide.[1,6,7] Overall the incidence and mortality of HCC is predicted to increase in many developed countries due to this shift in epidemiology from viral to metabolic risk factors.[8] This makes HCC an important clinical problem, for which it is estimated by 2025 more than 1 million individuals will be affected annually.[9]

### 1.1.2. Chronic liver disease

Chronic liver disease (CLD) is defined as the progressive injury of the liver parenchyma over a time of greater than 6 months. CLD encompasses a wide spectrum of disease stages from inflammation and steatosis to fibrosis, cirrhosis and eventual liver failure leading to either death or liver transplantation.[10] Cirrhosis and the resulting portal hypertension and synthetic liver failure leads to clinical complications such as varices, ascites, encephalopathy, hepatorenal syndrome, portopulmonary hypertension, hepatopulmonary syndrome, coagulopathy and bleeding diathesis, susceptibility to infection, jaundice, malnutrition and sarcopenia (figure 1.1).[11] Hence the health and life expectancy of cirrhotic patients even in the absence of HCC is severely compromised. HCC most commonly arises in liver cirrhosis but can also occur during earlier stages of liver disease.[7] There are many possible underlying aetiologies of CLD, these are broadly separated into MASLD, alcohol associated liver disease (ALD), chronic viral hepatitis, as well as autoimmune, biliary, vascular, drugs, toxins, genetic and cryptogenic causes (table 1.1).[12] Globally, chronic viral hepatitis (HCV or HBV) is the leading cause of CLD,[13] whereas in the UK, steatotic liver disease (SLD) is the most common cause of CLD.[14] SLD encompasses; MASLD (previously known as non-alcoholic fatty liver disease (NAFLD)) and its inflammatory state known as metabolic dysfunction-associated steatohepatitis (MASH) (previously known as non-alcoholic steatohepatitis (NASH)), ALD and MASLD with increased alcohol intake (MetALD).[15] MASLD is the fastest growth cause of CLD and is predicted to become the most common cause of CLD in the future.[13,15,16] Worryingly the burden of liver disease is increasing, with it being the third leading cause of premature death in the UK, and in contrast to other major diseases such as heart disease and cancer where the burden of disease is stable or reducing, the burden of liver disease continues to rise.[17] This is also driving the increasing prevalence of HCC.

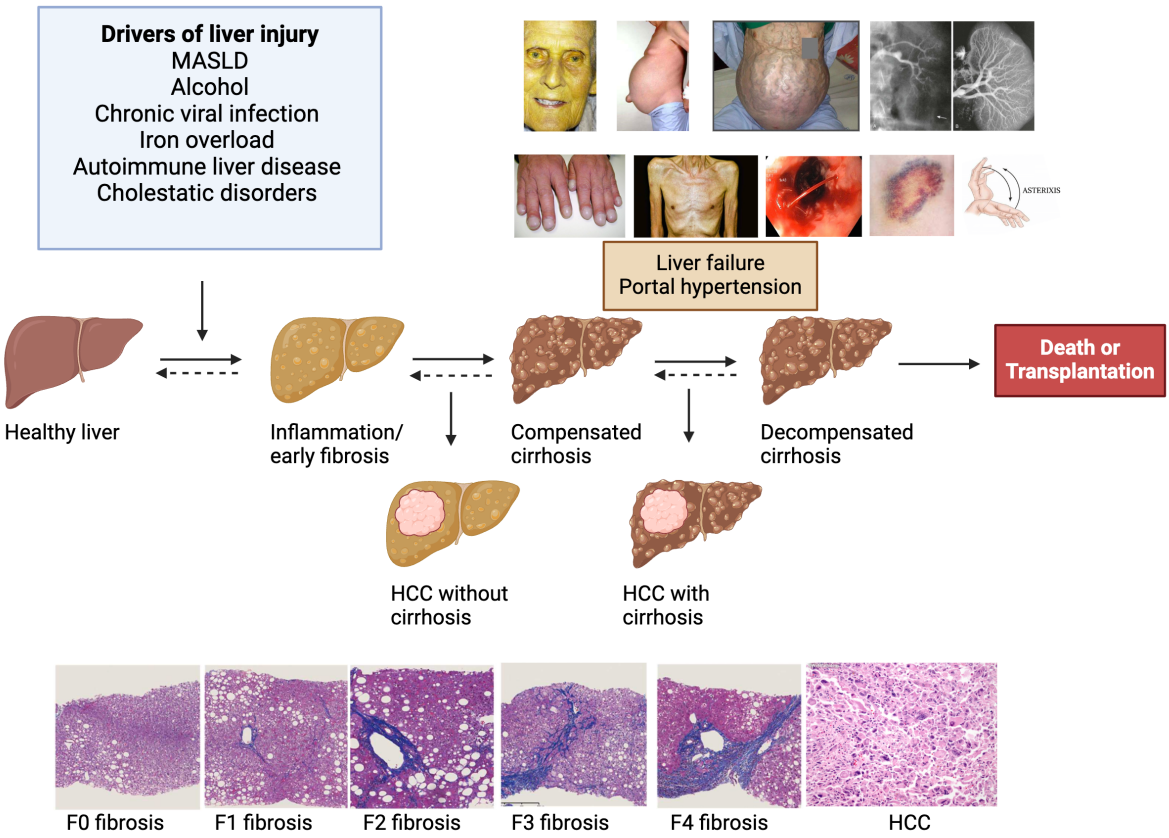



**Figure 1.1 – Natural history of chronic liver disease (CLD).** There are many potential drivers of CLD each of which causes liver damage and chronic inflammation. Over time this causes dysregulation in hepatic regeneration and leads to the development of fibrosis. Fibrosis is graded histologically using the metavir score system from F0 (no fibrosis) to F4 (cirrhosis).[18] Liver failure and portal hypertension develop as a result of cirrhosis and lead to clinical complications such as varices, ascites, encephalopathy, hepatorenal syndrome, portopulmonary hypertension, hepatopulmonary syndrome, coagulopathy and bleeding diathesis, susceptibility to infection, jaundice, malnutrition and sarcopenia. These complications can lead to death or need for liver transplantation. Hepatocellular carcinoma (HCC) most commonly develops on the background of cirrhosis but can also develop in CLD in the absence of cirrhosis. This background of chronic liver disease makes HCC more challenging to treat due to patients limited functional and hepatic reserve. Created with https://BioRender.com.

Steatotic liver disease (SLD)
- Metabolic dysfunction-associated steatotic liver disease (MASLD)
- Alcohol associated liver disease (ALD)
- MASLD with increased alcohol intake (MetALD)

Chronic viral hepatitis
- Hepatitis B virus (HBV)
- Hepatitis C virus (HCV)

Autoimmune
- Autoimmune hepatitis (AIH)
- Primary biliary cholangitis (PBC)
- Primary sclerosis cholangitis (PSC)
- Autoimmune cholangiopathy

Biliary
- Secondary biliary cirrhosis
- Cystic fibrosis

Vascular
- Budd chiari syndrome
- Hepatic congestion

Genetic
- Hemochromatosis
- Wilsons disease
- Alpha 1 antitrypsin disease
- Porphyria
- Glycogen storage disease
- Polycystic liver disease

Miscellaneous
- Drugs
- Toxins
- Parasites

Cryptogenic

**Table 1.1 – Aetiologies of chronic liver disease.**

### 1.1.3. The pre-cancerous niche

HCC almost always develops in the context of CLD and occurs in a multistep process driven by both the CLD microenvironment and aetiology specific factors. The altered liver microenvironment of CLD is a key driver in the development of HCC,[7] with the main drivers being; fibrosis, chronic inflammation and immune tolerance.[7] During the progression of CLD, fibrous scar tissue made up of extracellular matrix (consisting of various proteins, collagen type I and collagen type III) is deposited and eventually replaces normal tissues, resulting in disruption to liver architecture causing portal hypertension and compromising liver function.[19] Myofibroblasts and activated hepatic

stellate cells are the main drivers of this fibrotic process and also produce cytokines, pro-tumorigenic extracellular matrix, angiogenic factors and growth factors which all promote the development and progression of HCC.[20] Chronic inflammation is a unifying feature between all aetiologies of CLD and is a driver of tumour development, progression and metastatsis.[21] In MASLD the inflammatory aspect of the disease is known as MASH and is a driver of disease progression.[15] The CLD immune infiltrate is made up of both innate and adaptive immune cells all of which can have either pro-tumour or anti-tumour functions.[7,20] For example, neutrophils can promote hepatocarcinogenesis through reactive oxygen species (ROS) mediated deoxyribonucleic acid (DNA) damage and promotion of senescence.[22,23] In addition the immune microenvironment of the liver is highly tolerogenic compared to other organs due the constant flow of inflammatory stimuli from the portal circulation. This unique immune microenvironment combined with chronic inflammation leads to the development of pre-neoplastic lesions which bypass immune surveillance leading to the development of HCC. For HCC to progress immune evasion must be maintained, with the HCC tumour microenvironment being shown to be particularly immunosuppressive.[21] Aetiology specific risk factors also influence the development of HCC. For example HBV is responsible for direct mutagenesis through integration of viral DNA into hepatocytes, commonly resulting in TERT promoter mutations,[24] amongst others. Aflatoxin B1 can induce TP53 mutations.[25] The steatotic environment of MASLD causes lipotoxicity and oxidative stress, which can lead to DNA damage and promote hepatocarcinogenesis.[6] The genetic drivers of HCC are complex and described in detail elsewhere.[7,20] Some of the more common driver gene mutations include those in; the TERT promoter, the Wnt-β-catenin signalling pathway and the cell cycle control pathway (e.g. TP53, PTEN, RB1 and AANE1).[20]

### 1.1.4. HCC classification

Like in other cancers, attempts have been made to classify HCCs based on their molecular and immune characteristics.[26,27] This has demonstrated an inflamed and non-inflamed class based on the levels of immune infiltration. The inflamed class can be further split into immune active, immune exhausted and immune-like subclasses. The non-inflamed can be split into intermediate and excluded subclasses, based on differential expression of various immune cells, chemokines, checkpoint molecules

and antigen presentation.[26] These classes also partly align with features of the genetic or molecular landscape of HCC; with the non-inflamed class having increased Wnt-β-catenin signalling and TP53 mutations and the inflamed class having more TGFβ and PD1 signalling.[26] Although the development of this immunogenomic classification is an important step bringing HCC classification more in line with that of other cancers, it has yet to be incorporated into clinical practice.

### 1.1.5. HCC diagnosis, staging and management

Given that HCC most frequently develops in liver cirrhosis, professional societies recommend HCC screening in this patient group in the form of 6 monthly abdominal ultrasound (US) +/- serum alpha-fetoprotein (AFP) in the hope of being able to detect and diagnose HCC at an early stage, treatable with curative intent.[28-31] However, despite this, the majority of HCCs are diagnosed at later stages. This is partly due to the limitations of current screening modalities, but also the burden of undiagnosed cirrhotic patients not in screening programmes, alongside HCC cases arising in the absence of cirrhosis.[32]

Due to the unique vasculature of the liver the majority of HCCs can be diagnosed based on cross sectional imaging alone (contrast computed tomography (CT) or magnetic resonance imaging (MRI)), especially in the presence of liver cirrhosis.[28] When HCC arises in the absence of cirrhosis or if systemic therapies are being considered a histological diagnosis is usually confirmed following biopsy.[28]

Unlike most other cancers, the tumour node metastasis (TMN) staging has a limited role in clinical decision making, as the patients background liver disease, liver function and fitness are essential to consider. The Barcelona Clinic for Liver Cancer (BCLC) staging and treatment algorithm is more widely used.[33] This considers the tumour stage (size, number of nodules, portal vein invasion, extra-hepatic spread) as well as the patients liver function (Child-Pugh cirrhosis stage) and Eastern Cooperative Oncology Group (ECOG) performance status (PS) (figure 1.2). BCLC stage 0 and A are early stage HCCs with good liver function and performance status that can be treated with curative treatments such as liver resection, liver transplantation or ablation. BCLC stage B are intermediate stage HCCs with good liver function and

performance status for which locoregional therapies such as transarterial chemoembolization (TACE), selective internal radiation therapy (SIRT) and stereotactic ablative radiotherapy (SABR) may be utilized. BCLC stage C are those with advanced stage HCCs with good liver function and performance status, or those with early stage disease and preserved liver function, with mildly impaired PS. The BCLC algorithm recommends systemic therapies be used for BCLC C patients, with best supportive care (BSC) advised for all with BCLC D - HCCs are of advanced stage with poor liver function and/or more severely impaired performance status.

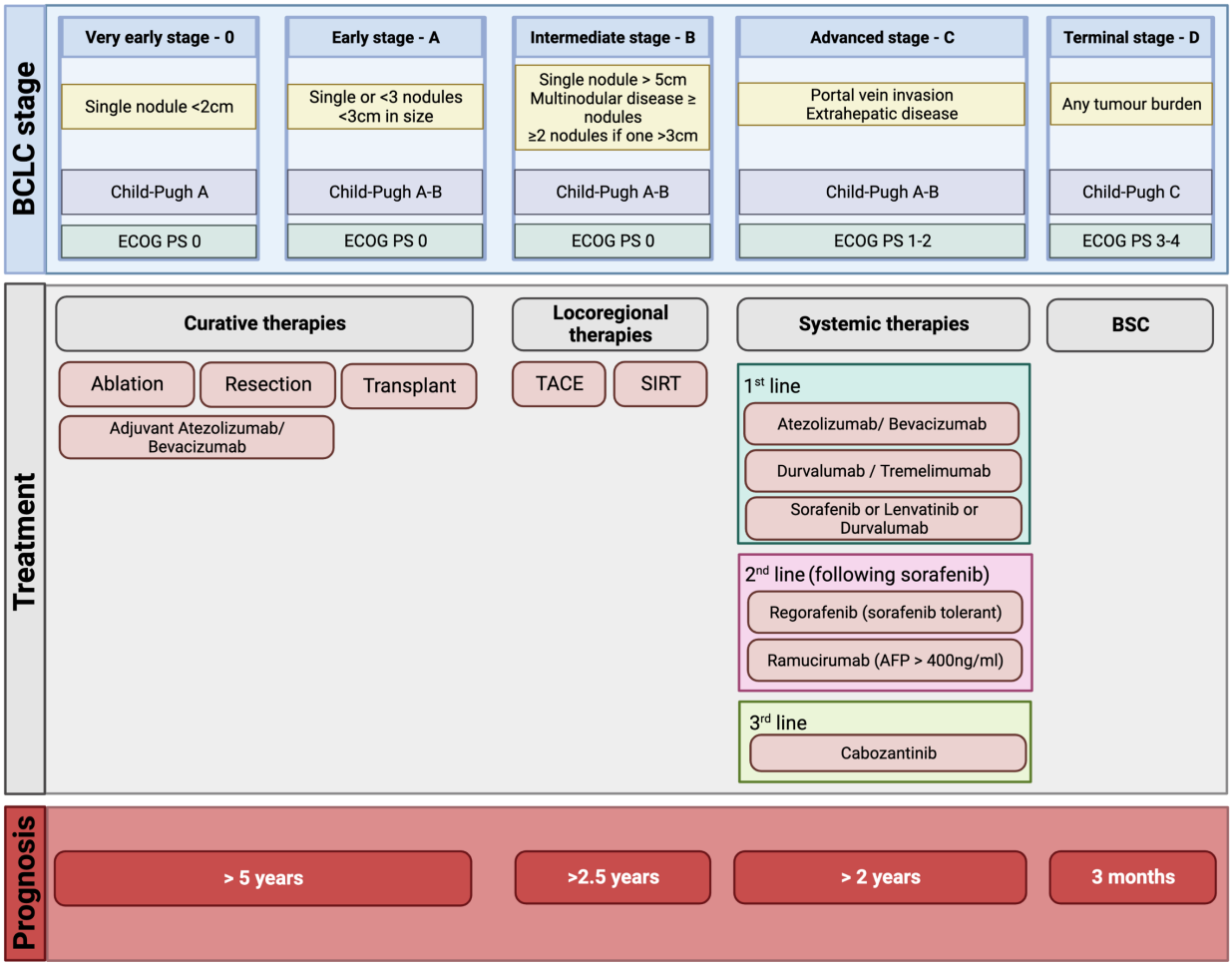



**Figure 1.2 – Hepatocellular carcinoma staging and management.** Barcelona Clinic for Liver Cancer (BCLC) algorithm considers tumour stage (size, number of nodules, extrahepatic metastasis), liver function (Child-Pugh cirrhosis stage) and ECOG patient performance status to aid treatment decisions and guide prognosis. Figure adapted from Reig et al.[33] Created with https://BioRender.com.

While the BCLC algorithm has been universally validated as a prognostic tool, its evidence base for treatment allocation has centred largely on cirrhotic patients with

viral hepatitis – who tend to be younger and fitter than typical UK patients. In the North East UK, patients tend to be older, with the metabolic syndrome and its associated comorbidities, often with mild to moderately impaired PS which has little to do with their cancer diagnosis. The majority of our patients fall within the BCLC C category, often with early stage disease, preserved liver function and age or comorbidity associated mildly impaired PS. These patients may be better served by selective locoregional therapies, rather than medical therapies. While BCLC stage is recorded for UK patients, decision making for treatment allocation is within the setting of an experienced multi-disciplinary team, following the strategy in figure 1.3.[34]

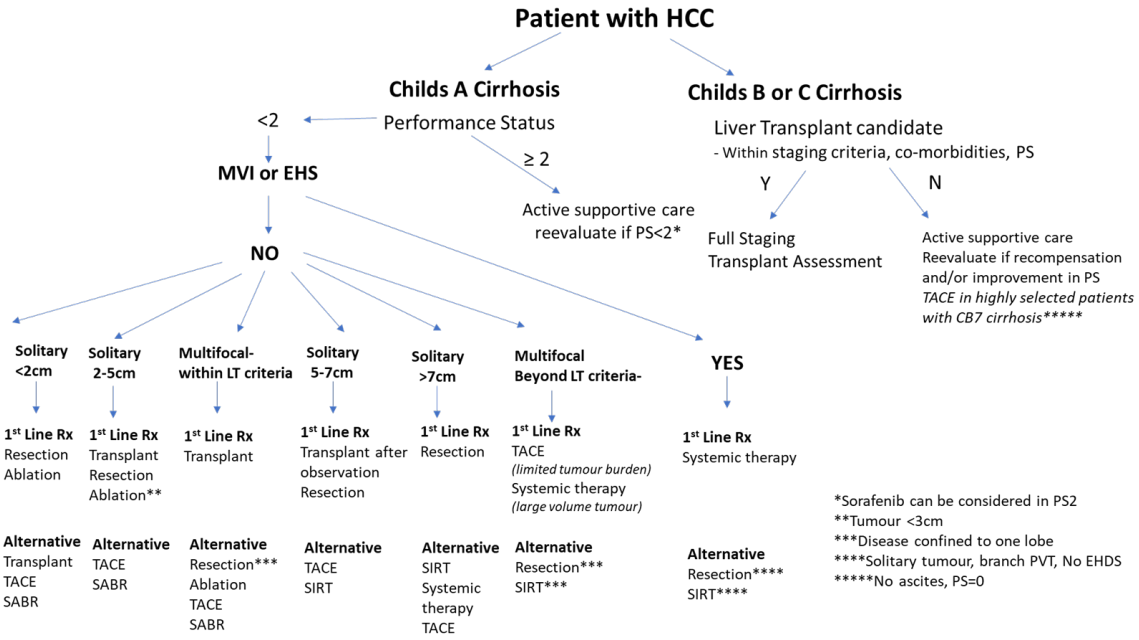



**Figure 1.3 – Hepatocellular carcinoma HCC treatment decision strategy in the UK**. In the UK there is a lower prevalence of viral hepatitis and a higher prevalence of MASLD compared to other countries. HCC patients are typically older and more comorbid. Therefore, although many are staged as BCLC C and would traditionally be recommended systemic therapy, many may benefit from locoregional therapies. The updated British Society of Gastroenterology (BSG) treatment algorithm in the setting of an experienced multi-disciplinary team reflects this shift. Figure adapted from Suddle et al with permission of authors.[34] EHS, extrahepatic disease spread; LT, liver transplant; MVI, microvascular tumour infiltration; PVT, portal vein thrombosis.

### 1.1.6. Systemic therapies for the treatment of HCC

Owing to the presence of underlying liver disease HCC patients do not tolerate systemic cytotoxic chemotherapies traditionally used to treat other cancers.[35] This means only targeted therapies such as small molecular inhibitors or immunotherapies tend to be used. Until recently the only first line systemic therapies for the treatment of HCC were the tyrosine kinase inhibitors, sorafenib and lenvatinib, which only gave a modest survival benefit.[36,37] Second line therapies include the multikinase inhibitors regorafenib and cabozantinib and the anti-vascular endothelial growth factor receptor 2 (anti-VEGFR2) antibody ramucirumab.[38-40] The landmark phase 3 IMBrave150 clinical trial demonstrated that the combination of atezolizumab, an inhibitor of the programmed cell death protein 1 (PD1) – programmed cell death ligand 1 (PDL1) lymphocyte immune checkpoint, with bevacizumab, a vascular endothelial growth factor A (VEGF-A) inhibitor, is a highly effective treatment for some patients with HCC, changing standard care.[41] Previous reports had suggested an HCC patient response rate of around 16-20%, using immune checkpoint inhibitors alone.[42,43] The atezolizumab/bevacizumab combination increased the response rate to 27.3%, compared to 11.9% for sorafenib, in association with improved progression free survival (median 6.8 months versus 4.3 months) and overall survival (median 19.2 months versus 13.4 months at 15.6 months median follow up).[41,44] Subsequently the phase 3 HIMALAYA clinical trial demonstrated effectiveness of another immune checkpoint inhibitor combination. Patients treated with tremelimumab (anti-cytotoxic T-lymphocyte associated protein 4 (CTLA4)) in combination with durvalumab (anti-PD1) had an improved overall survival compared to sorafenib with an objective response rate of 20.1%.[45] Additionally the IMbrave 050 has recently demonstrated an improved recurrence free survival with adjuvant atezolizumab/bevacizumab following surgical resection.[46] This has been recognised as a milestone in the treatment of HCC, but longer follow-up is required to determine the impact of adjuvant atezolizumab/bevacizumab on recurrence and overall survival.

However, many patients do not respond to immunotherapies which is one of the most important conundrums facing the immuno-oncology field. Bevacizumab impacts the microvascular tumour blood supply, but immuno-oncology combinations with therapies that target other components of the tumour microenvironment (TME) may

be more effective in some patients and as such, immune cells other than lymphocytes are now the subject of intense research.

I propose that the manipulation of neutrophils may make the HCC immune microenvironment more permissive to systemic immunotherapies.

### 1.1.7. Underlying CLD and response to systemic therapies

An interesting observation from post hoc subgroup analyses of the main immune checkpoint inhibitor clinical trials in HCC is that the underlying aetiology of liver disease may be a determining factor in therapy response.[47-49] This was based on the initial observation in the IMBrave150 trial that patients classified as having non-viral aetiology had a worse response rate and survival compared to those with viral aetiology.[41] As MASLD is one of the main non-viral aetiologies, one can extrapolate that MASLD may be associated with a poorer response compared to other aetiologies.[48] Indeed a meta-analysis which categorised MASLD vs non-MASLD aetiologies demonstrated a worse overall survival following PD1 or PDL1 blockade in MASLD versus non-MASLD aetiologies.[47] A subsequent retrospective study of 'real-world' patients treated with either lenvatinib or atezolizumab/bevacizumab showed that overall survival in MASLD patients treated with atezolizumab/bevacizumab was non superior to that of lenvatinib whereas in non-MASLD patients atezolizumab/bevacizumab was superior, further suggesting impaired immune checkpoint inhibitor effectiveness in MASLD.[49] These findings are interesting as obesity in other cancer types is reported to be associated with an improved response to PD1/PDL1 blockade, due to leptin associated signal transducer and activator of transcription 3 (STAT3) signalling and upregulation of T cell PD1 expression (figure 1.4).[50] This suggests that there is a fundamental difference in T cell responses to immune checkpoint blockade in the liver versus systemically and is an interesting area of future research.

The mechanisms underlying relative immune checkpoint inhibitor resistance in MASLD-HCC are incompletely understood, however CD8 and CD4 T cell dysfunction in the context of the metabolic environment of MASH have been proposed (figure 1.4).[47,51-54] An expansion of auto-aggressive CD8 T cells which are defined as tissue

resident ($CXCR6^+$), effector (Granzyme $B^+$) and exhausted (eomesodermin $(EOMES)^+$ and $PD1^+$) have been identified in the livers of both MASH patients and mice.[47,51] In MASH these are described as being induced through metabolic stimuli such as acetate and extracellular adenosine triphosphate (ATP) and functionally display MHC-class-I independent auto-aggressive killing, hence being directly implicated in the pathogenesis and progression of MASLD.[51] In the context of HCC these auto-aggressive CD8 T cells rather than being anti-tumour may promote the development of HCC through their induction of liver damage and inflammation.[47] Additionally MASLD has also been shown to impair antigen specific CD8 immunity against HCC due to an accumulation of immunosuppressive macrophages as well as direct metabolic impairment of CD8 T cells.[54,55] CD4 T cells are equally affected with the metabolic hepatic environment of MASLD causing mitochondrial dysfunction, oxidative damage and selective depletion of hepatic and intra-tumoural CD4 T cells, contributing to poor immune checkpoint inhibitor response.[53,54] To date the pre-clinical studies investigating immune checkpoint inhibitor resistance in MASLD-HCC have used anti-PD1 monotherapy,[47,55,56] which requires further validation in the context of anti-PDL1/ anti-VEGF combination therapy given that this is the current fist line systemic therapy used in clinical practice. Preliminary research suggests that pharmacological reversal of MASLD metabolic dysfunction with drugs such as metformin may help rescue immune checkpoint inhibitor response.[55] Another approach is to combine T cell immune checkpoint blockade with therapies that target immune cells beyond T cells in the tumour microenvironment. Combining anti-PD1 therapy with a small molecule inhibitor targeting the neutrophil chemokine receptor, C-X-C chemokine receptor 2 (CXCR2), has been shown to rescue immune checkpoint inhibitor response in pre-clinical models of MASH-HCC by re-programming tumour associated neutrophils.[56] This highlights neutrophils as a novel and potentially important therapeutic target in HCC that warrants further study.

Despite these initial reports this remains a controversial topic due to the retrospective nature of current clinical studies, limited aetiology classification and data collected in clinical trials and conflicting analyses.[57] To properly answer this conundrum large scale, prospective and real world data are awaited.

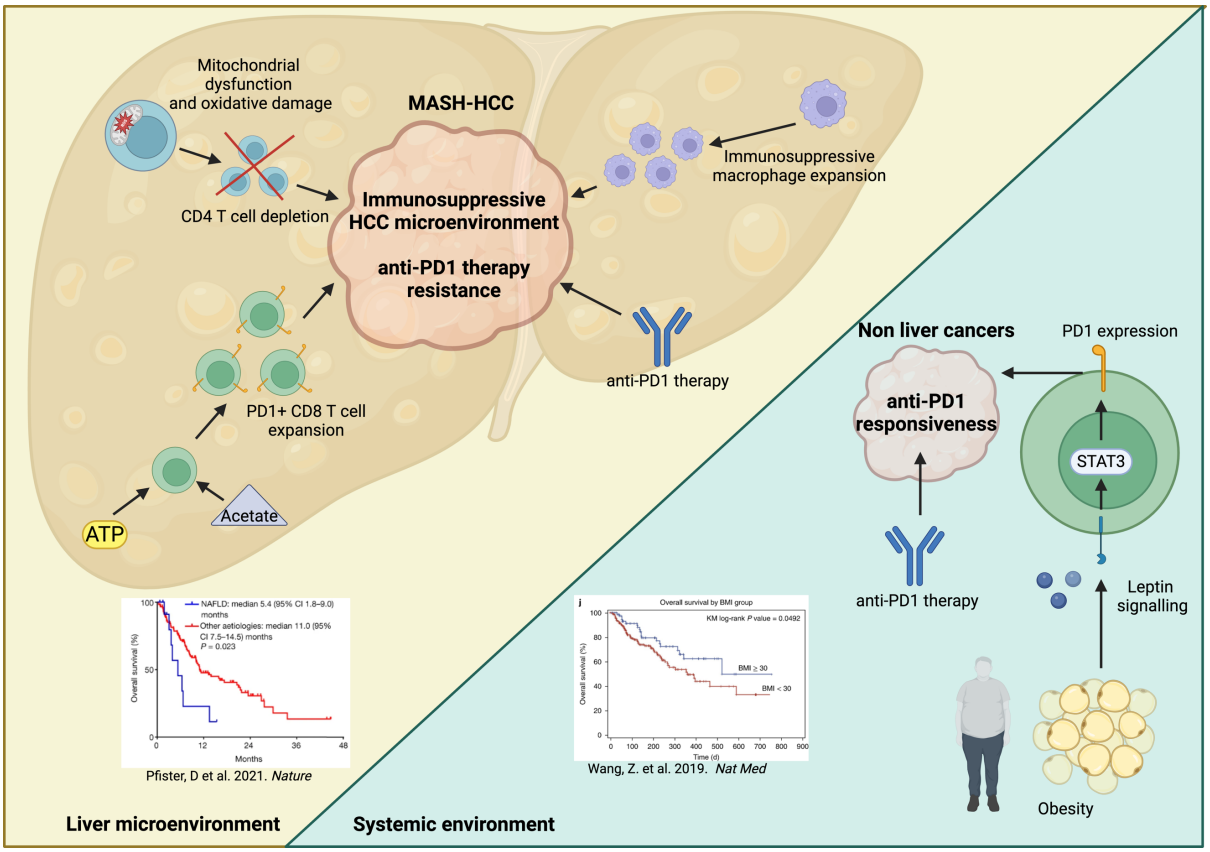



**Figure 1.4 – The immunosuppressive microenvironment of MASH-HCC and therapeutic response to PD1 therapy.** Preliminary clinical studies suggest that anti-PD1 monotherapy is poorly effective in MASH-HCC.[47,49] Suggested mechanisms underlying this are; 1. Acetate and extracellular ATP induced expansion of auto-aggressive and exhausted CD8 PD1$^{+}$ T cells.[47] 2. MASH induced mitochondrial dysfunction, oxidative damage and depletion of CD4 T cells.[52,53] 3. MASH induced expansion of immunosuppressive macrophages.[54] 4. MASH induced metabolic reprogramming of CD8 T cells.[55] Conversely clinical studies of non-liver cancers show that obesity is associated with improved responses to anti-PD1 therapy, possibly due to leptin induced PD1 upregulation of CD8 T cells.[50] Created with https://BioRender.com.

## 1.2. Neutrophils in health

### 1.2.1. Granulopoiesis

Neutrophils are the most abundant immune cells representing 50-70% of circulating leukocytes. Neutrophils are key mediators of the innate inflammatory response, being the first effector cells to arrive at sites of infection, inflammation and tissue damage.[58] In health the majority of the bone marrow is dedicated to granulopoiesis, producing over $1x10^{11}$ neutrophils daily.[59] The majority are held as a mobilisable reservoir, with only 1-2% entering the circulating under resting conditions.[59] During granulopoiesis hematopoietic stem cells differentiate into multipotent progenitor (MPP) cells followed by lymphoid-primed multipotent progenitors (LMPPs) and granulocyte-monocyte progenitors (GMPs). Under the stimulation of granulocyte colony-stimulating factor (G-CSF) GMPs undergo a number of maturation stages (myeloblast, promyelocyte, myelocyte, metamyelocyte, banded/ immature neutrophil) to eventually become mature neutrophils.[60] During this time they undergo changes in their expression of a variety of surface markers, granules (which contain proteins relevant to their function) and their nuclear morphology (changes from a round to a lobulated nucleus) (figure 1.5).[60]

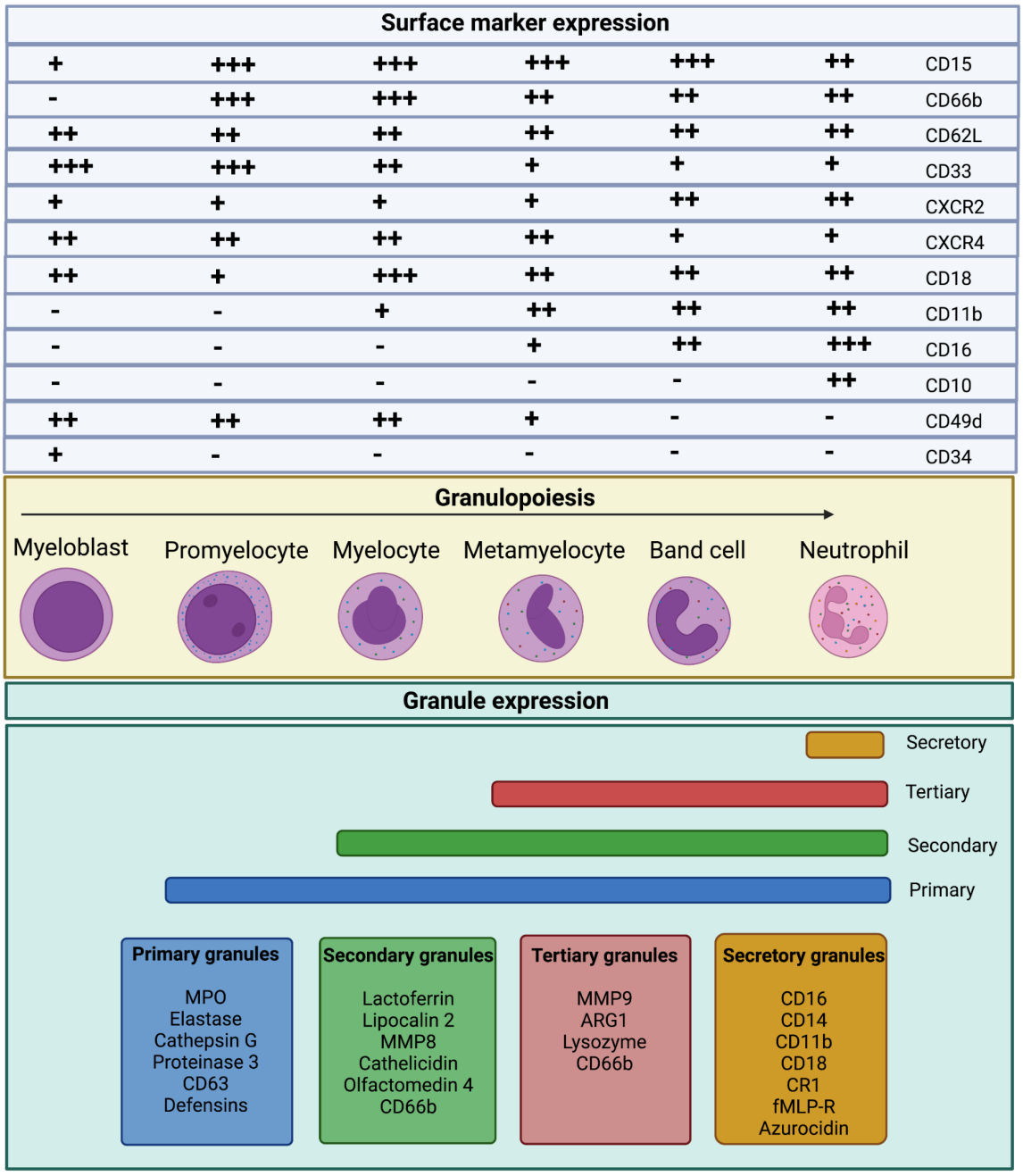



**Figure 1.5 – Neutrophil granulopoiesis.** The majority of the bone marrow is dedicated to neutrophil granulopoiesis. During granulopoiesis neutrophil precursors mature into terminally differentiated mature neutrophils. Each stage of maturation has different surface marker and granule expression. Neutrophil granules form during neutrophil differentiation and contain various proteins with anti-microbial or inflammatory functions. Created with https://BioRender.com.

### 1.2.2. Neutrophil aging, circadian rhythm and clearance

In health, neutrophil dynamics are closely dictated by circadian rhythms (figure 1.6).[61] In the morning there is a large release of neutrophils from the bone marrow into the

blood, then throughout the day neutrophils age and are recruited into tissues or cleared.[62] The main characteristics of aged neutrophils are an increased expression of CXCR4 and reduced expression of the integrin CD62L.[63,64] This increased CXCR4 expression allows enhanced recruitment via C-X-C Motif Chemokine Ligand 12 (CXCL12) and subsequent clearance by the reticular endothelial system of the bone marrow, liver and spleen.[64] Reduced CD62L expression is also an indication of neutrophil activation and degranulation.[65] Aged neutrophils additionally have an increased expression of CD16, CD10, CD11b, CD49d, TLR4, ICAM-1, CD24 and reduced expression of CXCR2, CD47 and Ly6G (Ly6G in mice only).[63,66-68] Aged neutrophils are also functionally distinct from fresh neutrophils with increased ROS activity and neutrophil extracellular trap (NET) formation.[69,70] Diurnal neutrophil ageing has been shown to be controlled by the clock protein BMAL1, which induces intrinsic neutrophil CXCL2 expression and subsequent CXCR2 signalling - which drives ageing and subsequent recruitment into tissues and/or clearance.[61] Detailed mechanistic studies in mice show that CXCR2 signalling drives neutrophil ageing whereas CXCR4 antagonises it.[61] This diurnal switching of neutrophils is thought to allow the optimal function of circulating neutrophils during the day, when injury and contact with pathogens is most likely, whilst promoting migration of neutrophils out of the circulation into tissues at night which protects against vascular injury whilst enabling continued tissue anti-microbial activity.[61,71] Additionally neutrophil ageing has also been shown to be influenced by the microbiome, metabolic syndrome, glucocorticoid signalling and cancer.[63,70,72-75]

An accelerated rate of neutrophil ageing has been reported in mice with dietary induced MASH.[75] Through the use of constitutively aged (MRP8 driven conditional knock out of CXCR4) and constitutively fresh (MRP8 driven conditional knock out of CXCR2) neutrophil models, neutrophil ageing was shown to exacerbate steatosis and fibrotic progression of MASH. Activation, degranulation and ageing of neutrophils causes reduced CD62L expression due to shedding.[65] Interestingly genetic or pharmacological depletion of CD62L in MASH pre-clinical models ameliorates liver disease and reduces the number of liver infiltrating neutrophils.[65] These studies strongly suggest an important role of neutrophil ageing in the pathogenesis of MASH.

In cancer, neutrophils are also reported to undergo accelerated ageing as well as directly promote tumour progression.[74,76,77] Aged neutrophils may promote tumour progression via release of neutrophil elastase (NE) stimulating increased tumour proliferation or by NET release and subsequent capturing of tumour cells in the pre-metastatic niche of lung cancer.[76,77]

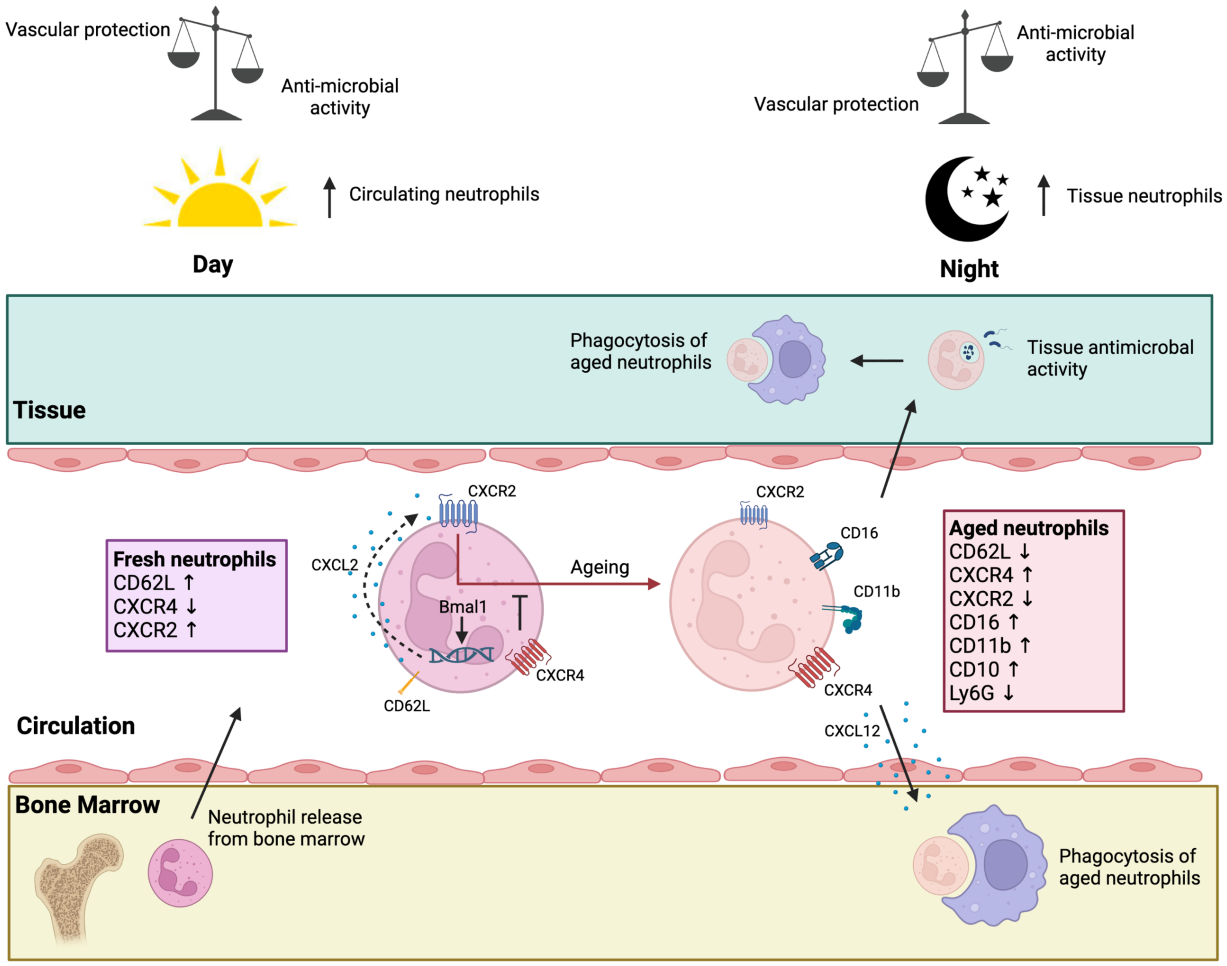



**Figure 1.6 – Neutrophil ageing and circadian clock.** Following mobilisation from the bone marrow into the circulation neutrophils undergo a process of ageing. Aged neutrophils have a distinct phenotype with the most well described changes being a reduction in CD62L expression and increase in CXCR4 expression. This increase in CXCR4 is thought to facilitate migration back into the bone marrow and reticular endothelial system where they can be cleared by macrophages. The process of neutrophil ageing has been shown to be controlled by the core circadian clock transcription factor Bmal1. This process is also responsible for circadian oscillations in the number of circulating neutrophils and the evolutionary reason behind this phenomenon is thought to be to balance anti-microbial activity (needed mostly in daylight when most likely to encounter pathogens) with vascular protection (needed at night when resting and pathogens less likely to be encountered). Created with https://BioRender.com.

### 1.2.3. Neutrophil trafficking

The release of neutrophils from the bone marrow into the circulation is tightly controlled by the action of CXCR2 and CXCR4 (figure 1.7). Bone marrow neutrophils express high levels of CXCR4 with bone marrow stromal cells expressing its ligand CXCL12, this interaction keeps them in the bone marrow. Factors such as G-CSF stimulate neutrophil release from the bone marrow to the circulation by inducing down regulation of CXCR4 and CXCL12 and upregulation of CXCR2.[78-82] The ligands for CXCR2 are CXCL1, CXCL2, CXCL3, CXCL5, CXCL6 and CXCL8 (in humans only) and are expressed by endothelial cells.[78] Once in the circulation neutrophils can be recruited to sites of inflammation and infection in a process called the leukocyte adhesion cascade.[83] In this process local inflammatory stimuli and chemokines induce the upregulation of adhesion molecules on endothelial cells and neutrophils (E and L-selectins, intracellular adhesion molecule 1/2 and integrins) to induce neutrophil tethering, rolling, adhesion and crawling on endothelial cells and finally transmigration into the tissue. Once in the tissue neutrophils are recruited to areas of infection/inflammation via CXCR2 ligands (CXCL1, CXCL2, CXCL3, CXCL5, CXCL6 and CXCL8) or necrotaxis-associated molecules such as formyl-methionyl-leucyl-phenyalanine (fMLP) and complement component C5a.[83,84] Neutrophil migration into tissues is also controlled by the sympathetic nervous systemic and circadian rhythm.[85,86] Neutrophils are short lived with a lifespan of 7-10 hours in the circulation,[87] although their survival may be more prolonged in tissues.[88] Neutrophils are cleared by several different mechanisms. Apoptotic neutrophils in tissues are cleared by phagocytic macrophages and dendritic cells and aged neutrophils in the circulation upregulate CXCR4 enabling them to return to the bone marrow for clearance.[67,89]

### 1.2.4. Antimicrobial and inflammatory actions of neutrophils

Neutrophils exert their antimicrobial and inflammatory functions through phagocytosis, ROS generation, degranulation and release of NETs (figure 1.7).[67,90,91] Phagocytosis is the process in which opsonized pathogens become engulfed within a neutrophil vacuole known as a phagosome.[91] Compared to other phagocytic cells neutrophil phagocytosis is a very rapid process occurring in as little as 20 seconds.[92] Once phagocytosis has occurred granules fuse with the phagosome and activated nicotinamide adenine dinucleotide phosphate (NADPH) oxidase produce ROS for

cytotoxic effect.[91] Respiratory burst describes the large increase in oxygen consumption associated with neutrophil ROS generated by the active NADPH oxidase complex (made up of 5 subunits; NOX2, CYBA, NCF4, NCF1 and NCF2).[91] These oxygen derivatives are highly cytotoxic towards pathogens however if released outside the neutrophil may cause bystander tissue damage.[93] In addition neutrophils also produce nitric oxide (NO) via inducible nitric oxide synthase (iNOS) activity which complements ROS activity.[94] Neutrophils contain 4 types of granules, each containing a variety of antimicrobial enzymes, adhesion and chemotactic receptors (figure 1.5). During degranulation these granules either fuse with the phagosome aiding phagocytic killing of pathogens or fuse with the plasma membrane resulting in extracellular release of their contents.[91] NETs are a network of decondensed chromatin, histones and granule products released into the extracellular space by neutrophils and primarily occur during a form of neutrophil cell death called NETosis.[95] NETs kill pathogens by trapping them in a network of chromatin and concentrated antimicrobial granules such as myeloperoxidase (MPO), NE, S100A8/9, LL-37 and lactoferrin.[95] NETosis has been shown to be stimulated by both inflammatory mediators such as tumour necrosis factor (TNF) and immune complexes as well as pathogen-associated molecular patterns (PAMPs).[95] Mechanistically ROS produced via NADPH oxidase, NE and MPO are vital in the generation of NETs.[95] In contrast to neutrophil phagocytosis and degranulation NETosis is a relatively slow process occurring over 2-4 hours.[96] In addition to these direct antimicrobial functions neutrophils also have immunomodulatory functions on a number of other immune cells such as dendritic cells, T cells, B cells, macrophages and natural killer (NK) cells, mainly via the secretion of various granule products or cytokines.[91]

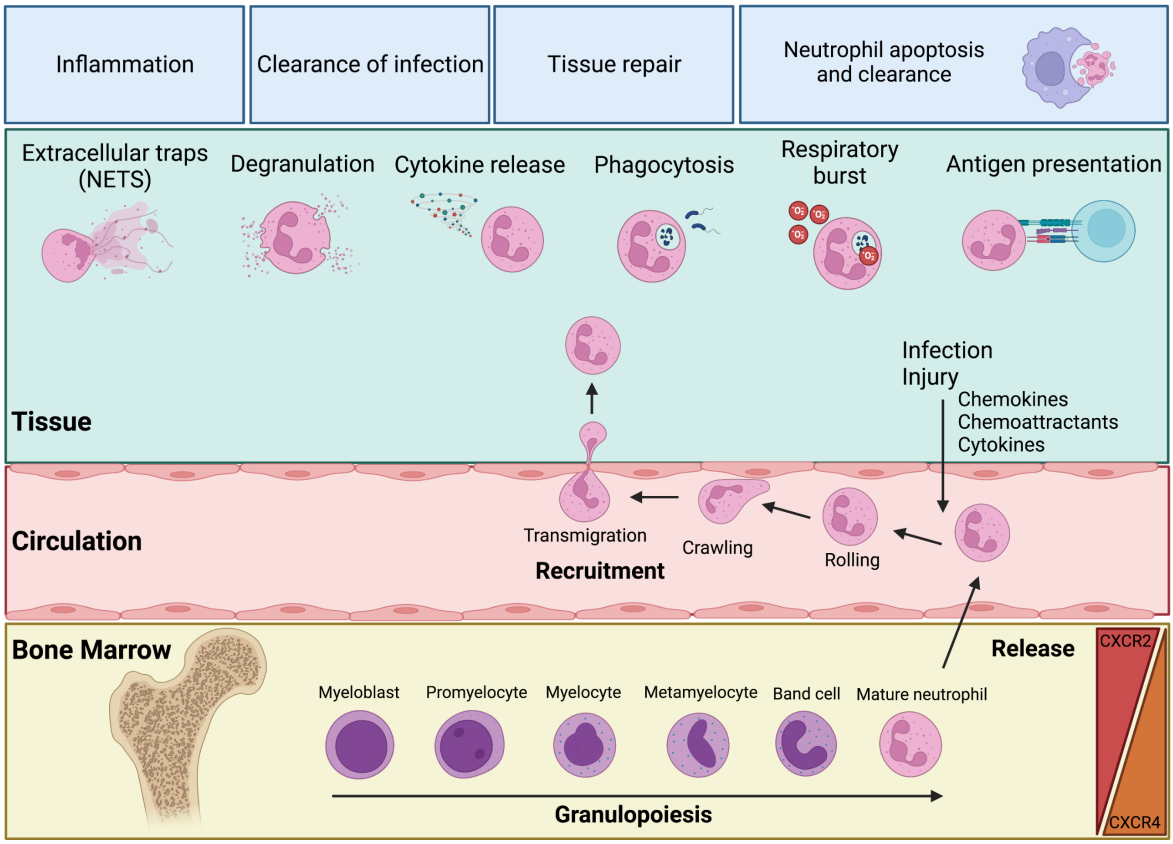



**Figure 1.7 – Recruitment and anti-microbial functions of neutrophils.** During granulopoiesis neutrophil precursors differentiate into mature neutrophils. The mobilisation of neutrophils from the bone marrow into the blood is controlled by CXCR2 and CXCR4 signalling. Once in the circulation neutrophils can be recruited into tissues via the actions of chemokines, cytokines and other chemoattractants. In order to exit the blood neutrophils need to engage with various selectins and integrins expressed on endothelial cells. This causes neutrophil rolling and crawling along the endothelium followed by transmigration between endothelial cells and into tissue. Once recruited neutrophils can exert multiple anti-microbial and inflammatory functions such as; 1. Produce NETs. 2. Release granule contents in a process known as degranulation. 3. Release cytokines which can further potentiate the inflammatory response. 4. Engulf bacteria in a process called phagocytosis. 5. Generate ROS either intracellular or extracellular. 6. Act as antigen presenting cells. These processes result in either ongoing inflammation, clearance of infection, tissue repair and eventual apoptosis and clearance of neutrophils by phagocytic cells such as macrophages. Created with https://BioRender.com.

### 1.2.5. Neutrophil heterogeneity in health

Neutrophils have traditionally been viewed as a homogenous cell type due to their terminally differentiate nature. However single cell RNA sequencing studies (scRNA-seq) have challenged this and are demonstrating a high degree of heterogeneity according to their maturation, tissue of residence, circadian rhythm as well as local and systemic stimuli.[64,71,88,97-100] Initial sc-RNA-seq studies describe 8 populations of neutrophils with 5 residing in the bone marrow and separating according to stage of maturation and 3 being found in blood.[99] These blood populations were initially thought to be pre-programmed in the bone marrow in order to perform specific functions. However a more recent study has demonstrated that neutrophils exist along a continuum of phenotypes as a result of time, maturation, tissue of residence and environmental stimuli such as inflammation and infection.[100] This developmental spectrum, termed the 'neutrotime' by the authors, demonstrates that neutrophils are not only highly heterogeneous but also display a high level of plasticity even after maturation in response to environmental cues.

## 1.3. Neutrophils in cancer

Until recently the role of neutrophils in cancer pathogenesis has been overlooked, in part because their lifespan was thought to be too short to have a significant impact.[101-103] However, over the past decade, neutrophils have become increasingly implicated in the pathology of a number of cancers including HCC.

### 1.3.1. The N1 and N2 spectrum

Morphologically, neutrophils have a distinctive appearance due to their multilobulated nucleus.[104] Phenotypically neutrophils can be defined by $CD15^{+}CD16^{+}CD66b^{+}CD14^{-}$ and $CD11b^{+}Ly6G^{+}$ surface marker expression in humans and mice respectively.[105,106] Due to technical difficulties such as the frailty of neutrophils following isolation, the vast majority of mechanistic studies of neutrophils have been carried out either in mouse models of cancer or in vitro with human cancer cell lines and isolated peripheral blood neutrophils.

Neutrophil heterogeneity and the existence of distinct neutrophil populations in cancer has only recently been recognized. Consequently, the classification and terminology

has been appropriated from the more established macrophage literature.[107] Fridlender *et al* were the first to apply similar terminology to neutrophils,[108] based on the observation that transforming growth factor beta (TGF-β) blockade ameliorated cancer progression whilst leading to an influx of myeloid cells into the tumour. They determined that TGF-β blockade exerted its anti-tumour mechanism by preventing the polarisation of neutrophils from an anti-tumour (N1) to a pro-tumour phenotype (N2).[108] N1 neutrophils were more cytotoxic towards cancer cells, also expressing higher levels of inflammatory chemokines compared to N2 neutrophils, with TGF-β driving tumour progression by inducing an N2 phenotype.[108] Numerous studies have followed, defining the phenotype of N1 and N2 neutrophils based on their density, morphological appearance, cell surface antigen expression, cytokine/chemokine expression and functional characteristics.[109-122] The spectrum of neutrophil phenotypes are detailed in figure 1.8.

Functionally N1 neutrophils have an increased oxidative burst, increased phagocytosis, increased migratory capacity, are non-suppressive towards T cells and have increased cytotoxicity towards tumour cells. N2 neutrophils are suppressive towards T cells and show poor cytotoxicity towards tumour cells.[118] However, there is considerable overlap - both in the phenotypes and functional mechanisms of N1 and N2 neutrophils. For example ROS production can be utilized by N1 neutrophils for tumour killing,[123] and by N2 neutrophils for T cell suppression.[124] It is possible, however, that the difficulty in distinguishing between N1 and N2 markers is compounded by mixed populations of neutrophils within tumours or tumour regions. In HCC peri-tumour neutrophils reportedly have different characteristics, functions and prognostic significance compared to intra-tumour neutrophils,[114] which would be lost using bulk phenotyping methods characterising neutrophils isolated from tumours. The application of single cell technologies may help resolve the nature of mixed populations, however significant technical challenges of isolating neutrophils from tissues whilst keeping them alive and preserving their native state along with the low abundance of RNA present in neutrophils makes this difficult. Thus far, studies employing single cell RNA sequencing and spatial transcriptomics of neutrophil populations are under-represented, compared to those of other immune cells.[125] Single cell proteomics is a technology currently being developed that could be

particularly useful for deciphering neutrophil phenotype at the single cell level due to the fact that neutrophils are not strongly influenced by transcriptional control.[126]

### 1.3.2. Low density neutrophils

Blood neutrophils are usually isolated on a density gradient where they localise to the high density fraction at the bottom of the gradient (often referred to as high density (HD) neutrophils, but more recently referred to as normal density (ND) neutrophils), separating from mononuclear cells found in the low density fraction at the top.[127] A population of low density (LD) neutrophils can be found mixed within the low density mononuclear layer and has been reported to correlate to disease stage in both patients with cancer and in tumour bearing mice.[118,128] Additionally they have also been reported in patients with autoimmune diseases such as systemic lupus erythematosus (SLE), rheumatoid arthritis,[129] psoriasis[130] and vasculitis,[131] infectious conditions such as human immunodeficiency virus,[132] sepsis,[133] and malaria,[134] inflammatory conditions such as obesity,[135] chronic graft versus host disease (cGVHD),[136] and alcoholic hepatitis[137] and as well as in healthy pregnancy.[138] The origin of LD neutrophils is poorly understood, however they are thought to be a heterogenous population of mixed maturity.[118] Immature LD neutrophils are described as having either a banded or myelocyte like morphology are thought by some to be immature neutrophils prematurely released from the bone marrow as part of the acute inflammatory response.[118,139-141] On the other hand mature LD neutrophils with a segmented morphology maybe activated ND neutrophils which have undergone degranulation and hence changed density.[118,134] So far attempts to characterise neutrophil function in relation to density have yielded mixed results. In SLE LD neutrophils have been shown to be more prone to forming NETs and hence implicated in auto-antigen presentation and driving inflammation.[142,143] Whereas in the context of cancer LD neutrophils have been demonstrated to be immunosuppressive with poor anti-cancer cytotoxicity (N2).[118] In the context of alcoholic hepatitis LD neutrophils have been reported as having a functionally exhausted phenotype with poor ROS response to lipopolysaccharide (LPS), reduced phagocytosis and reduced migratory ability.[137] Interestingly circulatory NET markers and LD neutrophils frequency was shown to increase following alcohol exposure.[137] In the context of cGVHD LD neutrophils were shown to be mostly $CD10^-$ immature neutrophils which functionally

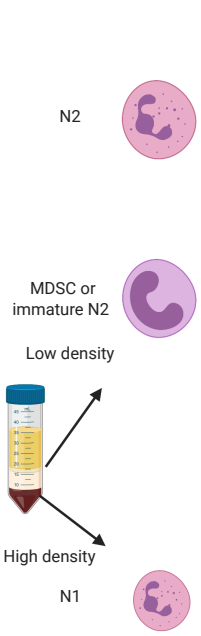
enhanced T cell proliferation and could differentiate into antigen-presenting neutrophil with increased HLA-DR and PDL1 expression.[136] Attempts to characterise neutrophils based on density have been further confused due to; the lack of continuity of some neutrophil markers between murine and human neutrophils (for example Ly6G is only expressed on murine neutrophils), inconsistent terminology (immature LD neutrophils referred to as polymorphonuclear myeloid derived suppressor cells by some groups) and lack of specific markers to differentiate these populations other than density.[67] Additionally the relationship between neutrophil function and density in tissue and tumour associated neutrophils has yet to be explored but will likely be confounded by the more complex isolation process making it difficult to isolate them in their native state.

### 1.3.3. Myeloid derived suppressor cells

Myeloid derived suppressor cells (MDSCs) are immature myeloid cells with the ability to suppress T cell activity and were first described in patients with cancer almost 40 years ago.[144,145] MDSCs are split into monocytic (M-MDSC) and polymorphonuclear (PMN-MDSC) categories. M-MDSCs are suppressive monocytes and are identified as having the monocyte phenotypic markers $CD11b^{+}CD14^{+}HLA\text{-}DR^{-/low}CD15^{-}$ in humans and $CD11b^{+}Ly6G^{-}Ly6C^{hi}$ in mice. PMN-MDSCs are suppressive granulocytes with the neutrophil phenotypic markers; $CD11b^{+}CD14^{-}CD15^{+}CD66b^{+}$ in humans and $CD11b^{+}LyG^{+}Ly6C^{int}$ in mice.[146] Morphologically M-MDSCs and PMN-MDSCs are almost identical to monocytes and neutrophils respectively with the exception of having some studies reporting an immature appearance.[118] Early studies of MDSCs in mice identify MDSCs as $CD11b^{+}Gr1^{+}$ which includes both M-MDSC and PMN-MDSC groups as Gr1 is a composite of both Ly6G and Ly6C markers.[146] MDSCs are principally found in significant numbers in the context of cancer and resolving infection and in the blood are differentiated from neutrophils in some studies on density centrifugated, with MDSCs being in the low-density fraction.[146,147] The fact that PMN-MDSCs express the same markers as neutrophils means that terms PMN-MDSCs and LD neutrophils are likely describing the same population in the blood however due to the inconsistent use of density separation along with markers which assess maturation it is unknown which neutrophil population PMN-MDSCs correspond to. Interesting the lectin-like low-density lipoprotein (LDL) receptor-1 (LOX-1) is reported to be an

identifying marker of PMN-MDSCs.[148] Therefore assessing LOX-1 expression of blood LD neutrophil populations may enable these populations to be matched.

In the context of cancer MDSCs have been shown to promote tumour progression through immune suppression, tissue remodelling and angiogenesis mechanisms.[144,146] MDSCs exert their immunosuppression functions through arginase 1 (ARG1), iNOS, indoleamine 2,3-dioxygenase (IDO), TGF-β, cyclooxygenase-2 (COX2) and interleukin (IL) 10 activity as well as ROS production.[121,144,146,149-151] Tissue remodelling and angiogenesis are stimulated by MDSCs through their secretion of VEGF, Bv8 and matrix metallopeptidase 9 (MMP9).[144,146]




| | Appearance | Identification markers | Maturation marker expression | Other phenotypic markers | Functional characteristics | Tumour functions |
|---|---|---|---|---|---|---|
| N2 | Mature<br>Segmented nucleus<br>Large | Human; $CD15^+CD16^+CD66b^+CD14^-$<br>Mouse; $CD11b^+Ly6G^+$ | Human; $CD11b^{high}$ $CD16^{high}$<br>Mouse; $CD11b^{high}$ | CXCL1, CXCL14, CXCL10<br>CCL2, CCL5, CCL17<br>CCR5<br>PDL1<br>VEGF<br>IL6<br>MMP9<br>ARG1, iNOS | ↓Oxidative burst<br>↓phagocytosis<br>↓migratory capacity<br>T cell suppression | Pro-tumour |
| MDSC or immature N2 | Immature<br>Segmented nucleus<br>Large | Human; $CD15^+CD16^+CD66b^+CD14^-$<br>Mouse; $CD11b^+Ly6G^+$ | Human; $CD11b^{int}$ $CD16^{int}$<br>Mouse; $CD11b^{int}$ | TGFβ<br>COX2<br>IL10<br>IDO<br>ARG1, iNOS<br>VEGF<br>Bv8<br>MMP9<br>LOX-1 | ↓Oxidative burst<br>↓phagocytosis<br>↓migratory capacity<br>T cell suppression | Pro-tumour |
| N1 | Mature<br>Segmented nucleus<br>Small | Human; $CD15^+CD16^+CD66b^+CD14^-$<br>Mouse; $CD11b^+Ly6G^+$ | Human; $CD11b^{high}$ $CD16^{high}$<br>Mouse; $CD11b^{high}$ | CD54, OX40L, 4-1BBL<br>CXCL13, CXCL10, CXCL4<br>CCL6, CCL2, CCL8, CCL3,<br>CCL7, CCL4<br>CCR5, CCR7<br>CXCR3, CXCR4<br>TNF-α<br>IL12, IL8, IL6 | ↑Oxidative burst<br>↑phagocytosis<br>↑migratory capacity<br>Cancer cytotoxicity | Anti-tumour |

**Figure 1.8 – Neutrophil phenotypes in cancer.** Blood neutrophil populations can be separated on density gradient centrifugation. Anti-tumour N1 neutrophils are found in the high density polymorphonuclear fraction whereas pro-tumour N2 neutrophils can be found in the low-density fraction along with mononuclear cells.[118] Pro-tumour N2 neutrophils can be further separated into mature N2 neutrophils and immature N2 neutrophils/MDSCs based on maturation marker expression and nuclear morphology.[118] There are a range of differentially expressed phenotypic markers however the gold standard to distinguish between these populations remains through the use of functional assays.[109-122] The relevance of high density and low-density neutrophils in tissues and tumours is unclear. Figure used for publication.[152] Created with https://BioRender.com.

### 1.3.4. Problems with current classification

Single cell technologies have demonstrated that neutrophils exhibit considerable phenotypic heterogeneity that may be highly dynamic and determined by the tissue in which they reside, circadian rhythm and age.[71,88] This casts questions over the current classification of neutrophils in cancer (N1, N2 and PMN-MDSCs) which suggests that phenotypes are fixed. To this end I suggest the current classification represents the extreme phenotypic fates and that in reality neutrophils likely exist across a spectrum of dynamic pro-tumour and anti-tumour states that vary according to their context. As single cell technologies are further refined to explore neutrophil phenotype in cancer this classification should be re-visited. Due to the similarities between PMN-MDSCs and neutrophils I will include studies of PMN-MDSCs but refer to them as neutrophils with a pro-tumour phenotype.

## 1.4. Neutrophils in HCC

### 1.4.1. Circulating neutrophils

Peripheral blood absolute neutrophil count and neutrophil-lymphocyte ratio (NLR) are widely observed as markers of advanced disease, poor prognosis and poor response to therapy in HCC.[153-167] In a study of 2 large independent HCC patient cohorts involving 1168 patients, neutrophils were the only cell type independently associated with outcome.[159] Higher neutrophil counts were independently associated with more advanced disease, worse performance status and poorer overall survival.[159] NLR and absolute neutrophil count are also reported to predict poor prognosis and response following treatments such as liver resection, liver transplantation, TACE and sorafenib therapy.[153,154,157,158,160-162,164-166] Of particular relevance NLR may also predict treatment responses to immunotherapies in HCC. In a small retrospective study of patients treated with nivolumab a lower post treatment NLR associated with a better treatment response and improved survival.[167] Interestingly a high NLR also appears to indicate a higher risk of developing HCC in both HBV and MASLD.[168,169] However, I urge caution with the use of NLR as a predictive tool in HCC since it also predicts survival in patients with liver cirrhosis without HCC.[170,171] Interestingly a recent study has reported NLR as being predictive of a better prognosis in HCC.[172] While this study appears in contradiction to the rest of the literature, the disease stage, underlying

aetiology, liver function and treatment received may underpin differences and were not reported.[172] NLR is also known to be a prognostic factor in other cancers including; intrahepatic cholangiocarcinoma, colorectal cancer, metastatic melanoma, prostate cancer, lung cancer, B cell lymphoma and renal cell carcinoma.[173-180] To date only one study has investigated the presence of LD neutrophils in HCC (referred to PMN-MDSCs by the authors) and reported an expansion of LD neutrophils in HCC patients compared to age and sex matched healthy controls.[156] Interestingly the expansion of LD neutrophils correlated to the absolute neutrophil count. However, a limitation of this study is lack of appropriate control, with chronic liver disease being a possible confounding factor.

### 1.4.2. Tumour associated neutrophils

Tumour associated neutrophils (TANs) are neutrophils found within or around a tumour. TANs are a marker of poor prognosis in HCC,[114,115,181-190] as well as in other cancers such as head and neck, glioma, gastric, pancreatic, melanoma and renal cell carcinoma.[191-197] There are conflicting reports as to whether it is peri-tumour or intra-tumour TANs that influence prognosis. Some studies report peri-tumour neutrophils as correlating with poor prognosis.[114,115,183,198,199] Whereas other studies report intra-tumour neutrophils as correlating with poor prognosis.[182,185,189,190,200] Although there is disparity on how the localisation of TANs affects prognosis in these studies there is consensus that a high number of TANs is a marker of poor prognosis. These observational studies should be interpreted with caution as they were carried out using tissue from patients undergoing liver resection with curative intent. In clinical practice these patients have early, localised disease with generally preserved liver function and good performance status. In western counties where, viral hepatitis is less prevalent and fatty liver diseases such as MASLD more common, only 15% of HCC patients are staged as having early disease and considered candidates for curative resection.[14] Therefore, these observations of TANs may not be generalisable to HCC patients with more advanced disease, which make up the majority of patients typically considered for systemic treatment.

### 1.4.3. Neutrophil heterogeneity in HCC

The majority of HCC scRNA-seq studies fail to provide a detailed characterisation of neutrophils, likely due to their fragile nature and low relative abundance of RNA.[201-204] However a recent scRNA-seq study conducted on 124 patients with primary liver cancers (HCC, ICC and HCC-ICC) undergoing surgical resection has provided the most detailed characterisation to date.[205] This study described 11 neutrophil subtypes that clustered according to the tissue of residence, with 3 being found in blood, 2 in background non-tumour liver and 6 in the tumour (2 exclusive to HCC, 2 exclusive to ICC and 4 found in both). Neutrophil maturity corresponded to tissue of residence with blood subgroups being the most immature, liver subgroups being of intermediate maturity and tumour neutrophils being the most mature. Interestingly there was a range of PDL1 expression, possibility alluding to different degrees of immunosuppressive/ protumour function between the subtypes. Additionally, the authors characterised neutrophils isolated from genetically engineered mouse models of both HCC and ICC, demonstrating a total of 12 mouse neutrophil subtypes, which appeared to be similar to those seen in human disease. This suggests that neutrophil heterogeneity in liver cancer is well conserved between mice and humans validating the use of mouse models as an experimental tool. Despite these exciting insights into neutrophil heterogeneity in HCC this study conducted very limited protein level or functional validation, which is problematic given that RNA abundance does not always correlate to protein expression.[206] Additionally the majority of neutrophils analysed came from the ICC samples. Further studies are needed to identify unique and specific protein markers which define these neutrophil populations as well as explore their functional role in the pathogenesis of HCC.

### 1.4.4. Tumour associated neutrophil recruitment and induction to a pro-tumour phenotype

Neutrophils are produced in vast numbers (over $1x10^{11}$ produced daily),[59] with the majority of the bone marrow dedicated to granulopoiesis in health.[58] An enormous reservoir of mobilisable neutrophils are held in the bone marrow under homeostatic conditions with only 1-2% circulating. The mobilisation of neutrophils from the bone marrow is tightly controlled by G-CSF, CXCR4 and CXCR2 expression as well as CXCL12 expression by the bone marrow stroma.[207,208] The recruitment of neutrophils

into tissues, tumours and sites of inflammation is controlled by the action of chemokines. The main chemokine receptors expressed by neutrophils are CXCR1 and CXCR2,[208] although other chemokine receptors such as CXCR4, CXCR6, C-C chemokine receptor (CCR) 5 and CX3C chemokine receptor 1 (CX3CR1) have been found to influence neutrophil recruitment.[28,209-213]

CXCL1, CXCL2, CXCL3, CXCL5, CXCL8, CXCL12, CXCL16 and chemokine (C-C motif) ligand 5 (CCL5) have been reported as being upregulated in HCC and to facilitate neutrophil recruitment into the tumour.[115,182,190,209,211-218] Tumour stromal cells may also induce neutrophil recruitment. CXCL2 and CXCL8 are secreted by tumour associated monocytes and have the effect of prolonging neutrophil survival, allowing intratumoural neutrophils to accumulate.[213] Similarly cancer associated fibroblasts (CAFs), hepatic stellate cells (HSCs) and tumour activated stromal cells secrete CXCL12.[209,212,213] Neutrophils have been noted to accumulate in the hypoxic regions of human HCCs.[210] This is mediated via hypoxia inducible factor (HIF) induced CCL26 expression from hypoxic HCC cells and subsequent neutrophil chemotaxis through CX3CR1.[210]

Non-chemokine neutrophil attractants also play a key role in neutrophil recruitment. S100A8 and S100A9 are calcium binding proteins expressed by myeloid cells and HCCs that are thought to promote neutrophil recruitment and disease progression.[23,219-221] S100A9 knockout mice display reduced neutrophil recruitment and protection from diethylnitrosamine (DEN) carcinogen induced HCC.[23] S100A8 and S100A9 recruit neutrophils via induction of hepatocyte CXCL1 and CXCL2 expression,[23,220] and also exert effects on neutrophil adhesion and receptor for advanced glycan end-products (RAGE) signalling[222,223]. S100A9 may preferentially recruit pro-tumour neutrophils.[224] Other factors that are raised in HCC and known to recruit neutrophils are TNF-α,[225,226] and VEGF.[227,228] The main mechanisms of tumour associated neutrophil recruitment have been summarised in figure 1.9.

Granulocyte-macrophage colony stimulating factor (GM-CSF), IL-6, TGF-β, prostaglandin E2 (PGE-2), hyaluronan fragments and hypoxia have all been found to drive the polarisation and accumulation of pro-tumour neutrophils in

HCC.[198,199,209,213,229-233] This is summarised in figure 1.9. GM-CSF stimulates neutrophils through PI3K/AKT MAPK JNK/ErK/p38 NF-kB signalling.[198] It also stimulates hepatocyte growth factor (HGF) release from neutrophils, which in itself has pro-metastatic actions.[121,198] HCC cells, CAFs and HSCs secrete IL-6 leading to pro-tumour polarisation, induction of PDL1 expression, enhanced neutrophil survival and accumulation both in the tumour and systemically.[209,230,231,233] Raised levels of GM-CSF and IL-6 are found in the serum of HCC patients and may drive pro-tumour polarisation systemically either in the bone marrow or blood.[198] HSCs further polarise pro-tumour neutrophils through PGE-2 expression and tumour activated stromal cells secrete TGF-β, a known inducer of the pro-tumour phenotype.[108,213,232] Within the TME, hyaluronan fragments and hypoxia may also induce pro-tumour neutrophils.[199,229] Hyaluronan fragments are produced by tumour cells and can activate pro-tumour neutrophils, prolonging their survival through interaction with toll-like receptor 4 (TLR4) and subsequent PI3K/AkT signalling.[199] Hypoxia induces the overexpression of ectonucleotide triphosphate diphosphohydrolase 2 (ENTPD2) and production of 5'-AMP by tumour cells which has the effect of promoting pro-tumour neutrophil accumulation within the TME.[229] S100A9 has also been shown to promote pro-tumour neutrophil polarisation and activation via TLR4 sigannling.[222]

Neutrophil recruitment into the tumour and polarisation to a pro-tumour phenotype are key steps that allow neutrophils to drive tumour progression. It is unclear whether neutrophils first undergo polarisation to a pro-tumour phenotype systemically followed by recruitment to the tumour or vice versa. An accumulation of circulating neutrophils with a pro-tumour phenotype is observed both in patients with cancer and in cancer models.[118,234,235] However, where these neutrophils undergo polarisation is unknown and may not be in the circulation as there is evidence that neutrophils can undergo reverse migration out of sites of inflammation and back into the systemic circulation.[236] Hence, pro-tumour neutrophils observed in the circulation may have been polarised within the TME where they have subsequently undergone reverse migration. Further detailed studies comparing the phenotypic and functional characteristics of tumour and systemic neutrophils as well as in vivo imaging studies are needed to investigate this important question.

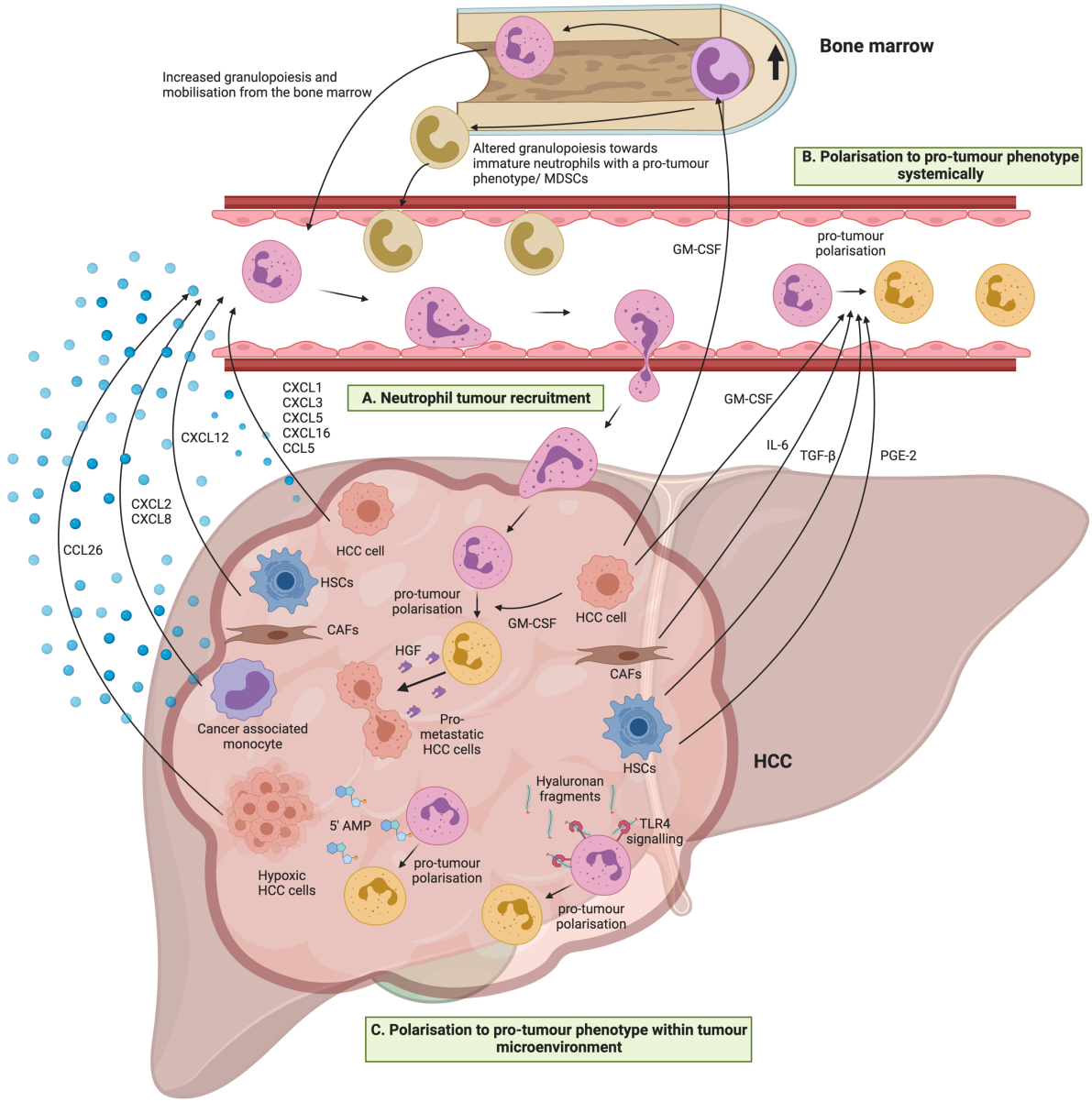



**Figure 1.9 – Neutrophil tumour recruitment and polarisation to a pro-tumour phenotype. A.** Neutrophil tumour recruitment. HCC tumour and stromal cells produce a number of neutrophil chemokines leading to neutrophil tumour recruitment. HCC cells produce; CXCL1, CXCL3, CXCL5, CXCL16 and CCL5.[115,182,190,211,214,215,218] HSCs and CAFs produce CXCL12.[209,212,213] Cancer associated monocytes produce CXCL2 and CXCL8.[213] Hypoxic tumour cells produce CCL26.[210] **B**. Systemic polarisation of neutrophils to a pro-tumour phenotype. This may occur in the bone marrow and/ or blood. In patients with HCC systemic levels of GM-CSF, IL-6, TGF-β and PGE-2 are elevated and known to polarise neutrophils to a pro-tumour phenotype.[108,198,209,213,230-233] GM-CSF is produced by HCC tumour cells and also increases granulopoiesis and mobilisation of neutrophils from the bone marrow. GM-CSF induces neutrophils to express HGF, which promotes metastasis.[198] Tumour activated stromal cells such as CAFs and HSCs produce IL-6, TGF-β and PGE-2.[209,213,230-233] **C.** Factors within the HCC tumour microenvironment also promote the polarisation of neutrophils to a pro-tumour phenotype. Tumour

hypoxia promotes polarisation of neutrophils to a pro-tumour phenotype through the overexpression of ENTPD2 and production of 5'-AMP.[229] Hyaluronan fragments within the tumour polarise neutrophils to a pro-tumour phenotype via TLR signalling.[199]. Created with https://BioRender.com. Figure also for publication.[152]

### 1.4.5. Role of neutrophils in tumour development

Preclinical studies demonstrate that both neutrophils and inflammation play an important role in early HCC tumorigenesis. Neutrophils are required for tumour development in the DEN carcinogen induced model of HCC, with selective neutrophil depletion ameliorating HCC development.[23] In this model neutrophils accumulate in the liver and promote tumorigenesis through ROS mediated telomere DNA damage.[23] Similarly neutrophils appear crucial for HCC development in the streptozotocin and high-fat diet treated mouse (STAM) model of MASH.[237] In this model neutrophil NET production appears to be key for pathogenesis as shown by the fact that NET inhibition by DNase treatment significantly reduces inflammation and subsequent tumour development.[237] Further investigation has demonstrated that NETs are capable of inducing the expansion of regulatory T cells (Tregs) via TLR4 signalling, hence further precipitating an immunosuppressive microenvironment in which HCC can arise.[238] In an inducible $kras^{v12}$ zebrafish model of HCC, rapid infiltration of neutrophils into the liver is observed upon $kras^{v12}$ induction creating an inflammatory environment.[239] Similar to other models of HCC, neutrophil depletion in this model ameliorates tumourgenesis.[239] Although these studies rely on preclinical models their findings are likely relevant to human HCC of which the majority develop on the background of chronic liver inflammation of which neutrophils make up a significant proportion of the inflammatory infiltrate.[240] The role of neutrophils in HCC development is summarised in figure 1.10.

### 1.4.6. Role of neutrophils in local tumour progression

Neutrophils promote HCC progression through a number of different mechanisms that include; immunosuppression of anti-tumour responses, direct enhancement of tumour cell growth and invasiveness and promotion of extracellular matrix remodelling and angiogenesis.[114,115,122,163,209,218,241-247] These are summarised in figure 1.10.

Neutrophils promote immunosuppression of anti-tumour responses mainly via their inhibitory action on T cells.[114,122,209,241,247] TANs in HCC express PDL1, the ligand for the T cell checkpoint receptor PD1, and can suppress both CD4 and CD8 T cell functions through the PDL1-PD1 interaction.[114,209] Engagement of PD1 on T cells is well known to directly inhibit T cell proliferation, cytokine production, cytotoxic activity as well indirectly inhibiting T cell function through promotion of Treg expansion.[248] Neutrophils also suppress CD4 and CD8 T cells via ARG1, iNOS and ROS activity.[144] ARG1 causes T cell suppression by depleting L-arginine, a crucial metabolite needed for T cell proliferation.[249] iNOS activity leads to the production of NO, which suppresses T cell proliferation and induces T cell apoptosis and ROS production by neutrophils is known to inhibit T cell activation.[250,251] In addition TANs induce CD4 T cells to express pro-tumour IL-10 and TGF-β whilst suppressing cytotoxic CD8 T cells.[241] IL-10 has the effect of suppressing CD4 T cell function indirectly through the inhibition of antigen presentation and inflammatory cytokine production as well as having a direct effect of inhibiting CD4 T cell proliferation.[252] TGF-β also promotes Treg differentiation and T cell exhaustion.[253] TANs additionally can recruit immunosuppressive macrophages and Tregs via CCL2 and CCL17 secretion, this being associated with resistance to sorafenib.[122] Of note. neutrophil depletion can improve response to sorafenib in pre-clinical models.[122,241] HCC associated neutrophils also inhibit NK cell function via ARG1, iNOS and ROS activity as well as NKp30 receptor engagement and membrane bound TGF-β1.[242,245,247] Neutrophils can inhibit the antigen presenting functions of Kupffer cells by reducing expression of CD86 and major histocompatibility complex class II (MHCII) and by increasing CD274 expression on Kupffer cells.[244]

Neutrophils may influence early tumour progression by promoting a stem cell like phenotype in HCC cells.[218] Stem cell like cancer cells are a key driver of disease progression and treatment resistance in HCC.[254] TANs induce HCC stem cell characteristics through release of bone morphogenetic protein 2 and TGF-β. Once stem cell like cancer cells develop, a positive feedback loop is established whereby further neutrophils are recruited via CXCL5.[218] Similarly neutrophils produce IL-6 and HGF which promote stem cell like features and proliferation.[119,198,243,255] Neutrophils further promote HCC progression through release of MMP9 a known promoter of

extracellular matrix remodelling, angiogenesis and TGF-β activation.[115,256] Studies on HCC resection tissue show that peritumoral neutrophils are a major source of MMP9 and that peritumoral neutrophil count corresponds with VEGF expression and vessel density at the tumour edge.[115] This suggests neutrophils stimulate angiogenesis to promote HCC growth at the tumour margin. Further work has shown that increased autophagy of TANs enhances their survival in the tumour microenvironment and is associated with MMP9 production.[246]

### 1.4.7. Role of neutrophils in tumour metastasis

TANs additionally play a role in promoting tumour metastasis (figure 1.10). In implantation models of HCC, injection of neutrophils increases metastasis whereas neutrophil depletion reduces metastasis.[198,218] In HCC patients the number of peritumoural neutrophils correlates to the presence of metastases and circulating neutrophils can increase the migration and invasive capacity of HCC cells in vitro.[163,199] Neutrophils may directly enhance the metastatic phenotype of HCC through NETs and by secretion of HGF, ROS, oncostatin M (OSM) and MMP9.[115,198,217,243,246,257,258] Neutrophils from HCC patients display enhanced NET formation compared to patients without HCC and a greater number of NETs are found in HCCs which have metastasised compared to those which have not.[258] Direct evidence for NETs in HCC metastasis was shown in a metastatic model of HCC in which Hepa1-6 cells were injected into the tail vein or spleen of immunocompetent mice. Here inhibition of NETs using DNase reduced the burden of both liver and lung metastasis.[258] HCC cells can internalise NET material activating TLR signalling and induce increased cell survival and a more invasive phenotype.[258] TANs are a source of HGF which can enhance the metastatic ability of HCC cells through c-Met activation.[198,243] Neutrophil ROS may also enhance the metastatic ability of HCC.[257] ROS in the presence of TGF-β1 induces HCC β3 integrin expression via p38 MAPK activation.[257] These induced cells have greater invasive capacity and display enhanced metastasis when injected into immunodeficient mice.[257] Neutrophil MMP9 and OSM promote both local disease progression and metastasis through angiogenesis, promotion of tumour cell mobility and TGF-β activation.[115,217,246,256,259]

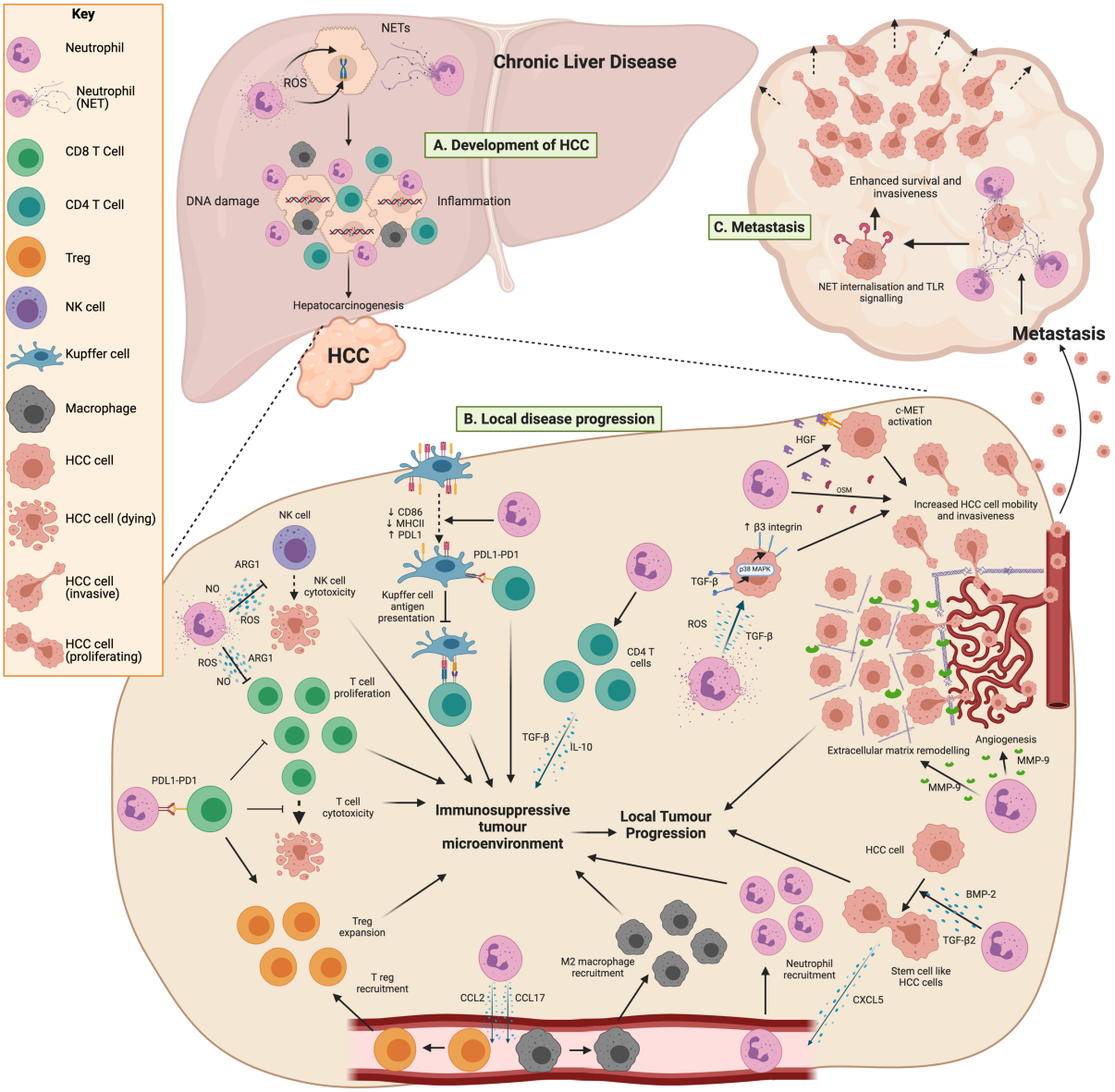



**Figure 1.10 – Neutrophil tumour promoting mechanisms in HCC**. **A.** Role of neutrophils in the development of HCC. Neutrophils drive hepatocarcinogenesis via ROS mediated DNA damage and through NET induced inflammation[23,237,239]. **B.** Role of neutrophils in local tumour progression. Neutrophils create an immunosuppressive tumour microenvironment through a number of mechanisms. Neutrophil PDL1 expression inhibits T cell proliferation and cytotoxicity as well as promoting the expansion of T regs.[114,209] Neutrophils can inhibit NK cell cytotoxicity and T cell proliferation through NO, ARG1 and ROS activity.[144,245,247] Neutrophils inhibit the antigen presenting abilities of Kupffer cells by inducing downregulation of CD86 and MHCII.[244] Neutrophils induce CD4 T cells to express immunosuppressive IL-10 and TGF-β.[241] Neutrophils promote tumour recruitment of pro-tumour Tregs and M2 macrophages via the expression of CCL2 and CCL17.[122] Neutrophils also induce cancer like stem cells which have greater proliferation and survival and recruit further tumour neutrophils via CXCL5.[218] **C**. Role of neutrophils in metastasis. Neutrophils produce VEGF to stimulate angiogenesis and produce MMP9 for extracellular remodelling which enables tumour invasion and mobilisation to the vasculature.[115,246] MMP9 can also release latent TGF-β.[256] Neutrophil ROS in the presence of TGF-β

causes upregulation of β3 integrin via p38 MAPK activation, which increases the metastatic potential of HCC cells.[257] Neutrophil HGF and OSM also increase the metastatic potential of HCC cells via c-MET activation.[198,217,243] At sites of HCC metastasis neutrophil NET production promotes metastatic development due to HCC cell internalisation of NETs and subsequent TLR signalling resulting in enhanced survival and invasiveness.[258] Created with https://BioRender.com. Figure used for publication.[152]

### 1.4.8. Potential anti-tumour functions of neutrophils

Although the vast majority of studies point to a pro-tumour role in HCC, neutrophils also have anti-tumour potential. For example neutrophil ROS such as hydrogen peroxide and NO have been shown to be cytotoxic towards cancer cells,[123,260,261] and neutrophils in early stage lung cancer have been shown to acquire an antigen presenting cell features with the capability of stimulating T cell responses.[111,262] Furthermore neutrophils express Fc receptors meaning antibody dependent cell mediated cytotoxicity (ADCC) can be elicited via trogoptosis.[263,264] Although current terminology implies a fixed dichotomy of neutrophil phenotypes in cancer, the application of single cell technologies in this field is likely to reveal a spectrum of both pro-tumour and anti-tumour phenotypes varying according to the tissue of residence, type of tumour microenvironment and disease stage. It is hoped that once we have a better understanding of this plasticity and range of functions in cancer that strategies to target and manipulate neutrophils from a pro-tumour to anti-tumour phenotype can be fully exploited.

## 1.5. Neutrophils as therapeutic targets in HCC

Pre-clinical work using mouse models of HCC has highlighted the potential therapeutic benefits of neutrophil targeted treatments in HCC, demonstrating that neutrophil depletion can reduce tumour burden and improve treatment response to other systemic therapies.[23,122,231,241] Although neutrophil depletion is effective in pre-clinical models, this approach is more challenging in patients due to the risk of severe infection associated with neutropenia. Traditional cytotoxic chemotherapy agents, which also commonly cause neutropenia, tend to be less well tolerated in patients with HCC, who often have cirrhosis with portal hypertension. With this in mind, most neutrophil therapies in development target specific neutrophil functions, such as tumour recruitment or manipulation of neutrophil phenotype from a pro-tumour to an anti-

tumour phenotype. The mechanisms of actions of neutrophil targeted therapies being developed in HCC are summarised in figure 1.11. Clinical trials investigating the use of neutrophil targeted therapies in HCC and other cancers are listed in table 1.2 and table 1.3 respectively.

### 1.5.1. Effect of conventional HCC therapies on neutrophils

The tyrosine kinase inhibitor Sorafenib has been the mainstay systemic treatment for advanced HCC for the last decade,[28] and is thought to work mainly through the inhibition of VEGF and subsequently tumour angiogenesis.[36] Studies suggest that patients receiving sorafenib prior to curative liver resection have a greater number of TANs compared to those not, with high numbers of TANs being associated with a worse prognosis.[122] One explanation for this is the development of tumour hypoxia following angiogenesis inhibition, driving further neutrophil recruitment and pro-tumour polarisation.[122,210,229] Combining sorafenib with neutrophil depletion has an additive effect in pre-clinical models.[122] Therefore combining tyrosine kinase inhibition with neutrophil targeted therapy is a treatment in which further research is warranted.

Radiotherapy in the form of SIRT and SABR can be used to treat locally advanced HCC.[28,265] Radiotherapy stimulates sterile inflammation and neutrophil ROS mediated tumour killing,[123] as well as having other effects on neutrophil dynamics and functions.[266] For example in a heterotopic model of HCC with multiple tumour sites, irradiation of one tumour site exerted anti-tumour effects on non-irradiated tumour sites, possibly being mediated by reductions in pro-tumour neutrophil polarisation through IL-6 and G-CSF.[266] The role of neutrophils in radiotherapy of human HCC is yet to be explored.

### 1.5.2. Chemokine inhibitors

One of the most promising targets for neutrophil based therapy is CXCR2. CXCR2 is the main neutrophil chemokine receptor and its ligands CXCL1, CXCL2, CXCL3, CXCL5, and CXCL8 have all been shown to influence neutrophil recruitment in HCC.[115,190,214-216,267] Because of the immunosuppressive actions of TANs on tumour infiltrating lymphocytes CXCR2 inhibition has been investigated in combination with T cell immune checkpoint inhibitors.[56] In pre-clinical models of MASLD associated HCC,

CXCR2 inhibition with the small molecule AZD5069 sensitised tumours to anti-PD1 therapy. The mechanism underlying this sensitisation is intriguing as contrary to reducing the frequency of TANs it increased their frequency. Further investigation demonstrated that CXCR2 inhibition resulted in a reprogramming of TAN phenotype from a mature pro-tumour phenotype to an immature, proliferative and anti-tumour phenotype.[56] These reprogrammed neutrophils partly mediated their anti-tumour functions through activation of both dendric cells and cytotoxic T cells.[56] A phase I/II clinical trial of AZD5069 in combination with anti-PDL1 is ongoing.[268] AZD5069 in combination with Durvalumab has already been trialled in metastatic pancreatic ductal adenocarcinoma (PDAC) with some indications of efficacy.[269]

CXCR4, CCR5 and CXCR6 are other chemokine receptors which have been shown to play a role in neutrophil recruitment in HCC.[182,209,211-213,270,271] Preclinical studies of CXCR6 and CCR5 inhibition have demonstrated anti-tumour efficacy, however are yet to reach clinical trials.[109,211,271,272] Preclinical studies show efficacy of CXCR4 inhibition in combination with anti-PD1 therapy,[273,274] with this combination showing early signs of efficacy in a phase I clinical trial of pancreatic and colorectal cancer.[275]

### 1.5.3. Cytokine Inhibitors

Tumour cytokines play a myriad of functions and are an important factor in the polarisation of pro-tumour neutrophils.[108,209,230,231,276] Directly inhibiting these cytokine pathways with the goal of manipulating neutrophils from a pro-tumour to an anti-tumour phenotype is a further therapeutic strategy.

IL-6 is a major cytokine that acts through STAT3 signalling to recruit and polarise neutrophils.[209,230,231,233] IL-6 blockade has a synergistic effect when used with anti-PDL1 therapy in pre-clinical models of HCC.[277] Icartin is a drug derived from a herbal Chinese remedy and has been shown to have neutrophil modulating effects via its actions on the IL-6/Janus kinase 2 (JAK2)/STAT3 pathway.[278-280] Early clinical trials in HCC have shown that it is safe and well tolerated with some signs of efficacy.[278]

TGF-$\beta$ is another important cytokine that induces neutrophils with a pro-tumour phenotype.[108] The TGF-$\beta$1 receptor type 1 inhibitor galunisertib has been tested in

combination with sorafenib in a few early clinical trials in HCC,[281,282] demonstrating a reasonable safety profile and improved median time to tumour progression compared to sorafenib alone.[282] An ongoing clinical trial is also evaluating its use with its use in combination with nivolumab.[283]

### 1.5.4. Oligonucleotide based therapies

CCAAT/enhancer binding protein alpha (C/EBP-α) is a key transcription factor regulating myeloid cell differentiation,[284,285] which is downregulated in pro-tumour neutrophils and has been linked to arrested maturation and various pro-tumour functions.[286] In pre-clinical studies upregulation of C/EBP-α suppresses HCC tumour progression.[287] MTL-CEBPA is a small activating RNA that upregulates C/EBP-α. In an initial clinical trial involving patients with advanced HCC, MTL-CEBPA was found to be safe and well tolerated.[288] Although the efficacy of MTL-CEBPA therapy alone was disappointing, three patients whom subsequently went on to receive sorafenib experienced a complete response, suggesting MTL-CEBPA therapy may sensitise to tyrosine kinase therapy, perhaps via its actions on pro-tumour neutrophils.[288]

### 1.5.5. Phosphodiesterase type 5 inhibition

Adoptive cell therapies are a promising class of immunotherapies now being used in the treatment of multiple cancers.[289] Cytokine induced killer cells (CIKs) are a type of adoptive cell therapy in development for the treatment of HCC,[290,291] however its effectiveness appears to be limited by immunosuppressive TANs with both in vitro and in vivo studies supporting this.[247] Tadalafil is a phosphodiesterase type 5 (PDE5) inhibitor that can inhibit pro-tumour neutrophil immunosuppressive through its negative activity on ARG1 and iNOS.[247] In a pre-clinical study tadalafil enabled the therapeutic effect of CIKs via its actions on immunosuppressive TANs.[247] A clinical trial is currently investigating the effects of tadalafil in combination with nivolumab and vancomycin.[292]

### 1.5.6. Histone deacetylase inhibitors

Histone deacetylase (HDAC) inhibitors non-specifically target pro-tumour neutrophils by inhibition of ARG1 and iNOS, as demonstrated by pre-clinical studies.[293,294] Belinostat and resminostat are the HDACs that have reached clinical trials in HCC,

showing good safety and some signs of efficacy.[295,296] Further research is needed to investigate the effects of HDACs on neutrophils in human HCC.

### 1.5.7. STAT3 inhibitors

The IL-6/STAT3 pathway is thought to be key in the pro-tumour polarisation and pro-tumour functions of neutrophils, making it an attractive therapeutic target.[163,194,209,297,298] To date one clinical trial of a STAT3 inhibitor (AZD9150) has been conducted in HCC, demonstrating a good safety profile with one patient achieving a partial response.[299] Clinical trials in HCC investigating other STAT3 inhibitors (TTI-101 and BBI608) either as monotherapy or in combination with sorafenib are ongoing.[300,301]

### 1.5.8. CD47-SIRPα checkpoint inhibitors

Engagement of CD47 with signal-regulatory protein alpha (SIRP-α) inhibits myeloid cell phagocytosis and ADCC forming a key myeloid immune checkpoint.[302] HCCs and other cancers upregulate CD47 in order to exploit this immune checkpoint.[264,302,303] Therapies disrupting the CD47-SIRP-α pathway are being explored in clinical trials in other cancers.[304] In HCC pre-clinical studies suggest a synergistic effect of CD47 blockade when used with other therapies such as sorafenib.[303,305,306] Clinical trials in HCC are awaited.

### 1.5.9. TRAIL receptor 2 agonists

TNF-related apoptosis inducing ligand receptor 2 (TRAIL-R2) agonists have been shown to selectively initiate apoptosis of pro-tumour neutrophils.[307-310] An early clinical trial investigating the use of the TRAIL-R2 antibody DS-8273a in patients with a variety of advanced cancers, including HCC, showed a selective depletion of low-density neutrophils with preservation of high-density neutrophils and other myeloid populations. This depletion in low density neutrophils was associated with better progression free surivial.[308] In a phase II clinical trial in HCC the TRAIL-R2 monoclonal antibody tigatuzumab in combination with sorafenib failed to achieve its primary endpoint, despite demonstrating a favourable safety profile.[311] TRAIL-R2 agonist in combination with immune checkpoint blockade offer an alternative and are being trialled in other cancers (Table 1.3).

### 1.5.10. S100A9 inhibition

S100A9 (also known as MRP14) is a calcium binding protein of the S100 family (which also includes S100A8 or MRP8) of alarmins. Alarmins are multifunctional endogenous molecules released in response to cell damage and infection to elicit immune cell recruitment and inflammation.[312] S100A9 has been shown to be a key mediator of neutrophil recruitment, activation and polarisation.[23,219,220,313-315] In the DEN HCC model, genetic knockout of S100A9 results in reduced liver neutrophil recruitment and reduced tumour burden.[23] S100A9 can be pharmacological manipulated with quinoline-3-carboxamides which target the interaction of S100A9 with its receptors TLR4 and RAGE.[316] The quinoline-3-carboxamide tasquinimod has demonstrated good anti-tumour efficacy in pre-clinical models of other cancers.[317-319] The effects of pharmacologically targeting S100A9 in HCC have yet to be tested. Interestingly in pre-clinical studies paquinimod, another quinoline-3-carboxamide, shows antifibrotic and immunomodulating activity in the context inflammatory chronic liver disease.[320]

### 1.5.11. Other novel therapeutic approaches

An approach which has demonstrated potential in pre-clinical studies of other cancers is activating neutrophils through a combination of TNF, CD40 agonism and a tumour binding antibody.[321] Mechanistically this combination was found to improve the mobilisation and infiltration of neutrophils into the tumours as well as enhance the tumour killing ability of neutrophils through complement C5a and leukotriene $B_4$ activity which stimulated ROS production in neutrophils via xanthine oxidase. Additionally this approach also activated dendritic cell populations and stimulated anti-tumour T cell activation.

Despite being highly effective in haematological malignancies, adoptive cell therapies such as chimeric antigen receptor (CAR) T cell therapy, have yet to be successfully used for the treatment of solid tumours.[322,323] A trial investigating the use of glypican-3 targeted CAR T cell therapy is currently ongoing in HCC.[324] One reason CAR T cell therapy has been unsuccessful in solid tumours is due to the limited ability of CAR T cells to infiltrate solid tumours due to the presence of extracellular matrix and tumour stroma.[325] An exciting alternative is the development of adoptive neutrophil therapies such as CAR neutrophils.[326,327] CAR neutrophils have been successfully generated

from human pluripotent stem cells and have shown anti-tumour efficacy in a humanised mouse model of glioblastoma.[326,327] The concept of CAR neutrophils is promising as neutrophils are better equipped to penetrate collagenous stroma due to their expression of metalloproteinases and their toxicity profile may be better than that of CAR T cells due to their short lifespan. In a pre-clinical model of MASH-HCC adoptive transfer of immature bone marrow neutrophils from LPS treated mice was able to sensitise tumour bearing mice to anti PD1 therapy, mechanistically inducing a similar effect to CXCR2 inhibition.[56] Together these studies have shown that neutrophils can be engineered and used as an adoptive therapy in HCC.

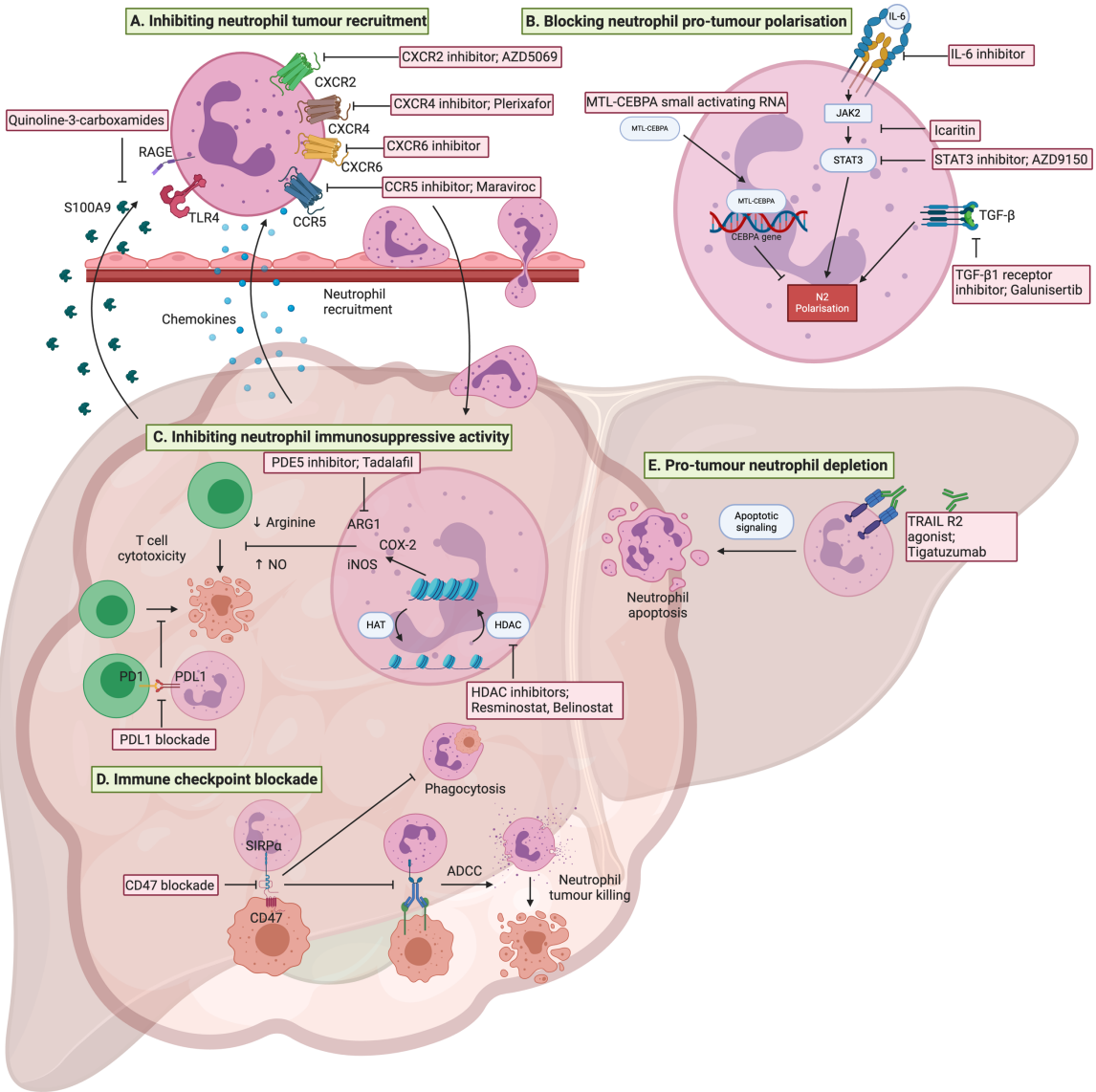



**Figure 1.11 – Neutrophil therapeutic targets in HCC**. **A.** Neutrophil recruitment to HCC. Recruitment of neutrophils into the tumour can be inhibited through blockade of a number of chemokine receptors.

The CXCR2 inhibitor AZD5069 is being trialled in HCC and other cancers.[328] The CCR5 inhibitor Maraviroc is being trialled in colorectal cancer and has shown therapeutic potential in pre-clinical models of HCC.[211,272] CXCR6 inhibitors have yet to enter clinical trials but pre-clinical data in HCC are promising.[271] S100A9 inhibitors such as quinoline-3-carboxamides, modulate the interaction between S100A9 and its receptors TLR4 and RAGE and have been shown to reduce tumour neutrophil recruitment in pre-clinical studies.[23,317-319] **B.** Pro-tumour neutrophil polarisation. Therapeutic targeting of IL-6/JAK2/STAT3 pathway, TGF-β signalling and the MTL-CEBPA transcription factor results in inhibition of neutrophil pro-tumour polarisation. The IL-6/JAK2/STAT3 pathway has a number of therapeutic targets. IL-6 inhibition has been shown to improve response to PDL1 blockade in pre-clinical HCC studies but has yet to be tested in clinical trials.[277] Icaritin has multiple effects on the IL-6/JAK2/STAT3 pathway with clinical trials so far demonstrating a good safety profile with signs of efficacy and modulating effects on pro-tumour neutrophils.[278-280] STAT3 inhibitors have been tested both as monotherapy and in combination with sorafenib in early clinical trials with results so far demonstrating a reasonable safety profile.[299] The TGF-β1 receptor inhibitor galunisertib has been tested in a variety of combinational therapies for HCC showing a good safety profile.[281,282] MTL-CEBPA is a small activating RNA which interferes with the pro-tumour functions of neutrophils. An initial clinical trial has suggested it sensitizes HCCs to subsequent treatment with tyrosine kinase inhibition.[288] **C.** Inhibition of neutrophil pro-tumour functions. Neutrophils inhibit T cell and NK cell cytotoxicity through ARG1 and iNOS activity.[144,245,247] This can be inhibited through the use of inhibitors such as tadalafil or HDAC inhibitors such as belinostat and resminostat.[247,294-296] Early clinical trials investigating these agents are ongoing. **D.** Immune checkpoint blockade. Neutrophils express a number of immune checkpoints. In HCC neutrophils have increased expression of PDL1 resulting in T cell inhibition. PDL1 inhibition in combination with VEGF inhibition is the first line systemic treatment of HCC, however the effect of PDL1 inhibition on neutrophils is yet to be explored. PDL1 inhibition is also being trialled in combination with CXCR2 blockade for the treatment of HCC.[268] HCC tumour cells expression high levels of CD47 which inhibits neutrophil tumour cell cytotoxicity (phagocytosis and ADCC) via its interaction with SIRPα.[302,303] Therapies targeting the CD47- SIRP-α immune checkpoint offer therapeutic potential in HCC and are in early clinical trials for the treatment of other cancers.[305,306] **E.** Pro-tumour neutrophil depletion. TRAIL R2 agonists have been shown to selectively deplete pro-tumour neutrophils by induction of apoptosis signalling, without depletion of other neutrophil and myeloid populations.[307-309] TRAIL R2 agonists are currently in early clinical trials for the treatment of HCC.[311] Created with https://BioRender.com. Figure used for publication.[152]

| Target | Drug Name | Trial Identifier | Phase | Combinations | Ref |
|---|---|---|---|---|---|
| **CXCR2** | AZD5069 | ISRCTN12669009 | I/II | Combination with Durvalumab | 268 |
| **TGF-β1 receptor** | Galunisertib | NCT02240433 | Ib | Combination with Sorafenib | 281 |
| | Galunisertib | NCT01246986 | II | Alone and in combination with sorafenib or Ramucirumab | 282 |
| | Galunisertib | NCT02423343 | Ib/II | Combination with Nivolumab | 329 |
| **STAT3** | TTI-10 | NCT03195699 | I | Monotherapy | 301 |
| | AZD9150 | NCT01839604 | I | Monotherapy | 299 |
| | BBI608 | NCT02279719 | I/II | Combination with Sorafenib | 300 |
| **C/EBPα** | MTL-CEBPA small activating RNA | NCT02716012 | I | Monotherapy | 288 |
| **IL-6/JAK2/STAT3** | Icaritin | NCT02496949 | I | Monotherapy | 278 |
| | | NCT01972672 | II | Monotherapy | 330 |
| | | NCT03236636 | III | Monotherapy | 331 |
| | | NCT03236649 | III | Monotherapy | 332 |
| **PDE5** | Tadalafil | NCT03785210 | II | In combination with Nivolumab and oral Vancomycin | 292 |
| **TRAIL-R2** | Tigatuzumab | NCT01033240 | II | Combination with Sorafenib | 311 |
| **HDAC** | Resminostat | NCT00943449 | II | Combination with Sorafenib | 295 |
| | Belinostat | NCT00321594 | I/II | Monotherapy | 296 |

**Table 1.2 – Neutrophil therapies for HCC in clinical trials.** Table used for publication.[152]

| Target | Drug Name | Trial Identifier | Cancer | Phase | Monotherapy or combination | Ref |
|---|---|---|---|---|---|---|
| **CXCR2** | AZD5069 | NCT02583477 | Pancreatic | Ib/II | Combination with Durvalumab | [269] |
| | AZD5069 | NCT03177187 | Prostate | I | Combination with Enzalutamide | [333] |
| | AZD5069 | NCT02499328 | Head and neck | Ib/II | Combination with Durvalumab | [334] |
| | SX-682 | NCT04477343 | Pancreatic | I | Combination with Nivolumab | [335] |
| | SX-682 | NCT04245397 | MDS | I | Monotherapy | [336] |
| | Reparixin | NCT02370238 and NCT02001974 | Breast | II | Combination with Paclitaxel | [337,338] |
| **CCR5** | Maraviroc | NCT03274804 | Colorectal | I | Combination with Pembrolizumab | [339] |
| | Maraviroc | NCT01736813 | Colorectal | I | Monotherapy | [340] |
| **TGF-β1 receptor** | Galunisertib | NCT02423343 | Solid tumours and NSCLC | Ib/II | Combination with Nivolumab | [283] |
| | Galunisertib | NCT02734160 | Pancreatic | Ib | Combination with Durvalumab | [341] |
| | Galunisertib | NCT01682187 | Malignant glioma | I | Alone or in combination with Lomustine | [342] |
| | Galunisertib | NCT02452008 | Prostate | II | Combination with Enzalutamide | [343] |
| **PDE5** | Tadalafil | NCT03785210 | Liver dominant colorectal or pancreatic cancer | I | Combination with Nivolumab and oral Vancomycin | [292] |
| | Tadalafil | NCT02544880 | Head and Neck | II | Combination with MUC1 vaccine | [344] |
| | Sildenafil | NCT00752115 | NSCLC | II/III | Combination with carboplatin and paclitaxel | [345] |

| | | | | | | |
|---|---|---|---|---|---|---|
| **CD47-SIRPα inhibition** | Hu5F9-G4 | NCT02953782 | Colorectal | I/II | Combination with Cetuximab | [346] |
| | TTI-621 | NCT02890368 | Solid tumours | I | Alone or in combination with other therapies | [347] |
| | AO-176 | NCT03834948 | Solid tumours | I | Alone or in combination with other therapies | [348] |
| | BI 765063 | NCT03990233 | Solid tumours | I | Alone or in combination with PD1 therapy | [349] |
| **TRAIL-R2** | DS-8273a | NCT02076451 | Solid tumours and Lymphoma | I | Monotherapy | [308] |
| | DS-8273a | NCT02991196 | Colorectal | I | Combination with Nivolumab | [350] |
| | DS-8273a | NCT02983006 | Melanoma | I | Combination with Nivolumab | [351] |
| **S100A9** | Tasquinimod | NCT00560482 | Prostate | II | Monotherapy | [352,353] |

**Table 1.3 – Neutrophil therapies for other cancers in clinical trials.** Table used for publication.[152]

## 1.6. Areas of future development

### 1.6.1. Improving murine and humanised pre-clinical models

Due to the short lifespan of neutrophils the majority of mechanistic studies have heavily relied on mouse models, which in HCC includes genetically engineered, chemotoxic and implantation models.[7,354] The majority of studies have used either the DEN chemotoxic or orthotopic/heterotopic implantation models. The DEN model is well established but has the disadvantage of there being a lengthy time to tumour development with variability depending on strain and sex of mice used.[354] Furthermore the mutational landscape of DEN tumours poorly represents that of human HCC.[355] Implantation models are rapid to establish and interrogate making them ideal for therapeutic testing, but they are limited in their recapitulation of underlying liver disease, or the chronicity with which tumours develop in situ.[354] Heterotopic models,

in which cell lines are often injected subcutaneously, fail to mimic the HCC tumour microenvironment, while the orthotopic models, which inject cell lines into a typically healthy liver, require imaging or surgical expertise.[354] Also, unless syngeneic cells are used, immunocompromised mice are needed to prevent immune rejection, thereby failing to model the full immune microenvironment.[354] Humanized models allow the implantation of human HCCs in mice with a human immune system allowing for a better approximation of the HCC immune landscape. The main drawbacks of humanized models are that human fetal or cord blood is required to reconstitute the immune system and these models do not currently support a fully functioning immune system.[356,357] For example many models do not support normal myeloid lineage development and do not develop proper humoral immune responses due to the lack of various stimulatory factors and the lack of normal lymphoid tissue development.[357] In addition the rest of the animal is not humanized meaning the background liver and other organs are still of mouse origin.

To study in vivo effects of neutrophils in HCC most studies have used neutrophil depletion models with the most common methods using anti-Gr-1 or anti-Ly6G antibodies.[358] Anti-Gr-1 is highly effective, however because it targets both Ly6G and Ly6C it also has the effect of depleting monocytes and macrophages.[358] Anti-Ly6G antibodies are highly specific to neutrophils but can cause incomplete neutrophil depletion, especially in the liver and in aged mice.[358-360] Anti-Ly6G antibody depletion alone is not fully effective because of the presence of newly circulating neutrophils from the bone marrow, which have lower surface membrane Ly6G expression.[360] This can be somewhat overcome by using a double antibody based approach.[360]

To better define the role of neutrophils in HCC, models using immunocompromised mice need to be avoided and the specific limitations of a particular model must be carefully considered when designing experiments. Ideally the results from one model should be validated in an additional model. As humanized models become more refined and capable of sustaining a more complete immune system, use of these models should be utilized given that they have the capacity to most closely resemble human HCC.

### 1.6.2. Understanding the role of neutrophils in chronic liver disease

As HCC develops on the background of chronic liver disease of varying aetiologies there are multiple disease processes involved other than that of HCC. For example, a diabetic patient with MASLD who develops HCC has at least 3 disease processes all of which maybe influencing neutrophil phenotype and function. Therefore, some of the changes in neutrophil phenotype and function seen in HCC maybe driven by chronic liver disease rather than HCC. Our understanding of how chronic liver disease and HCC interact to influence neutrophil function is further confounded by the fact that the majority of pre-clinical models of HCC do not replicate the conditions of chronic liver disease. Although the role of neutrophils in chronic liver disease is far from fully characterised, current research suggests that like in HCC they have a range of phenotypes and functions,[361] either driving inflammation and disease progression through MPO, ROS and NET production,[362,363] or contributing to disease resolution though HGF release and collagen degradation.[364,365] This demonstrates the importance of using models which combine HCC and chronic liver disease when doing mechanistic studies and using chronic liver disease as a comparison when studying neutrophils in human HCC.

### 1.6.3. Better characterisation of neutrophil heterogeneity

Despite several scRNA-seq studies demonstrating heterogeneity and plasticity of neutrophils in both health and disease,[64,71,88,97,99,100,205] further investigation is needed to validate this heterogeneity on both a protein and functional level. This will help to infer their relevance in disease. In terms of circulating neutrophil heterogeneity further work is needed to understand the biological relevance of normal- and low-density neutrophils, their dynamics, relationship to tissue neutrophils and function in terms of anti or pro-tumour functions. Outdated and confusing nomenclature such as PMN-MDSC, N1 and N2 should also be revisited and modified to reflect the more complex, heterogeneous and plastic nature neutrophils are now known to have.[100]

## 1.7. Conclusion

Neutrophils exhibit diverse functions and phenotypes in cancer. There is growing evidence that neutrophils are important in the pathogenesis of HCC, playing roles in tumourigenesis, local tumour progression and metastasis. The main mechanisms by

which neutrophils promote HCC is through suppression of anti-cancer immunity, direct enhancement of tumour cell survival, invasiveness and metastatic ability, promotion of extracellular matrix degradation and stimulation of angiogenesis. There are currently multiple neutrophil targeted therapies entering clinical trials for the treatment of HCC and other cancers. However, further work is needed to better define the role of neutrophil phenotypes in HCC and especially for TANs. For this to be achieved we require improved experimental models that more accurately represent the HCC TME along with a better understanding of neutrophil phenotypes in chronic liver disease.

## 2. Aims and Objectives

The focus of my PhD is to investigate how neutrophil heterogeneity, phenotype and function changes in HCC and how this may affect tumour progression. Although there is already a large amount of research about the role neutrophils play in cancer, there are limited data on the role of neutrophils in HCC with most studies being conducted in pre-clinical models. I aim to investigate how neutrophils change in human HCC and compare these changes to those in a pre-clinical model of HCC, with the aim of identifying conserved targets and pathways. I then aim to test the effect of therapeutically manipulating these pathways in a pre-clinical model to develop novel therapeutic strategies for the treatment of HCC. As an additional objective I aim to investigate immune checkpoint inhibitor responses in a pre-clinical model of MASH-HCC.

**Aim 1:** Investigate neutrophil phenotype and heterogeneity in HCC and chronic liver disease. HCC and chronic liver disease patient blood samples and liver/tumour tissue samples will be acquired through the HUNTER study alongside healthy control blood samples. Phenotypic and functional heterogeneity will be investigated by morphology, high dimensional flow cytometry and functional assays.

**Aim 2:** Investigate neutrophil phenotype and heterogeneity in mouse models of chronic liver disease and HCC. Neutrophils across different biological compartments will be phenotyped from control, chronic liver disease and HCC bearing mice using high dimensional flow cytometry, functional assays and cell tracking techniques. Mouse HCC neutrophil phenotypes will be compared to those found in human disease in order to identify common phenotypes and pathways which may represent novel therapeutic targets.

**Aim 3:** Assess the anti-tumour, immunological and systemic effects of targeting the neutrophil pathways identified in aims 1 and 2 using in vitro and in vivo models.

**Aim 4:** Investigate the effectiveness of anti-PDL1/anti-VEGF combination therapy in a mouse model of MASH-HCC and explore the relationship between tumour

location/microenvironment and treatment response. Investigate differential responses to anti-PDL1/anti-VEGF therapy in the hepatic MASLD microenvironment vs the systemic MASLD environment and explore the underlying immunological mechanisms.

# 3. Materials and Methods

## 3.1. Human blood characterisation

### 3.1.1. Human blood sample collection

HCC and CLD patient blood samples were obtained from hepatology outpatient clinics at Newcastle Hospitals NHS Foundation Trust with full ethical approval (HUNTER study, 19/NE/0251) and written informed consent. Healthy control blood samples were collected from volunteers at Newcastle University with full ethical approval and written informed consent. Eight ml of blood was collected into ethylenediaminetetraacetic acid (EDTA) coated vacutainers (BD, 367842). Basic clinical information of HCC and CLD patients was collected as per the HUNTER protocol. All blood samples were processed within 1-2 hours of collection.

### 3.1.2. General immune cell isolation

200-400 µl of whole blood was lysed in 2 ml of lysing buffer (BD Pharm Lyse, 555899) for 5-10 minutes after which osmolarity was restored by adding 1x Dulbecco's phosphate-buffered saline (DPBS-) modified without magnesium and calcium (Sigma-Aldrich, D8537). Samples were then washed twice and plated into a 96 well round bottom plate for staining.

### 3.1.3. Neutrophil isolation

Plasma was removed following slow centrifugated (300 xg for 20 minutes) and snap frozen. Erythrocytes were removed via dextran T500 (Pharmacosmos) sedimentation and the leukocyte rich top layer collected and washed in 1x DPBS-. Leukocytes were then resuspended in 55% Percoll PLUS (cytiva) and carefully layered on top of a double 81%, 70% Percoll PLUS gradient. Samples were then centrifuged at 700g for 20 minutes. This separates the LD neutrophils along with mononuclear cells from ND neutrophils and remaining erythrocytes (figure 3.1). The LD neutrophil/mononuclear layer and ND neutrophil layers were then collected into separate tubes and washed in 1x DPBS- before being plated into a 96 well round bottom plate for staining.

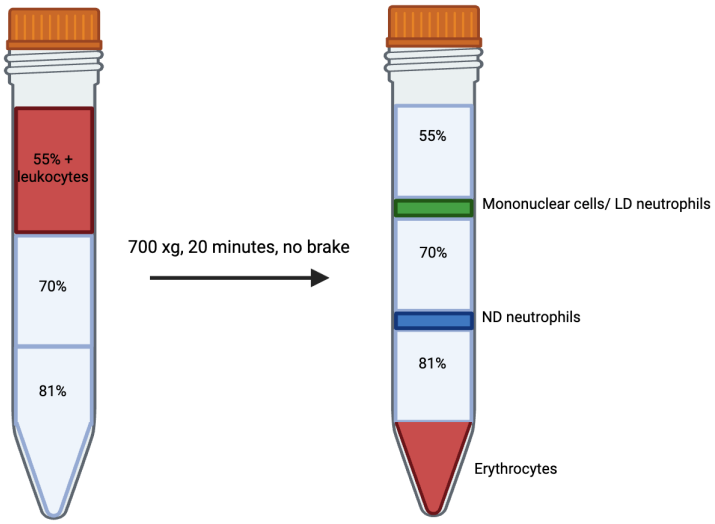



**Figure 3.1 – Human neutrophil density gradient separation.** Human peripheral blood LD neutrophil and ND neutrophil isolation using a 55%, 70%, 81% percoll gradient and density centrifugation. The LD neutrophils are found in the top 55%/70% band along with mononuclear cells. The ND neutrophils are found in the middle 70%/81% band and the erythrocytes pellet at the bottom. Created with https://BioRender.com.

## 3.2. HCC liver and tumour immune cell and neutrophil characterisation

### 3.2.1. Human HCC and liver tissue collection

Liver and tumour samples of patients undergoing surgical liver resection or diagnostic liver biopsy at Newcastle Hospitals NHS Foundation Trust were obtained with full ethical approval (HUNTER study, 19/NE/0251) and informed written consent. Surgical resection tissue was obtained under the direct supervision of a pathologist and placed into 1x DPBS- at 4°C. Liver and tumour biopsies were obtained by a radiologist and placed into 1x DPBS- at 4°C. All tissue samples were processed within 1-2 hours of collection. Basic clinical information of patients was collected as per the HUNTER protocol.

### 3.2.2. Surgical resection HCC liver and tumour immune cell isolation

Samples were first weighed then processed into a single cell suspension using the gentleMACS$^{TM}$ Octo Dissociator with heaters system (Miltenyi Biotec). This uses a combination of gentle mechanical and enzymatic digestion to produce a single cell suspension. The human tumour dissociation kit (Miltenyi Biotec, 130-095-929) was used following the manufactures protocol. Single cell suspensions were then passed

through a 100 µm cell strainer, washed and resuspended in 1x Hank's Balanced Salt Solution (HBSS-) modified without magnesium and calcium and with phenol red (Sigma-Aldrich, 55037C). To remove dead cells and contaminating hepatocytes samples were then layered on top of a 30% Percoll PLUS (cytiva) gradient and centrifuged at 1000 xg for 15 minutes. The dead cell layer was then removed, and the leukocyte and erythrocyte pellet washed in 1x DPBS-. Erythrocytes were then lysed in 1 ml of lysing buffer (BD Pharm Lyse, 555899) for 30 seconds after which osmolarity was restored by adding 1x DPBS-. Samples were then washed and plated into a 96 well round bottom plate for staining.

#### 3.2.3. Liver and tumour biopsy immune cell isolation

Samples were first weighed then processed into a single cell suspension using the TissueGrinder (Fast Forward Discoveries) system. This uses enzyme free mechanical digestion to produce a single cell suspension from small tissue samples. The manufacturers tumour protocol was followed. Following this the single cell suspension was centrifuged through a 100 µm cell strainer and washed in 1x DPBS- and plated into a 96 well plate for staining.

### 3.3. Human flow cytometry

#### 3.3.1. Flow cytometry surface marker cell staining

Dead cells were stained using LIVE/DEAD™ fixable blue dead stain kit (Invitrogen, L23105) diluted 1:1000 in 1x DPBS- for 10 minutes at room temperature. Mitochondrial staining was conducted simultaneously with MitoTracker™ Orange CMTMRos (Invitrogen, M7510) diluted at 1:10000 in 1x DPBS-. Samples were then washed in fluorescence-activated cell sorting (FACS) buffer (phosphate buffered saline (PBS) with 2% fetal bovine serum (FBS)) followed by Fc receptor blockage (Biolegend, human TruStain FcX, 422302) at 1:100 dilution in FACS buffer. Surface antigens were then stained for with a panel of pre-optimised fluorophore conjugated antibodies as per table 3.1 for 30 minutes at 4°C, then washed in FACS buffer. Cells were then fixed in formaldehyde solution made up to 4% (Sigma-Aldrich, F8775) for 10 minutes at 4°C, washed and resuspended in FACS buffer and stored in the dark at 4°C until samples could be run on the flow cytometer.

### 3.3.2. Flow cytometry intracellular phosphoflow staining

Following surface marker staining as above cells were then fixed in phosflow fix buffer I (BD, 557870) for 10 minutes at room temperature, washed in FACS buffer then resuspended in cold BD phosflow perm buffer III (BD, 558050) for nuclear permeabilization for 30 minutes at 4°C. Cells were then washed in FACS buffer and resuspended in a panel of pre-optimised phosphoflow antibodies (panel 7, table 3.1) and left overnight at 4°C before washing and being resuspended in FACS buffer.

### 3.3.3. Flow cytometry acquisition

General immune and neutrophil phenotyping samples were run on the Fortessa cytometer X20 (BD). Samples from functional neutrophil assays and phosphoflow staining were run on the FACSymphony cytometer (BD) in high throughput screening (HTS) mode. Appropriate voltages were applied using an all-stained sample. Fluorophores were compensated using single antibody-stained AbC total compensation beads (Invitrogen, A10497), LIVE/DEAD™ and MitoTracker™ Orange CMTMRos signal was compensated using single stained Amine Reactive Compensation (ArC) compensation beads (Invitrogen, A10346). To control for changes in the cytometer over time (e.g. laser power) neutrophil phenotyping samples were run alongside calibration beads (Thermo Scientific, Cyto-Cal Multifluor + Violet intensity calibrator beads, 11878293) with a set cytometer setting applied. In addition, these samples were re-compensated at each run. This means that any changes in cytometer performance could be tracked over time and corrected for allowing mean fluorescent intensities (MFIs) to be compared between different runs. For samples being run on HTS mode a set sample volume was run. For samples being run in tube mode, samples were run for a set time and the residual volume remaining measured with a pipette. This allowed calculation of the absolute volume of sample run and of the absolute event/ cell count per sample.

### 3.3.4. Human neutrophil cell sorting

Blood LD neutrophil, ND neutrophil and tissue isolated leukocyte samples were used for neutrophil cell sorting. Samples were stained for surface identification markers as above using a panel of pre-optimised fluorophore conjugated antibodies (panel 6) as per table 3.1. Due to limitations of reliably gaining access to FACS cell sorting

machines on the same day of isolations, samples were fixed using 4% formaldehyde (Sigma-Aldrich, F8775), washed, resuspended in FACS buffer and kept at 4°C in the dark until sorting. All samples were sorted between 24-48 hours after isolation. Cell sorting was conducted using the BD Aria Fusion FACS sorter (BD) using the gating strategy outlined in figure 3.2. Compensation was applied using single antibody-stained AbC total compensation beads (Invitrogen, A10497) or LIVE/DEAD$^{TM}$ fixable blue dead single stained ArC compensation beads (Invitrogen, A10346). Highly purified neutrophils were sorted into DPBS- containing Eppendorfs and used for cytospin analysis.

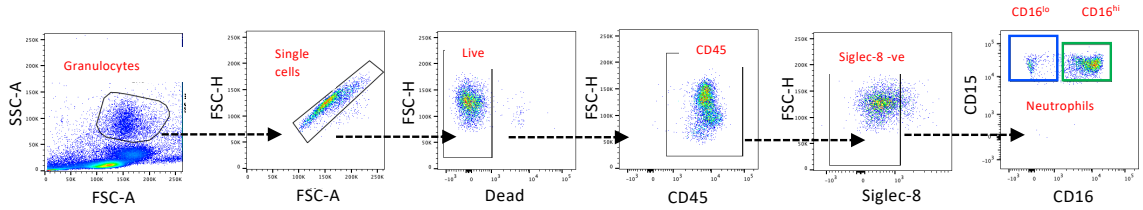



**Figure 3.2 – Flow cytometry neutrophil sorting gating strategy.** Forward scatter area (FSC-A) vs side scatter area (SSC-A) was used to identify granulocytes. FSC-A vs forward scatter height (FSC-H) was used to identify single cells. Live cells were gated on. Neutrophils were identified as being $CD45^{+}$, $Siglec\text{-}8^{-}$, $CD15^{+}$. $CD16^{low}$ and $CD16^{high}$ neutrophil populations were then identified and sorted.

### 3.3.5. Flow cytometry data analysis

Raw data was analysed using FlowJo v10 flow cytometry analysis software (BD). Gating strategies used are outlined in the relevant results sections. Numerical data were obtained by extracting population frequencies of leukocytes, absolute counts as well as MFIs of relevant surface markers for each population. To generate high dimensional plots an equal number events from each population of interest were concatenated into a shared data file using the downsample function. High dimensional analysis was then applied using the t-distributed stochastic neighbour embedding (tSNE), uniform manifold approximation and projection (UMAP) or triMAP functions. To reduce bias all parameters used in the experiment were applied to the high dimensional analysis. Conventional gating was then applied to concatenated data sets and layered on top of the high dimensional analysis to identify population separation/ similarity.

### 3.3.6. Human flow cytometry panels

1. Human general immune panel
   CD45 (FITC), CD8 (PerCP-Cy5.5), CD123 (PE), Siglec-8 (PE/Dazzle 594), CD11c (PE-Cy5), CD244 (PE-Cy7), CD163 (APC), CD4 (Alexa Fluor 700), CD27 (APC/Fire 750), CD3 (Brilliant Violet 421), CD16 (Brilliant Violet 510), CD14 (Brilliant Violet 605), CD19 (Brilliant Violet 650), HLA-DR (Brilliant Violet 711), CD15 (BUV395), LIVE/DEAD™ fixable blue, CD56 (BUV737)

2. Human neutrophil phenotyping panel
   SIRPα (FITC), MitoTracker™ Orange CMTMRos, Siglec-8 (PE/Dazzle 594), CD11b (PE-Cy5), PDL1 (PE-Cy7), CD66b (Alexa Fluor 700), CXCR2 (APC/Fire 750), CXCR4 (Brilliant Violet 421), CD16 (Brilliant Violet 510), CD62L (Brilliant Violet 605), CD10 (Brilliant Violet 785), CD15 (BUV395), LIVE/DEAD™ fixable blue, CD56 (BUV737)

3. Human ROS (DHR 123) assay panel
   Dihydrorhodamine 123 (DHR 123), Siglec-8 (PE/Dazzle 594), CD11b (PE-Cy5), CD66b (Alexa Fluor 700), CXCR2 (APC/Fire 750), CXCR4 (Brilliant Violet 421), CD16 (Brilliant Violet 510), CD62L (Brilliant Violet 605), CD10 (Brilliant Violet 785), CD15 (BUV395)

4. Human phagocytosis assay panel
   Escherichia coli BioParticles (Alexa fluor 488), CD41 (PerCP-Cy5), LOX-1 (PE), Siglec-8 (PE/Dazzle 594), CD11b (PE-Cy5), CD36 (APC), CD66b (Alexa Fluor 700), CXCR2 (APC/Fire 750), CXCR4 (Brilliant Violet 421), CD16 (Brilliant Violet 510), CD62L (Brilliant Violet 605), CD10 (Brilliant Violet 785), CD15 (BUV395), LIVE/DEAD™ fixable blue

5. Human migration assay panel
   CD41 (PerCP-Cy5), LOX-1 (PE), Siglec-8 (PE/Dazzle 594), CD11b (PE-Cy5), CD36 (APC), CD66b (Alexa Fluor 700), CXCR2 (APC/Fire 750), CXCR4 (Brilliant Violet 421), CD16 (Brilliant Violet 510), CD62L (Brilliant Violet 605), CD10 (Brilliant Violet 785), CD15 (BUV395), LIVE/DEAD™ fixable blue

6. Human neutrophil FACS sorting panel
   CD45 (FITC), Siglec-8 (PE/Dazzle 594), CD16 (Brilliant Violet 510), CD15 (BUV395), LIVE/DEAD™ fixable blue

7. Human neutrophil phosphoflow panel
   p-STAT3 (FITC), Siglec-8 (PE/Dazzle 594), CD11b (PE-Cy5), p-mTOR (APC), CD66b (Alexa Fluor 700), CXCR2 (APC/Fire 750), CXCR4 (Brilliant Violet 421), CD16 (Brilliant Violet 510), CD62L (Brilliant Violet 605), CD10 (Brilliant Violet 785), CD15 (BUV395), LIVE/DEAD™ fixable blue

8. LEGENDScreen panel
   CD45 (FITC), LEGENDScreen markers (PE), Siglec-8 (PE/Dazzle 594), CD16 (Brilliant Violet 510), CD15 (BUV395), LIVE/DEAD™ fixable blue

9. Imagestream panel
   CD45 (FITC), Siglec-8 (PE/Dazzle 594), CD15 (PE-cy7), CD16 (Brilliant Violet 510), CD41 (PE), CD36 (APC)

| Antigen | Fluorophore | Clone | Vendor | Dilution |
|---|---|---|---|---|
| SIRPα | FITC | SE5A5 | Biolegend | 1/200 |
| CD45 | FITC | 2D1 | Biolegend | 1/200 |
| CD4 | FITC | OKT4 | Biolegend | 1/200 |
| p-STAT3 | FITC | LUVNKLA | Invitrogen | 1/100 |
| CD8 | PerCP-Cy5.5 | SK1 | Biolegend | 1/200 |
| CD41 | PerCP-Cy5.5 | HIP8 | Biolegend | 1/200 |
| PD1 | PE | EH12.2H7 | Biolegend | 1/200 |
| CD123 | PE | 6H6 | Biolegend | 1/200 |
| LOX-1 | PE | 15C4 | Biolegend | 1/200 |
| p-AKT1 | PE | SDRNR | Invitrogen | 1/100 |
| Siglec-8 | PE/Dazzle 594 | 7C9 | Biolegend | 1/200 |
| CD11b | PE-Cy5 | ICRF44 | BD Biosciences | 1/200 |
| CD11c | PE-Cy5 | B-ly6 | BD Biosciences | 1/200 |

| | | | | |
|---|---|---|---|---|
| PDL1 | PE-Cy7 | 29E.2A3 | Biolegend | 1/200 |
| CD15 | PE-Cy7 | HI98 | Biolegend | 1/200 |
| CD163 | APC | VI M38 | Biolegend | 1/200 |
| CD36 | APC | 5-271 | Biolegend | 1/200 |
| p-mTOR | APC | MRRBY | Invitrogen | 1/100 |
| CD66b | Alexa Fluor 700 | G10F5 | Biolegend | 1/200 |
| CD4 | Alexa Fluor 700 | A161A1 | Biolegend | 1/200 |
| CXCR2 | APC/Fire 750 | 5E8 | Biolegend | 1/200 |
| CD27 | APC/Fire 750 | 113-16 | Biolegend | 1/200 |
| CD47 | Brilliant Violet 421 | CC2C6 | Biolegend | 1/200 |
| CXCR4 | Brilliant Violet 421 | 12G5 | Biolegend | 1/200 |
| CD3 | Brilliant Violet 421 | UCHT1 | Biolegend | 1/200 |
| CD16 | Brilliant Violet 510 | 3G8 | Biolegend | 1/200 |
| CD14 | Brilliant Violet 605 | M5E2 | Biolegend | 1/200 |
| CD62L | Brilliant Violet 605 | V S056 | Biolegend | 1/200 |
| CD36 | Brilliant Violet 605 | CB38 | Biolegend | 1/200 |
| CD19 | Brilliant Violet 650 | HIB19 | Biolegend | 1/200 |
| HLA-DR | Brilliant Violet 711 | G46-6 | BD Biosciences | 1/200 |
| PD1 | Brilliant Violet 750 | EH12.2H7 | Biolegend | 1/200 |
| CD10 | Brilliant Violet 785 | HI10a | Biolegend | 1/200 |
| CD15 | BUV395 | HI98 | BD Biosciences | 1/200 |
| CD3 | BUV395 | SP34-2 | BD Biosciences | 1/200 |
| CD56 | BUV737 | B159 | BD Biosciences | 1/200 |

**Table 3.1 – Human flow cytometry antibodies and dilutions.** Intracellular staining – phosphoflow staining protocol.

### 3.4. Human neutrophil functional assays

#### 3.4.1. Human neutrophil ROS assay

Freshly isolated neutrophils were plated into a round bottom 96 well plate in triplicate. Conditions; 1. control (DPBS- only). 2. Dihydrohodamine 123 (DHR 123) only. 3. DHR 123 + phorbol 12-myristate 13-acetate (PMA). DHR 123 only and DHR 123 + PMA samples were resuspended in 1 μM DHR 123 (Invitrogen, D23806) and incubated for

15 minutes at 37°C. Following this PMA (Merck, 16561-29-8) was spiked into the DHR 123 + PMA samples giving a final concentration of 100 nM and incubated for 30 minutes at 37°C. A panel of fluorophore conjugated antibodies (panel 3, table 3.1) was then spiked into each sample and incubated for a further 15 minutes. Following this samples were washed and resuspended in FACS buffer and kept in the dark at 4°C before being run fresh on the cytometer. All samples were run on the FACSymphony cytometer (BD) in HTS mode, within 1 hour of washing. Fluorophores were compensated using single antibody-stained AbC total compensation beads (Invitrogen, A10497). DHR 123 was compensated using a DHR 123 only stained sample.

### 3.4.2. Human neutrophil phagocytosis assay

Escherichia coli (K-12 strain) BioParticles, Alexa fluor 488 conjugate phagocytosis beads (Invitrogen, E13231) reconstituted at 10 mg/ml were mixed with Escherichia coli BioParticles Opsonizing Reagent (Invitrogen, E2870) at a 1:1 ratio and incubated at 37°C for 1 hour. 1 µl of reconstituted beads were used per samples. Following this opsonised beads were washed with DPBS- and resuspended in DPBS- at a volume of 50 µl per 1 µl of beads, giving a final concentration of 0.2 mg/ml. Freshly isolated neutrophil samples were then plated into a round bottom 96 well plate in duplicate. Conditions; 1. control (no beads). 2. test (beads). Control samples were resuspended in 50 µl DPBS- and test samples resuspended in 50 µl of diluted opsonised beads. Samples were then incubated for 30 minutes at 37°C. Following this samples were washed with cold DPBS- followed by LIVE/DEAD™ fixable blue dead staining (Invitrogen, L23105), Fc blockage (Biolegend, human TruStain FcX, 422302) and surface antigen staining (panel 4, table 3.1). Finally samples were fixed in 4% formaldehyde (Sigma-Aldrich, F8775), washed, resuspended in FACS buffer and kept at 4°C in the dark until samples were run on the FACSymphony cytometer (BD) in HTS mode. Fluorophores were compensated using single antibody-stained AbC total compensation beads (Invitrogen, A10497), LIVE/DEAD™ signal was compensated using single stained ArC compensation beads (Invitrogen, A10346). BioParticles Alexa fluor 488 signal was compensated using a neutrophil-bead sample without antibody staining.

### 3.4.3. Human neutrophil migration assay

Freshly isolated LD and ND neutrophils were plated into a round bottom 96 well plate in triplicate and resuspended in Roswell park memorial institute (RPMI) 1640 medium (Gibco, 11875101) containing 2% FBS. Different chemokine conditions were made up in RPMI 1640 with 2% FBS. Condition 1; CXCL2 (PeproTech, 300-39) 50 ng/ml. Condition 2; CXCL1 (PeproTech, 300-11) 50 ng/ml, CXCL3 (PeproTech, 300-40) 50 ng/ml, CXCL6 (PeproTech, 300-41) 50 ng/ml, CXCL7 (PeproTech, 300-14) 10 ng/ml and CXCL8 (PeproTech, 200-08) 50 ng/ml. Condition 3; CXCL12 (PeproTech, 300-28A) 50 ng/ml. These chemokine containing medias were added to the bottom well of a 5 µm transwell plate (Corning, 10555673) and LD or ND neutrophils resuspended in RPMI 1640 with 2% FBS added to the top well. Plates were then incubated at 37°C with 5% carbon dioxide for 4 hours. Following incubation, the contents of the lower and upper chambers were carefully resuspended and transferred to a new round bottom 96 well plate for staining. Following this samples were washed with cold DPBS- followed by LIVE/DEAD™ fixable blue dead staining (Invitrogen, L23105), Fc blockage (Biolegend, human TruStain FcX, 422302) and surface antigen staining (panel 5, table 3.1). Finally, samples were fixed in 4% formaldehyde (Sigma-Aldrich, F8775), washed, resuspended in FACS buffer and kept at 4°C in the dark until samples run on the FACSymphony cytometer (BD) in HTS mode. Fluorophores were compensated using single antibody-stained AbC total compensation beads (Invitrogen, A10497), LIVE/DEAD™ signal was compensated using single stained ArC compensation beads (Invitrogen, A10346).

## 3.5. ImageStream

### 3.5.1. ImageStream cell staining and preparation

LD and ND neutrophils were isolated as per the protocol above (3.1.3) and plated into a 96 well round bottom plate. Samples were then Fc blocked (Biolegend, human TruStain FcX, 422302) followed by surface antigen staining as per panel 9, table 3.1 for 30 minutes at 4°C, then washed in FACS buffer. Cells were then fixed in formaldehyde solution made up to 4% (Sigma-Aldrich, F8775) for 10 minutes at 4°C, washed and resuspended in FACS buffer at a concentration of $1x10^6$ cells per 50 µl

and transferred to an Eppendorf for storage until samples could be run on the ImageStream flow cytometer.

### 3.5.2. ImageStream experiment set up and acquisition

Samples were run on the ImageStream Mk II imaging flow cytometer (Cytek-Amnis). Table 3.2 outlines the channel-laser settings used. Laser voltages were set using an all-stained sample and experiment settings saved for all subsequent sample runs. Each sample was run through at 60x magnification at a slow flow rate with 50,000 total events recorded. For compensation single antibody-stained AbC total compensation beads (Invitrogen, A10497) were run with the same settings but with brightfield turned off.

| | | Excitation laser (nm) | | | | |
|---|---|---|---|---|---|---|
| Ch | Band (nm) | 405 | 488 | 561 | 642 | 785 |
| 1 | 430-480 | Brightfield | | | | |
| 2 | 480-560 | | CD45 (FITC) | | | |
| 3 | 560-595 | | PE (CD41) | | | |
| 4 | 595-640 | | Siglec-8 (PE-Dazzle 594) | | | |
| 5 | 640-745 | | | | | |
| 6 | 745-800 | | CD15 (PE-Cy7) | | | |
| 7 | 430-505 | | | | | |
| 8 | 505-570 | CD16 (Brilliant Violet 510) | | | | |
| 9 | 570-595 | Brightfield | | | | |
| 10 | 595-640 | | | | | |
| 11 | 640-745 | | | | CD36 (APC) | |
| 12 | 745-800 | | | | | |

**Table 3.2 – Laser configuration on ImageStream Mk II imaging flow cytometer and channel set up**.

### 3.5.3. ImageStream analysis

ImageStream data were analysed using the IDEAS v6.0 software (Amnis). First a compensation matrix was created by loading in the single antibody-stained AbC bead compensation samples. Any sample with a high compensation ratio was manually checked and re-gated to the line of best fit if needed. The compensated matrix was then saved as a .ctm file and applied to all further analysis. Samples were then gated

according to figure 3.3. Briefly, area_brightfield vs aspect ratio_brightfield was used to gate single cells and exclude focus beads. Then focused cells were gated for using a histogram based on gradient RMS_brightfield. Following this LD and ND neutrophils were gated for based on $CD45^+$, $Siglec\text{-}8^-$, $CD16^+$, $CD15^+$. Finally CD36 and CD41 expression was assessed. Corresponding single cell images from each of these populations were then obtained to assess the presence of neutrophil-platelet aggregates and the co-expression of CD36 and CD41.

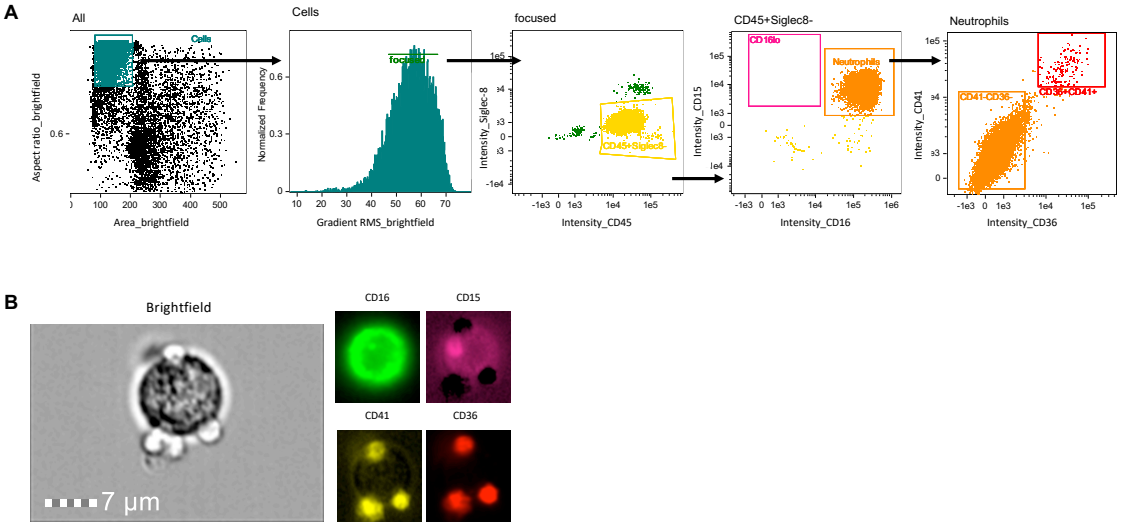



**Figure 3.3 – ImageStream gating strategy and image acquisition. A.** ImageStream gating strategy. Area vs aspect ratio of bright field was used to gate single cells and the peak of the gradient RMS_brightfield was used to gate cells in focus. Using intensities $CD45^+$ $Siglec\text{-}8^-$ cells were gated followed by $CD16^+$ $CD15^+$ to gate for neutrophils. Finally $CD36^+$ $CD41^+$ neutrophils were separated from $CD36^-$ $CD41^-$ neutrophils. **B**. Images of representative cells in brightfield, CD16, CD15, CD36 and CD41 cells were then obtained from each population.

## 3.6. LEGENDScreen

### 3.6.1. LEGENDScreen cell preparation and staining

LD neutrophil/ mononuclear cells and ND neutrophils were isolated and separated into different 15 ml falcon tubes as per the method above (3.1.3). LD neutrophil/ mononuclear cell and ND neutrophil samples were counted using the EVE automated cell counter (NanoEntek). Dead cells were stained using LIVE/DEAD™ fixable blue dead stain kit (Invitrogen, L23105) and samples were Fc receptor blocked (Biolegend,

human TruStain FcX, 422302). The LD neutrophil/ mononuclear cell sample was then barcoded with CD45 as per table 3.1 and incubated 30 minutes at 4°C, then washed twice in FACS buffer. Following this the LD neutrophil/ mononuclear cells and ND neutrophil samples were re-combined in 2:1 ratio and resuspended in a panel of pre-optimised fluorophore conjugated antibodies as per table 3.1, panel 8 for 30 minutes at 4°C, washed twice, and resuspended in FACS buffer at a concentration of $3x10^6$ cells per ml. The LEGENDScreen human PE kit (Biolegend, 700011) was reconstituted as per the manufacturers protocol and the cells were transferred into the plate giving a final staining cell concentration of $1x10^6$ per ml. The plate was incubated for 30 minutes at 4°C, washed twice in FACS buffer and finally the cells fixed in 4% formaldehyde (Sigma-Aldrich, F8775) for 10 minutes at 4°C, washed and resuspended in FACS buffer. Samples were kept overnight protected from light at 4°C before being run the next day (figure 3.4).

### 3.6.2. LEGENDScreen sample acquisition

The LEGENDScreen plates were run on the FACSymphony cytometer (BD) in HTS mode. Appropriate voltages were set using an all-stained sample. Fluorophores were compensated using single antibody-stained AbC total compensation beads (Invitrogen, A10497), LIVE/DEAD$^{TM}$ signal was compensated using single stained ArC beads (Invitrogen, A10346). The run was set up to record a minimum of 1000 LD neutrophil events (Siglec-8$^-$CD16$^+$CD15$^+$CD45$^+$).

### 3.6.3. LEGENDScreen analysis

Samples were gated using the gating strategy outlined in figure 3.4, with CD45 barcoding distinguishing LD from ND neutrophils. Screening markers of interest were all in PE. Isotype control samples were used to gate positive expression. The relative expression both in terms of % of neutrophil expression and absolute MFI could then be compared between LD CD16$^{high}$, LD CD16$^{low}$ and ND neutrophil populations. For both the LD CD16$^{high}$ vs ND neutrophil and LD CD16$^{high}$ vs LD CD16$^{low}$ neutrophil comparisons, markers with a greater than 1.5 fold increase in MFI or less than 0.8 fold increase in MFI in LD CD16$^{high}$ vs ND /LD CD 16$^{low}$ neutrophils were selected. These markers were then run through the Enrichr online analysis tool,[366] and gene ontology

biological pathway analysis applied to identify key upregulated and downregulated biological pathways between the populations.

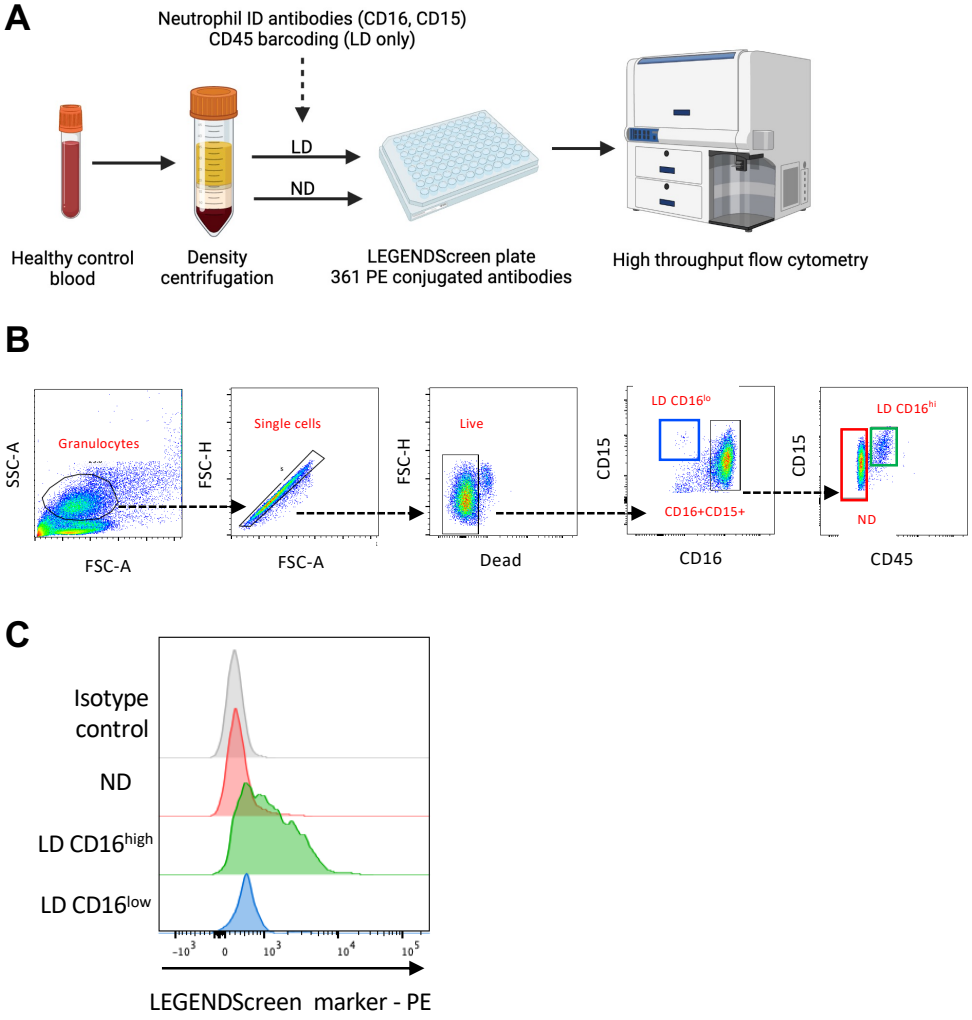



**Figure 3.4 – LegendScreen experiment set up and analysis**. **A.** Experiment set up LD and ND neutrophils were isolated and separated. LD neutrophils were barcoded with a CD45 antibody then recombined with the ND neutrophils. The combined population was stained with neutrophil identification antibodies and plated into the LegendScreen assay plates with each well containing a different PE conjugated antibody. Plates were then run through the cytometer in HTS mode. **B.** Gating strategy. Neutrophils were gated first, then CD45 positivity used to separate LD from ND neutrophils. LD CD16$^{low}$ neutrophils were also gated for. **C**. Screening markers of interest were all in PE. Isotype control samples were used to gate positive expression. The relative expression both in terms of % of neutrophil expression and absolute MFI could then be compared between LD CD16$^{high}$, LD CD16$^{low}$ and ND neutrophil populations.

## 3.7. Cytospin

### 3.7.1. Cytospin preparation

Freshly FACS sorted unfixed neutrophil populations were resuspended in DPBS- to give a concentration of $0.5x10^6$ cells per ml and added to a Shandon cytofunnels (epredia, 1102548). Cytofunnels were then mounted onto slides (Thermo scientific, 12312148, Epredia SuperFrost Plus) using Shandon cytoclips (epredia, 59910052) and filter cards (epredia, 5991022). Slides were then centrifuged at 300 rpm on high acceleration/ deceleration for 3 minutes using the Shandon cytopin 3 centrifuge and carefully removed from the cytofunnels.

### 3.7.2. Cytospin nuclear cell staining

The cell monolayer area was circled with a hydrophobic marker pen. Cells were then fixed in formaldehyde solution made up to 4% (Sigma-Aldrich, F8775) for 5 minutes at room temperature followed by 2 washes in 1x DPBS-. Nuclei were then stained with Giemsa (Sigma-Aldrich, 32884) diluted 1:10 in 2% Tween-DPBS- for 5 minutes at room temperature. Finally, cells were washed in deionised water and left to dry before microscopy analysis.

### 3.7.3. Cytospin nuclear staining image analysis

Giemsa nuclear stained slides were analysed on the Nikon Eclipse Upright microscope and NIS-Elements BR analysis software. The number of nuclear lobes of each neutrophil was manually counted and classified as either; banded (1 lobe), mature (2-3 lobes) or mature (>4 lobes) or unclassifiable (smudged/ burst nucleus).

### 3.7.4. Cytospin immunofluorescence cell staining and microscopy

The cell monolayer area was circled with a hydrophobic marker pen. Cells were then fixed in formaldehyde solution made up to 4% (Sigma-Aldrich, F8775) for 5 minutes at room temperature followed by washing in 1x PBS. Samples were then blocked in 20% swine serum for 45 minutes. The primary antibody in 20% swine serum was added as per table 3.3 and incubated overnight at 4°C. Samples were then washed in tris-buffered saline with tween 20 (TBST) and secondary antibody added as per table 3.3 and incubated for 1 hour at room temperature. Following this samples were washed

in TBST and incubated with Hoechst 33342 (ThermoScientific, 62249) diluted to 1:1000 in tris-buffered saline (TBS) for 15 minutes at room temperature. Following another wash in 1x PBS samples were mounted with Vectashield (Vector, H-1000) and analysed on the Zeiss Axio Observer D1 microscope with the ZEN Pro 2012 Blue Edition software.

| Antigen | Primary antibody | Secondary antibody |
|---|---|---|
| MPO | Goat pAb to human MPO, AF3667, R&D, 1/100 dilution | Donkey anti-goat Alexa Fluor 488, A-11055, ThermoFisher, 1/200 dilution |

**Table 3.3 – antibodies used for immunofluorescence staining**. pAb; polyclonal antibody.

## 3.8. In vivo models

### 3.8.1 Ethical statement and animal husbandry

All animal experiments were performed in accordance with a UK Home Office licence (PP8854860), were conducted in line with ARRIVE guidelines and the UK Animal (Scientific Procedures) Act 1986 and were subject to review by the Newcastle Ethical Review Committee. Mice were housed at the Newcastle University Comparative Biology Centre in specific pathogen-free conditions, were maintained on a 12-hour light-dark cycle in a tightly controlled climate (19°C-22°C at 45%-65% humidity) and had unrestricted access to food and water. The welfare of animals was accessed daily and whilst undergoing experimentation animals were weighed at least weekly and their clinical condition scored. Any animal reaching a pre-specified severity score was humanely killed using a schedule 1 approved method. Veterinary advice was also sought in designing experiments and if there were animal welfare concerns.

### 3.8.2. Mouse strains

C57BL/6 mice were purchased from the Jackson Laboratory. Male, aged matched C57BL/6 mice were used in all experiments. Neutrophil specific *Cxcr2* knockout mice (*Cxcr2*$^{DNeut}$) were generated by crossing *Mrp8*$^{cre}$ with *Cxcr2*$^{fl/fl}$ mice. In experiments using *Cxcr2*$^{DNeut}$ mice age and sex matched *Cxcr2*$^{fl/fl}$ mice were used as cre negative controls. These mice were kindly donated by Professor Tom Bird at the Beatson Institute for cancer research. Breeding and genotyping were done at the Beatson

Institute for cancer research before mice were transferred to Newcastle University Comparative Biology Centre.

### 3.8.3. Dietary induced MASH model – modified western diet model

Male C57BL/6 mice were fed either a normal chow plus drinking water or a modified western diet (Envigo, TD.120528) plus sugar water (23.1 g/L fructose and 18.9 g/L glucose) from 6 weeks of age. Mice were kept on diet for a minimum of 12 weeks before experimentation. 12 weeks on the modified western diet is sufficient to induce significant steatohepatitis and obesity. During this time mice were weighed and scored weekly.

### 3.8.4. Intrahepatic HCC model

Male C57BL/6 mice were pre-dosed with buprenorphine (0.05 mg/kg) and put under general anaesthesia using isoflurane. They then underwent laparotomy, manual exposure of the liver and injection of a strain matched hepatoma (Hep 53.4) cell line into the left lobe. One million Hep 53.4 cells were injected in DPBS- with 25% matrigel (corning, 354230), an injection volume of 30 µl was used to minimise leak from the injection tract. For mice undergoing a sham procedure the same volume of DPBS- with 25% Matrigel but with no cells was injected. Following implantation, the livers were replaced and laparotomy closed. Tumours were then allowed to grow for up to 6 weeks before the mice were harvested. Mice were regularly weighed, scored, and palpated to assess for disease progression.

### 3.8.5. Subcutaneous HCC model

Male C57BL/6 mice were put under general anaesthesia using isoflurane and Hep 53.4 cells were injected subcutaneously into the left flank. In total 10 million Hep 53.4 cells were injected in a volume of 50 µl made up of 25% Matrigel (corning, 354230). Tumours were allowed to grow up to 6 weeks with the tumour area measured at least twice weekly using a pair of digital callipers. Mice were humanely culled if the tumours ulcerated or exceeded predefined humane endpoints.

### 3.8.6. Cancer therapies

Tumours were allowed to engraft and grow for 2 weeks post implantation before starting anti-cancer treatments. This is to simulate advanced, established tumours

which are encountered in clinical practice for patients undergoing systemic therapy for their HCC. Whilst on treatments mice were monitored daily for any welfare issues and drug toxicities. Appropriate control treatments were given to mice in control groups. For antibodies an isotype matched isotype control antibody was given and for small molecule inhibitors the vehicle solution administered. Mice were treated for a total of 2 weeks then harvested. Cancer therapies are detailed in table 3.4 and 3.5.

| Antibody | Clone | Isotype | Details | Dose | Route | Frequency |
|---|---|---|---|---|---|---|
| Anti-PDL1 | 10F.9G2 | Rat IgG2b | Biolegend, 124329 | 200 µg | IP | Twice weekly |
| Anti-PD1 | RMP1-14 | Rat IgG2a | Biolegend, 114122 | 200 µg | IP | Twice weekly |
| Anti-VEGFA | 2G11-2A05 | Rat IgG2a | Biolegend, 512810 | 100 µg | IP | Twice weekly |
| IgG2b isotype control | RTK4530 | Rat IgG2b | Biolegend, 400668 | 200 µg | IP | Twice weekly |
| IgG2a isotype control | RTK2758 | Rat IgG2a | Biolegend, 400574 | 200 µg or 100 µg | IP | Twice weekly |
| Anti-S100A8 | n/a | Rabbit IgG | Obtained from collaborator[315] | 200 µg | IP | Twice weekly |
| Anti-S100A9 | n/a | Rabbit IgG | Obtained from collaborator[315] | 200 µg | IP | Twice weekly |

**Table 3.4 – Monoclonal antibody therapies.** IP; intraperitoneal.

| Drug | Target | Vehicle | Details | Dose | Route | Frequency |
|---|---|---|---|---|---|---|
| AZD1480 | JAK2 | HPMC | MedChemExpress, HY-10193 | 20 mg/kg | OG | Twice daily |
| AZ12601011 | ALK5 | HPMC | MedChemExpress, HY-122856 | 50 mg/kg | OG | Twice daily |

**Table 3.5 – Small molecule inhibitor therapies.** HPMC; hydroxypropyl methylcellulose, OG; oral gavage.

### 3.8.7. Mouse tail vein blood collection

Mice were restrained and the tail veins punctured with a 24G needle. 10 µl of blood was collected with a 20 µl pipette tip and immediately placed into 10 ml of DPBS- in a 15 ml falcon tube. This dilution was enough to prevent coagulation. Pressure was then

applied to the tail vein puncture site and haemostasis ensured before returning mice to their home cage. For studies involving serial tail vein bleeds no more than 7.5% of blood volume was sampled over a week period as per laboratory animal science association (LASA) guidelines.

### 3.8.8. Mouse harvests

At the end of studies mice were humanely culled by putting them under isoflurane general anaesthesia and performing cardiac puncture to collect between 500-800 µl of blood which was collected into EDTA coated vacutainers (BD, 367842) and Eppendorf's. The EDTA samples were used for cell isolations and the Eppendorf sample left for 10 minutes and centrifuged for serum collection. Livers were dissected out, weighed and tumour burden measured by taking 3 measurements in 3 different planes using a pair of electric callipers. Sections of liver and tumour were collected into ice cold DPBS- for cell isolation, into cassettes for fixation and paraffin embedding and into Eppendorf's for snap freezing. Subcutaneous tumours were carefully dissected out from the subcutaneous tissue layer, weighed and measured in 3 planes with a pair of electric callipers. Following this, subcutaneous tumours were cut up, divided and placed into ice cold DPBS- for cell isolations, cassettes for fixation and paraffin embedding and into Eppendorf's for snap freezing. Spleens and femurs were also harvested into ice cold DPBS- for cell isolations.

## 3.9. Mouse immune cell isolations

### 3.9.1. Bone marrow isolation

Femur bones were cut away from muscles and the bone ends cut with scissors. The bone ends were carefully cannulated with a 24G needle and 10 ml of HBSS- flushed through into a petri dish using a 10 ml syringe. The bone marrow clumps were carefully aggregated by passing through a syringe and passed through a 100 µm cell strainer to remove any bone fragments. Bone marrow cells were then pelleted and washed twice in DPBS-. Red cells were lysed in 1 ml of lysing buffer (BD Pharm Lyse, 555899) for 30 seconds after which osmolarity was restored by adding DPBS-. Cell pellets were transferred to a round bottom 96 well plate for staining and or functional assays.

### 3.9.2. Whole blood immune cell isolation

100-200 µl of EDTA anticoagulated blood was lysed in 2 ml of lysing buffer (BD Pharm Lyse, 555899) for 2 minutes after which osmolarity was restored by adding DPBS-. Samples were then washed twice and plated into a 96 well round bottom plate for staining.

### 3.9.3. Tail vein blood immune cell isolation

Falcon tubes containing blood diluted in 10 ml DPBS- were centrifuged and the whole blood pellet collected. Erythrocytes were lysed by adding 500 µl of lysing buffer (BD Pharm Lyse, 555899) for 30 seconds after which osmolarity was restored by adding DPBS-. Cell pellets were transferred to a round bottom 96 well plate for staining.

### 3.9.4. Blood neutrophil isolation

3 ml of histopaque-1119 (Sigma-Aldrich, 11191) was added to a 15 ml falcon tube and 3 ml of histopaque-1077 (Sigma-Aldrich, 10771) was carefully layered on top. 500-1000 µl of EDTA anticoagulated blood was made up to 6 ml by adding DPBS-. The DPBS- diluted blood was then carefully layered on top of the histopaque-1077 layer. Samples were then centrifuged at 700 xg for 30 minutes with the brake switched off. This resulted in the separation of 3 cell bands (figure 3.5). At the DPBS- -histopaque-1077 interface were the mononuclear cell / LD neutrophil population. At the histopaque-1077- histopaque-1119 interface were the ND neutrophil population and beneath the histopaque-1119 layer were the erythrocytes. The mononuclear cell/ LD neutrophil and ND neutrophil populations were collected separately and washed in DPBS-. Contaminating erythrocytes were lysed by resuspending cell pellets in lysing buffer (BD Pharm Lyse, 555899) for 30 seconds after which osmolarity was restored by adding DPBS-. Samples were then washed twice and plated into a 96 well round bottom plate for staining and or functional assays.

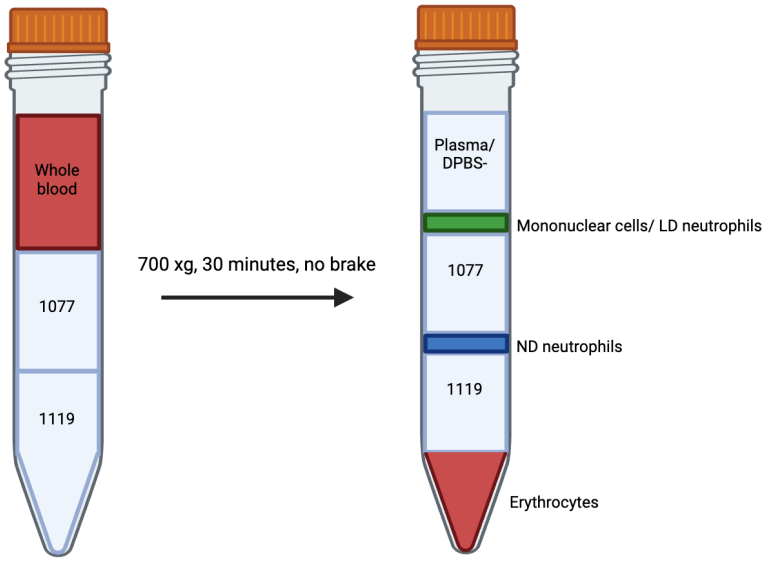



**Figure 3.5 – Mouse peripheral blood LD and ND neutrophil isolation**. The LD neutrophils are found in the top plasma – histopaque-1077 band. The ND neutrophils are found in the middle histopaque-1077 – histopaque-1119 band. The erythrocytes pellet are at the bottom. Created with https://BioRender.com.

### 3.9.5. Spleen immune cell isolation

Whole spleens were passed through a 100 µm cell strainer through the combination of light dissociation with a syringe plunger and rinsing with HBSS-. Dissociated splenocytes were then washed twice in DPBS- to remove debris. Erythrocytes were removed by resuspending pellets in 1 ml lysing buffer (BD Pharm Lyse, 555899) for 30 seconds after which osmolarity was restored by adding DPBS-. Samples were then washed twice and plated into a 96 well round bottom plate for staining and or functional assays.

### 3.9.6. Liver and tumour immune cell isolation

Samples were first weighed then processed into a single cell suspension using the gentleMACS$^{TM}$ Octo Dissociator with heaters system (Miltenyi Biotec). This uses a combination of gentle mechanical and enzymatic digestion to produce a single cell suspension. The mouse liver dissociation kit (Miltenyi Biotec, 130-105-807) was used following the manufactures protocol. Single cell suspensions were then passed through a 100 µm cell strainer, washed and resuspended in HBSS-. To remove dead cells and contaminating hepatocytes samples were then layered on top of a 30% Percoll PLUS (cytiva, 17544501) gradient and centrifuged at 1000 xg for 15 minutes.

The dead cell layer was then removed, and the leukocyte and erythrocyte pellet washed in 1x DPBS-. Erythrocytes were then lysed in 1 ml of lysing buffer (BD Pharm Lyse, 555899) for 30 seconds after which osmolarity was restored by adding 1x DPBS-. Samples were then washed twice and plated into a 96 well round bottom plate for staining and or functional assays.

### 3.10. Mouse flow cytometry

#### 3.10.1. Flow cytometry surface marker cell staining

Dead cells were stained using LIVE/DEAD™ fixable blue dead stain kit (Invitrogen, L23105) diluted 1:1000 in 1x DPBS- for 10 minutes at room temperature. Mitochondrial staining was conducted simultaneously with MitoTracker™ Orange CMTMRos (Invitrogen, M7510) diluted at 1:10000 in 1x DPBS-. Samples were then washed in FACS buffer followed by Fc receptor blockage (Biolegend, TruStain FcX, 101320) at 1:100 dilution in FACS buffer. Surface antigens were then stained for with a panel of pre-optimised fluorophore conjugated antibodies as per table 3.6 for 30 minutes at 4°C, then washed in FACS buffer. Cells were then fixed in formaldehyde solution made up to 4% (Sigma-Aldrich, F8775) for 10 minutes at 4°C, washed and resuspended in FACS buffer and stored in the dark at 4°C until samples could be run on the flow cytometer.

#### 3.10.2. Flow cytometry intracellular marker cell staining

Following surface marker staining samples were fixed and permeabilized with either the Cytofix/Cytoperm kit (BD, 554714) or the Transcription factor staining buffer set (eBiosciences, 00-5523-00) as per the manufactures protocol. Following permeabilization intracellular antigens were stained for with a panel of pre-optimised fluorophore conjugated antibodies (table 3.6 and panels 5 and 6) for 30 minutes at 4°C, then washed in perm wash (BD, 557885) and resuspended in FACS buffer and stored in the dark at 4°C until samples could be run on the flow cytometer.

#### 3.10.3. Flow cytometry intracellular phosphoflow staining

Following surface marker staining as above cells were fixed in phosflow fix buffer I (BD, 557870) for 10 minutes at room temperature, washed in FACS buffer then

resuspended in cold BD phosflow perm buffer III (BD, 558050) for nuclear permeabilization for 30 minutes at 4°C. Cells were then washed in FACS buffer and resuspended in a panel of pre-optimised phosphoflow antibodies (table 3.6, panel 2 and 3) and left overnight at 4°C before washing and being resuspended in FACS buffer.

### 3.10.4. Flow cytometry acquisition

All mouse flow cytometry samples were run on the FACSymphony cytometer (BD) in HTS mode. Appropriate voltages were applied using an all-stained sample. Fluorophores were compensated using single antibody-stained AbC total compensation beads (Invitrogen, A10497), LIVE/DEAD™ and MitoTracker™ Orange CMTMRos signal was compensated using single stained ArC compensation beads (Invitrogen, A10346). A fixed volume of each sample was run through the cytometer, this allowed calculation of the absolute event/ cell count per sample.

### 3.10.5. Flow cytometry data analysis

Raw data were analysed using FlowJo v10 flow cytometry analysis software (BD). Gating strategies used are outlined in the relevant results sections. Numerical data were obtained by extracting population frequencies of leukocytes, absolute counts as well as MFIs of relevant surface markers for each population. To generate high dimensional plots an equal number events from each population of interest were concatenated into a shared data file using the downsample function. High dimensional analysis was then applied using the tSNE, UMAP or triMAP functions. To reduce bias all parameters used in the experiment were applied to the high dimensional analysis. Conventional gating was then applied to concatenated data sets and layered on top of the high dimensional analysis to identify population separation/ similarity.

### 3.10.6. Mouse flow cytometry panels

1. Mouse general immune panel
   CD4 (FITC), Ly6C (PerCP-Cy5.5), PD1 (PE), CXCR2 (PE/Dazzle 594), CD103 (PE-Cy5), CD3 (PE-Cy7), MHC-2 (APC), CD45 (Alexa Fluor 700), CD8 (APC/Fire 750), CCR7 (Brilliant Violet 421), CD11b (Brilliant Violet 510), CD11c

(Brilliant Violet 605), PDL1 (Brilliant Violet 650), SIRPα (Brilliant Violet 711), NK1.1 (Brilliant Violet 750), XCR1 (Brilliant Violet 785), Ly6G (BUV395), CD86 (BUV563), CD80 (BUV615), F4/80 (BUV661), CD19 (BUV805), LIVE/DEAD™ fixable blue

2. Mouse neutrophil phosphoflow panel
   p-STAT3 (FITC), Ly6C (PerCP-Cy5.5), p-AKT1 (PE), CXCR2 (PE/Dazzle 594), C-kit (PE-Cy5), CD101 (PE-Cy7), p-mTOR (APC), CD45 (Alexa Fluor 700), CXCR4 (Brilliant Violet 421), CD11b (Brilliant Violet 510), CD62L (Brilliant Violet 650), Ly6G (BUV395), LIVE/DEAD™ fixable blue

3. Mouse in vitro phosphoflow panel
   p-STAT3 (FITC), Ly6C (PerCP-Cy5.5), CXCR2 (PE), CD3 (PE-Cy7), CD45 (Alexa Fluor 700), CXCR4 (Brilliant Violet 421), CD11b (Brilliant Violet 510), CD62L (Brilliant Violet 650), NK1.1 (Brilliant Violet 750), Ly6G (BUV395), F4/80 (BUV661), CD19 (BUV805), LIVE/DEAD™ fixable blue

4. Mouse bone marrow neutrophil panel
   CXCR2 (FITC), Ly6C (PerCP-Cy5.5), MitoTracker™ Orange CMTMRos, CD34 (PE/Dazzle 594), C-kit (PE-Cy5), CD16/32 (APC), CD45 (Alexa Fluor 700), CD115 (APC/Fire 750), CXCR4 (Brilliant Violet 421), CD11b (Brilliant Violet 510), PDL1 (Brilliant Violet 650), Ly6G (BUV395), LIVE/DEAD™ fixable blue

5. Mouse intracellular neutrophil panel
   Ly6C (PerCP-Cy5.5), PD1 (PE), NOS2 (PE-Cy7), CD45 (Alexa Fluor 700), SIRPα (APC/Fire 750), CD47 (Brilliant Violet 421), CD11b (Brilliant Violet 510), Ly6G (BUV395), LIVE/DEAD™ fixable blue

6. Mouse T cell panel
   Tbet (FITC), CD127 (PerCP-Cy5.5), EOMES (PE), CTLA4 (PE/Dazzle 594), PD1 (PE-Cy7), CD8 (Alexa Fluor 700), CXCR3 (APC/Fire 750), Foxp3 (Brilliant Violet 421), CD4 (Brilliant Violet 510), CD244 (Brilliant Violet 605), CD62L (Brilliant Violet 650), CXCR6 (Brilliant Violet 711), CD3 (BUV395), CD44 (BUV563), NKp46 (BUV661), CD28 (BUV737), LIVE/DEAD™ fixable blue

7. Mouse ROS (DHR 123) assay panel

   DHR 123, Ly6C (PerCP-Cy5.5), CXCR2 (PE/Dazzle 594), CD45 (Alexa Fluor 700), CD11b (Brilliant Violet 510), CD62L (Brilliant Violet 650), Ly6G (Brilliant Violet 785), LIVE/DEAD™ fixable blue

8. Mouse phagocytosis assay panel

   Zymosan A BioParticles (Alexa fluor 488), Ly6C (PerCP-Cy5.5), CXCR2 (PE/Dazzle 594), CD45 (Alexa Fluor 700), CD11b (Brilliant Violet 510), CD62L (Brilliant Violet 650), Ly6G (BUV395), LIVE/DEAD™ fixable blue

9. Mouse migration assay panel

   Ly6C (PerCP-Cy5.5), CXCR2 (PE/Dazzle 594), CD45 (Alexa Fluor 700), CD11b (Brilliant Violet 510), CD62L (Brilliant Violet 650), Ly6G (BUV395), LIVE/DEAD™ fixable blue

10. Mouse neutrophil Bromodeoxyuridine (BrdU) panel

    BrdU (FITC), Ly6C (PerCP-Cy5.5), CXCR2 (PE), CD101 (PE-Cy7), CD36 (APC), CD45 (Alexa Fluor 700), CD41 (APC/Fire 750), CXCR4 (Brilliant Violet 421), CD11b (Brilliant Violet 510), CD62L (Brilliant Violet 650), Ly6G (BUV395), LIVE/DEAD™ fixable blue

11. Mouse bone marrow BrdU panel

    BrdU (FITC), Ly6C (PerCP-Cy5.5), CXCR2 (PE), CD34 (PE/Dazzle 594), C-kit (PE-Cy5), CD16/32 (APC), CD45 (Alexa Fluor 700), CD115 (APC/Fire 750), CXCR4 (Brilliant Violet 421), CD11b (Brilliant Violet 510), CD62L (Brilliant Violet 650), Ly6G (BUV395), LIVE/DEAD™ fixable blue

| Antigen | Fluorophore | Clone | Vendor | Dilution |
|---|---|---|---|---|
| CXCR2 | FITC | SA045E1 | Biolegend | 1/200 |
| CXCR2 | PE | SA045E1 | Biolegend | 1/200 |
| CXCR2 | PE/Dazzle 594 | SA045E1 | Biolegend | 1/200 |
| T-bet | FITC | 4B10 | Biolegend | 1/200 |
| CD4 | FITC | RM4-5 | Biolegend | 1/200 |
| p-STAT3 | FITC | LUVNKLA | Invitrogen | 1/100 |
| BrdU | FITC | | BD biosciences | 1/100 |
| Ly6C | PerCP-Cy5.5 | HK1.4 | Biolegend | 1/800 |
| PD1 | PE | 29F.1A12 | Biolegend | 1/200 |
| EOMES | PE | W17001A | Biolegend | 1/200 |
| p-AKT1 | PE | SDRNR | Invitrogen | 1/100 |
| CD34 | PE/Dazzle 594 | HM34 | Biolegend | 1/200 |
| CTLA4 | PE/Dazzle 594 | UC10-4B9 | Biolegend | 1/200 |
| C-kit | PE-Cy5 | 2B8 | Biolegend | 1/200 |
| CD103 | PE-Cy5 | 2E7 | Biolegend | 1/200 |
| NOS2 | PE-Cy7 | CXNFT | eBiosciences | 1/200 |
| CD101 | PE-Cy7 | Moushi101 | Invitrogen | 1/200 |
| MHC2 | APC | M5/114.15.2 | Biolegend | 1/200 |
| CD16/32 | APC | 93 | Biolegend | 1/200 |
| p-mTOR | APC | MRRBY | Invitrogen | 1/100 |
| CD36 | APC | HM36 | Biolegend | 1/200 |
| CD45 | Alexa Fluor 700 | 30-F11 | Biolegend | 1/200 |
| CD8A | Alexa Fluor 700 | 53-6.7 | Biolegend | 1/200 |
| CD115 | APC/Fire 750 | AFS98 | Biolegend | 1/200 |
| SIRPα | APC/Fire 750 | P84 | Biolegend | 1/200 |
| CD41 | APC/Fire 750 | MWReg30 | Biolegend | 1/200 |
| CD8A | APC/Fire 750 | 53-6.7 | Biolegend | 1/200 |
| CXCR3 | APC/Fire 750 | CXCR3-173 | Biolegend | 1/200 |
| CD47 | Brilliant Violet 421 | Miap301 | Biolegend | 1/200 |
| CXCR4 | Brilliant Violet 421 | L276F12 | Biolegend | 1/200 |
| Foxp3 | Brilliant Violet 421 | MF-14 | Biolegend | 1/200 |

| | | | | |
|---|---|---|---|---|
| CCR7 | Brilliant Violet 421 | 4B12 | Biolegend | 1/200 |
| CD11b | Brilliant Violet 510 | M1/70 | BD Biosciences | 1/200 |
| CD11c | Brilliant Violet 605 | N418 | Biolegend | 1/200 |
| CD62L | Brilliant Violet 650 | MEL-14 | Biolegend | 1/200 |
| PDL1 | Brilliant Violet 650 | 10F.9G2 | Biolegend | 1/200 |
| CXCR6 | Brilliant Violet 711 | SA051D1 | Biolegend | 1/200 |
| SIRPα | Brilliant Violet 711 | P84 | BD Biosciences | 1/200 |
| NK1.1 | Brilliant Violet 750 | PK136 | BD Biosciences | 1/200 |
| Ly6G | Brilliant Violet 785 | 1A8 | Biolegend | 1/200 |
| XCR1 | Brilliant Violet 785 | ZET | Biolegend | 1/200 |
| Ly6G | BUV395 | 1A8 | BD Biosciences | 1/200 |
| CD3 | BUV395 | 12A2 | BD Biosciences | 1/200 |
| CD44 | BUV563 | IM7 | BD Biosciences | 1/200 |
| CD86 | BUV563 | PO3 | BD Biosciences | 1/200 |
| F4/80 | BUV661 | T45-2342 | BD Biosciences | 1/200 |
| CD80 | BUV615 | 16-10A1 | BD Biosciences | 1/200 |
| NKp46 | BUV661 | 29A1.4 | BD Biosciences | 1/200 |
| CD28 | BUV737 | 37.51 | BD Biosciences | 1/200 |
| CD19 | BUV805 | 1D3 | BD Biosciences | 1/200 |

**Table 3.6 – Mouse flow cytometry antibodies and dilutions**. Intracellular staining – phosphoflow staining protocol. Intracellular staining – BrdU staining protocol. Intracellular staining – transcription factor staining protocol. Intracellular staining – cytofix/cytoperm protocol.

## 3.11. Mouse neutrophil functional assays

### 3.11.1. Mouse neutrophil ROS assay

Freshly isolated neutrophils were plated into a round bottom 96 well plate in triplicate. Conditions; 1. control (DPBS- only), 2. DHR 123 only and 3. DHR 123 + PMA. DHR 123 only and DHR 123 + PMA samples were resuspended in 1 µM DHR 123 (Invitrogen, D23806) and incubated for 15 minutes at 37°C. Following this PMA (Merck, 16561-29-8) was spiked into the DHR 123 + PMA samples giving a final concentration of 100 nM and incubated for 30 minutes at 37°C. A panel of fluorophore conjugated antibodies (table 3.6, panel 7) was then spiked into each sample and

incubated for a further 15 minutes. Following this samples were washed and resuspended in FACS buffer and kept in the dark at 4°C before being run fresh on the cytometer. All samples were run on the FACSymphony cytometer (BD) in HTS mode, within 1 hour of staining. Fluorophores were compensated using single antibody-stained AbC total compensation beads (Invitrogen, A10497). DHR 123 was compensated using a DHR 123 only stained sample.

### 3.11.2. Mouse neutrophil phagocytosis assay

Zymosan A (S. cerevisiae) BioParticles, Alexa fluor 488 conjugate phagocytosis beads (Invitrogen, Z23373) reconstituted at 10 mg/ml were resuspended at 0.2 mg/ml in DPBS- with 25% serum (obtained from a sex, age, and strain matched mouse) and incubated at 37°C for 1 hour for opsonisation. The beads were then washed twice and resuspended in DPBS- with 1% serum at 0.2 mg/ml. Freshly isolated neutrophils were plated out into a 96 round bottom plate in duplicate. Conditions; control (no beads) and test (beads). Control samples were resuspended in 50 µl DPBS- and test samples resuspended in 50 µl of diluted opsonised beads. Samples were then incubated for 30 minutes at 37°C. Following this samples were washed with cold DPBS- followed by LIVE/DEAD™ fixable blue dead staining (Invitrogen, L23105), Fc blockage (Biolegend, TruStain FcX, 101320) and surface antigen staining (table 3.6, panel 8). Samples were then fixed in 4% formaldehyde (Sigma-Aldrich, F8775), washed, resuspended in FACS buffer and kept at 4°C in the dark until samples run on the FACSymphony cytometer (BD) in HTS mode. Fluorophores were compensated using single antibody-stained AbC total compensation beads (Invitrogen, A10497), LIVE/DEAD™ signal was compensated using single stained ArC compensation beads (Invitrogen, A10346). BioParticles Alexa fluor 488 signal was compensated using a neutrophil-bead sample without antibody staining.

### 3.11.3. Mouse neutrophil migration assay

Freshly isolated neutrophils were plated into a round bottom 96 well plate in duplicate and resuspended in RPMI 1640 (Gibco, 11875101) containing 2% FBS. CXCL2 (PeproTech, 250-15) at a concentration of 50 ng/ml was made up in RPMI 1640 with 2% FBS and added to the bottom well of a 5 µm transwell plate (Corning, 10555673). RPMI 1640 with 2% FBS were added to the bottom well for control samples.

Neutrophils resuspended in RPMI 1640 with 2% FBS were added to the top wells. Plates were then incubated at 37°C with 5% carbon dioxide for 4 hours. Following incubation the contents of the lower and upper chambers were carefully resuspended and transferred to a new round bottom 96 well plate for staining. Following this samples were washed with cold DPBS- followed by LIVE/DEAD™ fixable blue dead staining (Invitrogen, L23105), Fc blockage (Biolegend, TruStain FcX, 101320) and surface antigen staining (table 3.6, panel 9). Finally samples were fixed in 4% formaldehyde (Sigma-Aldrich, F8775), washed, resuspended in FACS buffer and kept at 4°C in the dark until samples run on the FACSymphony cytometer (BD) in HTS mode. Fluorophores were compensated using single antibody-stained AbC total compensation beads (Invitrogen, A10497), LIVE/DEAD™ signal was compensated using single stained ArC compensation beads (Invitrogen, A10346).

## 3.12. BrdU neutrophil tracking experiment

### 3.12.1. BrdU administration

Tumour bearing or sham, western diet or control diet mice received 2 mg of BrdU (Sigma-Aldrich, 19-160) via intra-peritoneal (IP) injection and were then harvested at various timepoints post injection (1, 2, 3, 4 and 6 days). Bone marrow, blood LD, blood ND, spleen, liver and tumour neutrophils were then isolated as above and stained (figure 3.6).

### 3.12.2. BrdU flow cytometry staining

Dead cells were stained using LIVE/DEAD™ fixable blue dead stain kit (Invitrogen, L23105) diluted 1:1000 in 1x DPBS- for 10 minutes at room temperature. Samples were then washed in FACS buffer followed by Fc receptor blockage (Biolegend, TruStain FcX, 101320) at 1:100 dilution in FACS buffer. Surface antigens were then stained for with a panel of pre-optimised fluorophore conjugated antibodies (table 3.6, panels 10 and 11) for 30 minutes at 4°C, then washed in FACS buffer. BrdU staining was then conducted using a pre-optimised commercial kit (BD Pharmingen FITC BrdU flow kit, 559619). The manufacturers protocol was followed which involved an initial fixation/permeabilization step with BD cytofix/cytoperm buffer, an additional permeabilization step with BD cytoperm permeabilization buffer plus, a DNase

incubation step and finally staining of BrdU with the FITC conjugated antibody provided. Samples were then washed and resuspended in FACS buffer and stored at 4°C until they could be run on the flow cytometer the following day.

### 3.12.3. BrdU flow cytometry acquisition and data analysis

Samples were run on the Fortessa cytometer X20 (BD). Appropriate voltages were applied using an all-stained sample. Fluorophores were compensated using single antibody-stained AbC total compensation beads (Invitrogen, A10497), LIVE/DEAD™ signal was compensated using single stained ArC compensation beads (Invitrogen, A10346). Raw data were analysed using FlowJo v10 flow cytometry analysis software (BD). Gating strategies outlined in figure 3.6 were used.

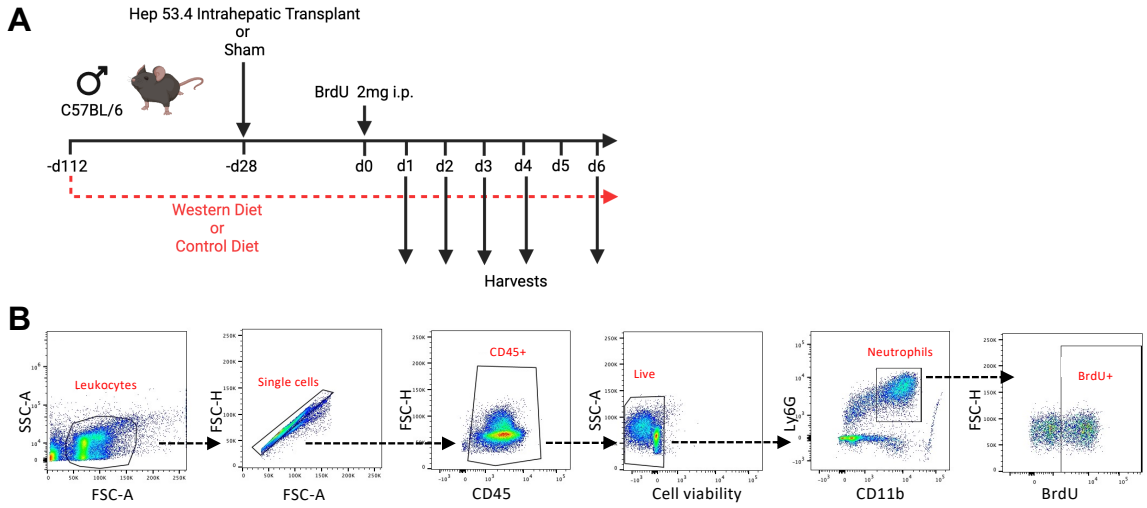



**Figure 3.6 – BrdU tracking experiment design and flow cytometry gating. A.** BrdU experiment overview. **B.** BrdU gating strategy.

## 3.13. Histology

### 3.13.1. Tissue processing and slide preparation

Following harvest as above; liver, tumour and spleen tissue was place into labelled cassettes and put in 10% formalin (Sigma-Aldrich, HT501128) for 24 hours. Following this formalin was replaced with 70% ethanol and left for another 24 hours. Tissues were then paraffin embedded with an automated tissue processor. Microscopy sides were prepared by cutting 5 µm tissue slices with a microtome and mounting them onto slides (Thermo scientific, 12312148, Epredia SuperFrost Plus).

### 3.13.2. Haematoxylin and Eosin (H&E) stain

Formalin fixed paraffin embedded (FFPE) 5 µm mounted slides were dewaxed in clearene for 5 minutes x2, then rehydrated in 100% ethanol, followed by 70% ethanol for 5 minutes each. Slides were then washed in running deionised water before being placed in Mayer Haematoxylin (Sigma-Aldrich, MHS32) for 5 minutes. Slides were then rinsed in deionised water and placed in Scott's water for 1 minute, then rinsed again in deionised water and placed in Eosin (Sigma-Aldrich, E4009) for 2 minutes, then washed three times in 100% ethanol. Slides were then transferred through a series of clearene washes each for 5 minutes then mounted with pertex (CellPath) and coverslips then left to dry.

### 3.13.3. Immunohistochemistry (IHC)

FFPE 5 µm mounted slides were dewaxed in clearene for 5 minutes x2, then rehydrated in 100% ethanol, followed by 70% ethanol for 5 minutes each. To block endogenous perixoidase activity slides were incubated in methanol with 0.6% hydrogen peroxidase (Sigma-Aldrich, H1009) for 15 minutes then washed in PBS. Various antigen retrieval techniques were used depending on the antibody used (table 3.7). To block endogenous avidin and biotin an avidin/biotin blocking kit was used (Vector, SP-2001) and to block non-specific binding 20% swine serum was added. Following this the primary antibody diluted in 20% swine serum was added at a pre-optimised concentration (table 3.7) and incubated overnight at 4°C. The following day slides were washed with PBS and incubated with a secondary biotinylated antibody at a pre-optimised concentration (table 3.7) for 1 hour at room temperature. Slides were then washed in PBS and incubated with Vectastain Elite ABC-HRP Reagent (Vector, PK-6100) for 45 minutes at room temperature. Following this staining was visualised using DAB substrate (3,3'-diaminobenzidine) as per the DAB Substrate Kit, Peroxidase Kit protocol (Vector, SK-4100). To counter stain slides were stained in Mayer haematoxylin followed by incubation in Scotts water. Finally slides were dehydrated through graded alcohols (50%, 75%, 100%, 100%) for 5 minutes each, transferred through clearene then mounted with pertex (CellPath) and coverslips then left to dry.

| Antigen | Antigen retrieval | Primary antibody | Secondary antibody |
|---|---|---|---|
| CD4 | Trish ETDA (pH9) + Tween, Microwave 20 minutes | Rabbit mAb to mouse CD4, EPR19514, abcam, 1/400 dilution | Goat anti-rabbit biotin conjugated, BA-1000-1.5, Vector, 1/600 dilution |
| CD8 | Trish ETDA (pH9) + Tween, Microwave 20 minutes | Rabbit mAb to mouse CD8, EPR21769, abcam, 1/1000 dilution | Goat anti-rabbit biotin conjugated, BA-1000-1.5, Vector, 1/600 dilution |
| Ly6G | Trish ETDA (pH9) + Tween, Microwave 20 minutes | Rabbit mAb to mouse Ly6G, E6Z1T, cell signalling, 1/2000 dilution | Goat anti-rabbit biotin conjugated, BA-1000-1.5, Vector, 1/600 dilution |
| αSMA | Citrate, Microwave 20 minutes | Mouse mAb to αSMA, FITC conjugated, 1A4, Sigma-Aldrich, 1/1000 dilution | Goat anti-FITC biotin conjugated, BA-0601-.5, Vector, 1/300 dilution |
| F4/80 | Trish ETDA (pH9) + Tween, Microwave 20 minutes | Rabbit mAb to mouse F4/80, D2S9R, cell signalling, 1/2000 dilution | Goat anti-rabbit biotin conjugated, BA-1000-1.5, Vector, 1/600 dilution |
| PD1 | Trish ETDA (pH9) + Tween, Microwave 20 minutes | Rabbit mAb to mouse PD1, EPR20665, abcam, 1/2000 dilution | Goat anti-rabbit biotin conjugated, BA-1000-1.5, Vector, 1/600 dilution |
| CD11c | Trish ETDA (pH9) + Tween, Microwave 20 minutes | Rabbit mAb to mouse CD11c, D1V9Y, cell signalling, 1/1000 dilution | Goat anti-rabbit biotin conjugated, BA-1000-1.5, Vector, 1/600 dilution |
| Ki67 | Trish ETDA (pH9) + Tween, Microwave 20 minutes | Rat mAb to Ki67, SolA15, Invitrogen, 1/20,000 dilution | Goat anti-rat biotin conjugated, BA-9400, Vector, 1/200 dilution |

**Table 3.7 – Antibodies used for immunohistochemistry along with corresponding antigen retrieval and dilutions**. mAb; monoclonal antibody.

### 3.13.4. Image analysis

All brightfield microscopy analysis was conducted using a Nikon Eclipse Upright microscope and NIS-Element BR (Nikon) analysis software. Cell counts were performed using the automatic object counter function. Pixel colour thresholds were set on areas of positive staining and restrictions based on area and circularity set to give a best fit object count. Once set this thresholding was saved and applied to all slides of the same stain. For liver and tumour cell count analysis a minimum of 10 images at 200x magnification were used per mouse. For H&E lipid analysis of liver and tumours a minimum of 10 images at 100x magnification were used per mouse. For tumour analysis images were taken bisecting across the whole width of the tumour in order to account for intratumorally heterogeneity.

### 3.14. Cell culture

Hep 53.4 cells (Cell Lines Service, 400200) are a hepatoma cell line derived from a primary HCC of a C57BL/6J mouse. Hep 53.4 cells were expanded in Dulbecco's Modified Eagle Medium -high glucose (DMEM) (Sigma-Aldrich, D5796) supplemented with 10% FBS, penicillin-streptomycin and L-glutamine at 37°C with 5% carbon dioxide and cryopreserved at a low passage number. For each tumour implantation experiment a fresh batch of Hep 53.4 cells was expanded. Cells were regular screened for mycoplasma infection using a PCR detection kit (Sigma-Aldrich, MP0035).

### 3.15. In vitro AZD1480 experiments

#### 3.15.1. In vitro effect of AZD1480 on leukocytes

Bone marrow, blood and spleen leukocytes were harvested and isolated from 4 C57BL/6J mice as above and plated into a 96 well round bottom plate in RPMI 1640 (Gibco, 11875101) with 2% FBS and IL-6 (Peprotech 216-16) at 5 μM. AZD1480 in Dimethylsulfoxide (DMSO) was added to test samples to give a final drug concentration of 5 μM. An equal volume of DMSO was added to control samples. Leukocytes were then incubated for 4 hours at 37°C with 5% carbon dioxide. Following incubation samples were washed with 1x DPBS- and stained with a panel of pre-optimised surface marker and intracellular phosphoflow antibodies as described above (table 3.5, panel 3).

#### 3.15.2. In vitro effect of AZD1480 on Hep 53.4 proliferation

Hep 53.4 cells were plated into a 24 well culture plate in at 50,000 cells per well in DMEM supplemented with 10% FBS, penicillin-streptomycin and L-glutamine and IL-6 (Peprotech 216-16) at 5 μM. For test samples AZD1480 in DMSO was added to give a final concentration of 5 μM, 10 μM and 50 μM. For control samples an equal volume of DMSO was added. Plates were incubated at 37°C with 5% carbon dioxide. Samples were taken at 0, 24, 48 and 72 hours for a resazurin assay to measure cell proliferation. Resazurin assays were performed by taking off the DMEM in the wells, adding 200 μl of resazurin diluted 1:10 in DMEM and incubating for 3 hours at 37°C with 5% carbon dioxide. Following this 50 μl of the resazurin in each well was then transferred to an

opaque 96 well plate and florescence read on a plate reader. The relative florescence unit (RFU) correlates to the degree of cellular proliferation.

### 3.16. Statistics

Statistical analysis for all data were conducted using GraphPad Prism version 9.5.1 for Mac (GraphPad). All data have been graphed as either bar graphs displaying mean +/- the standard error of the mean (SEM) or as box and whisker plots displaying median +/- interquartile range (IQR) with minimum and maximum. Sample numbers are detailed in each results figure. Where possible individual values have also been graphed to give a better representation of each data set. Before applying statical comparisons between groups normality was assessed to best decide the most appropriate statistical test. This was done both by looking at the distribution of each data set by eye and by applying normality tests such as D'Agostino-Pearson, Shapiro-Wilk, Anderson-Darling and Kolmogorov-Smirnov. To statistically compare the means of 3 or more unmatched groups defined by one factor with a normal distribution, a one-way analysis of variance (ANOVA) test was applied with a Tukey post-hoc test for multiple comparisons. If the data sets were not normally distributed, then a Kruskal-Wallis nonparametric test was applied with a Dunn's multiple comparisons test. To statistically compare the means of 2 unmatched groups with a normal distribution an unpaired t-test was applied. If the groups were not normally distributed a Mann-Whitney test was applied. p values of $<0.05$ were taken as statistically significant. The statistical test used in each analysis is outlined in the results figure legends.

# 4. Neutrophil heterogeneity and phenotype in hepatocellular carcinoma and chronic liver disease

## 4.1. Introduction

A growing body of evidence suggests that neutrophils are altered in states of chronic inflammation and that this can drive disease progression in cancer. In HCC the main mechanisms that neutrophils are thought to drive HCC progression are through suppression of anti-tumour immunity and promotion of tumour growth through the induction of extracellular matrix remodelling and angiogenesis as well as the direct enhancement of tumour cell invasiveness. Most studies in HCC are based on pre-clinical models which often fail to recapitulate the underlying liver disease and complex patient variability. Furthermore, recent studies suggest a greater degree of neutrophil heterogeneity than previously thought suggesting the existence of multiple neutrophil subtypes each with a different phenotype and role in pro-tumour or anti-tumour immunity.

To get a better understanding of the effects of HCC and CLD on neutrophil phenotype and heterogeneity I characterised circulating neutrophils from HCC and CLD patients as well as healthy controls. To get a better understanding of how neutrophils change when they enter the liver and tumours, I isolated neutrophils from surgical resections and biopsies of HCC patients.

## 4.2. Circulating immune cell characterisation

### 4.2.1. Patient clinical characterisation

In total 25 HCC patients, 16 CLD patients and 8 healthy controls were recruited and blood samples collected. The demographics of recruits are summarised in table 4.1. CLD and HCC patients recruited were similar in terms of gender (HCC 84% male, CLD 75% male), cirrhosis stage (Child-Pugh A/B/C %, HCC 85/12/0, CLD 92/8/0), aetiology of CLD (HCC 54% and CLD 44% MASLD or MetALD) and performance status (PS 0/1/2/3/4 %, HCC 36/52/4/8/0 and CLD 31/57/6/6/0). There were slight differences in age (median age HCC 73 vs CLD 60) and cirrhosis status (HCC 52% cirrhotic, CLD 75% cirrhotic). There was also a difference in age in the healthy control group with

them generally being younger compared to the HCC and CLD patients. For HCC patients there was a range of modes of presentation (surveillance/ Incidental/ symptomatic 32/32/36%), disease stage (BCLC stage A/B/C/D 44/28/20/8%) and treatments received.

| | | **HCC** | **CLD** | **Healthy control** |
|---|---|---|---|---|
| Number | | 25 | 16 | 8 |
| Age (median) | | 73 | 60 | 24-62 |
| Gender | Male | 21 (84) | 12 (75) | 4 (50) |
| | Female | 4 (16) | 4 (25) | 4 (50) |
| Cirrhosis | Yes | 13 (52) | 12 (75) | |
| | No | 12 (48) | 4 (25) | |
| Cirrhosis stage | A | 11 (85) | 11 (92) | |
| | B | 2 (15) | 1 (8) | |
| | C | 0 (0) | 0 (0) | |
| Aetiology | MASLD | 6 (25) | 4 (25) | |
| | ALD | 3 (13) | 7 (44) | |
| | MetALD | 7 (29) | 3 (19) | |
| | Hereditary haemochromatosis | 2 (8) | 2 (12) | |
| | Other | 6 (25) | 0 (0) | |
| ECOG PS | 0 | 9 (36) | 5 (31) | |
| | 1 | 13 (52) | 9 (57) | |
| | 2 | 1 (4) | 1 (6) | |
| | 3 | 2 (8) | 1 (6) | |
| | 4 | 0 (0) | 0 (0) | |
| BCLC stage | A | 11 (44) | | |
| | B | 7 (28) | | |
| | C | 5 (20) | | |
| | D | 2 (8) | | |
| Treatment | Ablation | 5 (20) | | |
| | Resection | 5 (20) | | |
| | TACE | 3 (12) | | |
| | SIRT | 2 (8) | | |
| | Atezo/bev | 3 (12) | | |

| | | | | |
|---|---|---|---|---|
| | Sorafenib | 2 (8) | | |
| | BSC | 5 (20) | | |
| HCC mode of presentation | Surveillance | 8 (32) | | |
| | Incidental | 8 (32) | | |
| | Symptomatic | 9 (36) | | |

**Table 4.1 – Demographics and clinical characteristics of patients**. number (%).

### 4.2.2. Gating strategy

The frequency of various immune populations was determined using flow cytometry analysis on whole blood. Immune populations were identified using the gating strategy outlined in figure 4.1. Leukocytes were first identified using the forward scatter area (FSC-A) and side scatter area (SSC-A) plot. This excludes debris which are low in both FSC-A and SSC-A. Next single cells were identified by selecting cells that had a proportional FSC-A to forward scatter height (FSC-H). Live cells were identified as being negative for the dead cell stain and immune cells identified as being $CD45^+$. Next monocytes were identified as being HLA-$DR^+$ and $CD11c^+$ and subsequently classical, intermediate, and non-classical monocyte subpopulations identified according to CD14 and CD16 expression. Basophils and plasmacytoid dendritic cells (pDCs) were identified on HLA-DR expression and as being $CD123^+$. Neutrophils were identified as being $CD15^+$ and siglec-$8^-$. Eosinophils were identified as being $CD15^+$ and siglec-$8^+$. B cells were identified as being $CD19^+$. T cells were identified as being $CD3^+$ and $CD56^-$ and classified as being $CD8^+$ or $CD4^+$. NK T cells were identified as being $CD3^+CD56^+$. Finally NK cells were identified as being $CD3^-CD56^+$. These populations were also identified on high dimensional t-SNE analysis.

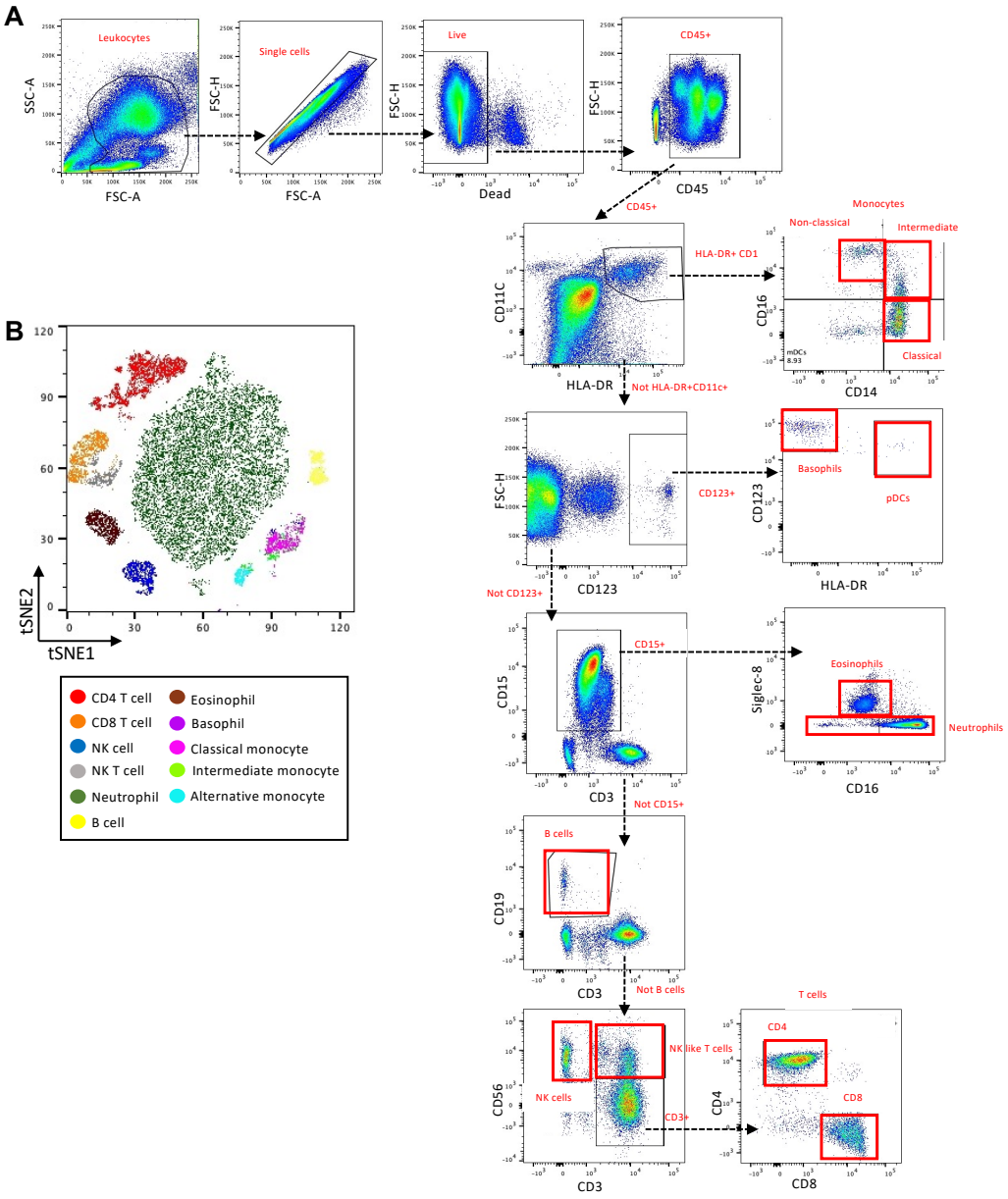



**Figure 4.1 – Gating strategy used for leukocyte populations in human whole blood. A.** Leukocytes were gated using FSC-A vs SSC-A. Single cells were gated using FSC-A vs FSC-H. Live cells were gated as being negative for the dead cell stain. Immune cells were gated on $CD45^+$. Monocytes were gated on CD11c and HLA-DR and categorised as being either classical, intermediate or non-classical based on CD14 and CD16 expression. Basophils and pDCs were gated on CD123 and HLA-DR expression. Neutrophils were gated on $CD15^+$ and siglec-$8^-$ and eosinophil on $CD15^+$ siglec-$8^+$. B cells were gated on $CD19^+$. T cells were gated as being $CD56^-$ and $CD3^+$ then separated into $CD8^+$ and $CD4^+$. NK T cells were gated on $CD3^+$ and $CD56^+$. NK cells were gated as $CD3^-$ $CD56^+$. **B**. These populations were also identified on high dimensional t-SNE analysis.

### 4.2.3. Circulating immune cell frequencies

Both CLD and HCC patients had a significantly higher frequency of circulating neutrophils compared to healthy controls (figure 4.2 A). CLD and HCC patients also had a significantly lower frequency of circulating T cells compared to healthy controls (Figure 4.2 B) with this being driven mainly by a reduction in CD8 compared to CD4 T cells (figure 4.2 C and D). There was also a trend to a reduction in circulating NK T cells in CLD and HCC compared to healthy controls (figure 4.2 E). There were no significant differences in circulating NK cells, basophils, eosinophils, B cells and monocyte populations between the groups (figure 4.2 F-L).

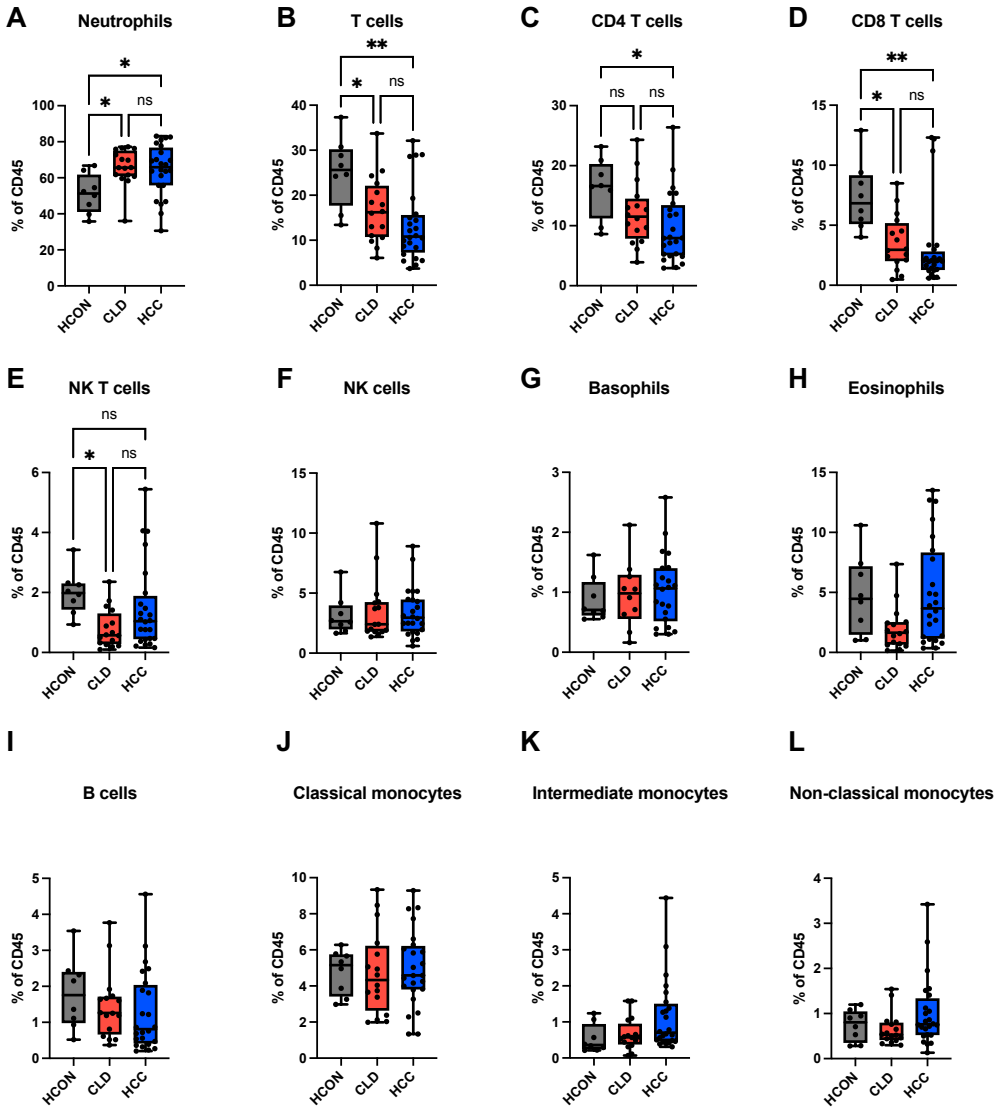



**Figure 4.2 – Frequency of circulating leukocyte populations in HCC patients, CLD patients and healthy controls**. Graphs showing the frequencies (% of $CD45^+$ cells) of **A**. Neutrophils. **B**. T cells. **C**. CD4 T cells. **D**. CD8 T cells. **E**. NK T cells. **F**. NK cells. **G**. Basophils. **H**. Eosinophils. **I**. B cells. **J**.

Classical monocytes. **K**. Intermediate monocytes. **L**. Non-classical monocytes. P values calculated using a one-way ANOVA with Tukey post-hoc test *p<0.05, **p<0.01, ***p<0.001, ns non-significant. HCON n=8, CLD n=16, HCC n=25.

### 4.3. Circulating neutrophil population frequencies

After identifying that the frequency of circulating neutrophils was increased in HCC and CLD the next step was to investigate circulating neutrophil heterogeneity. Based on the literature different circulating neutrophil populations can be isolated based on their density. Therefore, density separation was applied to blood samples and flow cytometry analysis conducted to assess for the presence of circulating neutrophil populations and their frequencies.

#### 4.3.1. Gating strategy

Density separation samples were stained with human panel 2, run through the flow cytometer and gated as per figure 4.3. Granulocytes were identified based on their high granularity (SSC) on FSC-A vs SSC-A. Single cells were identified by selecting cells that had a proportional FSC-A to FSC-H. Live cells were identified as being dead stain negative. Eosinophils were then excluded by gating for siglec-8 negative cells. Neutrophils were identified as being $CD15^{+}$.

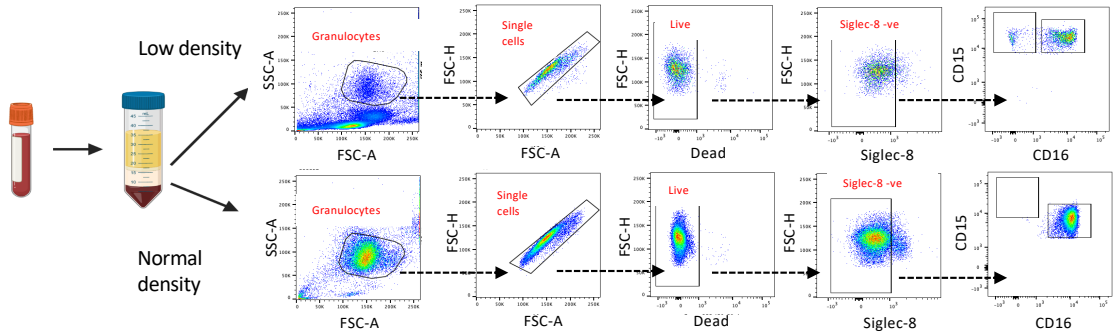



**Figure 4.3 – Neutrophil density separation gating strategy**. Granulocytes were gated based on FSC-A vs SSC-A as being the population of high granularity. Single cells were gated using FSC-A vs FSC-H. Live cell were gated by gating dead stain negative cells. Eosinophil were excluded out by gating for siglec-8 negative cells. Neutrophils were then gated as being $CD15^{+}$.

#### 4.3.2. Frequencies of circulating neutrophil populations

Neutrophils were identified in both the normal-density and low-density fractions. In the low-density fraction 2 populations of low-density neutrophils were identified based on

CD16 expression: low density CD16 high (LD CD16$^{high}$) and low density CD16 low (LD CD16$^{low}$) (figure 4.4 A). The frequency of LD CD16$^{low}$ neutrophils was unchanged between healthy controls, CLD patients and HCC patients (figure 4.4 B). There was a significant increase in the frequency of LD CD16$^{high}$ neutrophils in both CLD patients and HCC patients compared to healthy controls (figure 4.4 C). The frequency of ND neutrophils was the same between groups (figure 4.4 D). This suggests that the increased frequency of circulating neutrophils in CLD and HCC patients compared to healthy controls is being driven by an expansion of the LD CD16$^{high}$ neutrophil population.

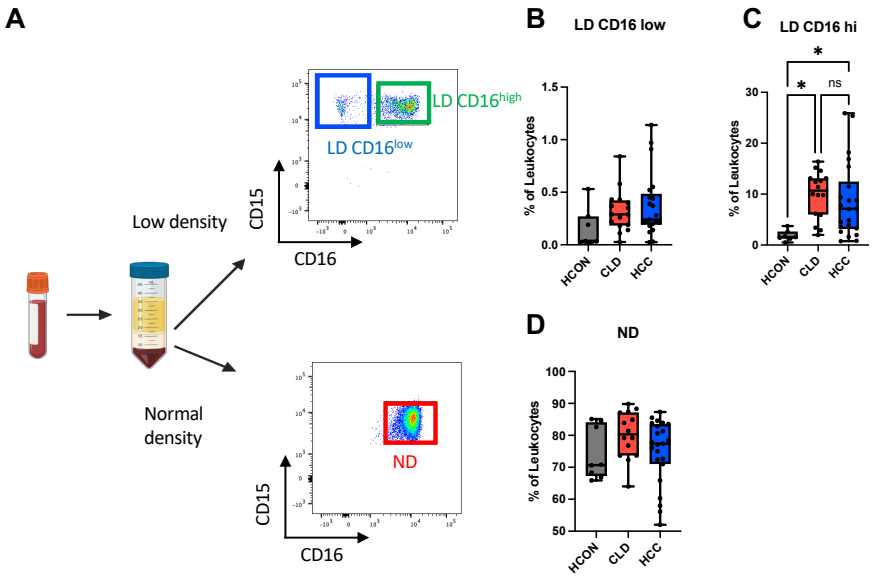



**Figure 4.4 – Neutrophil populations following density separation. A**. Representative plots showing the 3 circulating neutrophil populations. The low density (LD) CD16 low (LD C16$^{low}$), LD CD16$^{high}$ and normal density (ND) neutrophils. **B**. Quantification of LD CD16$^{low}$ neutrophil frequency. **C**. Quantification of LD CD16$^{high}$ neutrophil frequency. **D**. Quantification of ND neutrophil frequency. P values calculated using a one-way ANOVA with Tukey post-hoc test *p<0.05, **p<0.01, ***p<0.001, ns non-significant. HCON n=8, CLD n=16, HCC n=25.

## 4.4. Focused characterisation of circulating neutrophil populations

The next step was to conduct a focused morphological, phenotypic and functional assessment of these populations to determine their relevance in the context of CLD and HCC.

### 4.4.1. Nuclear morphology and immunofluorescence analysis

Cytospins of FACS sorted LD CD16$^{low}$, LD CD16$^{high}$ and ND populations were collected and stained (figure 4.5 A). All populations were confirmed to be neutrophils as indicated by their myeloperoxidase expression (figure 4.5 B). Each population had a very different nuclear morphology. ND neutrophils had a typical mature neutrophil appearance with a segmented nucleus with 2-3 lobes and occasional band nucleus (figure 4.5 B). LD CD16$^{high}$ neutrophils had a mature-aged nuclear morphology with typically hypersegmented nuclei (figure 4.5 B). On the other hand, LD CD16$^{low}$ neutrophils had an immature, neutrophil precursor morphology with a large oval nucleus (figure 4.5 B). This was confirmed on quantitative analysis of nuclear morphology showing that ND neutrophils mostly had 2-3 nuclear lobes (figure 4.5 C) whereas LD CD16$^{high}$ neutrophils mostly had 2-3 or >4 nuclear lobes (figure 4.5 D). This suggests that LD CD16$^{low}$ neutrophils are likely immature neutrophil progenitors, ND neutrophils are mature, resting neutrophils and LD CD16$^{high}$ neutrophils are activated, aged neutrophils.

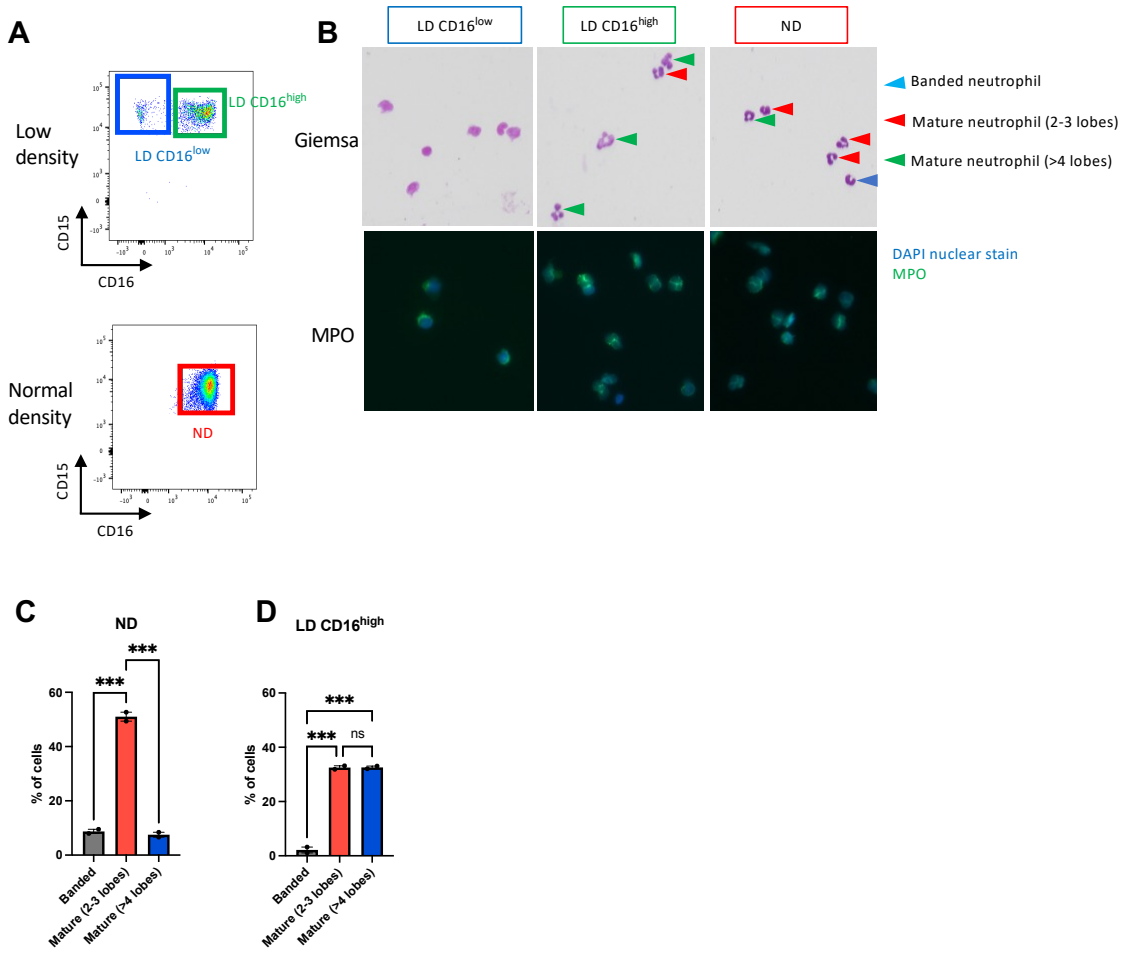


**Figure 4.5 – LD CD16$^{low}$, LD C16$^{high}$ and ND neutrophil morphology and MPO expression. A.** Representative flow cytometry plots of circulating neutrophil populations. **B**. Representative giemsa and immunofluorescence MPO staining of circulating neutrophil populations. **C-D**. Quantification of nuclear morphology and number of nuclear lobes in LD CD16$^{high}$ and ND neutrophil populations. P values calculated using a one-way ANOVA with Tukey post-hoc test *p<0.05, **p<0.01, ***p<0.001, ns non-significant. n=2.

### 4.4.2. Phenotype

Circulating neutrophil populations were then phenotyped using a focused flow cytometry panel (human panel 2). Unbiased high dimensional analysis demonstrated that the circulating neutrophil populations clustered separately on UMAP analysis (figure 4.6 A) with differential expression of CD16, CD15, CXCR2, CXCR4, CD66b, CD11b, CD10 and CD62L (figure 4.6 B). Quantitative analysis of relative expression (presented as MFIs) of various maturation markers, activation markers and chemokine receptors showed significant differences in expression between circulating neutrophil populations. LD CD16$^{low}$ neutrophils expressed significantly less CD16 compared to LD CD16$^{high}$ neutrophils and ND neutrophils (figure 4.6 C). Both LD CD16$^{high}$ and LD CD16$^{low}$ neutrophils expressed more CD15 than ND neutrophils (figure 4.6 D). LD CD16$^{low}$ neutrophils expressed more CD66b than LD CD16$^{high}$ and ND neutrophils (figure 4.6 E). LD CD16$^{high}$ neutrophils expressed more CD11b than LD CD16$^{low}$ and ND neutrophils (figure 4.6 F). LD CD16$^{high}$ neutrophils expressed more CD10 than LD CD16$^{low}$ and ND neutrophils, ND neutrophils expressed more CD10 than LD CD16$^{low}$ neutrophils (figure 4.6 G). ND neutrophils expressed more CD62L than LD CD16$^{high}$ and LD CD16$^{low}$ neutrophils, LD CD16$^{high}$ neutrophils expressed more CD62L than LD CD16$^{low}$ neutrophils (figure 4.6 H). ND neutrophils expressed more CXCR2 than LD CD16$^{high}$ and LD CD16$^{low}$ neutrophils, LD CD16$^{high}$ neutrophils expressed more CXCR2 than LD CD16$^{low}$ neutrophils (figure 4.6 I). There were no differences in CXCR4 expression (figure 4.6 J). LD CD16$^{low}$ neutrophils expressed more PDL1 than both LD CD16$^{high}$ and ND neutrophils (figure 4.6 K). There was no difference in SIRP$\alpha$ expression (figure 4.6 L) or mitochondrial mass as assessed by mitotracker orange staining (figure 4.6 M). There was no difference in neutrophil phenotype between HCC patients, CLD patients and healthy controls (data not shown).

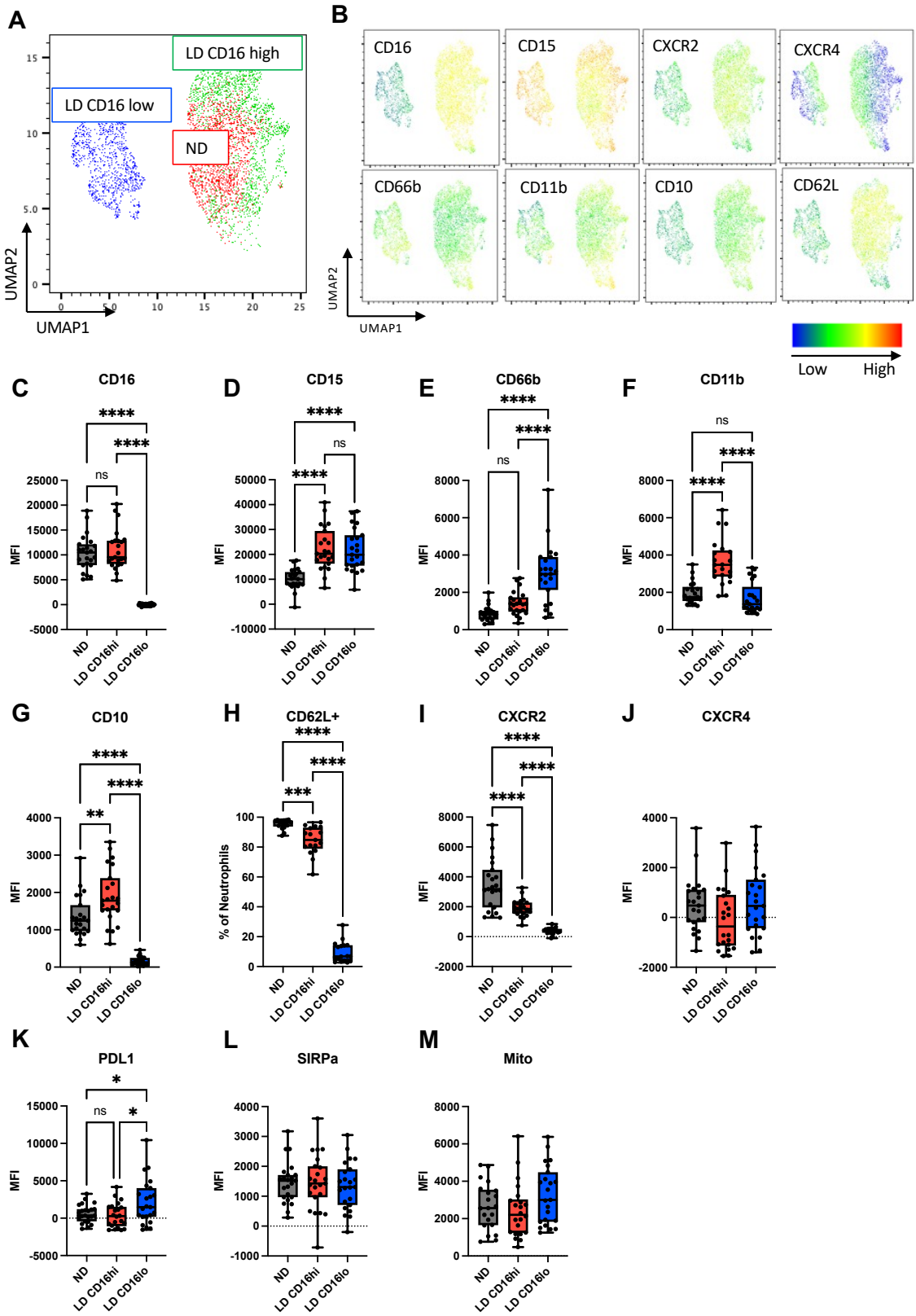



**Figure 4.6 – Phenotypical analysis of circulating neutrophil populations. A**. Unbiased high dimensional UMAP analysis of circulating neutrophil population phenotype, demonstrating distinct phenotypes as represented by the unique clustering of each population. **B**. Heatmap of CD16, CD15, CXCR2, CXCR4, CD66b, CD11b, CD10 and CD62L overlaid on UMAP populations. **C**. Quantification

CD16 expression. **D**. Quantification of CD15 expression. **E**. Quantification of CD66b expression. **F**. Quantification of CD11b expression. **G**. Quantification of CD10 expression. **H**. Quantification of CD62L expression (% positive neutrophils). **I**. Quantification of CXCR2 expression. **J**. Quantification of CXCR4 expression. **K**. Quantification of PDL1 expression. **L**. Quantification of SIRP$\alpha$ expression. **M**. Quantification of mitotracker orange staining, which is a measure for mitochondrial mass. P values calculated using a one-way ANOVA with Tukey post-hoc test *p<0.05, **p<0.01, ***p<0.001, ****p<0.0001, ns non-significant. HCON n=8, CLD n=16, HCC n=25.

### 4.4.3. Functional assays

To assess functional differences between the different circulating neutrophil populations a sub-cohort of HCC patient, CLD patient and healthy control blood was collected, neutrophils isolated and various functional assays performed. On assessing ROS activity LD CD16$^{high}$ neutrophils had significantly less basal ROS activity than LD CD16$^{low}$ and ND neutrophils (figure 4.7 A and C). Whereas LD CD16$^{high}$ neutrophils had significantly more PMA stimulated ROS activity compared to LD CD16$^{low}$ and ND neutrophils (figure 4.7 B and C). On assessing phagocytosis both ND and LD CD16$^{high}$ neutrophils had a high phagocytosis capacity, whereas LD CD16$^{low}$ neutrophils had a significantly lower phagocytosis capacity (figure 4.7 D and E). On assessing ability to migrate to various chemokines ND neutrophils had the greatest migration to CXCL2 and CXCL1, 3, 6, 7 and 8 (figure 4.7 F and G). LD CD16$^{high}$ neutrophils had a smaller migration to these chemokines whereas LD CD16$^{low}$ neutrophils had very low migration (figure 4.7 F and G). There were no differences in migration to CXCL12 (figure 4.7 H).

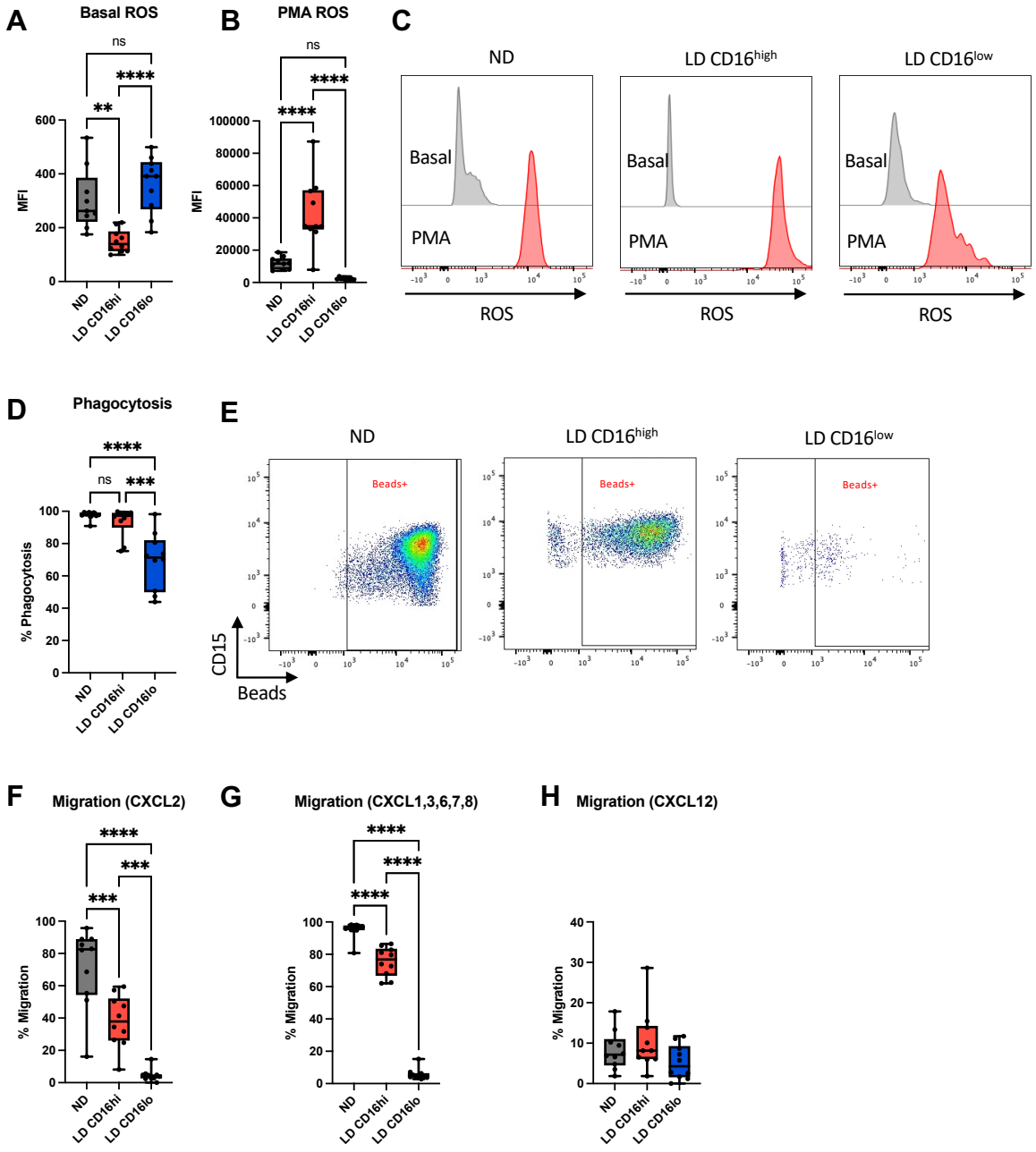



**Figure 4.7 – Circulating neutrophil population functional assays. A.** Quantification of basal ROS activity as assessed by DHR 123. **B**. Quantification of PMA stimulated ROS activity as assessed by DHR 123. **C**. Representative histograms showing MFI of basal and stimulated ROS as assessed by DHR 123 in the circulating neutrophil populations. **D**. Quantification of phagocytosis capacity of each circulating neutrophil populations, shown as percentage of neutrophils positive for phagocytosis beads. **E**. Representative scatter plots of circulating neutrophil populations and phagocytosis bead positivity. **F**. Quantification of neutrophil migration to CXCL2. **G**. Quantification of neutrophil migration to CXCL1, CXCL3, CXCL6, CXCL7 and CXCL8. **H**. Quantification of neutrophil migration to CXCL12. P values calculated using a one-way ANOVA with Tukey post-hoc test *p<0.05, **p<0.01, ***p<0.001, ****p<0.0001, ns non-significant. n=10.

### 4.5. Unbiased characterisation of circulating neutrophil populations

To further investigate the identity and phenotype of the circulating neutrophil populations I used the LEGENDScreen assay. This is an unbiased approach which analyses the expression of 361 cell surface markers. From this data I was able to compare the expression of each of these surface markers between the different circulating neutrophil populations.

#### 4.5.1. LEGENDScreen LD CD16$^{high}$ vs ND comparison

Comparison between LD CD16$^{high}$ vs ND populations (figure 4.8 A) demonstrated 9 markers with a greater than 1.5 fold increased expression in LD CD16$^{high}$ vs ND populations and 6 markers with a less than 0.8 fold increase in LD CD16$^{high}$ vs ND populations (figure 4.8 B). CD41, CD61, CD9 and CD36 were greater expressed on LD CD16$^{high}$ neutrophils and are typical platelet markers. CD33 and LOX-1 have previously been described as markers of PMN-MDSCs.[146,148] Increased CD63 expression is a known marker of neutrophil degranulation.[367] As demonstrated in the targeted flow cytometry analysis CXCR2 and CD62L were confirmed as being lowly expressed on LD CD16$^{high}$ neutrophils compared to ND neutrophils. Again, reduced CD62L expression is a known marker of neutrophil degranulation.[367] Gene set enrichment analysis (GSEA) of the 9 most upregulated markers in the LD CD16$^{high}$ population highlighted neutrophil degranulation and neutrophil activation as being key pathways upregulated by these markers (figure 4.8 C). The upregulation of CD41, CD36 and LOX-1 in LD CD16$^{high}$ neutrophils compared to ND neutrophil was confirmed in a separate cohort of healthy volunteer samples (figure 4.8 D-F). Taken together these results suggest that LD CD16$^{high}$ neutrophils are aged and activated neutrophils which have undergone some degree of degranulation (hyper-segmented morphology, CXCR2$^{high}$, CXCR4$^{low}$, CD66b$^{high}$, CD63$^{high}$, CD62L$^{low}$, CD10$^{high}$, CD11b$^{high}$) and are the population described by others as PMN-MDSCs (CD33$^{+}$, LOX-1$^{+}$) and may contain neutrophil platelet aggregates (NPAs) (CD41$^{+}$, CD61$^{+}$, CD36$^{+}$, CD9$^{+}$).

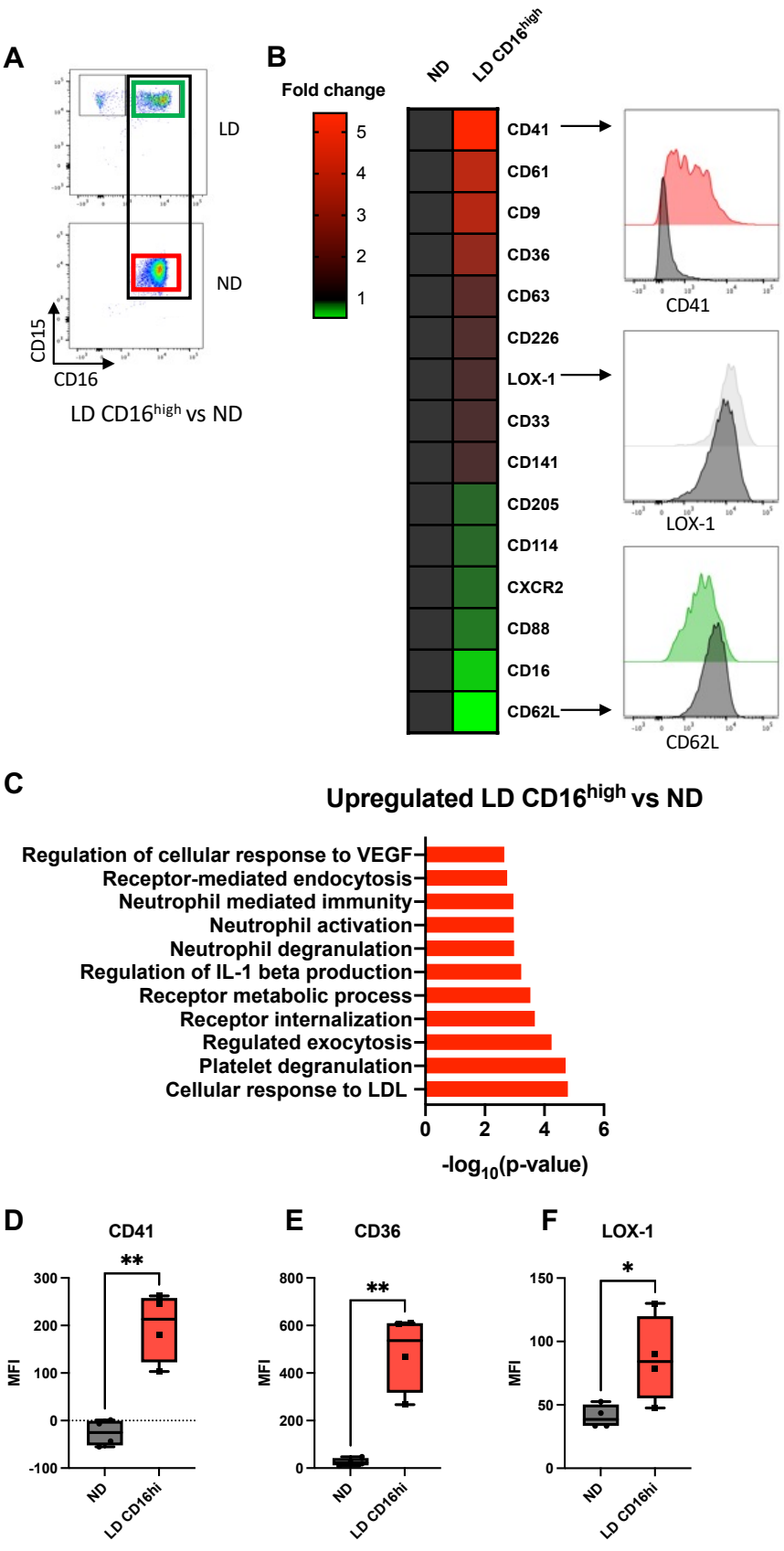



**Figure 4.8 – LEGENDScreen comparison LD CD16$^{high}$ vs ND neutrophils. A.** Representative scatter plots of LD CD16$^{high}$ vs ND neutrophil populations. **B.** Heatmap demonstrating surface markers with a greater than 1.5 fold increased expression or less than 0.8 fold increased expression in LD CD16$^{high}$ vs

ND neutrophils, along with representative histogram plots. **C**. Gene set enrichment analysis (GSEA) showing top 11 GO Biological Process pathways (Enrichr) represented as log10 of P-value. **D**. Quantification of CD41 expression on a separate cohort of healthy volunteer blood, n=4. **E**. Quantification of CD36 expression on a separate cohort of healthy volunteer blood, n=4. **F**. Quantification of LOX-1 expression on a separate cohort of healthy volunteer blood, n=4. P values calculated using an unpaired t-test *p<0.05, **p<0.01, ***p<0.001, ****p<0.0001, ns non-significant.

### 4.5.2. Neutrophils expressing CD41 and CD36 are neutrophil-platelets aggregates

Neutrophils do not usually express CD41, CD61, CD9 or CD36. Typically, these are platelets markers. Therefore, to further investigate a separate cohort of healthy volunteer blood was analysed. This confirmed that both CD41 and CD36 are more highly expressed on LD CD16$^{high}$ neutrophils compared to ND neutrophils and that they are co-expressed (figure 4.9 A-C). An explanation for expression of platelet markers on neutrophils is the presence of neutrophil-platelet aggregates (NPAs).[368] To confirm this the ImageStream system was utilised to visually confirm the presence of NPAs. This demonstrated the presence of NPAs in LD CD16$^{high}$ neutrophils on both brightfield and antibody immunofluorescence (figure 4.9 D-E).

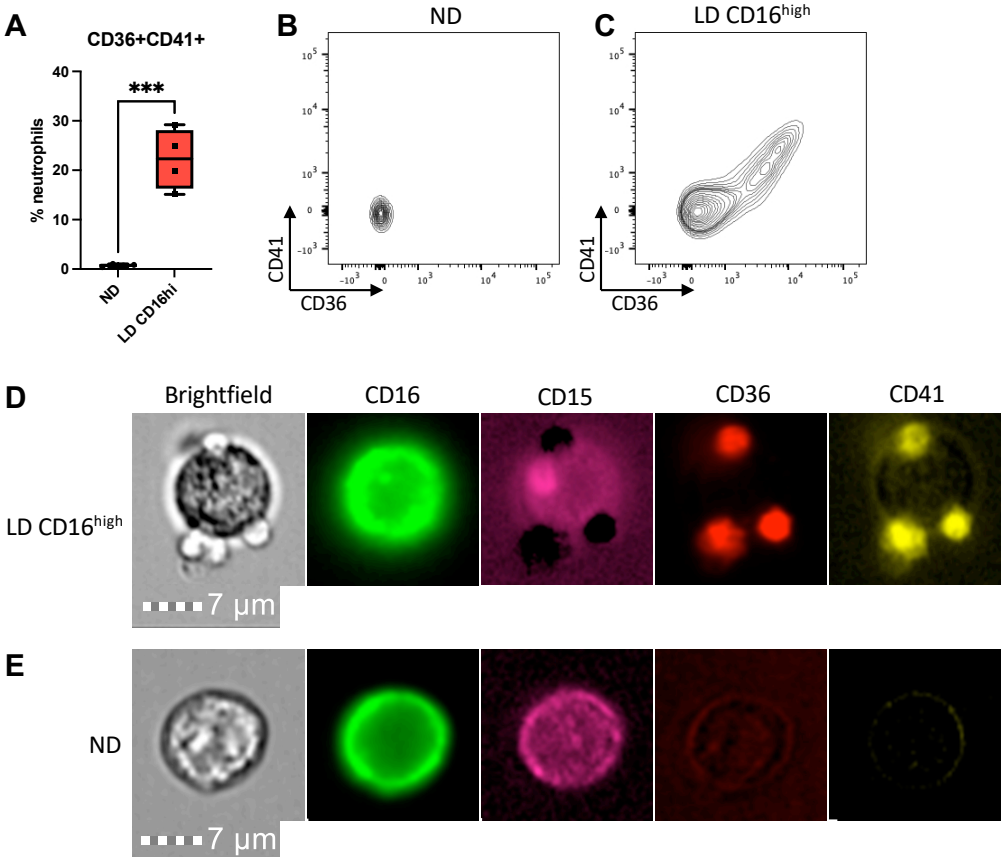



**Figure 4.9 – Confirmation of neutrophil-platelet aggregates in LD CD16$^{high}$ neutrophils. A**. Quantification of CD36 and CD41 co-expression in a cohort of healthy volunteers, n=4. **B**. Representative scatter plot demonstrating lack of CD36$^{+}$CD41$^{+}$ ND neutrophils. **C**. Representative scatter plot demonstrating presence of CD36$^{+}$CD41$^{+}$ LD CD16$^{high}$ neutrophils. **D**. Representative brightfield, CD16, CD15, CD36 and CD41 antibody florescence ImageStream images (60x magnification) of LD CD16$^{high}$ neutrophils. **E**. Representative brightfield, CD16, CD15, CD36 and CD41 antibody florescence ImageStream images (60x magnification) of ND neutrophils. P values calculated using an unpaired t-test *p<0.05, **p<0.01, ***p<0.001, ****p<0.0001, ns non-significant.

### 4.5.3. LEGENDScreen LD CD16$^{high}$ vs LD CD16$^{low}$ comparison

Comparison between LD CD16$^{low}$ vs LD CD16$^{high}$ neutrophil populations (figure 4.10 A) demonstrated 38 markers with a greater than 1.5 fold increased expression in LD CD16$^{low}$ vs LD CD16$^{high}$ neutrophil populations and 55 markers with a less than 0.8 fold increase in LD CD16$^{low}$ vs LD CD16$^{high}$ (figure 4.10 B-C). GSEA of the 38 most upregulated markers in the LD CD16$^{low}$ vs LD CD16$^{high}$ neutrophils highlighted neutrophil myeloblast, megakaryocyte and haematopoietic stem cell pathways as being up regulated (figure 4.10 D). GSEA of the 55 most downregulated markers in the LD CD16$^{low}$ vs LD CD16$^{high}$ neutrophils highlighted secretory granules, specific

granules, tertiary granules and platelet granules as being down regulated (figure 4.10 E). The down regulation of platelet granules is likely explained by lack of LD $CD16^{low}$ CD36, CD41, CD61 and CD9 expression, indicating the absence of NPAs. Taken together this suggests that the LD $CD16^{low}$ population are immature precursor neutrophils. Given their large oval nucleus, their cell surface marker expression ($CD16^{low}$, $CD15^{high}$, $CD49d^{+}$, $CXCR2^{low}$, $CXCR4^{high}$ and $CD10^{low}$), lack of specific, secretory and tertiary granules and reduced migratory and phagocytic function they are most likely promyelocytes.

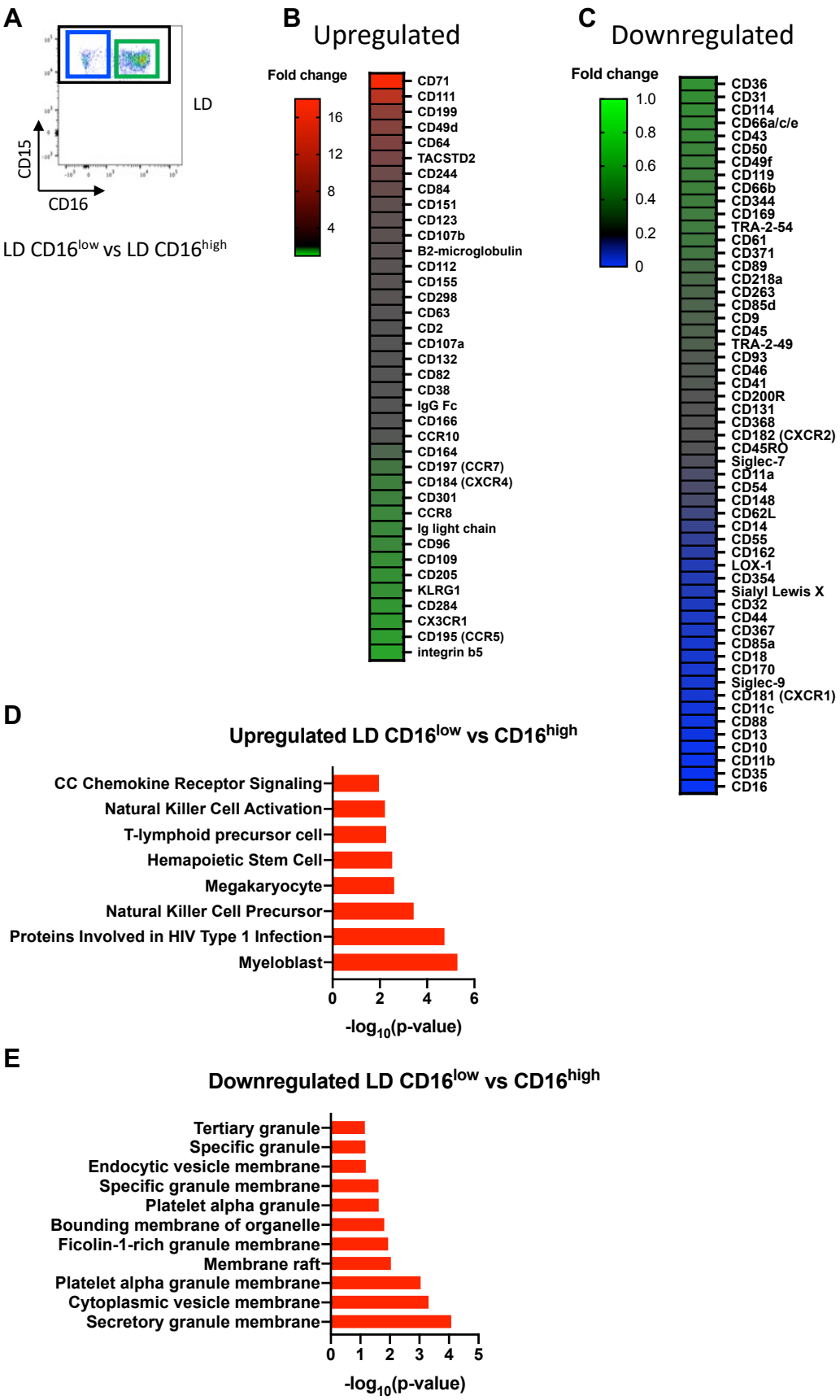



**Figure 4.10 – LEGENDScreen comparison LD CD16$^{low}$ vs LD CD16$^{high}$. A.** Representative scatter plots of LD CD16$^{low}$ vs LD CD16$^{high}$ neutrophil populations. **B.** Heatmap demonstrating surface markers

with a greater than 1.5 fold increased expression in LD CD16$^{low}$ vs LD CD16$^{high}$ neutrophils. **C.** Heatmap demonstrating surface markers with a less than 0.8 fold increased expression in LD CD16$^{low}$ vs LD CD16$^{high}$ neutrophils. **D**. GSEA of the 38 most upregulated surface markers in LD CD16$^{low}$ vs LD CD16$^{high}$ neutrophils showing GO Biological Process pathways (Enrichr) represented as log10 of P-value. **E**. GSEA of the 55 most down regulated surface markers in LD CD16$^{low}$ vs LD CD16$^{high}$ neutrophils showing GO Biological Process pathways (Enrichr) represented as log10 of P-value.

### 4.6. Dynamic characterisation of circulating neutrophil populations

To further test whether ND neutrophils are mature resting neutrophils and LD CD16$^{high}$ neutrophils are activated/aged/degranulated neutrophils an in vitro stimulation experiment was conducted. This gave a read out of the effects of both time and activation on neutrophil density and phenotype.

#### 4.6.1. Effects of PMA stimulation on neutrophil density and phenotype

To assess the effects of neutrophil activation on neutrophil density and phenotype PMA was added to whole blood. Whilst unstimulated blood mainly consisted of ND neutrophils, PMA stimulated blood mainly consisted of LD CD16$^{high}$ neutrophils (figure 4.11 A-B). This suggests that following stimulation ND neutrophils become LD CD16$^{high}$ neutrophils. This was further validated in a cohort of healthy volunteer blood in which isolated ND neutrophils were stimulated with PMA and then phenotyped. This demonstrated that ND neutrophils took on a LD CD16$^{high}$ phenotype following PMA stimulation as demonstrated by an increased expression of CD15 and CD11b, a decrease in CD62L and CXCR2 expression, and an increase in CXCR4 expression (figure 4.11 C-G).

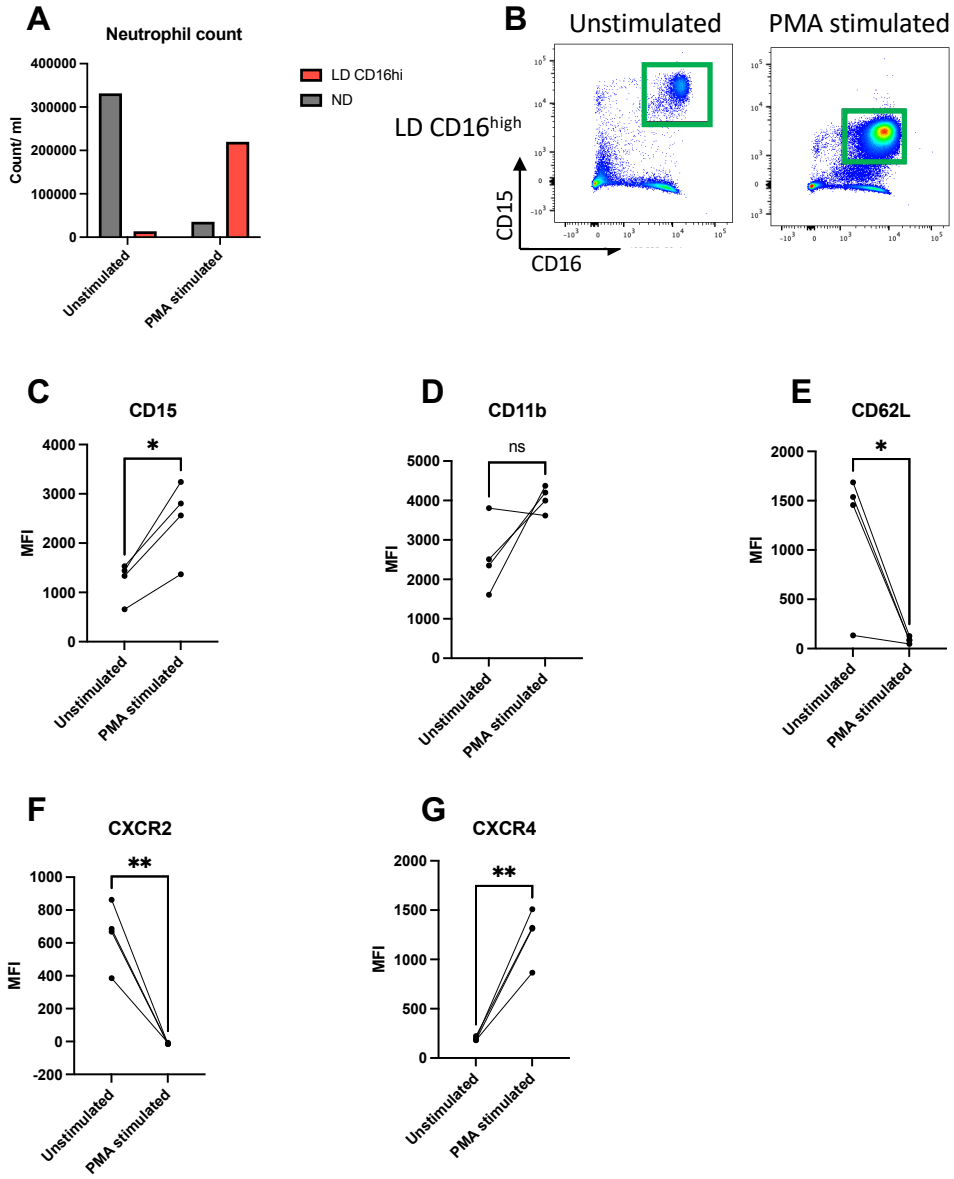



**Figure 4.11 – Effects of PMA stimulation on neutrophil density and phenotype. A.** Quantification of the number of ND and LD CD16$^{high}$ neutrophils isolated from unstimulated vs PMA stimulated whole blood, n=1. **B**. Representative scatter plots of LD CD16$^{high}$ neutrophils isolated from unstimulated and PMA stimulated whole blood. **C**. CD15 expression of unstimulated vs PMA stimulated ND neutrophils, n=4. **D**. CD11b expression of unstimulated vs PMA stimulated ND neutrophils, n=4. **E**. CD62L expression of unstimulated vs PMA stimulated ND neutrophils, n=4. **F**. CXCR2 expression of unstimulated vs PMA stimulated ND neutrophils, n=4. **G**. CXCR4 expression of unstimulated vs PMA stimulated ND neutrophils, n=4. P values calculated using an unpaired t-test *p<0.05, **p<0.01, ***p<0.001, ****p<0.0001, ns non-significant.

### 4.6.2. Effects of time and ageing on neutrophil density and phenotype

To assess the effects of time and ageing on neutrophil density and phenotype an isolation timecourse experiment was conducted. Blood was collected from 4 healthy volunteers and aliquots density separated at 0, 4 and 8 hours (figure 4.12 A). The number of LD CD16$^{high}$ neutrophils increased throughout the timecourse. There was a small insignificant increase between 0-4 hours but a large statistically significant increase between 4-8 hours (figure 4.12 B-C). This suggests that as a result of neutrophil ageing and time ND neutrophils become LD CD16$^{high}$ neutrophils. The phenotype of the LD CD16$^{high}$ neutrophils also changed throughout the timecourse (figure 4.12 D-M). Interestingly their phenotype became more like ND neutrophils with a reduction in CD16, CD15, CXCR2, CD66b, CD11b, CD10, CD41 and CD36 expression throughout the time course (figure 4.12 D-M). The change in ND neutrophil phenotype was not as dramatic (figure 4.12 N-W). Although ND neutrophil did become more aged and degranulated as shown by increased CXCR4 expression and reduced CD62L expression respectively (figure 4.12 Q-R). Interestingly ND neutrophil CD11b expression decreased during the timecourse which is the opposite to the effect of PMA stimulation (figure 4.12 T and figure 4.11 D). This suggests that the effects of time/ageing and PMA stimulation are different although they both induce transformation of ND neutrophils to LD CD16$^{high}$ neutrophils.

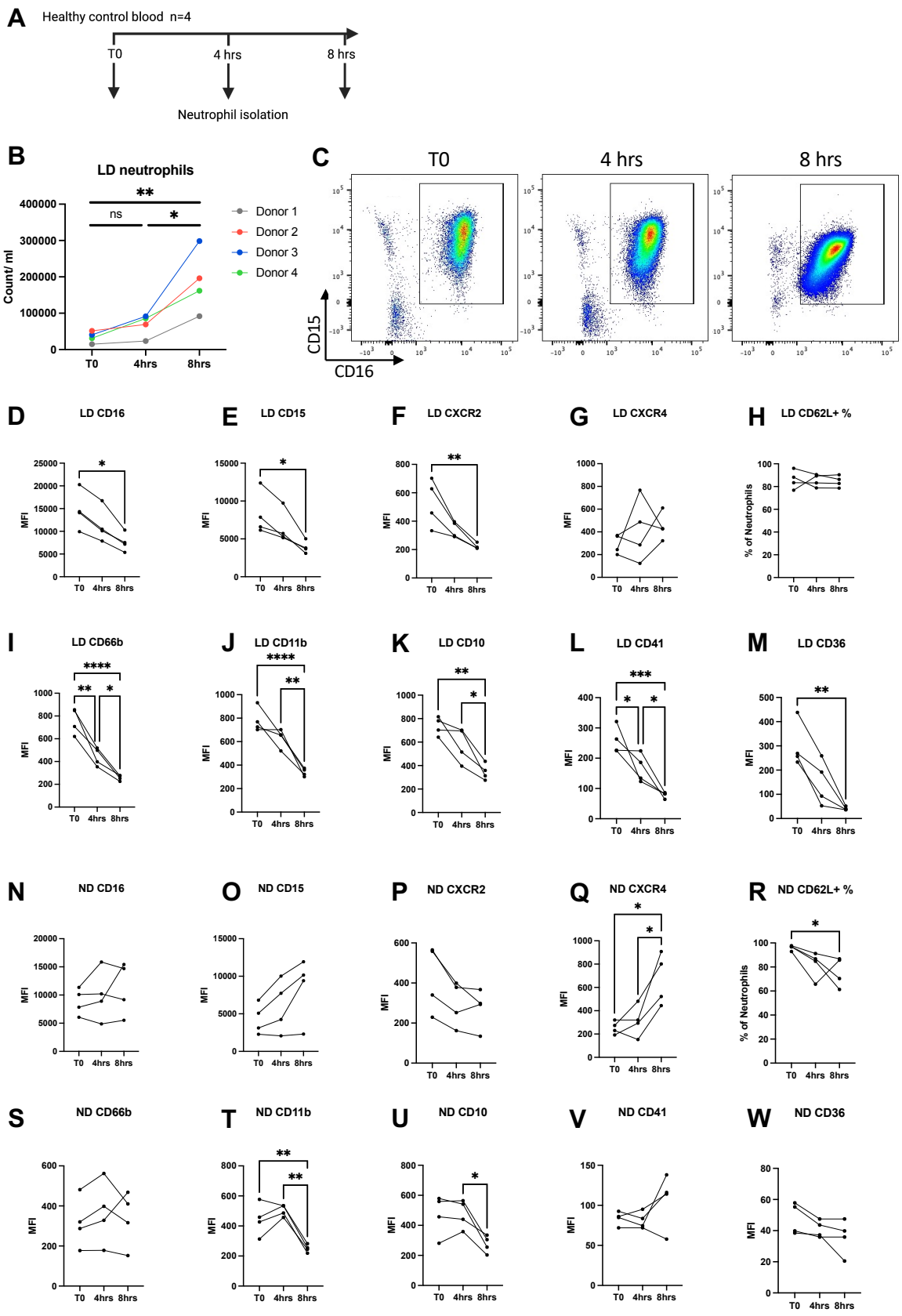



**Figure 4.12 – Effects of time and ageing on neutrophil density and phenotype. A.** Timecourse experiment design. **B**. Quantification of LD CD16$^{high}$ neutrophil count during timecourse. **C**. Representative scatter plots of LD CD16$^{high}$ population during timecourse. **D-M**. LD CD16$^{high}$ neutrophil

phenotype during timecourse showing CD16, CD15, CXCR2, CXCR4, CD62L, CD66b, CD11b, CD10, CD41 and CD36 expression. **N-W**. ND neutrophil phenotype during timecourse showing CD16, CD15, CXCR2, CXCR4, CD62L, CD66b, CD11b, CD10, CD41 and CD36 expression. P values calculated using a one-way ANOVA with Tukey post-hoc test *p<0.05, **p<0.01, ***p<0.001, ****p<0.0001, ns non-significant. n=4.

## 4.7. Neutrophil phenotype and function in healthy controls versus CLD and HCC patients

Next neutrophils were phenotypically and functionally compared between healthy controls, CLD and HCC patients.

### 4.7.1. Neutrophil phenotype

Comparing ND neutrophils both CLD and HCC neutrophils had a significantly lower expression of CXCR2 compared to healthy control neutrophils (figure 4.13 A). CLD neutrophils had significantly lower expression of CXCR4 compared to HCC and healthy control neutrophils (figure 4.13 B). HCC neutrophils had a significantly increased expression of CD15 compared to CLD and healthy control neutrophils (figure 4.13 C). HCC neutrophils had a significantly reduced expression of PDL1 compared to CLD neutrophils (figure 4.13 D). There were no differences in CD66b, CD11b, CD10, CD62L, SIRPα and mitochondrial mass (figure 4.13 E-J).

Comparing LD $CD16^{high}$ neutrophils both CLD and HCC neutrophils had a significantly lower expression of CXCR2 compared to healthy control neutrophils (figure 4.13 K). HCC neutrophils had a significantly higher expression of CXCR4 compared to CLD and healthy control neutrophils (figure 4.13 L). HCC neutrophils had a significantly increased expression of CD15 compared to CLD neutrophils (figure 4.13 M). CLD neutrophils had a significantly increased expression of PDL1 compared to HCC and healthy control neutrophils (figure 4.13 N). There was no difference in CD66b, CD11b, CD10, CD62L, SIRPα and mitochondrial mass (figure 4.13 O-T).

From these comparisons CXCR2 expression stands out as being reduced in both ND and LD $CD16^{high}$ neutrophils in HCC patients compared to CLD patients and healthy controls (figure 4.13 A, K, U).

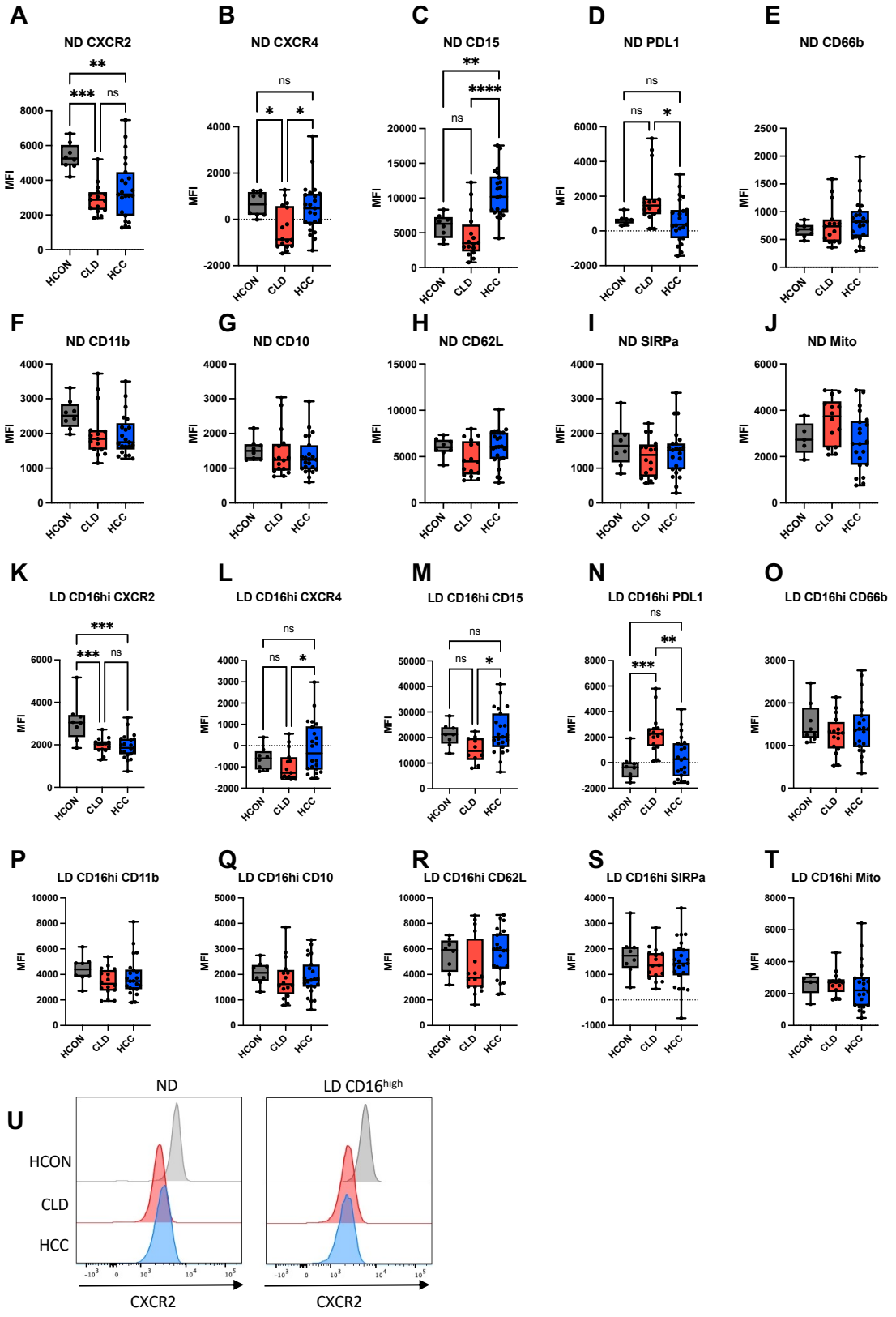



**Figure 4.13 – Neutrophil phenotype in HCC patients, CLD patients and healthy controls. A-J.** Quantification of CXCR2, CXCR4, CD15, PDL1, CD66b, CD11b, CD10, CD62L, SIRPα and MitoTracker™ Orange CMTMRos expression in ND neutrophils. **K-T.** Quantification of CXCR2, CXCR4,

CD15, PDL1, CD66b, CD11b, CD10, CD62L, SIRPα and MitoTracker™ Orange CMTMRos expression in LD CD16$^{high}$ neutrophils. **U**. Representative histograms of CXCR2 expression on ND and LD CD16$^{high}$ neutrophils in HCC, CLD and healthy controls (HCON). P values calculated using a one-way ANOVA with Tukey post-hoc test *p<0.05, **p<0.01, ***p<0.001, ****p<0.0001, ns non-significant. HCON n=8, CLD n=16, HCC n=25.

### 4.7.2. Neutrophil functional assays

In the ND population there was no difference in basal or PMA stimulated ROS between HCC, CLD and healthy control neutrophils (figure 4.14 A-B). In the LD CD16$^{high}$ population there was no difference in basal or PMA stimulated ROS between HCC, CLD and healthy control neutrophils (figure 4.14 C-D).

In the ND population there was no difference in phagocytosis ability between HCC vs CLD vs healthy control neutrophils (figure 4.14 E). In the LD CD16$^{high}$ population there was a significantly reduced phagocytosis activity in HCC neutrophils compared to CLD an healthy control neutrophils (figure 4.14 F).

In the ND population HCC neutrophils had a significantly reduced percentage migration to CXCL2 compared to CLD and healthy control neutrophils (figure 4.14 G). CLD neutrophils also had a non-significantly reduced percentage migration to CXCL2 compared to healthy control neutrophils. This is consistent with the phenotyping data showing a reduction in CXCR2 expression in HCC and CLD neutrophils compared to healthy control neutrophils (figure 4.13 A, K, U) as CXCR2 is the chemokine receptor for CXCL2. There were no differences in ND neutrophil migration to the CXCL1,3,6,7,8 cocktail and there was a small but significant reduction in ND neutrophil migration to CXCL12 in HCC compared to CLD neutrophils (figure 4.14 H-I). In the LD CD16$^{high}$ population there were no differences in migration to CXCL2, the CXCL1,3,6,7,8 cocktail and CXCL12 between HCC, CLD and healthy control neutrophils (figure 4.14 J-L).

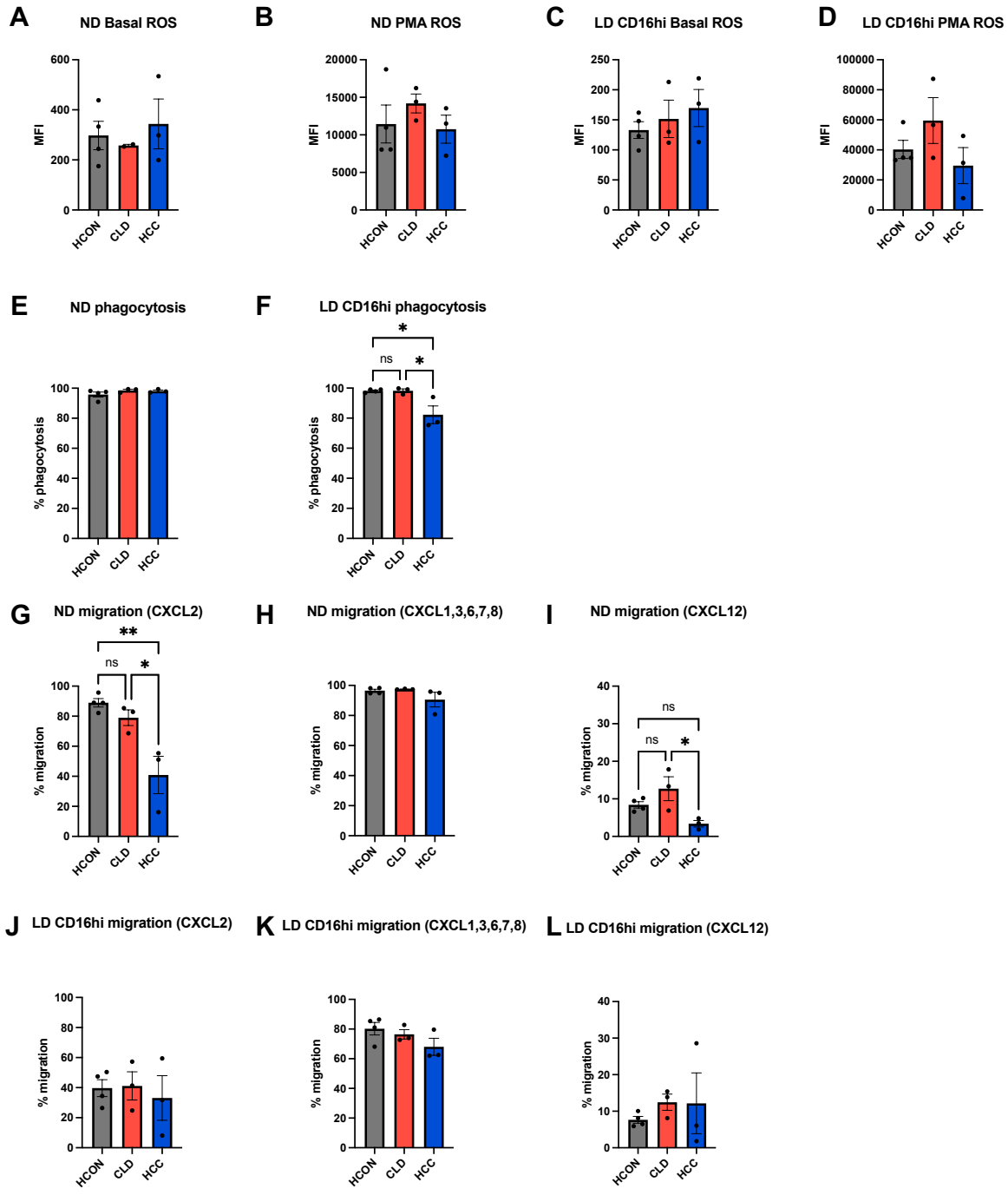



**Figure 4.14 – Neutrophil function in HCC patients, CLD patients and healthy controls. A.** Quantification of basal ROS in ND neutrophils. **B**. Quantification of PMA stimulated ROS in ND neutrophils. **C**. Quantification of basal ROS in LD CD16$^{high}$ neutrophils. **D**. Quantification of PMA stimulated ROS in LD CD16$^{high}$ neutrophils. **E**. Quantification of phagocytosis percentage in ND neutrophils. **F**. Quantification of phagocytosis percentage in LD CD16$^{high}$ neutrophils. **G**. Quantification of ND neutrophil migration to CXCL2. **H**. Quantification of ND neutrophil migration to CXCL1,3,6,7,8. **I**. Quantification of ND neutrophil migration to CXCL12. **J**. Quantification of LD CD16$^{high}$ neutrophil migration to CXCL2. **K**. Quantification of LD CD16$^{high}$ neutrophil migration to CXCL1,3,6,7,8. **L**. Quantification of LD CD16$^{high}$ neutrophil migration to CXCL12. P values calculated using a one-way

ANOVA with Tukey post-hoc test *p<0.05, **p<0.01, ***p<0.001, ****p<0.0001, ns non-significant.. HCON n=4, CLD n=3, HCC n=3.

### 4.8. Tumour, liver and blood immune cell frequencies in HCC patients undergoing surgical resection

I collected 4 matched blood, liver and tumour samples from patients undergoing surgical resection for their HCC. One of these tumour samples was necrotic and failed to isolate live leukocytes so has not been included in the analysis. To analyse the general immune landscape the same flow cytometry panel and gating strategy as outlined in figure 4.1 was used. A rich immune infiltrate was noted in both liver and tumour samples which was overall different to that found in peripheral blood (figure 4.15 A). Neutrophils made up a relatively small proportion of the immune infiltrate in the tumour and liver compared to blood (figure 4.15 B). T cells were generally enriched in liver and tumour compared to blood (figure 4.15 C-E) with CD8 T cells being particularly enriched (figure 4.15 E). NK cells and NK T cells were enriched in the background liver compared to the tumour and blood (figure 4.15 F-G). B cells, eosinophils, basophils and monocytes made up a relatively small proportion of immune cells in all compartments (figure 4.15 H-M).

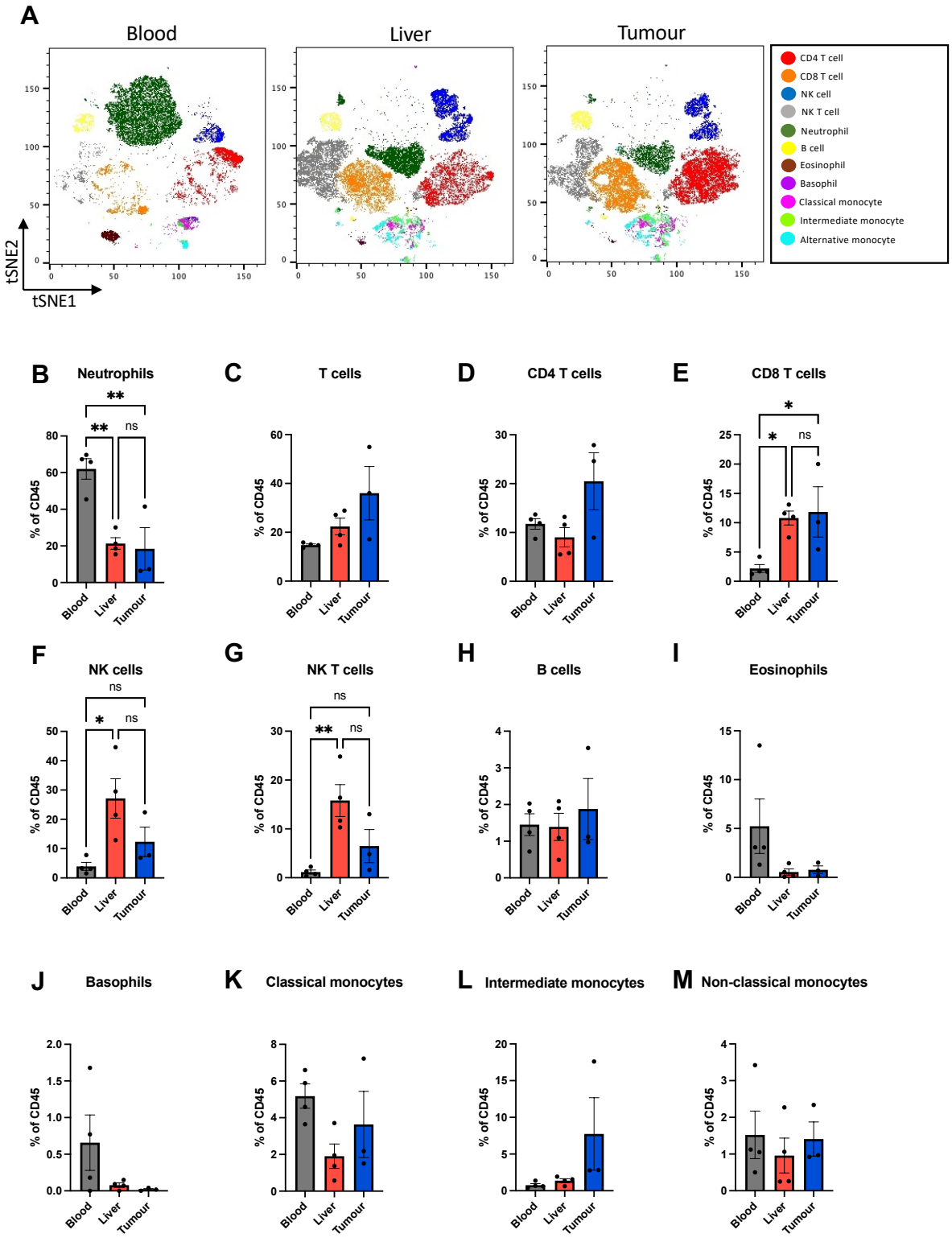



**Figure 4.15 – Tumour, liver and blood immune cell frequencies in HCC patients undergoing surgical resection. A.** tSNE plots representing the immune environments of blood vs liver vs tumour. **B-M.** Quantification of neutrophil, T cell, CD4 T cell, CD8 T cell, NK cell, NK T cell, B cell, eosinophil, basophil, classical monocyte, intermediate monocyte and non-classical monocyte frequencies in blood vs liver vs tumour compartments. P values calculated using a one-way ANOVA with Tukey post-hoc test *p<0.05, **p<0.01, ***p<0.001, ****p<0.0001, ns non-significant. Blood n=4, liver n=4, tumour n=3.

### 4.9. Tumour, liver and blood neutrophil phenotype in HCC

Using the neutrophil phenotyping panel I compared the phenotype of neutrophils isolated from the blood, liver and tumour compartments. High dimensional analysis demonstrated that neutrophils cluster according to their biological compartment with blood ND, blood LD CD16$^{high}$, blood LD CD16$^{low}$, liver and tumour neutrophils forming separate clusters (figure 4.16 A). These populations clustered separately due to differential expression of CD16, CD15, CD62L, CD10, CD11b, PDL1, CD66b and CXCR2 (figure 4.16 B). Interestingly the 3 tumour samples clustered in 2 separate clusters indicating that the neutrophil phenotype between the tumours was different (figure 4.16 A). Although not statistically significant liver and tumour neutrophils generally had a more activated and aged phenotype with reduced CD16 expression, increased CD15, CD66b, CD11b and CD10 expression and reduced CD62L and CXCR2 expression compared to blood neutrophils (figure 4.16 C-I). CXCR4 expression was comparable (figure 4.16 J) and expression of immune checkpoints such as PDL1 and SIRPα generally increased in liver and tumour neutrophils compared to blood neutrophils (figure 4.16 K-L). Mitochondrial mass was unchanged (figure 4.16 M).

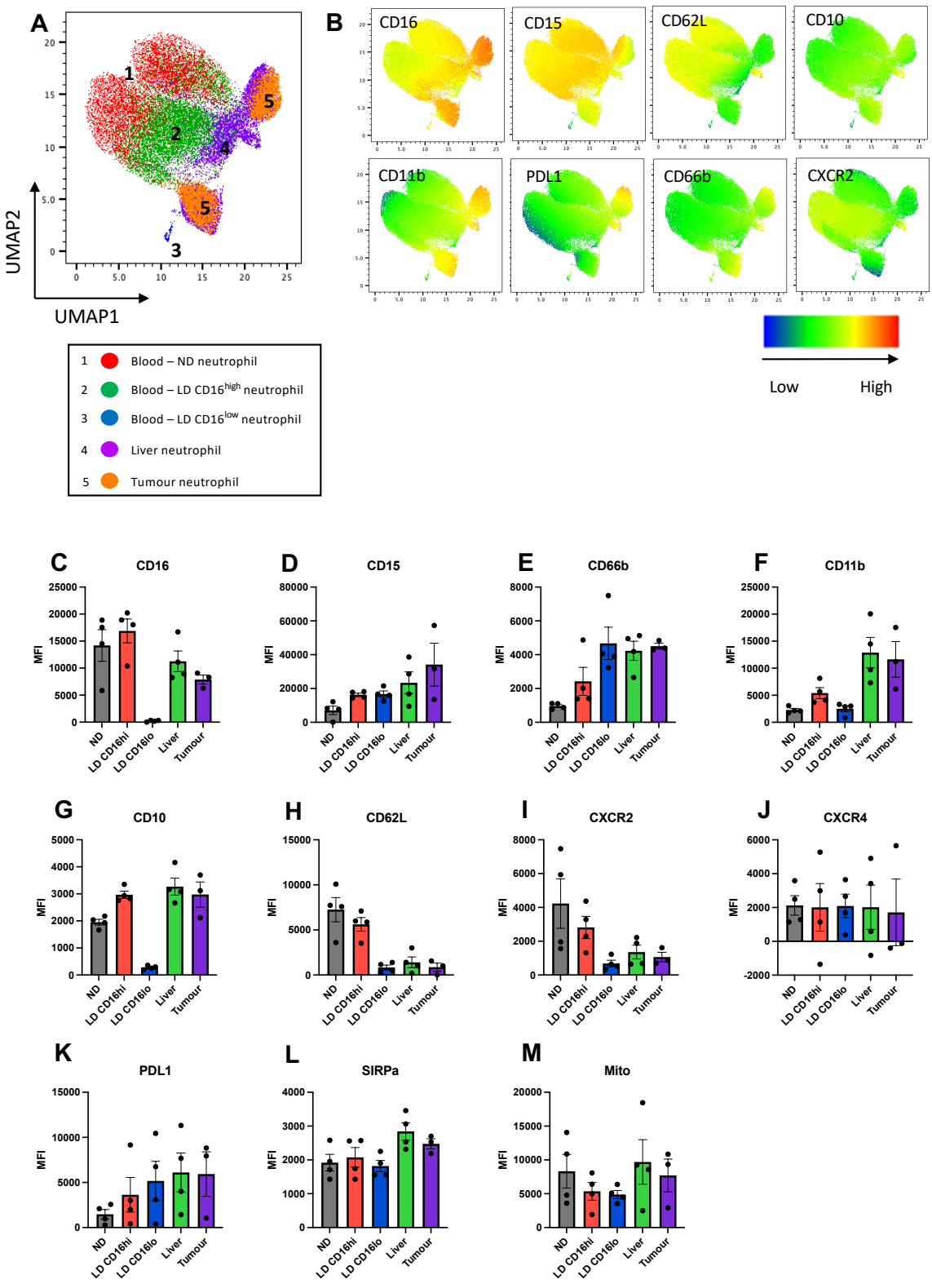



**Figure 4.16 – Tumour, liver and blood neutrophil phenotype in HCC patients undergoing surgical resection. A.** Unbiased high dimensional UMAP analysis of blood, liver and tumour neutrophil phenotype, demonstrating distinct phenotypes as represented by the unique clustering of each population. **B**. Heatmap of CD16, CD15, CD62L, CD10, CD11b, PDL1, CD66b and CXCR2 overlaid on the UMAP populations**. C-M.** Quantification of CD16, CD15, CD66b, CD11b, CD10, CD62L, CXCR2,

CXCR4, PDL1, SIRPα and MitoTracker™ Orange CMTMRos expression in blood, liver and tumour neutrophils. P values calculated using a one-way ANOVA with Tukey post-hoc test, all comparisons statistically non-significant. ND n=4, LD CD16$^{high}$ n=4, LD CD16$^{low}$ n=4, liver n=4, tumour n=3.

### 4.10. Conclusion

Neutrophil frequency is increased in the peripheral blood of both HCC and CLD patients compared to healthy controls. When further characterising circulating neutrophils there are 3 populations distinguished by their density and CD16 expression; ND, LD CD16$^{high}$ and LD CD16$^{low}$ neutrophils. It is the LD CD16$^{high}$ population which is differentially increased in HCC and CLD patients compared to healthy controls. These populations are confirmed as neutrophils based on their expression of MPO. LD CD16$^{low}$ neutrophils are most likely immature precursor neutrophils as indicated by their large oval nucleus, reduced CD16, CD11b, CD10 and CD62L expression, reduced secretory, specific and tertiary granule expression, increased CXCR4 expression and reduced stimulated ROS, phagocytosis and migratory functional ability. ND neutrophils are most likely mature resting neutrophils as indicated by their segmented nuclear morphology, positive expression of CD16, CD15, CD66b, CD11b, CD10 and CD62L. High expression of CXCR2. Lower stimulated ROS, high phagocytosis ability and high migratory ability. LD CD16$^{high}$ neutrophils are likely mature, aged and activated neutrophils as indicated by their high expression of CD15, CD11b, CD66b, CD63 and CD10. Lower expression of CXCR2 and CD62L. High stimulated ROS but lower phagocytosis ability. I further confirmed this hypothesis by conducting in vitro experiments where I demonstrated that both time and artificial activation caused an expansion of LD CD16$^{high}$ neutrophils. It is also the LD CD16$^{high}$ population which is likely the PMN-MDSC population described by others in the literature since they are low density and have high expression of LOX-1 and CD33. Therefore my findings are consistent with the literature which show that PMN-MDSCs (which I call LD CD16$^{high}$ neutrophils) are increased in the circulation of HCC patients compared to healthy controls.[156] In addition, I show that this increase is not specific to HCC but is also seen in CLD. This suggests that the increase in this population is related to the state of chronic inflammation as both are present in HCC and CLD. Furthermore, I characterised the immune microenvironment of the tumours and livers of HCC patients undergoing surgical resection. This showed that intra-tumoral neutrophils have a different phenotype to liver neutrophils and blood

neutrophils. In particular they have a more activated and aged phenotype as indicated by having a higher expression of CD66b, CD11b and CD10 and a lower expression of CXCR2 and CD62L. Liver and tumour neutrophils also had a generally higher expression of PDL1 compared to blood neutrophils which is consistent with them having an immunosuppressive pro-tumour phenotype.

# 5. Neutrophil heterogeneity and phenotype in a pre-clinical model of MASH-HCC

## 5.1. Introduction

My human data is limited by the very small number of matched tumour, liver and blood samples and the inability to evaluate neutrophil dynamics in vivo and investigate neutrophil changes during granulopoiesis. Therefore, to do this, I needed to use a pre-clinical model. In addition, I wanted to test the observations made in patients experimentally which again would require using a pre-clinical model. Therefore, I first evaluated a pre-clinical model of HCC to see how closely the changes in neutrophils compared to my observations in HCC patients. I hypothesised that I would see similar changes in neutrophil phenotype and dynamics in response to both CLD and HCC compared to my patient study. Then having identified common changes to neutrophils in both patients and pre-clinical models I would attempt to target these changes therapeutically in the pre-clinical model to further understand the underlying biology and identify potential neutrophil specific therapeutic targets.

## 5.2. Clinical characterisation of model

I chose to use an orthotopic MASH-HCC pre-clinical model because of the relatively short run time of the model and because it has previously been validated and published.[56,369] I started by first broadly characterising the clinical phenotype of the model as well and the general immune changes induced both by the dietary aspect of the model (MASH) as well as the orthoptic tumour aspect of the model (HCC).

### 5.2.1. MASH model characterisation – clinical phenotype

For the dietary aspect of the model 6-week-old male C57BL/6 mice were placed on either a high fat and high fructose diet (western diet) or normal chow (control diet). I weighed the mice weekly and harvested mice after 12 weeks to characterise their liver disease (figure 5.1 A). Western diet mice rapidly gained weight over the 12 weeks compared to control diet mice (figure 5.1 B). At 12 weeks western diet mice had a mean weight of 43.5 g SEM ± 1.1 g and control diet mice had a mean weight of 33.8 g SEM ± 0.96 g (figure 5.1 C). On macroscopic examination of the livers western diet mice had much larger and paler looking livers compared to control diet mice (figure

5.1 D). Western diet livers had a mean percentage of body weight of 8.2% SEM ± 0.29% compared to 5.7% SEM ± 0.13% in control diet mice (figure 5.1 E). Spleen weight as a percentage of body weight did not differ (figure 5.1 F). Histological examination of livers with H&E staining demonstrated significant steatosis in the livers of western diet mice compared to control diet mice (figure 5.1 G-H). However there was only a slight non statistically significant increase in fibrosis as indicated by αSMA staining (figure 5.1 I-J).

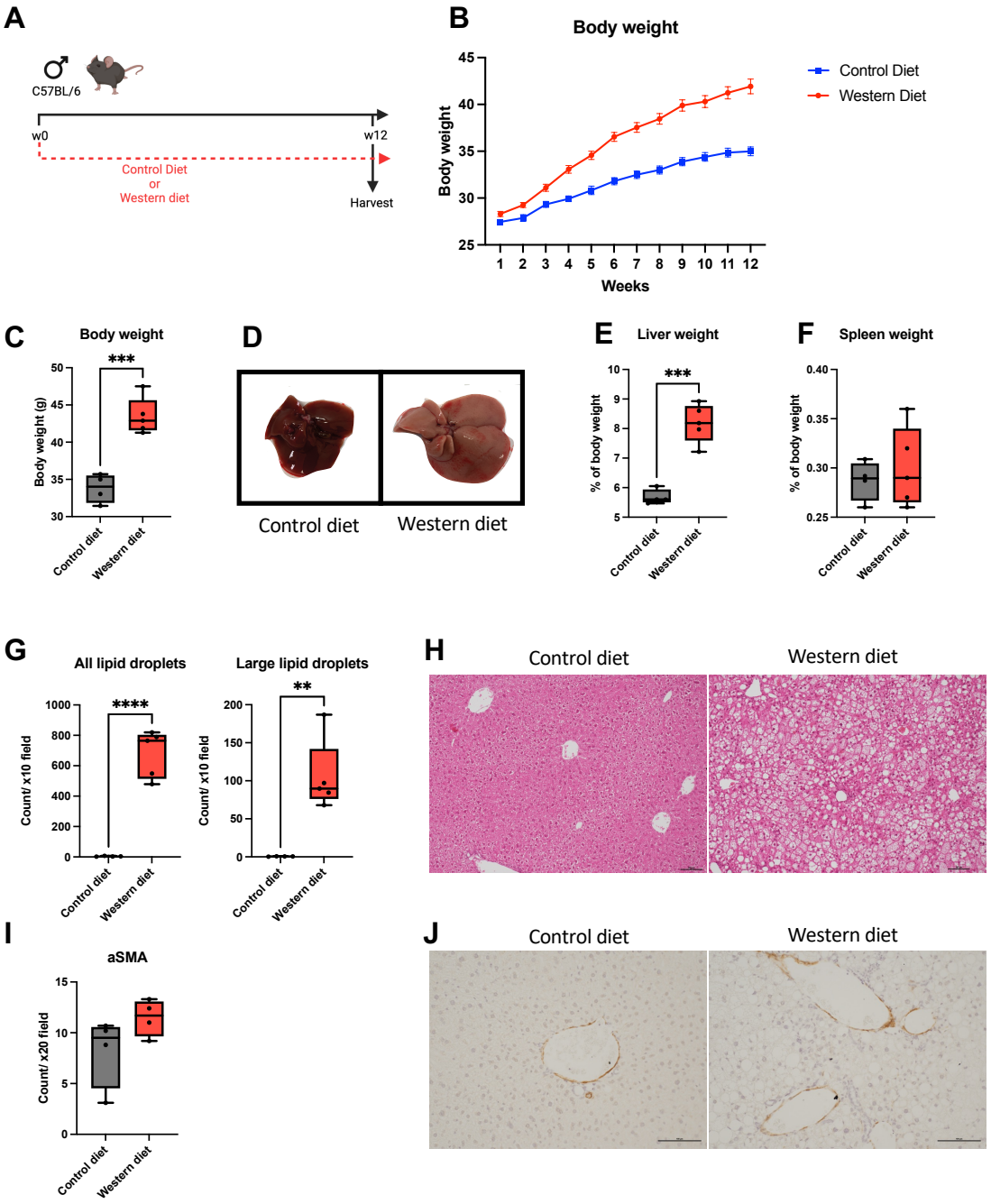


**Figure 5.1 – MASH model – clinical phenotype. A.** Schematic outlining dietary model of MASH. **B**. Quantification of mean body weight on western diet over the 12 week time course. **C**. Quantification of body weight on western vs control diet at week 12. **D**. Representative images of macroscopic appearance of western diet vs control diet livers. **E**. Quantification of liver weight as a percentage of body weight on western vs control diet at week 12. **F**. Quantification of spleen weight as a percentage of body weight on western vs control diet at week 12. **G**. Quantification of all and large lipid droplet counts on H&E staining of western and control diet livers at week 12. **H**. Representative images of H&E staining of western diet and control diet livers, at 100x magnification. **I**. Quantification of αSMA staining of western and control diet livers at week 12. **J**. Representative images of αSMA staining of western diet and control diet livers, at 200x magnification. P values calculated using an unpaired t-test *p<0.05, **p<0.01, ***p<0.001, ****p<0.0001, ns non-significant. Control diet n=4, western diet n=5.

### 5.2.2. MASH model characterisation – liver immune infiltrate

I next looked at the immune infiltrate of the livers of western diet vs control diet fed mice to characterise the degree of steatohepatitis. I used both flow cytometry and immunohistochemistry.

#### 5.2.2.1 Flow cytometry gating strategy – tissue

Dissociated livers were stained with a panel of antibodies (mouse panel 1) and run through the flow cytometer. Immune populations were identified using the gating strategy outlined in figure 5.2. Single cells were identified by selecting cells that had a proportional FSC-A to FSC-H. Live $CD45^+$ cells were gated on, and leukocytes identified on FSC-A vs SSC-A. NK cells, T cells and NK T cells were identified on CD3 vs NK1.1. T cells were then further categorised as being CD4 or CD8. Of the $CD3^-$ $NK1.1^-$ population, B cells and neutrophils were identified on Ly6G vs CD19. Of the $Ly6G^-CD19^-$ population, mature dendritic cells were identified as being $CD11c^+$ $MHCII^+$. Mature dendritic cells (DCs) could then be further classified as being monocytic dendritic cells (moDCs), conventional dendritic cells type 1 (cDC1) or conventional dendritic cells type 2 (cDC2) based on Ly6C, XCR1 and CD11b expression. From the not mature DC gate macrophages and immature DCs could be identified on F4/80 and CD11c expression. Macrophages could then be further classified as being either resident, recruited $Ly6C^+$ or recruited $Ly6C^-$ macrophages. Lastly of the $CD11c^-F4/80^-$ population monocytes could be identified as being $CD11b^+$ then further classified as $Ly6C^+$ and $Ly6C^-$ monocytes. These populations were also identified on high dimensional t-SNE analysis (figure 5.2 B).

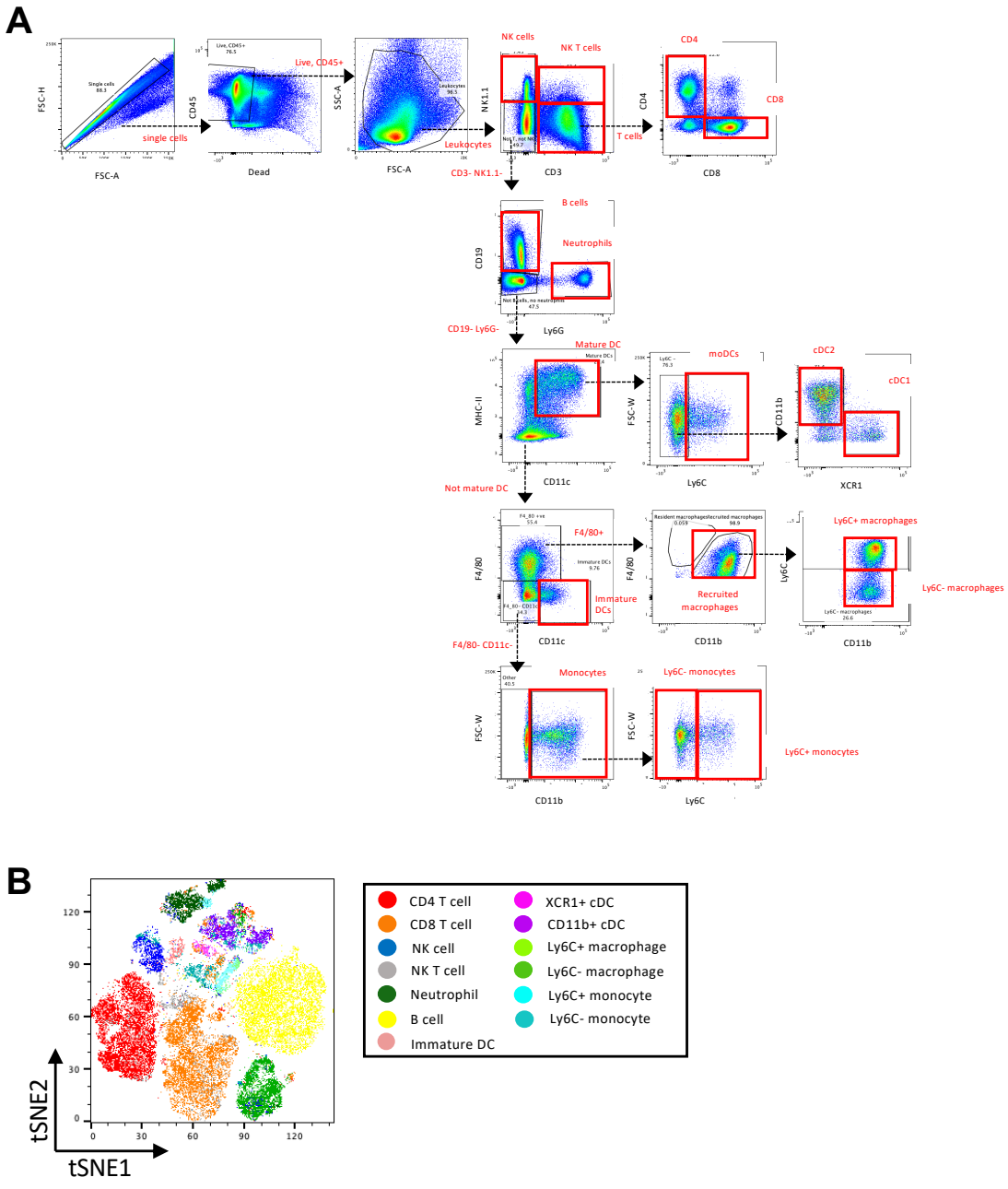



**Figure 5.2 – Mouse general immune cell panel gating strategy for tissue. A.** Gating strategy**.** Single cells were identified on FSC-A vs FSC-H. Live CD45$^{+}$ cells were gated and leukocytes identified on FSC-A vs SSC-A. NK cells, T cells and NK T cells were identified on CD3 vs NK1.1 and CD4 and CD8 T cells identified. B cells and neutrophils were identified on Ly6G vs CD19. Mature dendritic cells were identified as being CD11c$^{+}$ MHCII$^{+}$. Mature DCs could then be further classified as being monocytic moDC, cDC1 or cDC2 based on Ly6C, XCR1 and CD11b expression. Macrophages and immature DCs could be identified on F4/80 and CD11c expression. Macrophages could then be further classified as being either resident, recruited Ly6C$^{+}$ or recruited Ly6C$^{-}$ macrophages. Monocytes could be identified

as being CD11b$^{+}$ then further classified as Ly6C$^{+}$ and Ly6C$^{-}$ monocytes. **B**. These populations were also identified on high dimensional t-SNE analysis.

#### 5.2.2.2. MASH model – liver immune infiltrate

Flow cytometry analysis of dissociated livers demonstrated a rich immune infiltrate of western diet livers compared to control diet livers with almost all immune cell types being enriched (figure 5.3 A). There was a significant increase in the numbers of neutrophils in western diet livers (figure 5.3 B). There was also a significant increase in CD8 T cells, macrophages, monocytes and DCs (figure 5.3 B). IHC analysis confirmed an increase in neutrophils and a preferential increase in CD8 T cells (figure 5.3 C-H). Together this data show that this dietary model closely resembles MASH without significant fibrosis. These results indicate that this is a good model to investigate immune changes and chronic inflammatory changes in as patient studies also show an increase in liver neutrophils and CD8 T cells in MASH.[370]

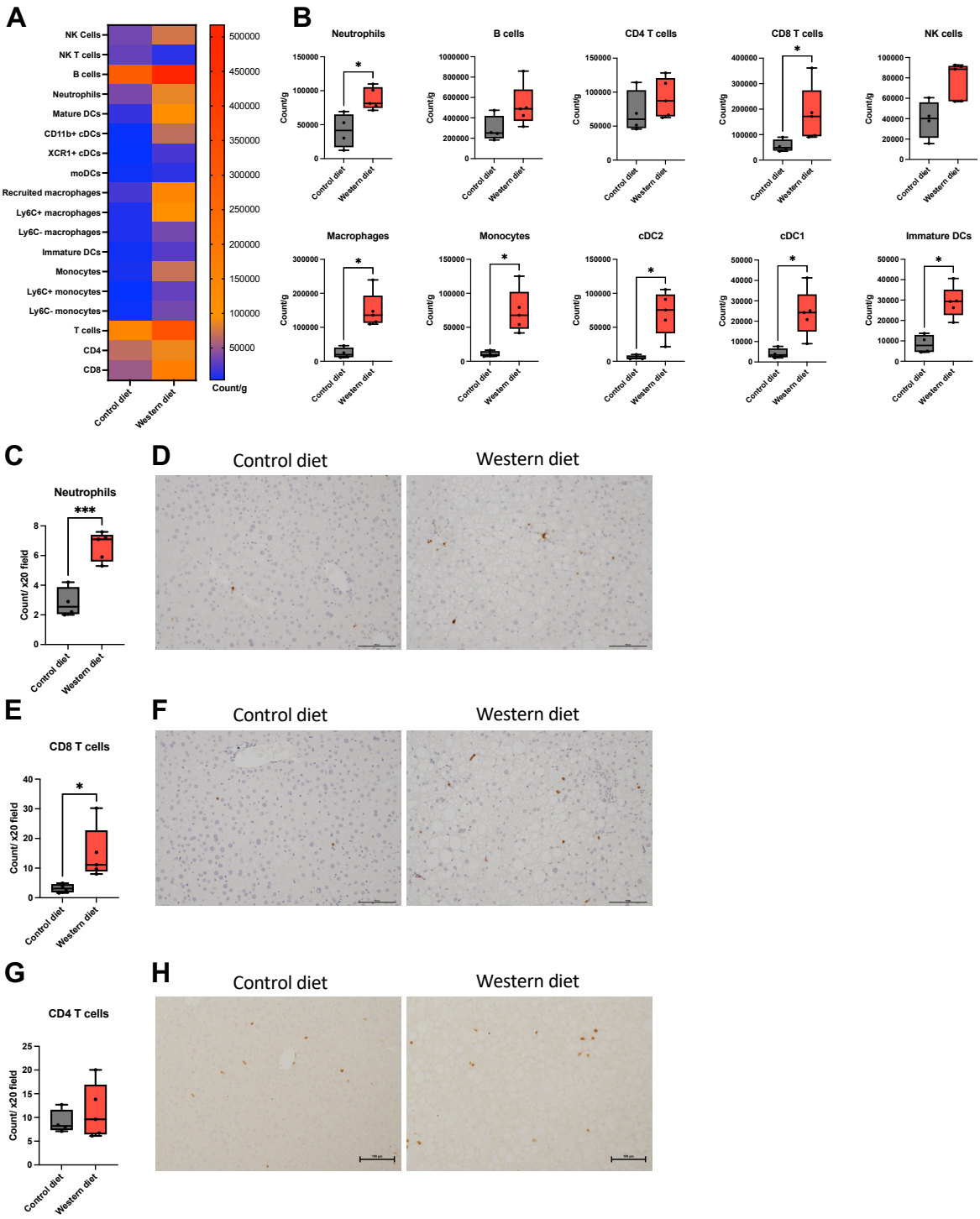



**Figure 5.3 – MASH model – liver immune infiltrate. A**. Heatmap demonstrating immune cell counts in western diet vs control diet livers as assessed by flow cytometry. **B.** Quantification of immune cell counts in western vs control diet livers as assessed by flow cytometry. **C**. Quantification of neutrophil counts in western diet vs control diet livers as assessed by IHC. **D.** Representative images of Ly6G IHC staining for neutrophils, at 200x magnification. **E**. Quantification of CD8 T cells counts in western diet vs control diet livers as assessed by IHC. **F**. Representative images of CD8 IHC staining, at 200x magnification. **G.** Quantification of CD4 T cells counts in western diet vs control diet livers as assessed by IHC. **H**. Representative images of CD4 IHC staining, at 200x magnification. P values calculated

using an unpaired t-test *p<0.05, **p<0.01, ***p<0.001, ****p<0.0001, ns non-significant. Control diet n=4, western diet n=5.

### 5.2.3. Orthotopic HCC model characterisation – clinical phenotype

For the tumour model a strain matched hepatoma cell line (Hep 53.4) was orthotopically transplanted into the livers of mice which had been on the western diet for 12 weeks. As a control procedure sham surgeries were performed in which laparotomy was performed but no cells injected into the liver. I then harvested mice at 2, 4 and 6 weeks (figure 5.4 A). Following surgery both sham and cancer injected mice lost weight as a direct result of the surgery (figure 5.4 B). As the tumours progressed from 4 to 6 weeks cancer bearing mice started to loss body weight rapidly whereas sham mice regained their pre-surgery weight (figure 5.4 B). Throughout the time course the tumour burden increased; 2 week median tumour volume 410 $mm^3$, 4 week median tumour volume 1199 $mm^3$, 6 week median tumour volume 1973 $mm^3$ (figure 5.4 C-D). At 4 and 6 weeks when there was significant tumour burden splenomegaly also occurred (figure 5.4 E). Microscopic examination of tumours demonstrated relatively avascular and fibrotic tumours with a rich stroma (figure 5.4 F-H). The background liver was steatotic (figure 5.4 F).

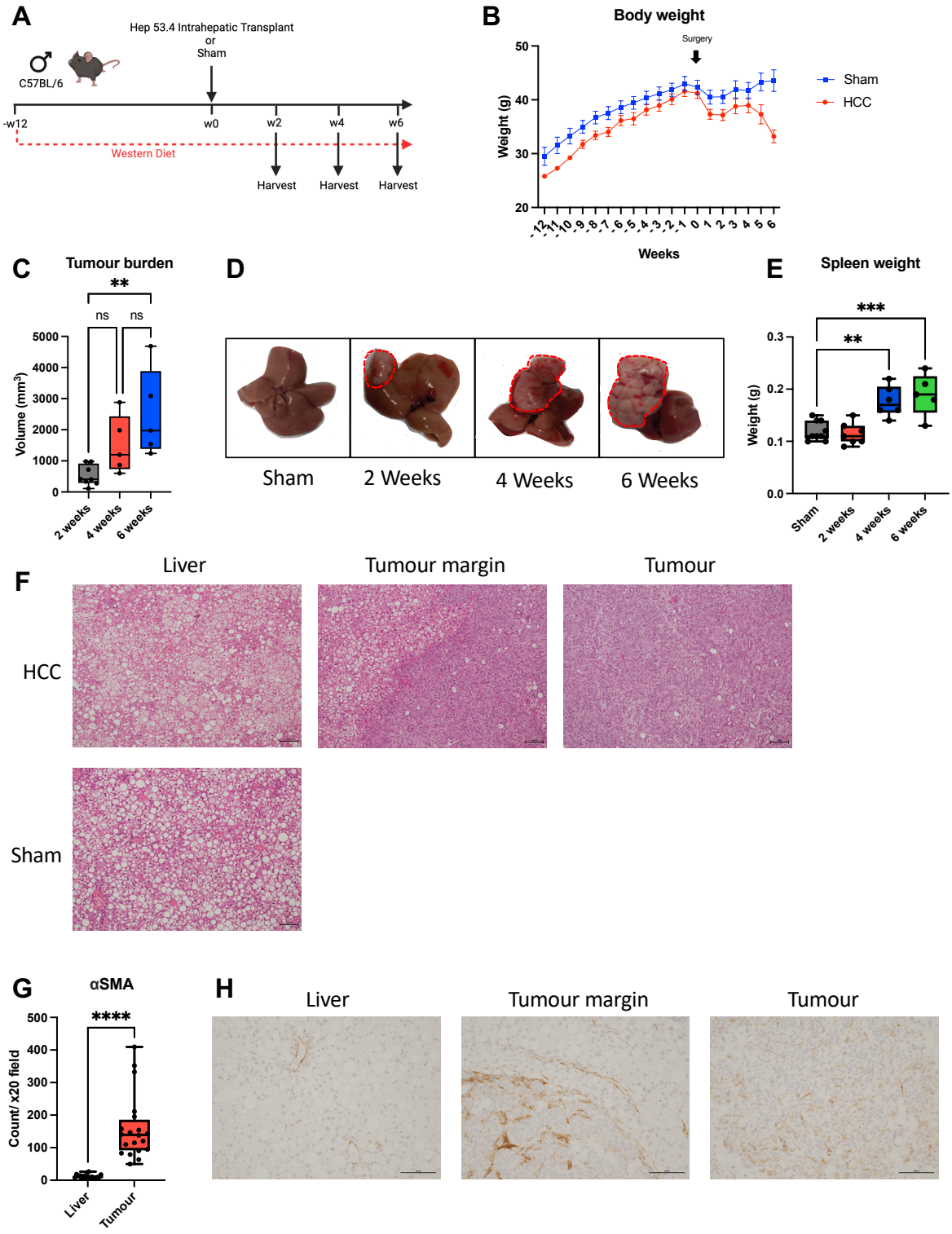



**Figure 5.4 – Orthotopic HCC model – clinical phenotype. A.** Schematic outlining orthotopic transplant model. **B**. Quantification of body weight between cancer bearing and sham control mice throughout the experiment, sham n=15, HCC n=19. **C**. Quantification of tumour burden/ volume throughout the time course, 2 weeks n=8, 4 weeks n=5, 6 weeks n=5. **D**. Representative images of livers/tumours throughout the time course. **E.** Quantification of spleen weight throughout the time course, sham n=9, 2 weeks n=8, 4 weeks n=5, 6 weeks n=5**. F**. Representative images of H&E staining of background liver, tumour margin, tumour and sham livers. At 100x magnification. **G**. Quantification

of αSMA staining in matched tumours vs background livers, n=20. **H**. Representative images of αSMA staining in matched background liver, tumour margin and tumour samples, at 200x magnification. P values calculated using a one-way ANOVA with Tukey post-hoc test (C, E) or an unpaired t-test (G) *p<0.05, **p<0.01, ***p<0.001, ****p<0.0001, ns non-significant.

### 5.2.4. Orthotopic HCC model characterisation – immune infiltrate

To evaluate the immune infiltrate of the orthotopic tumours I used both flow cytometry and IHC. Using the same flow cytometry panel and gating strategy as in figure 5.2 a rich immune infiltrate was identified in the tumours (figure 5.5 A-C). Most immune cells were enriched in the tumours compared to the background liver (figure 5.5 B). CD8 T cells were the most abundant leukocytes, followed by CD4 T cells and B cells, then neutrophils, macrophages and mature DCs (figure 5.5 C). This was confirmed on IHC analysis showing a predominantly T cell infiltrate with comparatively less neutrophils in the tumours (figure 5.5 D-G). Therefore, this orthotopic model most closely resembles HCC on the background of non-fibrotic MASH. The tumours themselves closely resemble immune hot HCCs and depending on the time point taken can either be early stage (2 weeks) or advanced stage (4-6 weeks). The fact that the tumours are immune hot makes this a good model for studying the effects of immunotherapies.

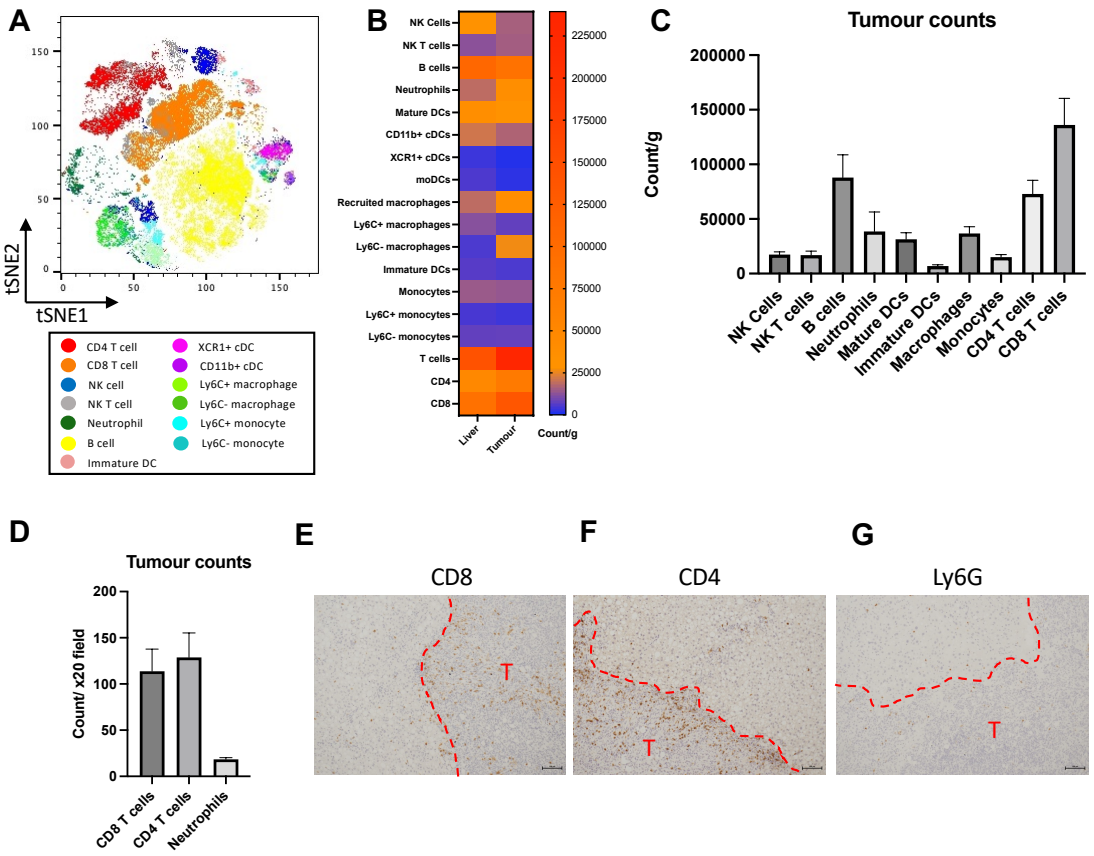



**Figure 5.5 – Orthotopic HCC model – immune infiltrate. A.** tSNE plot representing the tumour immune infiltrate assessed by flow cytometry. **B**. Heatmap demonstrating immune cell counts in the tumour vs background liver assessed by flow cytometry. **C**. Quantification of immune cell counts assessed by flow cytometry. **D**. Quantification of immune count in tumours assessed by IHC. **E**. Representative image of tumour CD8 IHC staining, at 200x magnification. **F**. Representative image of tumour CD4 IHC staining, at 200x magnification. **G**. Representative image of tumour Ly6G IHC staining, at 200x magnification. n=4.

## 5.3. Blood immune cell frequencies in the western diet and western diet – orthotopic HCC models

### 5.3.1. Flow cytometry gating strategy – blood

Whole lysed blood was stained with a panel of antibodies (mouse panel 1) and run through the flow cytometer. Immune populations were identified using the gating strategy outlined in figure 5.6. Single cells were identified by selecting cells that had a proportional FSC-A to FSC-H. Live $CD45^+$ cells were gated on, and leukocytes identified on FSC-A vs SSC-A. NK cells, T cells and NK T cells were identified on CD3 vs NK1.1. T cells were then further categorised as being CD4 or CD8. Of the $CD3^-$

NK1.1$^-$ population, B cells and neutrophils were identified on Ly6G vs CD19. Of the Ly6G$^-$CD19$^-$ population, monocytes were then identified as being CD11b$^+$. Monocytes were then further split into Ly6C$^+$ and Ly6C$^-$ populations. These populations were also identified on high dimensional t-SNE analysis (figure 5.6 B).

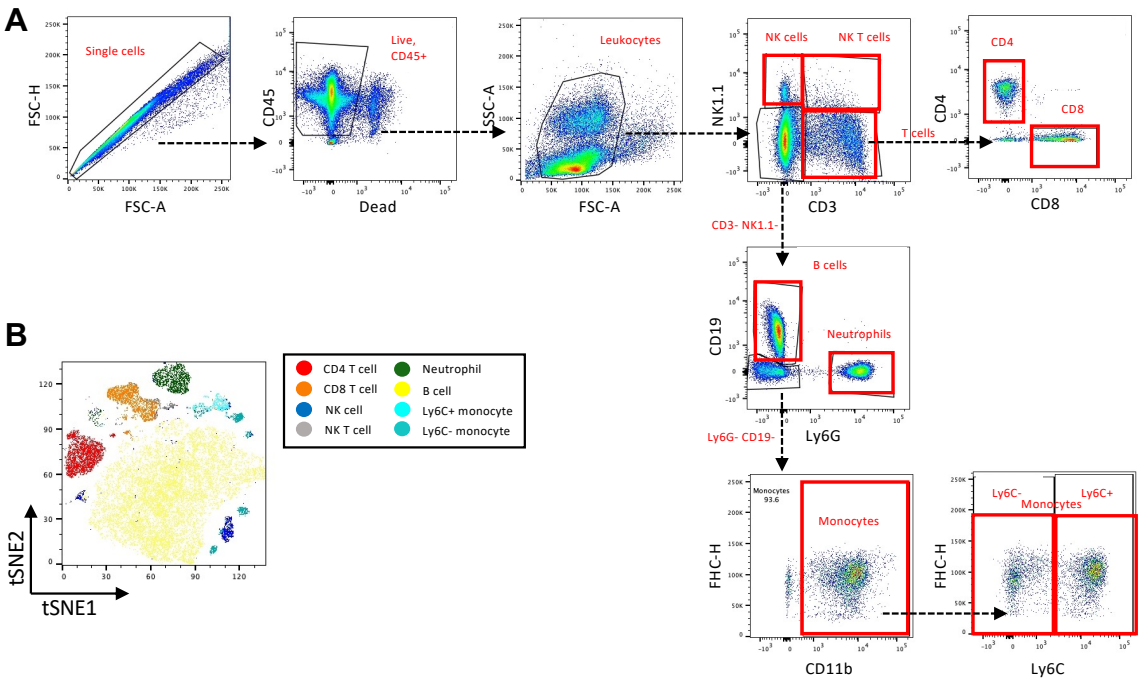



**Figure 5.6 – Mouse general immune cell panel gating strategy for blood. A.** Gating strategy**.** Single cells were identified on FSC-A vs FSC-H. Live CD45$^+$ cells were gated and leukocytes identified on FSC-A vs SSC-A. NK cells, T cells and NK T cells were identified on CD3 vs NK1.1 and CD4 and CD8 T cells identified. B cells and neutrophils were identified on Ly6G vs CD19. Monocytes could be identified as being CD11b$^+$ then further classified as Ly6C$^+$ and Ly6C$^-$ monocytes. **B**. These populations were also identified on high dimensional t-SNE analysis.

### 5.3.2. Blood immune cell frequencies

As an initial experiment and to make a comparison to my patient data I started by characterising the frequencies of circulating immune cells in the pre-clinical model. I started by making the comparison between control diet (CD) mice (equivalent to healthy controls), western diet sham mice (WD-sham) (equivalent to CLD patients) and western diet HCC (WD-HCC) mice (equivalent to HCC patients). This demonstrated a significant increase in the frequency of circulating neutrophils in WD-HCC mice compared to WD-Sham and CD mice (figure 5.7 A and B). In addition, there was also a decrease in the frequency of circulating T cells in both WD-HCC and WD-Sham mice compared to CD mice with this being driven by a preferential reduction in

CD8 T cells (figure 5.7 C-E). Overall, there was a reduction in circulating NK T cells in WD-Sham mice and no differences in circulating NK cells, B cells and monocytes (figure 5.7 F-I). These results are similar to what I found in patients (figure 4.2).

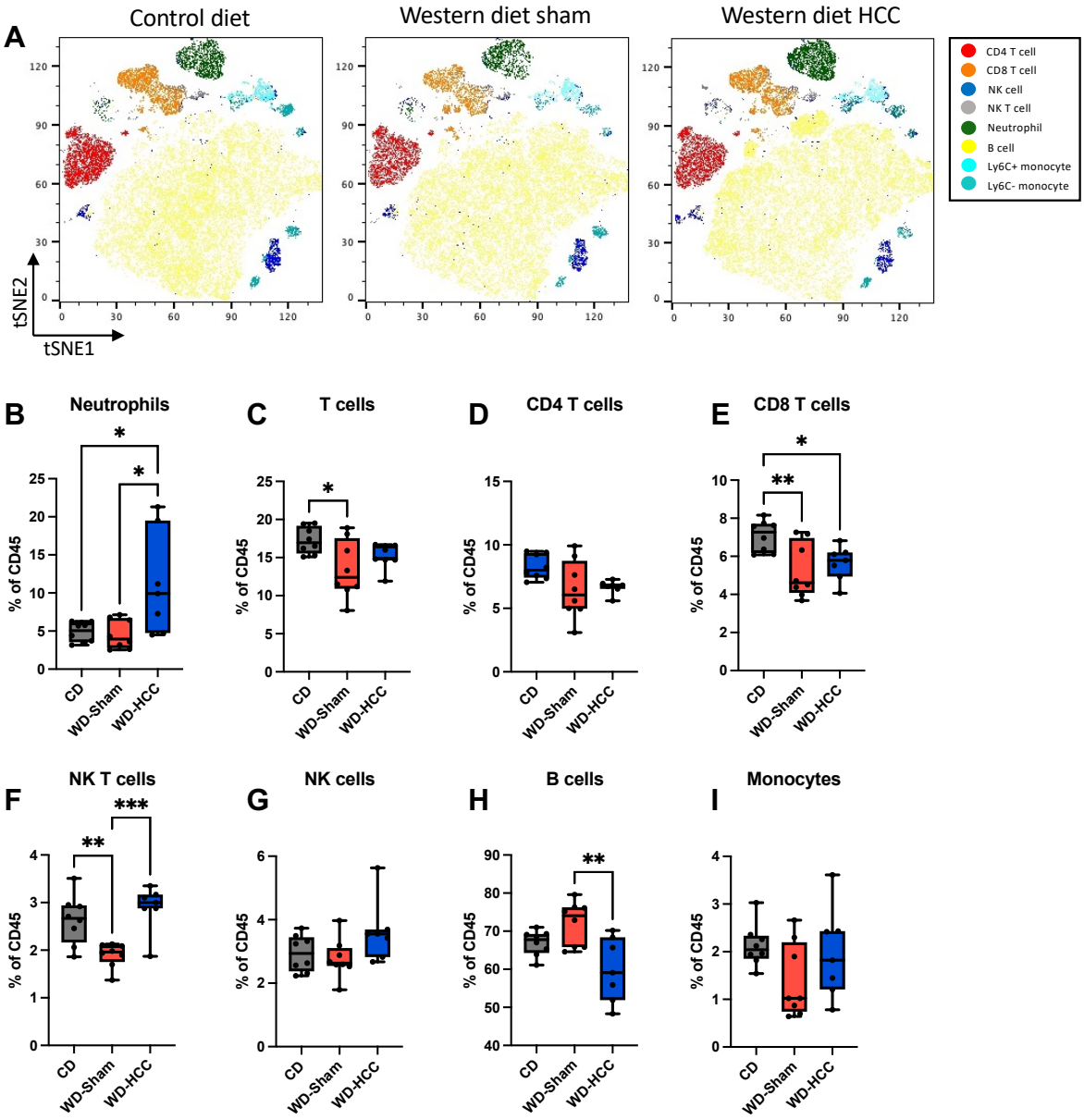



**Figure 5.7 – Circulating immune cell frequencies in the pre-clinical model. A.** tSNE plots representing the circulating immune cell populations as assessed by flow cytometry. In CD, WD-Sham and WD-HCC mice. **B-I.** Quantification of circulating neutrophil, T cell, CD4 T cell, CD8 T cell, NK T cell, NK cell, B cell and monocyte frequency in CD, WD-Sham and WD-HCC mice. P values calculated using a one-way ANOVA with Tukey post-hoc test. *p<0.05, **p<0.01, ***p<0.001, ****p<0.0001, ns non-significant. CD n=8, WD-sham n=8, WD-HCC n=7.

### 5.4. Pre-clinical model circulating neutrophil heterogeneity and phenotype

After identifying that the frequency of circulating neutrophils was increased in WD-HCC mice compared to CD mice the next step was to investigate circulating neutrophil heterogeneity and confirm whether this increase was being driven by an expansion of LD neutrophils as seen in my patient study.

#### 5.4.1. Circulating ND and LD gating strategy

Following density separation blood samples were stained with mouse panels 2, 4 or 5, run through the flow cytometer and gated as per figure 5.8. Leukocytes were identified on FSC-A vs SSC-A, then single cells identified by selecting cells that had a proportional FSC-A to FSC-H. Next live cells were gated on followed by $CD45^+$. Neutrophils were then identified based on being $CD11b^+Ly6G^+$.

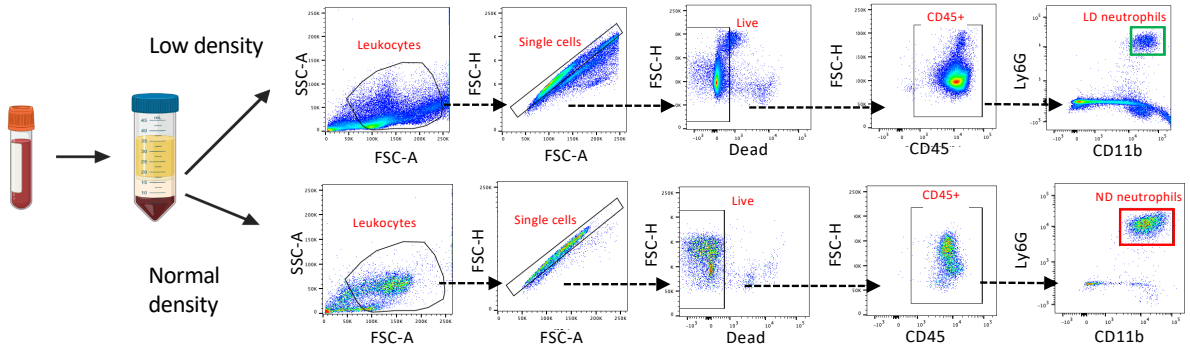



**Figure 5.8 – Mouse blood neutrophil density gating strategy**. Leukocytes were gated on FSC-A vs SSC-A followed by single cells on FSC-A vs FSC-H. Next live cells were gated on as being negative of the dead cell dye. Neutrophils were then identified as being $CD45^+CD11b^+Ly6G^+$.

#### 5.4.2. Frequency and phenotype of circulating neutrophil populations

Like in my patient study neutrophils were identified in both the normal-density and low-density fractions (figure 5.9 A). The frequency of LD neutrophils was significantly increased in tumour bearing mice compared to control mice (figure 5.9 B) whilst the frequency of ND neutrophils was unchanged. Therefore similar to in my patient study the increase in circulating neutrophil frequency was driven by an expansion of LD neutrophils. Nuclear morphology confirmed these populations as neutrophils based on their segmented nucleus with the LD neutrophils appearing more hyper segmented (figure 5.9 A).

Phenotypic analysis of ND and LD neutrophils demonstrated that LD neutrophils had a more activated phenotype compared to ND neutrophils as showed by their increased Ly6G and CD11b expression along with their reduced CD62L expression (figure 5.9 C-E). LD neutrophils also had a more aged and mature phenotype as demonstrated by their reduced CD62L, C-kit and CXCR2 expression and increased CXCR4 expression (figure 5.9 E-H). In terms of immune checkpoints LD neutrophils had increased SIRPα and CD47 expression and similar PDL1 expression compared to ND neutrophils (figure 5.9 I-K). In terms of intracellular markers LD neutrophils had reduced NOS2 expression (figure 5.9 L). LD neutrophils had similar mitochondrial mass (figure 5.9 M). LD neutrophils were a similar size to ND neutrophils as indicated by FSC-A but had reduced granularity as indicated by SSC-A (figure 5.9 N-O). Together this suggests that LD neutrophils are more activated, aged and degranulated compared to ND neutrophils in this pre-clinical model. Unlike in humans I did not identify an immature LD population of neutrophils.

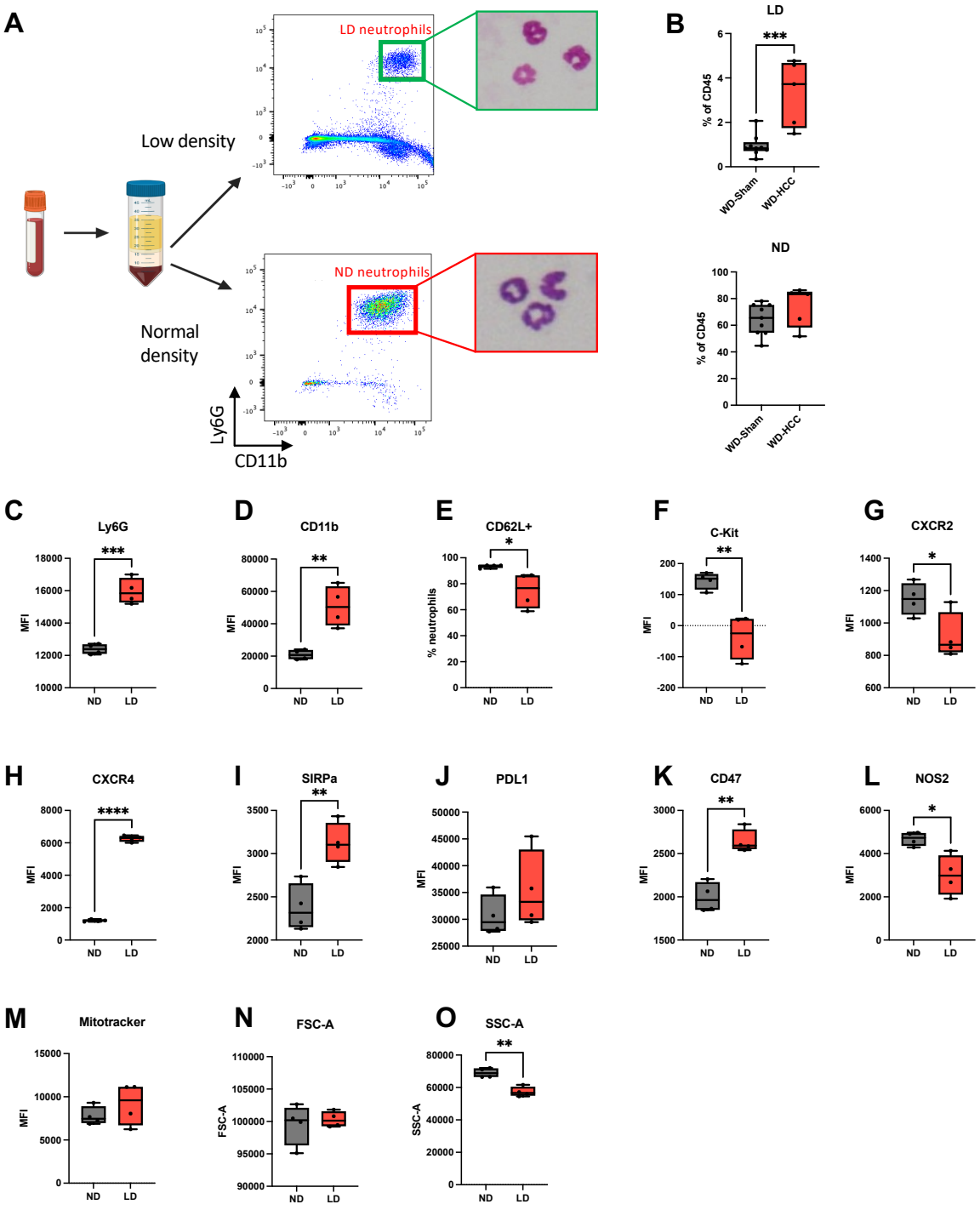



**Figure 5.9 – Pre-clinical model - frequency and phenotype of circulating neutrophil populations.** **A.** Representative plots showing the LD and ND neutrophil populations and Giemsa stains of FACS sorted populations. **B.** Quantification of LD and ND neutrophil frequency. **C-O**. Quantification of Ly6G, CD11b, CD62L, C-kit, CXCR2, CXCR4, SIRPα, PDL1, CD47, NOS2, mitotracker orange staining (measure for mitochondrial mass), FSC-A, and SSC-A. P values calculated using an unpaired t-test *p<0.05, **p<0.01, ***p<0.001, ****p<0.0001, ns non-significant. n=4.

### 5.4.3. Circulating neutrophil platelet marker expression

Like in my patient study LD neutrophils were found to have increased expression of the platelet markers CD36 and CD41 compared ND neutrophils (figure 5.10 A-B). Again, CD36 and CD41 were found to be co-expressed in LD neutrophils and indicated the presence of neutrophil-platelet aggregates (figure 5.10 C-D).

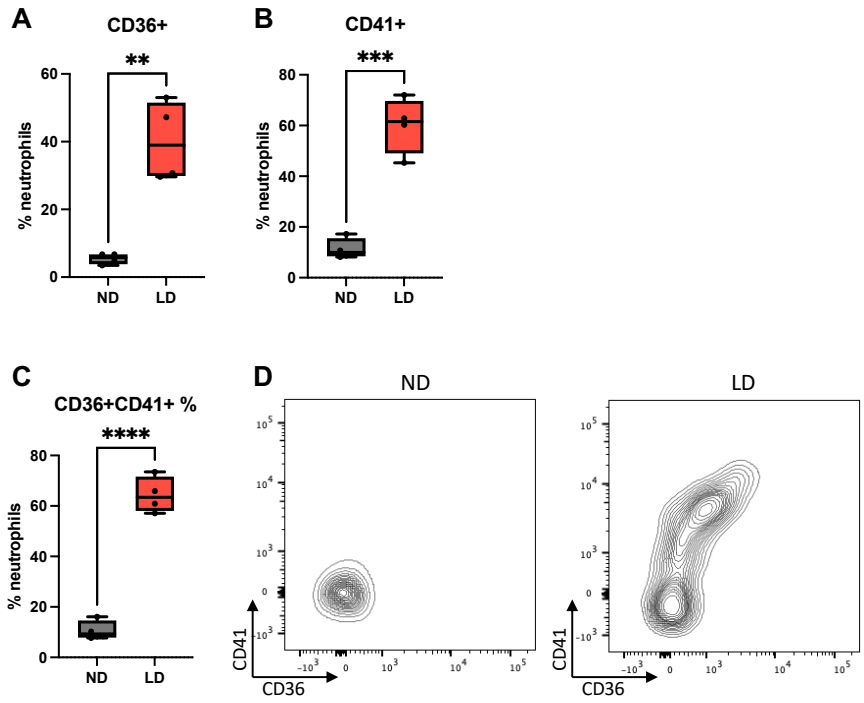



**Figure 5.10 – Pre-clinical model - circulating neutrophil CD36 and CD41 expression. A.** Quantification of CD36 expression. **B.** Quantification of CD41 expression. **C.** Quantification of CD36 and CD41 co-expression. **D**. Representative flow cytometry plot demonstrating CD36 and CD41 co-expression in LD neutrophils. P values calculated using an unpaired t-test *p<0.05, **p<0.01, ***p<0.001, ****p<0.0001, ns non-significant. n=4.

### 5.4.4. Circulating neutrophil functional assays

To assess functional differences between the different circulating LD and ND neutrophil populations I performed various functional assays. On assessing ROS activity LD neutrophils had significantly more basal ROS activity compared to ND neutrophils (figure 5.11 A). Whereas LD neutrophils had significantly less (PMA) stimulated ROS activity compared to ND neutrophils (figure 5.11 B). Together this shows that ND neutrophils have a greater capacity for stimulated ROS generation compared to LD neutrophils (figure 5.11 C-D). LD neutrophils also had a reduced phagocytosis capacity compared to ND neutrophils (figure 5.11 E-F) and reduced

migratory capacity to CXCL2 (figure 5.11 G). Together this suggests that in this pre-clinical model LD neutrophils are already activated and functionally exhausted in terms of ROS capacity.

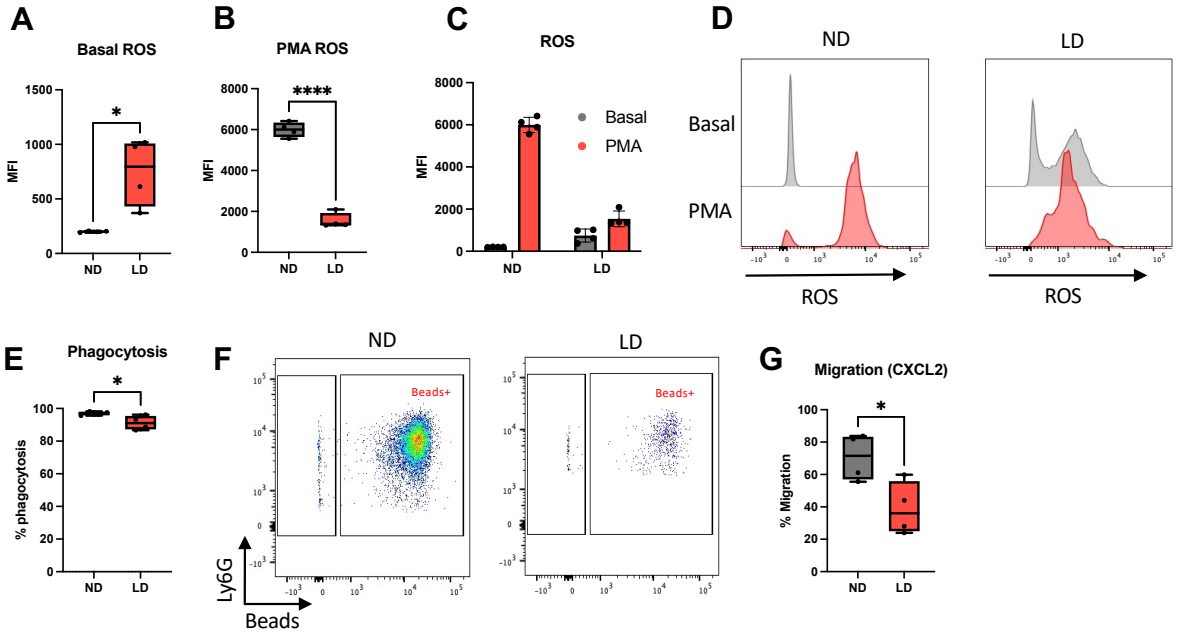



**Figure 5.11 – Pre-clinical model - circulating neutrophil functional assays. A.** Quantification of basal ROS. **B.** Quantification of PMA stimulated ROS. **C.** Quantification of ROS capacity on PMA stimulation. **D.** Representative histograms of basal and PMA stimulated ROS expression. **E.** Quantification of phagocytosis. **F.** Representative flow cytometry plot showing bead phagocytosis. **G**. Quantification of migration to CXCL2. P values calculated using an unpaired t-test *p<0.05, **p<0.01, ***p<0.001, ****p<0.0001, ns non-significant. n=4.

### 5.4.5. Comparison of mouse and human circuiting neutrophil populations

Overall, the mouse LD neutrophils appear to correspond to the LD CD16$^{high}$ population found in humans. Both populations are expanded in HCC (figure 5.9 and figure 4.4) and have an activated and aged phenotype as demonstrated by their increased expression of CD15/Ly6G, CD11b and reduced expression of CXCR2 and CD62L compared to ND neutrophils (figure 5.12 A-B). In addition, they are both associated with neutrophil platelet aggregates as shown by their expression of CD36 and CD41 which are typical platelet markers (figure 5.12 A-B). Functionally they both have reduced phagocytosis and migratory ability to CXCL2 (figure 5.12 C-D). There were however differences between the mouse and human LD neutrophils. Whereas mouse LD neutrophils had dramatically increased CXCR4 expression compared to ND

neutrophils, human LD CD16$^{high}$ neutrophils did not (figure 5.12 A-B). Mouse LD neutrophils were less granular as shown by their reduced SSC-A compared to ND neutrophils, however the opposite was found human LD CD16$^{high}$ neutrophils. Functionally mouse LD neutrophils had high basal ROS activity, but a poor PMA stimulated ROS activity compared to ND neutrophils, the opposite was found in human LD CD16$^{high}$ neutrophils (figure 5.12 C-D).

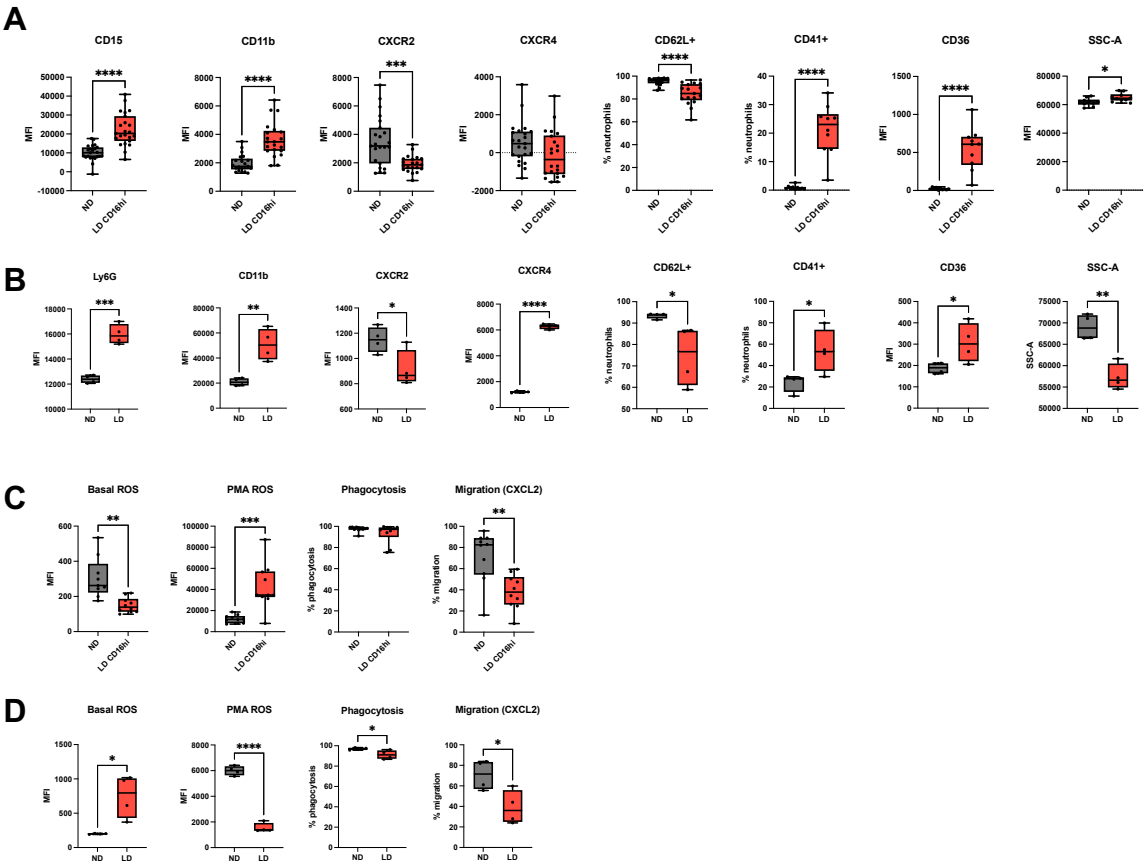



**Figure 5.12 – Mouse LD vs human LD CD16$^{high}$ neutrophil comparison. A.** Quantification of CD15, CD11b, CXCR2, CXCR4, CD62L, CD41, CD36 expression and SSC-A in human ND and LD CD16$^{high}$ neutrophils, n=10. **B**. Quantification of Ly6G, CD11b, CXCR2, CXCR4, CD62L, CD41, CD36 expression and SSC-A in mouse ND and LD neutrophils, n=4. **C.** Quantification of functional assays (basal ROS, PMA stimulated ROS, phagocytosis and migration to CXCL2) in human ND and LD CD16$^{high}$ neutrophils, n=10. **D.** Quantification of functional assays (basal ROS, PMA stimulated ROS, phagocytosis and migration to CXCL2) in mouse ND and LD neutrophils, n=4. P values calculated using an unpaired t-test *p<0.05, **p<0.01, ***p<0.001, ****p<0.0001, ns non-significant.

## 5.5. Experimental manipulation of neutrophil ageing and the effect on LD neutrophils

As the LD neutrophils have an aged phenotype, I wanted to test whether the ageing process results in them becoming low density and whether this can be manipulated. I also wanted to investigate the origin of LD neutrophils; whether they arise from aged ND circulating neutrophils or whether they originate directly from the bone marrow. To do this I conducted a neutrophil specific genetic knockout experiment of CXCR2 and a BrdU neutrophil tracking experiment.

### 5.5.1. The effect of neutrophil specific CXCR2 deletion on circulating neutrophil populations

CXCR2 signalling is a well described inducer of neutrophil ageing. Diurnal neutrophil ageing is controlled by the clock protein BMAL1 which induces CXCL2 and subsequent autocrine signalling via its receptor CXCR2 to drive neutrophil ageing (summarised in figure 1.6).[61] I therefore investigated whether LD neutrophils could be found in a neutrophil specific CXCR2 knockout model as well as looking at their phenotype and functional characteristics. I obtained 10-week-old male *Cxcr2*$^{DNeut}$ mice from the Cancer Research UK Scotland Institute. My control for this experiment were age matched *Cxcr2*$^{fl/fl}$ cre negative controls mice (figure 5.12 A). The nuclear morphology of neutrophils in *Cxcr2*$^{DNeut}$ mice was the same as in *Cxcr2*$^{fl/fl}$ (figure 5.12 B). CXCR2 expression was confirmed to be selectively knocked out in the neutrophils of *Cxcr2*$^{DNeut}$ mice (figure 5.13 C-D), although like in my patient data (figure 4.17) liver neutrophils in *Cxcr2*$^{fl/fl}$ mice were noted to have low expression of CXCR2 compared to blood neutrophils. *Cxcr2*$^{DNeut}$ neutrophils had comparable basal and PMA stimulated ROS compared to *Cxcr2*$^{fl/fl}$ neutrophils (figure 5.13 E) but had a significantly reduced migration capacity to CXCL2 (figure 5.13 F). Interestingly there was no difference in the proportions of circulating ND and LD neutrophils between *Cxcr2*$^{DNeut}$ and *Cxcr2*$^{fl/fl}$ mice (figure 5.13 G-I). Therefore despite selectively knocking out CXCR2 expression in neutrophils and potentially ameliorating neutrophil ageing the percentage of circulating LD neutrophils did not change.

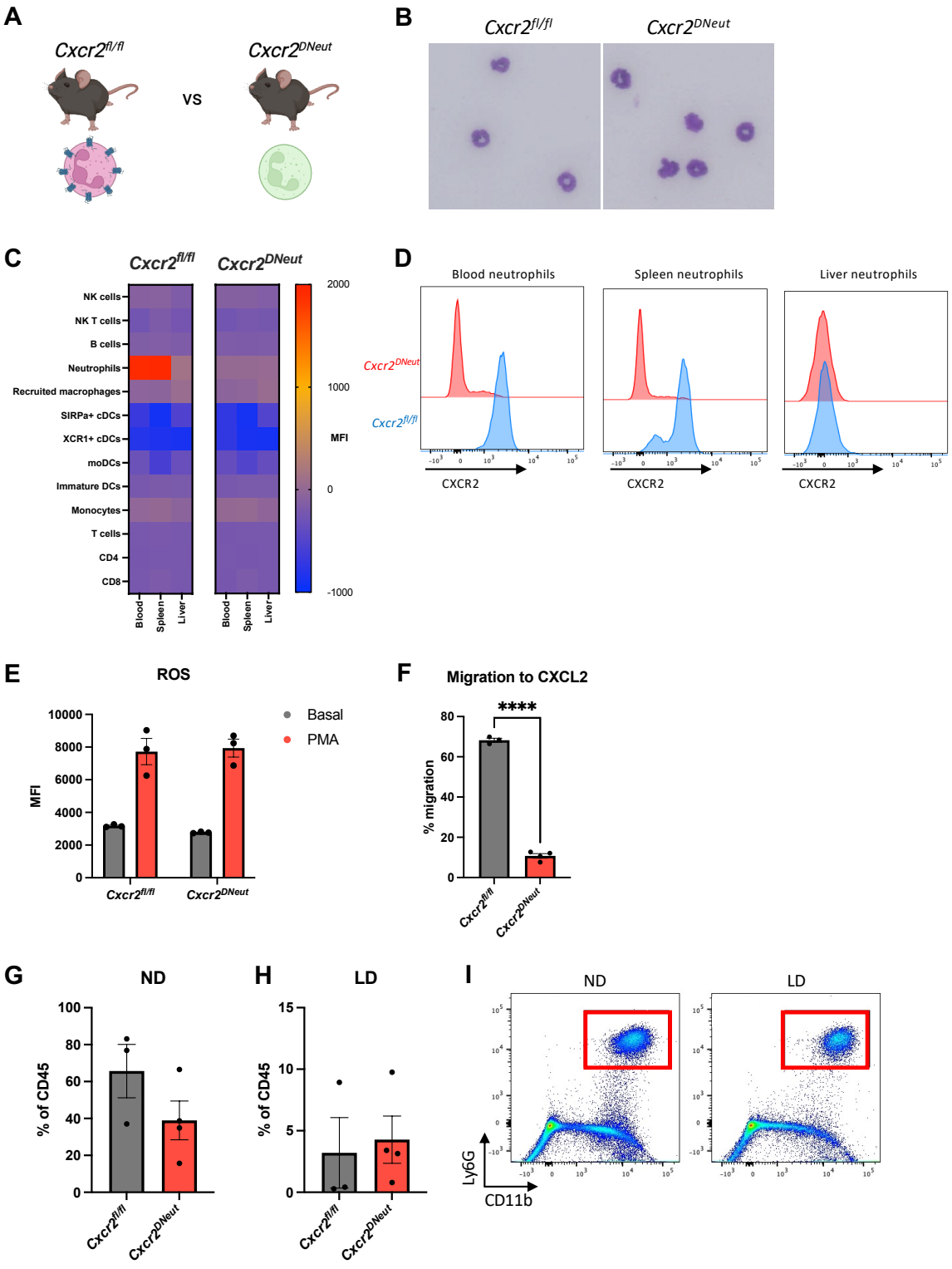



**Figure 5.13 – The effect of neutrophil specific CXCR2 deletion on circulating neutrophil populations. A.** Experiment design/ genetics. **B.** Giemsa stain of circulating neutrophils. **C.** Heatmap demonstrating the relative expression of CXCR2 on blood, spleen and liver isolated leukocytes in *Cxcr2*$^{DNeut}$ and*Cxcr2*$^{fl/fl}$ mice, n=4. **D.** Representative histograms demonstrating CXCR2 expression in blood, spleen and liver isolated neutrophils from *Cxcr2*$^{DNeut}$ vs *Cxcr2*$^{fl/fl}$ mice. **E.** Quantification of basal and PMA stimulated ROS in neutrophils from *Cxcr2*$^{DNeut}$ vs *Cxcr2*$^{fl/fl}$ mice, n=3. **F**. Quantification of

migration to CXCL2 in neutrophils isolated from *Cxcr2*$^{DNeut}$ vs *Cxcr2*$^{fl/fl}$ mice, n=3. **G.** Quantification of ND neutrophil frequency in *Cxcr2*$^{DNeut}$ vs *Cxcr2*$^{fl/fl}$ mice, *Cxcr2*$^{fl/fl}$ n=3, *Cxcr2*$^{DNeut}$ n=4. **H.** Quantification of LD neutrophil frequency in *Cxcr2*$^{DNeut}$ vs *Cxcr2*$^{fl/fl}$ mice, *Cxcr2*$^{fl/fl}$ n=3, *Cxcr2*$^{DNeut}$ n=4. **I.** Representative plot of ND and LD fractions isolated from *Cxcr2*$^{DNeut}$ mice. P values calculated using an unpaired t-test *p<0.05, **p<0.01, ***p<0.001, ****p<0.0001, ns non-significant.

### 5.5.2. BrdU neutrophil tracking experiment to establish the origin of circulating LD neutrophils

To establish the dynamics and origin of LD neutrophils in vivo I conducted a BrdU tracking experiment. Following administration, BrdU is only incorporated into proliferating cells. Neutrophils are terminally differentiated cells therefore only proliferating neutrophil pre-cursors in the bone marrow will incorporate BrdU. Therefore using this system, I could track neutrophils from the bone marrow migrating to the blood and other biological compartments.

#### 5.5.2.1. BrdU tracking validation and flow cytometry gating strategy

I validated BrdU as a method for tracking neutrophils in WD-HCC mice. Each mouse was given an intra-peritoneal injection of BrdU 2 mg. Following this, mice were harvested at various timepoints or tail vein blood collected and leukocytes isolated and stained with mouse panels 10 or 11, run through the flow cytometer and gated as per figure 5.14 A-B. Leukocytes were identified on FSC-A vs SSC-A, then single cells identified by selecting cells that had a proportional FSC-A to FSC-H. Next live cells were gated on followed by CD45$^{+}$. Neutrophils were then identified based on being CD11b$^{+}$Ly6G$^{+}$. Following this BrdU positive neutrophils could be gated (figure 5.14 B). On day 1 bone marrow immature precursor neutrophils had BrdU positivity whereas neutrophils in other biological compartments did not (figure 5.14 C). On day 2 mature bone marrow neutrophils became BrdU positive and on day 3 blood, spleen, liver and tumour neutrophils started to become positive (figure 5.14 C-D). After day 4 there was higher neutrophil BrdU positivity in the blood, spleen, liver and tumour compared to the bone marrow (figure 5.14 C-D). This shows how BrdU positivity shifts from the bone marrow to the blood then to spleen, liver and tumour over the time course and validates this as a model for tracking neutrophils in vivo.

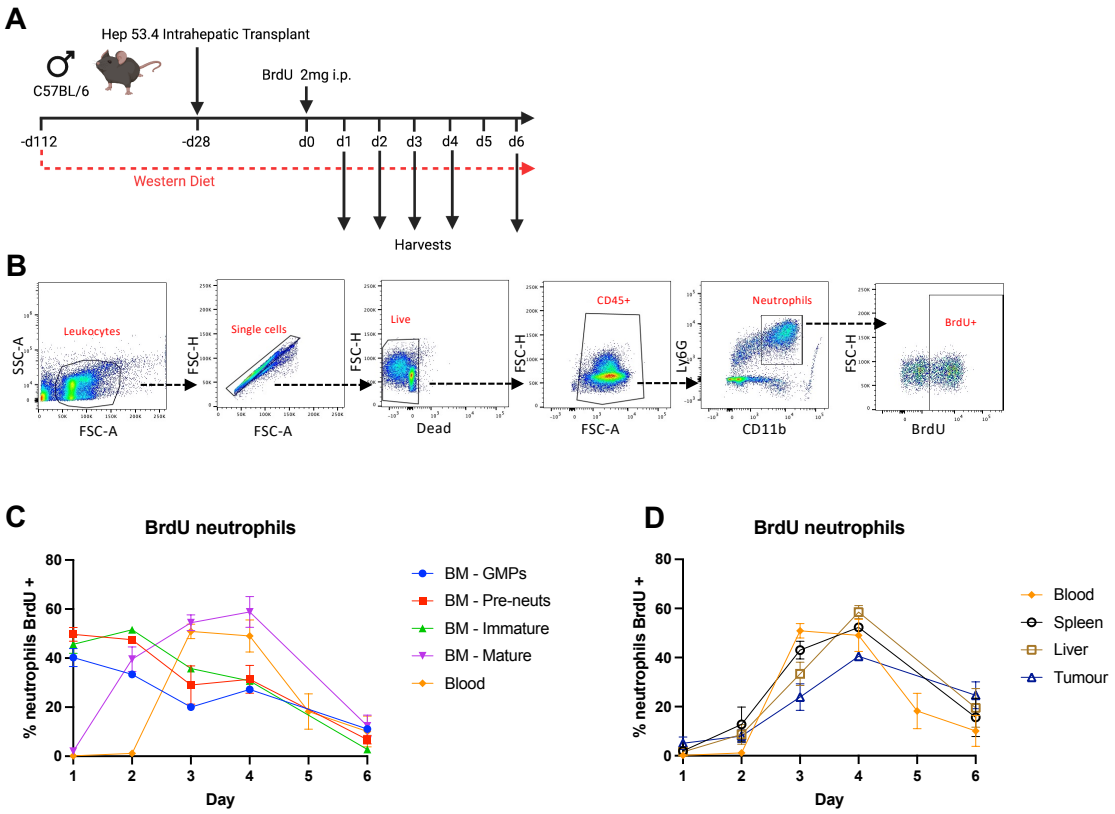



**Figure 5.14 – BrdU tracking validation and flow gating strategy. A.** Schematic outlining BrdU tracking validation experiment. **B.** Gating strategy. Leukocytes were gated on FSC-A vs SSC-A followed by single cells on FSC-A vs FSC-H. Next live cells were gated on as being negative of the dead cell dye. Neutrophils were then identified as being $CD45^{+}CD11b^{+}Ly6G^{+}$. Following this BrdU positive neutrophils could be gated. **C**. Quantification of the percentage of BrdU positive neutrophils in bone marrow neutrophil populations and in the blood. **D.** Quantification of the percentage of BrdU positive neutrophils in the blood, spleen, liver and tumour. n=4.

### 5.5.2.2. BrdU tracking of ND and LD neutrophils

BrdU positivity was tracked in WD-HCC mice because of the higher frequency of LD neutrophils as demonstrated in figure 5.9. Following BrdU administration (figure 5.15 A) there was a significantly higher frequency of BrdU positive LD neutrophils compared to ND neutrophils at the early day 2 timepoint (figure 5.15 B-C). From the previous experiment I knew this to be the earliest time point BrdU positive neutrophils are found in the blood (figure 5.14C). Therefore this suggests that the LD neutrophils at this timepoint have migrated out of the bone marrow as LD neutrophils rather than as ND neutrophils which have subsequently aged into LD neutrophils. At days 4 and 6 following BrdU administration there was a significantly raised frequency of BrdU

positive LD compared to ND neutrophils (figure 5.15 B-C) with LD BrdU positive neutrophils appearing to accumulate. This may suggest that either LD neutrophils are more long lived than ND neutrophils and/or that LD neutrophils have also come from other compartments such as ND neutrophils or tissue neutrophils which then accumulate in the LD fraction. Therefore this experiment demonstrates that at least some LD circulating neutrophils migrate out of the bone marrow as LD neutrophils and that LD neutrophils may also accumulate and be more long lived. They may also be ND or tissue neutrophils which have aged.

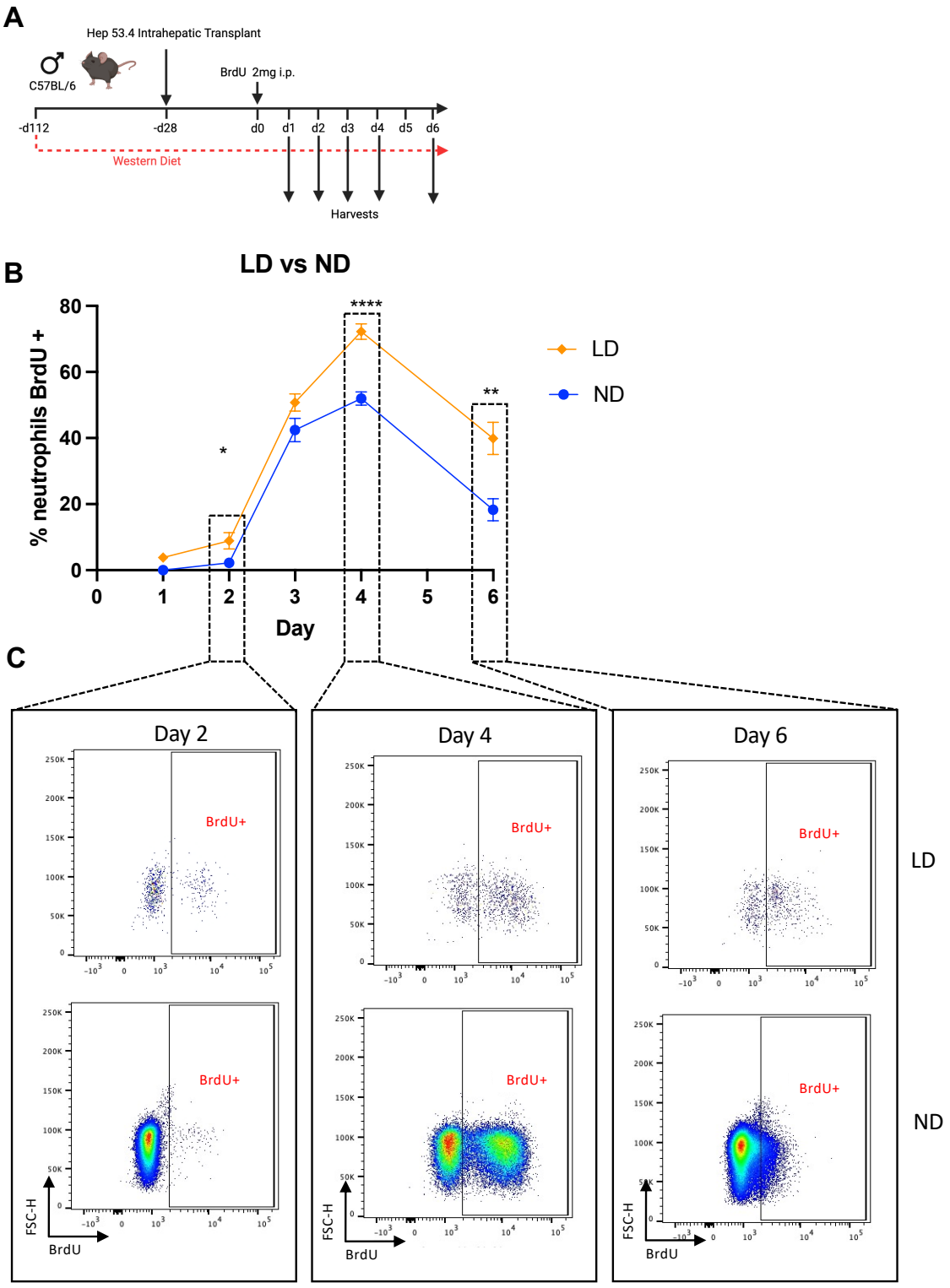



**Figure 5.15 – BrdU tracking of ND and LD neutrophils in WD-HCC mice. A.** Schematic outlining BrdU tracking validation experiment. **B**. Quantification BrdU positivity in LD vs ND neutrophils throughout the time course. **C**. Representative plots of BrdU positivity in LD and ND neutrophils at day 2, 4 and 6 following BrdU administration. P values calculated using an unpaired t-test *p<0.05, **p<0.01, ***p<0.001, ****p<0.0001, ns non-significant. n=8.

## 5.6. Neutrophil dynamics across biological compartments

### 5.6.1. Frequency of bone marrow, spleen, liver and tumour neutrophils in HCC

Following confirmation that circulating LD neutrophils are enriched in WD-HCC compared to WD-sham mice I next investigated the frequency of neutrophils in the bone marrow, spleen, liver and tumours of tumour bearing mice compared to sham controls (figure 5.16 A). This demonstrated an increase in neutrophil frequency across biological compartments. Neutrophil frequency was increased in the spleen and livers of WD-HCC mice compared to WD-Sham mice (figure 5.16 B-E). Neutrophils were also more frequent in the tumours of mice compared to the background liver tissue (figure 5.16 F-H). In the bone marrow granulocyte-monocyte progenitors (GMPs), pre-neuts, immature and mature neutrophils were identified according to the gating strategy outlined in figure 5.16 and validated by morphological analysis (figure 5.16 I). In the bone marrow there was a preferential increase in the frequency of early neutrophil progenitors – GMPs and pre-neuts (figure 5.16 J-K) with no increase in immature or mature bone marrow neutrophils (figure 5.16 L-M). Taken together these results suggest that in tumour bearing mice there is an accumulation of neutrophils across all biological compartments that is driven by an altered state of granulopoiesis and release from the bone marrow. One explanation for the preferential increase of GMPs and pre-neuts in the bone marrow but no increase in immature or mature neutrophils could be due to the premature release of these bone marrow populations into the circulation of tumour bearing mice.

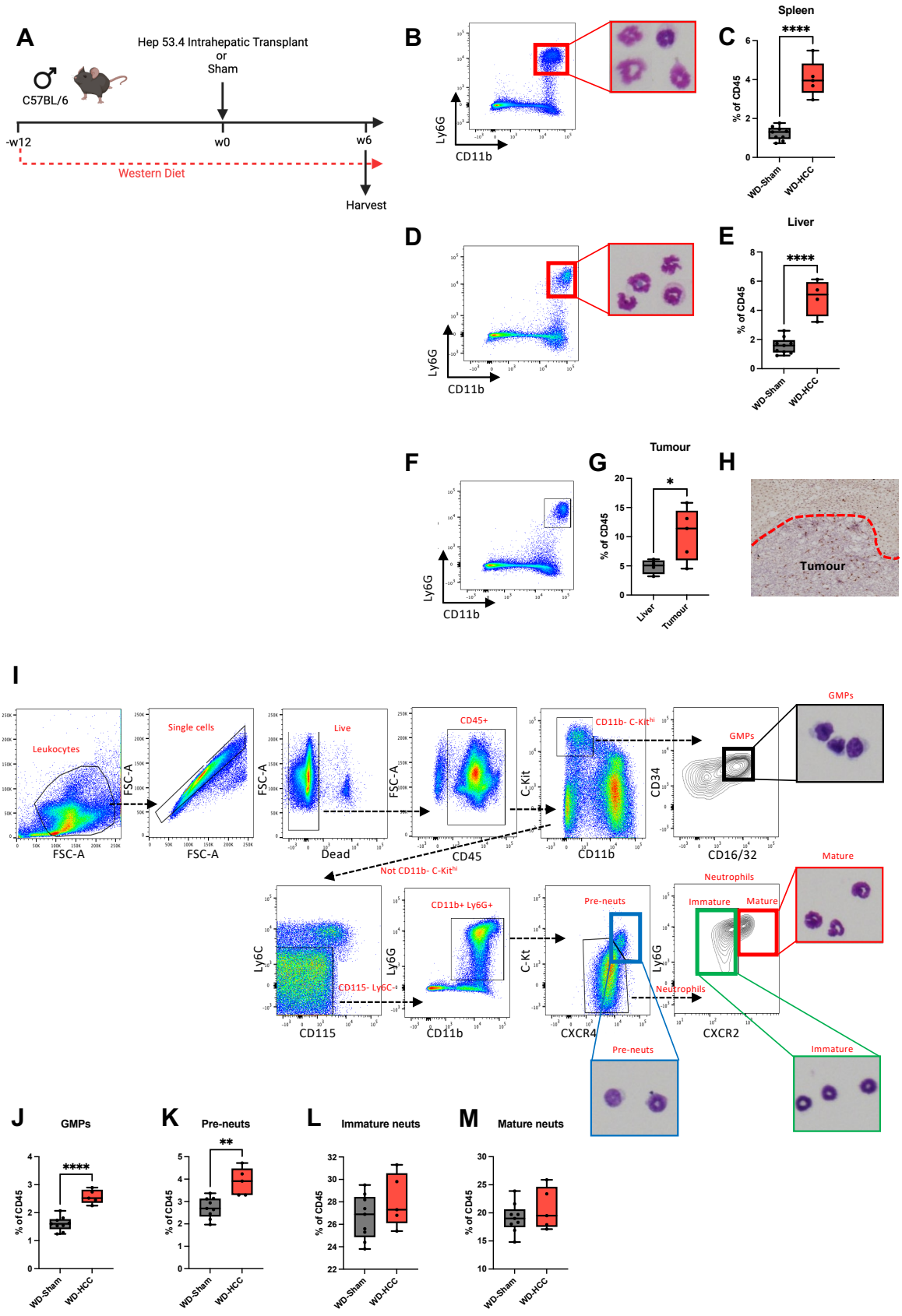



**Figure 5.16 – Frequency of bone marrow, spleen, liver and tumour neutrophils in WD-HCC vs WD-Sham mice. A.** Schematic outlining experiment comparing neutrophil frequencies in WD-HCC vs WD-Sham mice. **B**. Representative flow plot of spleen neutrophils from WD-HCC mice and

representative nuclear morphology on giemsa staining. **C.** Quantification of the frequency of spleen neutrophils in WD-HCC vs WD-Sham mice. **D.** Representative flow plot of liver neutrophils from WD-HCC mice and representative nuclear morphology on giemsa staining. **E.** Quantification of the frequency of liver neutrophils in WD-HCC vs WD-Sham mice. **F.** Representative flow plot of tumour neutrophils from WD-HCC mice. **G.** Quantification of the frequency of neutrophils in the tumours vs background liver of WD-HCC mice. **H.** Representative Ly6G IHC staining demonstrating the rich neutrophil infiltrate within the tumours of WD-HCC mice compared to the surrounding liver. **I.** Gating strategy to identify bone marrow neutrophil populations. Leukocytes were identified on FSC-A vs SSC-A, then single cells on FSC-A vs FSC-H. Next live cells were selected as being dead stain negative then $CD45^+$ selected. GMPs were identified as being $CD11b^-C\text{-}kit^{high}$ as well as $CD34^+CD16/32^+$. Of the not $CD11b^-C\text{-}kit^{high}$ population pre-neuts were identified as being $CD115^-Ly6C^-CD11b^+Ly6G^-$ then $CXCR4^{high}C\text{-}kit^{high}$. Of the $CXCR4^{low}C\text{-}kit^{low}$ population mature neutrophils were identified as being $CXCR2^{high}$ and immature neutrophils as being $CXCR2^{low}$. This gating strategy was adapted from Evrard et al.[371] Bone marrow neutrophil populations were validated on giemsa staining and morphological analysis. **J.** Quantification of GMP frequency in WD-HCC vs WD-Sham mice. **K**. Quantification of pre-neut frequency in WD-HCC vs WD-Sham mice. **L**. Quantification of immature bone marrow neutrophil frequency in WD-HCC vs WD-Sham mice. **M.** Quantification of mature bone marrow neutrophil frequency in WD-HCC vs WD-Sham mice. P values calculated using an unpaired t-test *p<0.05, **p<0.01, ***p<0.001, ****p<0.0001, ns non-significant. WD-sham n=9, WD-HCC n=5.

### 5.6.2. Dynamic changes in granulopoiesis associated with HCC

To further investigate changes in granulopoiesis induced by HCC I conduced a BrdU tracking experiment to get a measure of how neutrophil dynamics in the bone marrow are altered by HCC (figure 5.17 A). This demonstrated no significant changes in GMP and pre-neut BrdU positivity in WD-HCC vs WD-Sham (figure 5.17 B-C). But did show significantly more BrdU positivity in immature bone marrow neutrophils at day 1 and mature neutrophils at day 1 and 2 in WD-HCC compared WD-Sham mice (figure 5.17 D-G). Of the BrdU positive neutrophils in the bone marrow on day 3 there was significantly reduced expression of CD62L in WD-HCC compared to WD-Sham mice (figure 5.17 H-I). Together these findings suggest that there is an accelerated rate of granulopoiesis in HCC as well as an increased amount of neutrophil ageing and activation in the bone marrow. This may demonstrate that not only is granulopoiesis accelerated in the context of HCC but there is also abnormal activation and ageing of neutrophils occurring in the bone marrow which results an abnormal aged and pre-activated neutrophil being released from the bone marrow. It maybe these which are the LD circulating neutrophils I am observing in both HCC patients and HCC bearing mice.

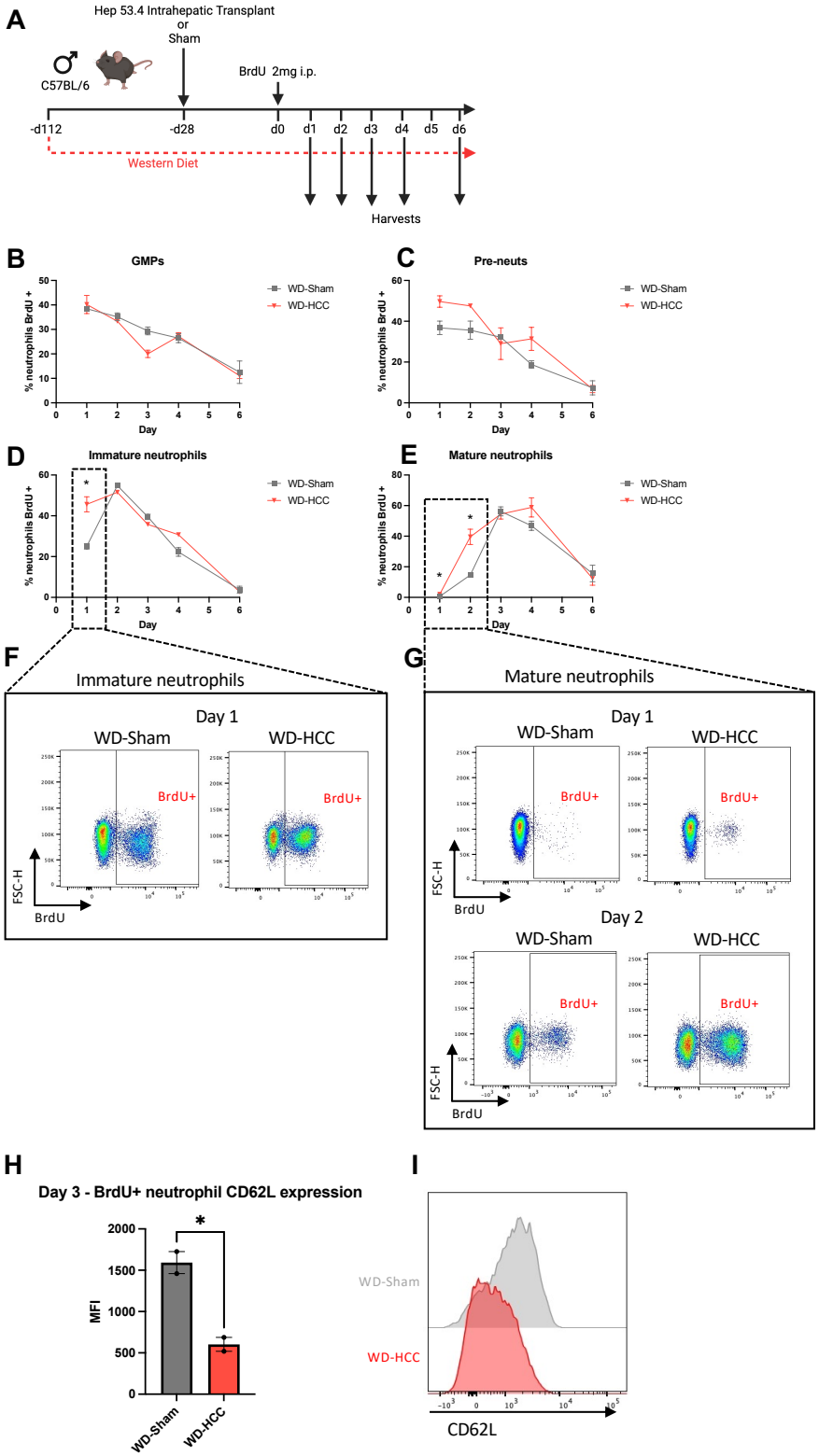



**Figure 5.17 – Altered granulopoiesis associated with HCC. A.** Schematic outlining BrdU tracking experiment. **B.** Quantification of GMP BrdU positivity in WD-HCC vs WD-Sham throughout the time course, n=2-4 each timepoint. **C.** Quantification of pre-neut BrdU positivity in WD-HCC vs WD-Sham throughout the time course, n=2-4 each timepoint. **D.** Quantification of immature bone marrow

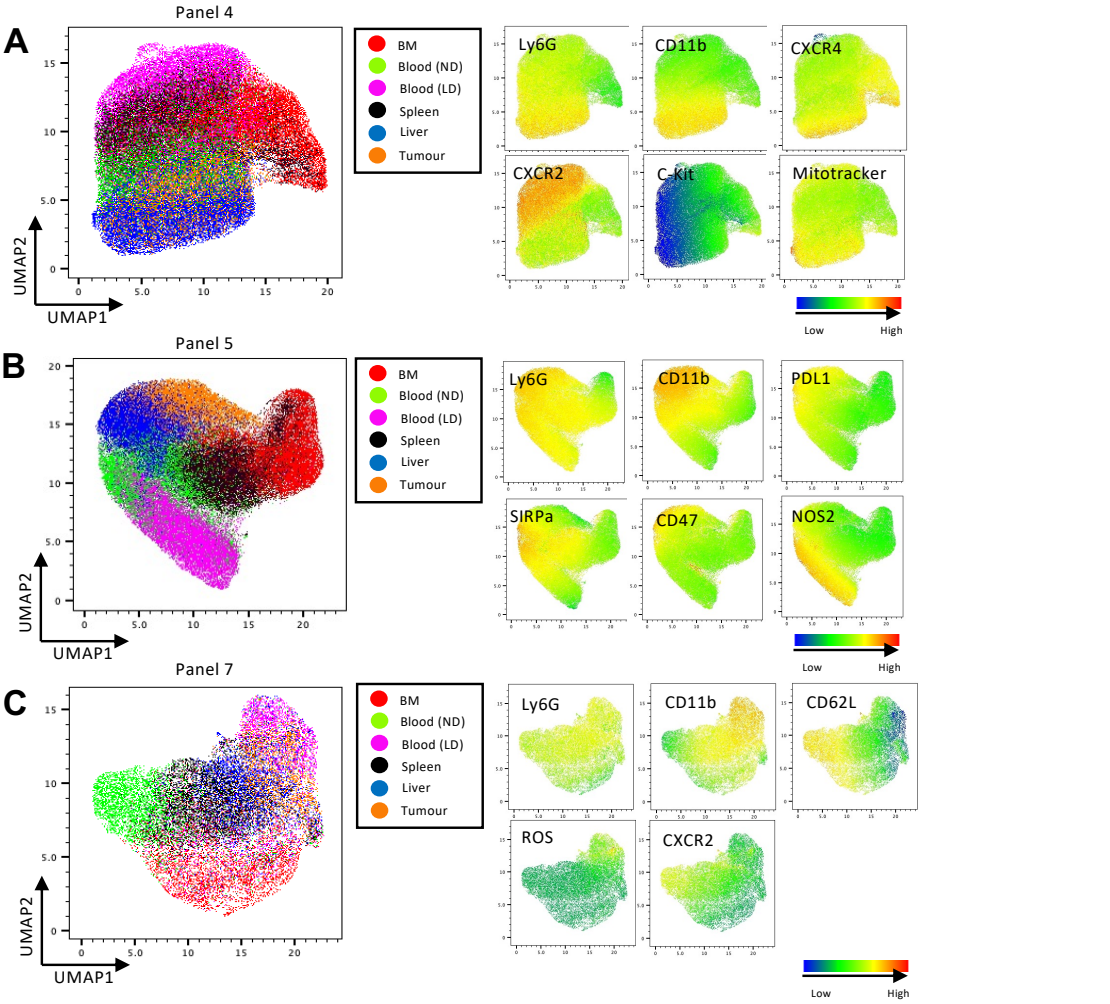
neutrophil BrdU positivity in WD-HCC vs WD-Sham throughout the time course, n=2-4 each timepoint. **E.** Quantification of mature bone marrow neutrophil BrdU positivity in WD-HCC vs WD-Sham throughout the time course, n=2-4 each timepoint. **F.** Representative plot of BrdU positivity in immature bone marrow neutrophils on day 1. **G.** Representative plot of BrdU positivity in mature bone marrow neutrophils on day 1 and 2. **H.** Quantification of CD62L expression in mature day 3 BrdU positive neutrophils in WD-HCC vs WD-Sham, n=2. **I.** Representative histogram of CD62L expression in WD-HCC vs WD-Sham mature bone marrow $BrdU^+$ neutrophils on day 3. P values calculated using an unpaired t-test *p<0.05, **p<0.01, ***p<0.001, ****p<0.0001, ns non-significant.

### 5.7. Neutrophil phenotype and function across biological compartments

In order to assess how neutrophil phenotype changes as they migrate from the bone marrow to the blood then to organs I conducted phenotyping and functional assays of neutrophils isolated from the different biological compartments in WD-HCC mice.

#### 5.7.1. Neutrophil phenotype across biological compartments

On high dimensional analysis neutrophils from the bone marrow, blood ND, blood LD, spleen, liver and tumour clustered in distinct populations according to their tissue of residence (figure 5.18 A-C). As neutrophils migrate from the bone marrow to the blood then spleen, liver and tumour they are found to be more mature and activated as demonstrated by increasing expression of Ly6G and CD11b and reducing expression of C-kit (figure 5.18 D-F). They also became more aged with reducing CXCR2 and CD62L expression and increasing CXCR4 expression (figure 5.18 G-I). There was also varying levels of expression of the immune checkpoint receptors PDL1, SIRPα and CD47 (figure 5.18 J-L). PDL1 is the ligand for PD1 and induces T cell immunosuppression.[372] Tumour and liver neutrophils had the highest expression of PDL1 suggesting that they are an immunosuppressive population of neutrophils (figure 5.18 J). The CD47- SIRPα immune checkpoint acts as an immune checkpoint for innate phagocytic cells, inhibiting phagocytosis.[302] Again like PDL1 expression CD47 expression was highest in liver and tumour neutrophils (figure 5.18 L). This suggests that these neutrophil populations are inhibiting their clearance from the liver and tumour allowing them to be more long lived and more immunosuppressive. Intracellular NOS2 and mitochondrial mass also varied between compartments (figure 5.18 M-N).


A
Panel 4
BM
Blood (ND)
Blood (LD)
Spleen
Liver
Tumour
UMAP1
UMAP2
Ly6G
CD11b
CXCR4
CXCR2
C-Kit
Mitotracker
Low
High
B
Panel 5
PDL1
SIRPa
CD47
NOS2
C
Panel 7
CD62L
ROS

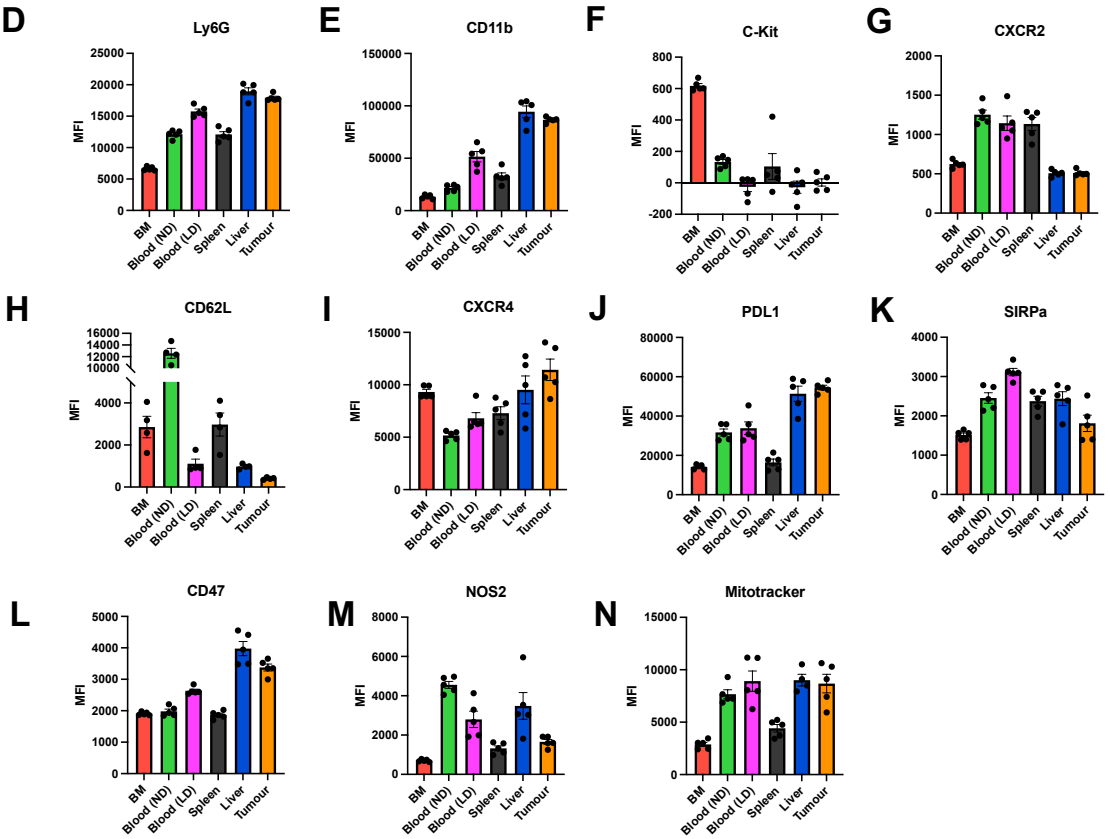

D
Ly6G
E
CD11b
F
C-Kit
G
CXCR2
H
CD62L
I
CXCR4
J
PDL1
K
SIRPa
L
CD47
M
NOS2
N
Mitotracker
MFI
BM
Blood (ND)
Blood (LD)
Spleen
Liver
Tumour

**Figure 5.18 – Neutrophil phenotype across biological compartments. A.** Flow cytometry panel 4 UMAP analysis of bone marrow, blood, liver and tumour neutrophil phenotype. **B.** Flow cytometry panel 5 UMAP analysis of bone marrow, blood, liver and tumour neutrophil phenotype. **C.** Flow cytometry panel 7 UMAP analysis of bone marrow, blood, liver and tumour neutrophil phenotype. **D-N.** Quantification of Ly6G, CD11b, C-kit, CXCR2, CD62L, CXCR4, PDL1, SIRPα, CD47, NOS2 and mitochondrial mass in bone marrow (BM), blood LD and ND, spleen, liver and tumour neutrophils. n=5.

### 5.7.2. Neutrophil functional assays across biological compartments

In line with the phenotyping data (figure 5.18) neutrophils across the different biological compartments also had different functional abilities in terms of ROS production, migration to CXCL2 and phagocytosis (figure 5.19 A-D). Blood LD and tumour neutrophils had the highest basal ROS (figure 5.19 A) whereas blood ND, liver and tumour neutrophils had the highest PMA stimulated ROS (figure 5.19 B). Ability to migrate to CXCL2 generally correlated with CXCR2 expression with blood ND and spleen neutrophils having the highest migration percentage, blood LD and liver neutrophils having an intermediate migration percentage and bone marrow and tumour neutrophils having the least migration percentage (figure 5.19 C). Bone marrow neutrophils displayed the least phagocytosis activity and blood ND neutrophils the greatest phagocytosis activity (figure 5.19 D). Tumour neutrophils displayed the least phagocytosis activity compared to blood ND, blood LD, spleen and liver neutrophils (figure 5.19 D). Taken together these data suggest that tumour neutrophils are high producers of ROS and poor at phagocytosis compared to neutrophils in other compartments. ROS production in the tumour microenvironment is known to be a potent suppressor of cytotoxic T cells,[250] and again points to intra-tumour neutrophils in this preclinical model as being immunosuppressive and pro-tumour in nature, confirming neutrophils to be a potential therapeutic target in HCC.

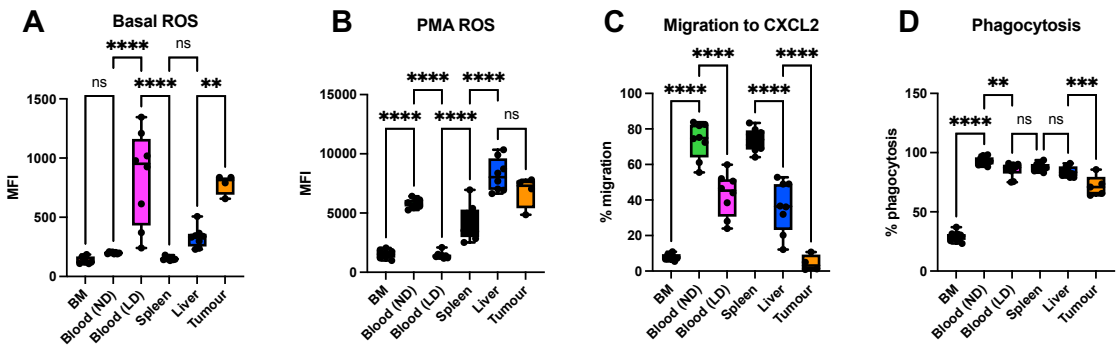



**Figure 5.19 – Neutrophil functional assays across biological compartments. A.** Quantification of basal ROS activity. **B.** Quantification of PMA stimulated ROS activity. **C.** Quantification of percentage migration to CXCL2. **D.** Quantification of the phagocytosis percentage. P values calculated using a one-way ANOVA with Tukey post-hoc test *p<0.05, **p<0.01, ***p<0.001, ****p<0.0001, ns non-significant. BM n=8, blood (ND) n=8, blood (LD) n=8, spleen n=8, liver n=8, tumour n=5.

## 5.8. Effect of HCC on neutrophil phenotype and function

Next I investigated whether HCC had any effect on neutrophil phenotype and function across the different biological compartments.

### 5.8.1. Effect of HCC on neutrophil phenotype

Neutrophils from WD-HCC mice had significantly reduced Ly6G expression compared to WD-Sham controls in the bone marrow, blood LD, spleen and liver (figure 5.20 A and C). Similarly, in WD-HCC mice neutrophils from the tumour had reduced Ly6G expression compared to neutrophils from the background liver (figure 5.20 B). There are reports that neutrophil Ly6G expression reduces as neutrophil age and/or activate.[67,373] I therefore conduced an in vitro PMA stimulation experiment with neutrophils isolated from different compartments of WD-HCC mice (figure 5.20 D). This demonstrated that PMA stimulation induced a significant reduction in Ly6G expression in spleen, liver and tumour neutrophils as well as a trend to reduction in bone marrow and blood LD neutrophils (figure 5.20 D). Together these data suggest that HCC induces ageing and activation of neutrophils across biological compartments. These changes may in fact start in the bone marrow due to an altered state of granulopoiesis as also supported by data showing a preferential expansion of early neutrophil progenitors (figure 5.16 J-M) and accelerated granulopoiesis (figure 5.17).

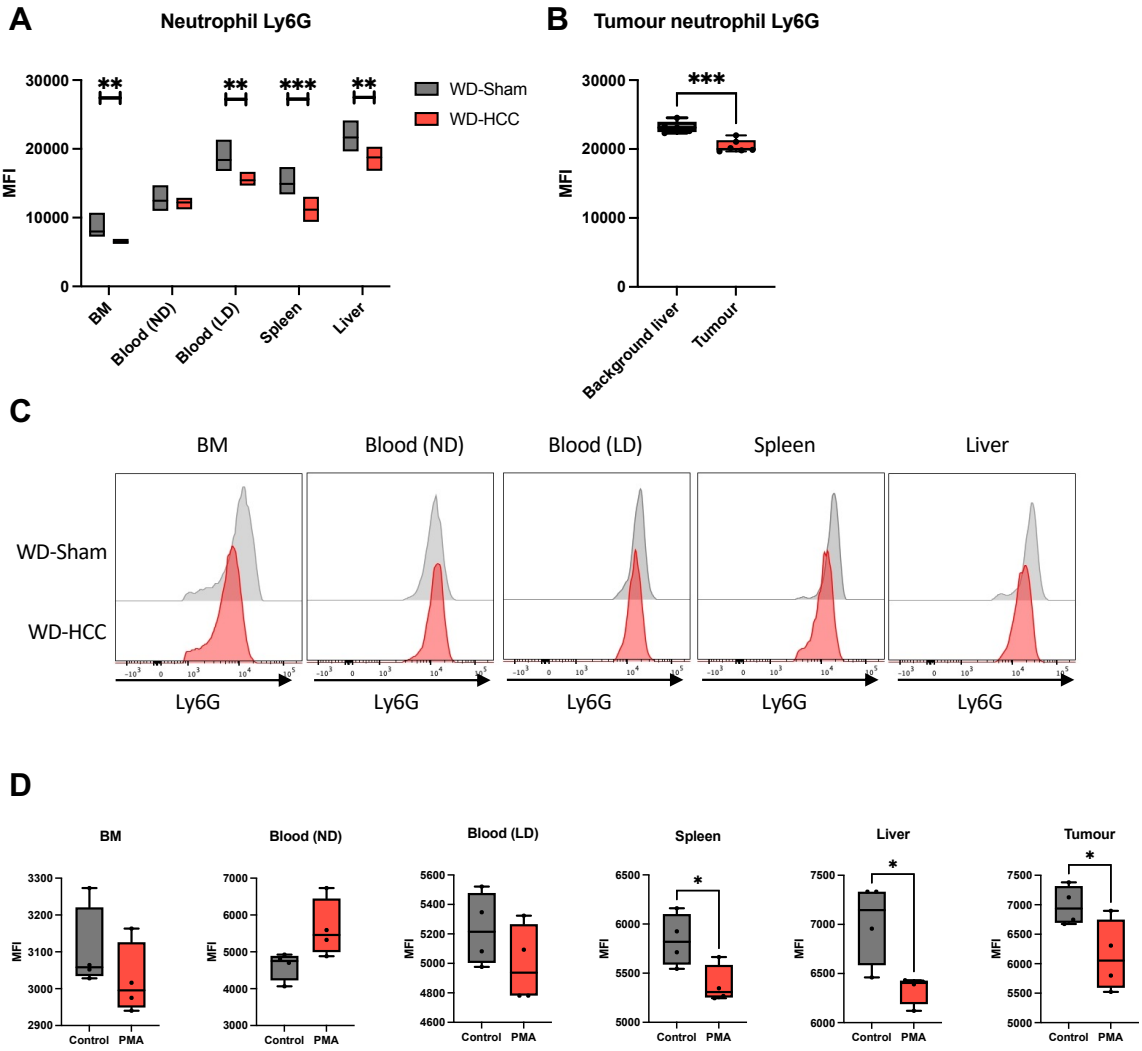



**Figure 5.20 – Effect of HCC on neutrophil phenotype. A.** Quantification of neutrophil Ly6G expression in WD-HCC vs WD-Sham mice, n=6. **B.** Quantification of tumour vs background liver neutrophil Ly6G expression in WD-HCC mice, n=6. **C.** Representative histograms demonstrating neutrophil Ly6G expression in WD-HCC vs WD-Sham mice. **D**. In vitro PMA stimulation experiment of neutrophils from WD-HCC mice. Quantification of neutrophil Ly6G expression following PMA stimulation, n=4. P values calculated using an unpaired t-test *p<0.05, **p<0.01, ***p<0.001, ****p<0.0001, ns non-significant.

### 5.8.2. Effect of HCC on neutrophil function

Functionally there was no difference in basal or PMA stimulated ROS in neutrophils from any compartments between WD-HCC and WD-Sham mice (figure 5.21 A). In bone marrow neutrophils there was a significantly increased percentage migration to CXCL2 in WD-HCC vs WD-Sham (figure 5.21 C) which corresponded to increased CXCR2 expression in WD-HCC bone marrow neutrophils (figure 5.21 D). This again indicates altered granulopoiesis in HCC-bearing mice with the bone marrow

neutrophils being more mature and supports the data presented in figure 5.16 and 5.17. There was no difference in percentage migration to CXCL2 between WD-HCC vs WD-Sham blood LD, blood ND, spleen and liver neutrophils (figure 5.21 E). There was no difference in phagocytosis capacity between WD-HCC and WD-Sham neutrophils (figure 5.21 F).

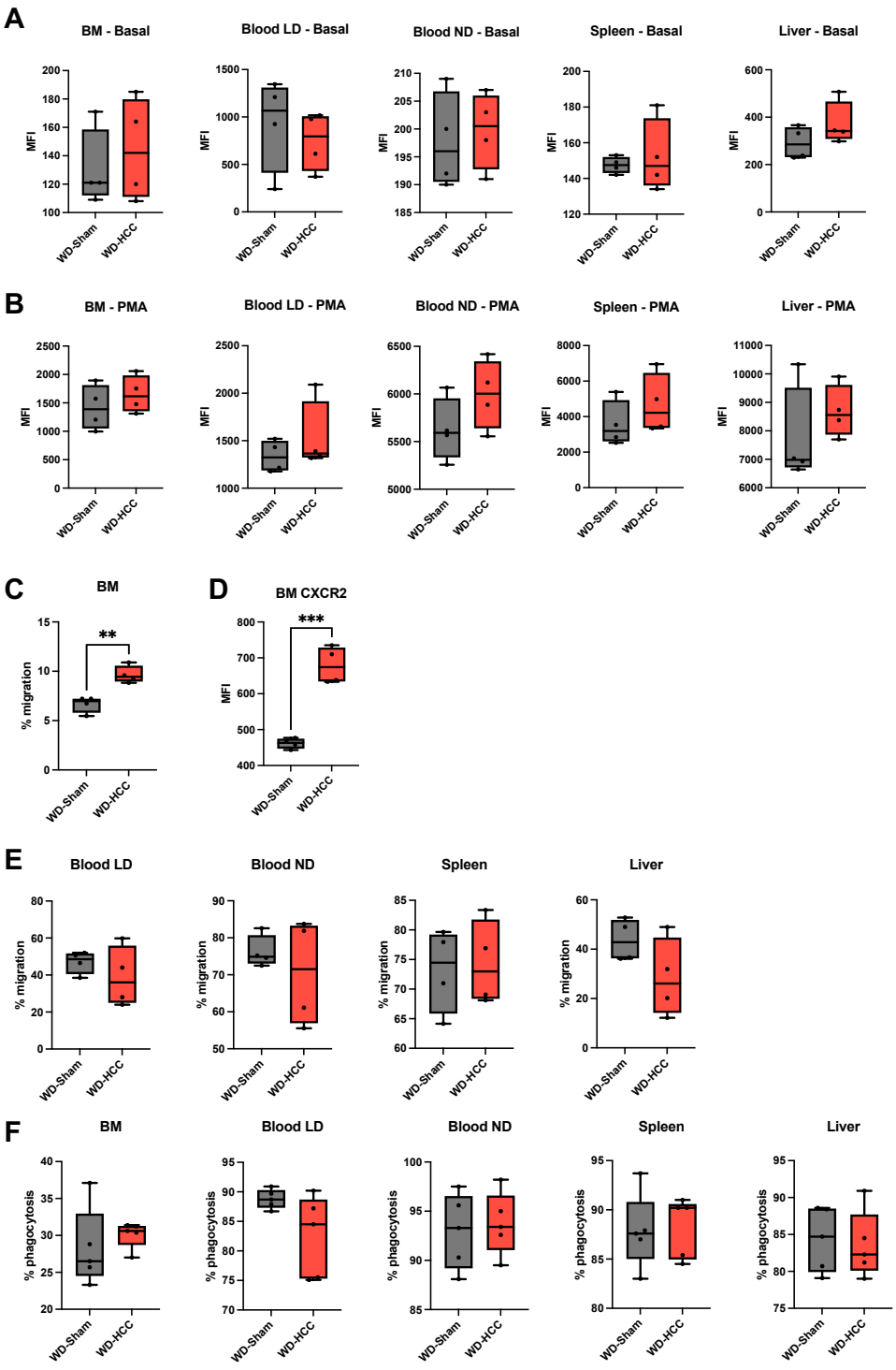


**Figure 5.21 – Effect of HCC on neutrophil function. A.** Quantification of basal ROS in BM, blood LD, blood ND, spleen and liver neutrophils from WD-HCC vs WD-Sham mice, n=4. **B**. Quantification of PMA stimulated ROS in BM, blood LD, blood ND, spleen and liver neutrophils from WD-HCC vs WD-Sham mice, n=4. **C.** Quantification of BM neutrophil migration to CXCL2 in WD-HCC vs WD-Sham, n=4. **D.** Quantification of BM neutrophil CXCR2 expression in WD-HCC vs WD-Sham, n=4. **E.** Quantification of blood LD, blood ND, spleen and liver neutrophil migration to CXCL2 in WD-HCC vs WD-Sham, n=4. **F**. Quantification of BM, blood LD, blood ND, spleen and liver neutrophil phagocytosis in WD-HCC vs WD-Sham, n=5. P values calculated using an unpaired t-test *p<0.05, **p<0.01, ***p<0.001, ****p<0.0001, ns non-significant.

## 5.9. Conclusion

I have validated a pre-clinical model of HCC on the background of non-fibrotic MASH in which rapidly progressive tumours are produced. This model has similar effects on neutrophils as I described in human HCC patients. There is an increase in the frequency of circulating neutrophils in HCC bearing mice, with this being driven by a preferential increase in LD neutrophils. LD neutrophils in this model closely resemble the LD CD16$^{high}$ population I describe in HCC patients. Phenotypically they are mature, activated and aged as demonstrated by their increased CD11b and CXCR4 expression and reduced CD62L, C-kit and CXCR2 expression. They also co-express the platelet markers CD36 and CD41 suggesting the presence of NPAs. Functionally mouse LD neutrophils resemble human LD CD16$^{high}$ neutrophils in that they have reduced migration tendency to CXCL2 and reduced phagocytosis capacity. The main difference between mouse and human circulating neutrophils is that I could not identify a corresponding immature population in mice to the LD CD16$^{low}$ population found in humans. Additionally, mouse and human LD neutrophils had opposite ROS profiles with mouse LD neutrophils having a high basal ROS and low PMA stimulated ROS and human LD CD16$^{high}$ neutrophils having a low basal ROS and high PMA stimulated ROS. Using pre-clinical models, I did some further investigation into the origin of LD neutrophils. To investigate whether they are a direct result of ageing through the Bmal1-CXCR2 pathway I used a neutrophil specific CXCR2 knockout mouse. This demonstrated that despite CXCR2 being knocked out in neutrophils there were still a similar proportion of LD neutrophils compared to controls with a comparable phenotype. This suggests that LD neutrophils are more than just aged ND neutrophils or at least there are other mechanisms to ageing independent to Bmal1-CXCR2. To ascertain the origin of LD neutrophils I performed a BrdU tracking experiment. This

demonstrated BrdU signal in the LD neutrophils before the ND neutrophils suggesting that LD neutrophils are formed in the bone marrow and are released into the circulation as such. This points to an altered state of granulopoiesis in HCC which is driving their production.

Like my findings in patients, I found that neutrophils in different biological compartments (bone marrow, blood, spleen, liver, tumour) have distinct phenotypes and functions. Tumour neutrophils had the highest expression of ROS and PDL1 suggesting immunosuppressive/ pro-tumour functions. Tumour neutrophils in mice like in humans had an activated and aged phenotype as demonstrated by higher expression of CD11b and CXCR4 and reduced expression of CXCR2 and CD62L. In addition to the expansion of circulating neutrophils I also found an increase in neutrophil frequency across other biological compartments such as the bone marrow, spleen and liver. I found evidence of this expansion being driven by altered granulopoiesis with increased frequencies of early neutrophil progenitors and an increased rate of granulopoiesis, confirmed using BrdU tracking, in HCC-bearing mice compared to controls.

There were also HCC induced changes in neutrophil phenotype. There was a reduction in Ly6G expression in bone marrow, blood LD, spleen and liver neutrophils from HCC-bearing mice compared to controls. An explanation for this is that there is accelerated ageing and activation of neutrophils in all biological compartments in HCC bearing mice and was supported by an in vitro PMA stimulation experiment showing reduced Ly6G expression following PMA activation.

Therefore, from both my patient study and pre-clinical models I have identified LD neutrophils with this activation/ageing/degranulation phenotype as being conserved and as being a potential therapeutic target. Tumour neutrophils also have this activation/ageing/degranulation phenotype and again this highlights neutrophil activation/ageing/degranulation as a possible therapeutic target.

# 6. Testing neutrophil targeted therapies in a pre-clinical model of MASH-HCC

## 6.1. Introduction

From my patient and pre-clinical studies, I have identified an expansion of LD circulating neutrophils which have an activated, aged and degranulated phenotype. I have also found that tumour neutrophils have an activated, aged and degranulated phenotype compared to neutrophils in other biological compartments. My next goal was to target LD neutrophils and/or neutrophil activation, ageing and degranulation experimentally in the pre-clinical models already described and characterised with the aim of assessing effects on tumour burden and neutrophil biology.

## 6.2. Targeting the JAK2-STAT3 pathway

The Janus kinase – signal transducer and activator of transcription (JAK-STAT) signalling pathway is involved in multiple cellular processes and allows rapid membrane to nucleus signalling.[374] The JAK-STAT3 pathway is of interest because it a common downstream pathway to both CXCR2 and IL-6 signalling in neutrophils.[209,375] CXCR2 signalling has been showed to be central to neutrophil mobilisation from the bone marrow and subsequent recruitment to HCC tumours as well as being crucial to neutrophil ageing.[61,115,208] Furthermore in pre-clinical studies there is evidence to suggest that inhibition of CXCR2 signalling can reprogram tumour neutrophils from a pro-tumour to anti-tumour phenotype and re-sensitise treatment resistant HCC to anti-PD1 immune checkpoint inhibtion.[56] IL-6 has been shown to stimulate the pro-tumour polarisation of neutrophils resulting in $PDL1^{+}$ immunosuppressive neutrophils which can suppress cytotoxic T cells.[209,230,231] STAT3 itself is also a regulator of emergency granulopoiesis.[376] This makes the JAK-STAT3 signalling pathway an attractive therapeutic target in neutrophils affecting multiple processes such as granulopoiesis, tumour recruitment, ageing and pro-tumour activation/polarisation. The CXCR2, IL-6, JAK2-STAT3 signalling pathways are outlines in figure 6.1. There are 4 different JAK non-receptor tyrosine protein kinases with JAK2 being well described as being an upstream regulator of STAT3.[374,377] AZD1480 is a small molecule inhibitor of JAK2 and has been shown to potently block

STAT3 signalling.[378] I therefore used this drug as one of my therapeutic agents of interest.

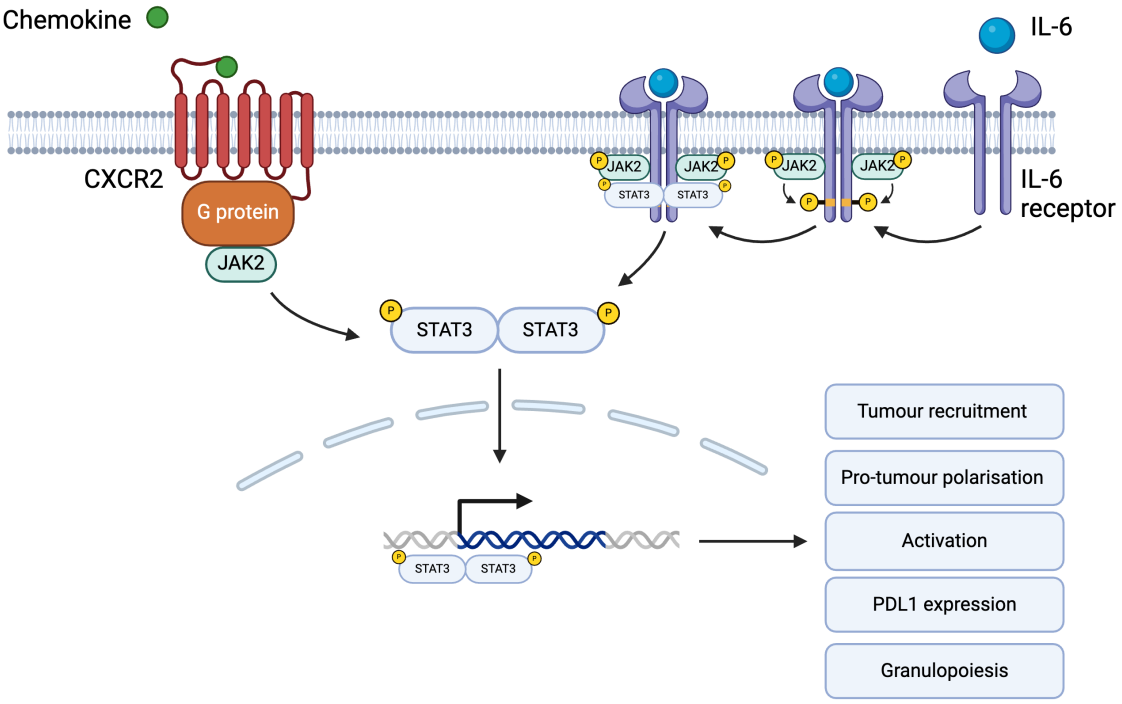



**Figure 6.1 – JAK2-STAT3 signalling pathway and its relation to IL-6 and CXCR2 in neutrophils.** The JAK-STAT3 pathway is activated by a diverse set of receptors including cytokine receptors, G-protein coupled receptors and toll like receptors and appears to be conserved across evolution.[377] JAK-STAT3 signalling allows rapid membrane to nucleus signalling. The IL-6 receptor is a cytokine receptor and when bound to IL-6 dimerizes and leads to the binding of JAK2 to the cytoplasmic tail of gp130 and the phosphorylation of STAT3. STAT3 then dissociates from the receptor, forms homodimers which then enter the nucleus to regulate transcription. CXCR2 is a G protein-coupled receptor when stimulated by its ligand and G-protein bound catalyses the conversion of guanine nucleotides and activates JAK2 which can directly phosphorylate STAT3 leading to homodimers which enter the nucleus and regulate transcription.[374,377] STAT3 mediated transcription has been shown to regulate neutrophils granulopoiesis, tumour recruitment, pro-tumour polarisation/activation and PDL1 expression.[374-377] Created with https://BioRender.com.

### 6.2.1. Neutrophil p-STAT3 expression in HCC

I measured phosphorylated STAT3 (p-STAT3) expression in neutrophils isolated from the tumours, livers and blood of HCC patients undergoing percutaneous tumour/liver biopsy. Tumour neutrophils had the highest expression of p-STAT3 with blood neutrophils having the least p-STAT3 expression and liver neutrophils having an intermediate p-STAT3 expression (figure 6.2 A-B). Likewise in neutrophils isolated from HCC-bearing mice, tumour neutrophils also expressed the most p-STAT3 (figure

6.2 C-D). In HCC-bearing mice LD circulating neutrophils expressed more p-STAT3 than ND circulating neutrophils however this difference was small in comparison to that of tumour neutrophils (figure 6.2 C-D). Because JAK2-STAT3 signalling is also a key pathway in tumour cells I looked at p-STAT3 expression in the HCC cell line used to implant in the pre-clinical model. This demonstrated that the Hep 53.4 tumour cells had low expression of p-STAT3 compared to the tumour neutrophils (figure 6.2 E-F). In addition, I looked at p-STAT3 expression in other immune cells isolated from the blood of HCC-bearing mice. This again showed that neutrophils had the highest p-STAT3 expression of all circulating immune cells (figure 6.2 G-H). Therefore, although the JAK2 small molecule inhibitor I was going to use for my therapeutic experiment was not neutrophil specific, neutrophils had the highest degree of JAK2-STAT3 activity of all cells, including tumour cells, as demonstrated by them expressing the highest amount of p-STAT3.

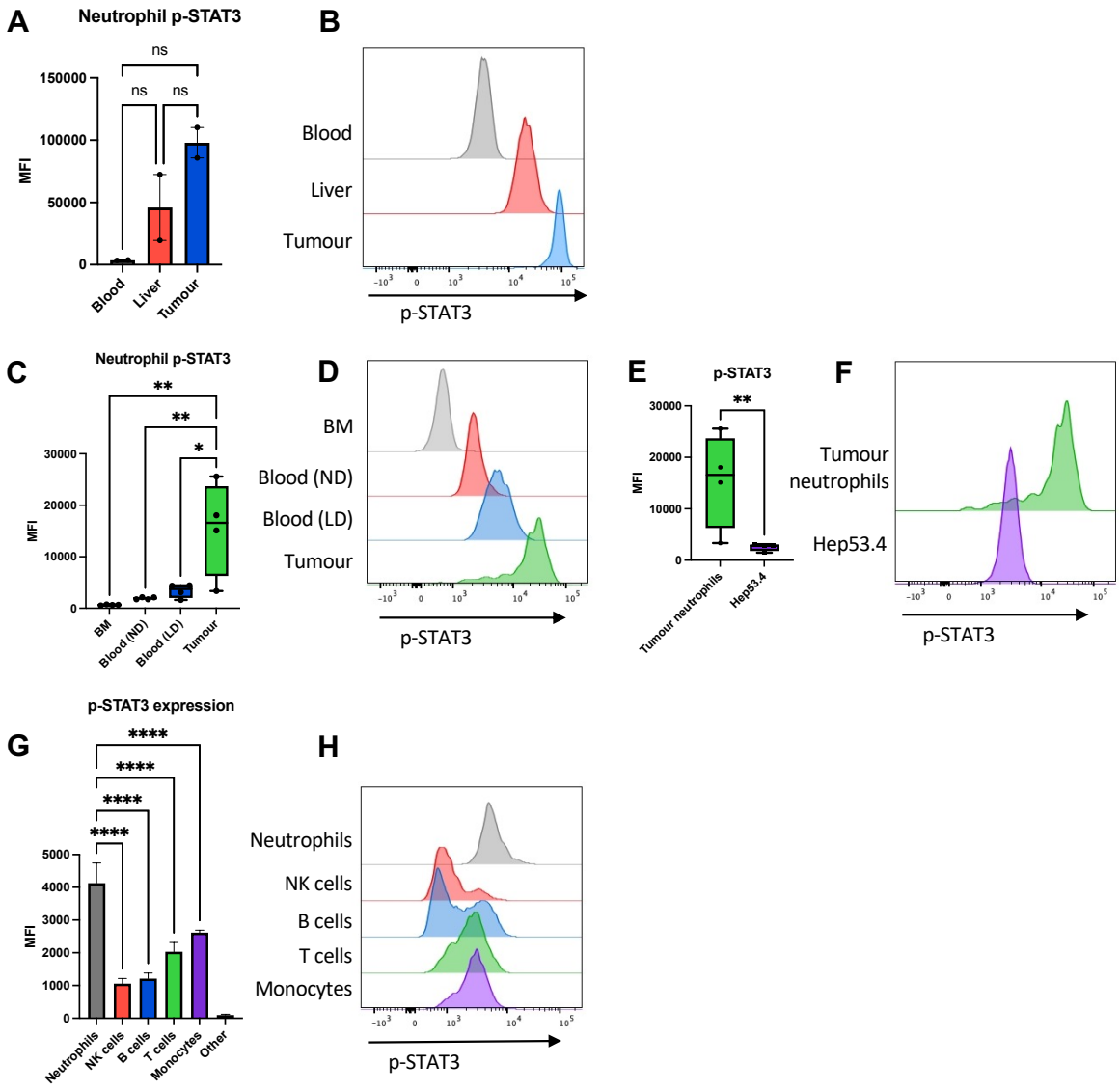



**Figure 6.2 – Neutrophil p-STAT3 expression in HCC patients and pre-clinical models. A.** Quantification of p-STAT3 expression in blood, liver and tumour neutrophils of HCC patients undergoing percutaneous tumour/liver biopsy, n=2. **B.** Representative histograms of neutrophil p-STAT3 expression in blood, liver and tumour neutrophils of HCC patients undergoing percutaneous biopsy. **C.** Quantification of p-STAT3 expression in bone marrow, blood ND, blood LD and tumour neutrophils from HCC-bearing mice, n=4. **D**. Representative histograms of neutrophil p-STAT3 expression in the bone marrow, blood ND, blood LD and tumour of HCC-bearing mice. **E.** Quantification of tumour neutrophil and Hep 53.4 p-STAT3 expression, n=4. **F**. Representative histograms of tumour neutrophil and Hep 53.4 p-STAT3 expression. **G.** Quantification of p-STAT3 expression in the circulating immune cells of HCC-bearing mice, n=4. **H.** Representative histograms of p-STAT3 expression in the circulating immune cells of HCC-bearing mice. P values calculated using a one-way ANOVA with Tukey post-hoc test (A, C, G) or an unpaired t-test (E) *p<0.05, **p<0.01, ***p<0.001, ****p<0.0001, ns non-significant.

### 6.2.2. Effect of JAK2 inhibition on neutrophils ex vivo

Blood leukocytes were harvested from adult, male C57BL/6 mice and plated into media containing IL-6 to mimic in vivo IL-6 exposure in HCC-bearing mice. The JAK2 small molecule inhibitor AZD1480 or DMSO vehicle control was added, and samples incubated for 4 hours after which samples were stained and run through flow cytometry analysis (figure 6.3 A). AZD1480 was used at a concentration of 5 μM. This was based on previous in vitro studies demonstrating complete JAK2 inhibition without cell toxicity at this concentration.[378,379] AZD1480 successfully inhibited JAK2-STAT3 activity as demonstrated by a reduction in p-STAT3 expression (figure 6.3 B-C). JAK2-STAT3 inhibition led to alterations in neutrophil phenotype with AZD1480 treated neutrophils expressing more CD11b and CD62L and less CXCR4 compared to controls (figure 6.3 D-E). This may show that AZD1480 causes an alternate state of activation and reduced neutrophil ageing through its inhibition on the JAK2-STAT3 pathway.

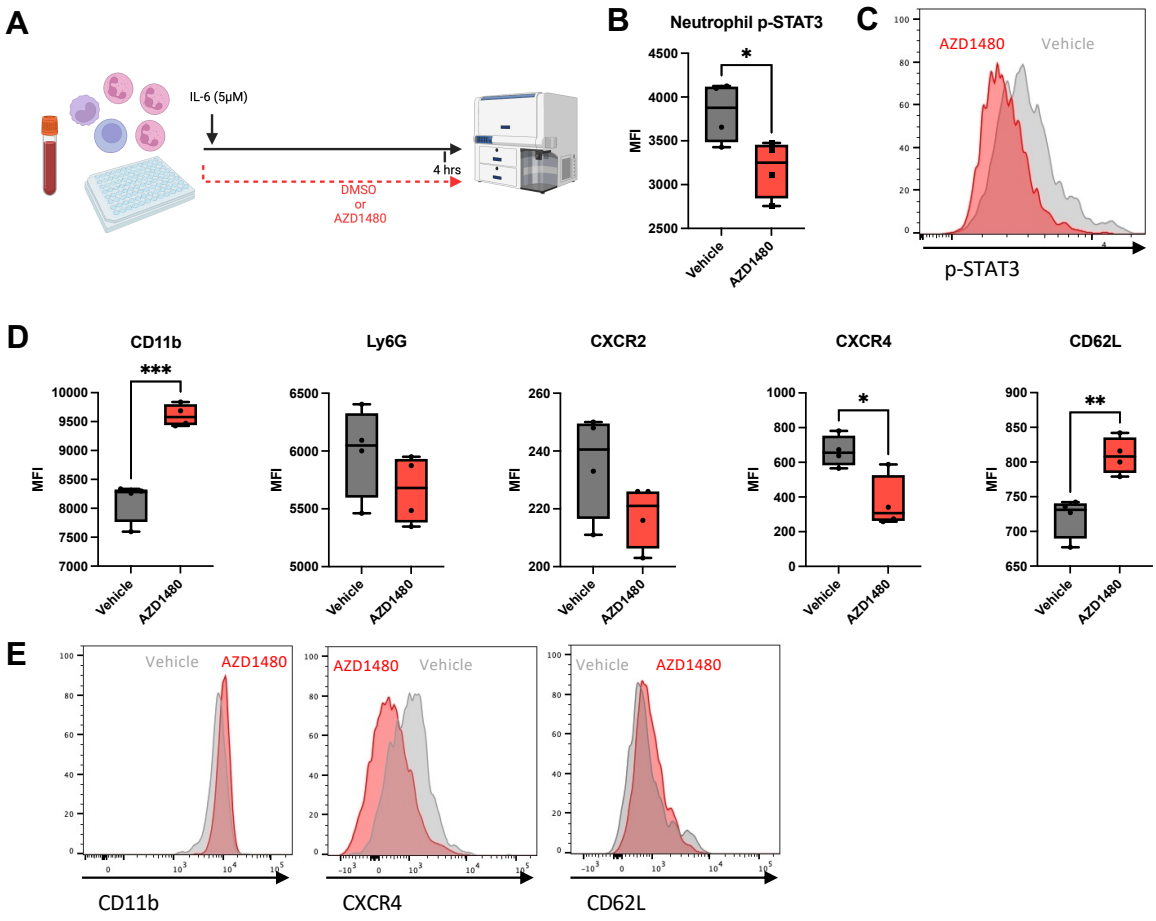



**Figure 6.3 – Ex vivo effect of AZD1480 on neutrophils. A.** Schematic outlining ex vivo experiment to test the effect of AZD1480 on neutrophils. **B.** Quantification of neutrophil p-STAT3 expression in AZD1480 vs vehicle treated neutrophils. **C.** Representative histogram demonstrating p-STAT3

expression in AZD1480 vs vehicle treated neutrophils. **D.** Quantification of CD11b, Ly6G, CXCR2, CXCR4 and CD62L expression in in AZD1480 vs vehicle treated neutrophils. **E.** Representative histograms demonstrating CD11b, CXCR4 and CD62L expression in in AZD1480 vs vehicle treated neutrophils. P values calculated using an unpaired t-test *p<0.05, **p<0.01, ***p<0.001, ****p<0.0001, ns non-significant. n=4.

### 6.2.3. Effect of JAK2 inhibition on Hep 53.4 cells in vitro

To test the direct anti-tumour effect of AZD1480 I conducted an in vitro culture experiment with the Hep 53.4 cells (figure 6.4 A). AZD1480 used at 5 μM, the same concentration as used for the ex vivo neutrophil experiment (figure 6.3) only demonstrated a very small anti-proliferative effect at 72 hours compared to the vehicle (figure 6.4 B). AZD1480 used at 10 μM demonstrated significant anti-proliferative activity at all timepoints and AZD1480 used at 50 μM demonstrated significant cytotoxicity at all timepoints (figure 6.4 B). Interestingly AZD1480 had the effect of increasing p-STAT3 expression in Hep 53.4 cells in a dose dependent manner (figure 6.4 C-D). This may suggest some degree of compensatory activity possibly via JAK1 activity which also feeds into STAT3.

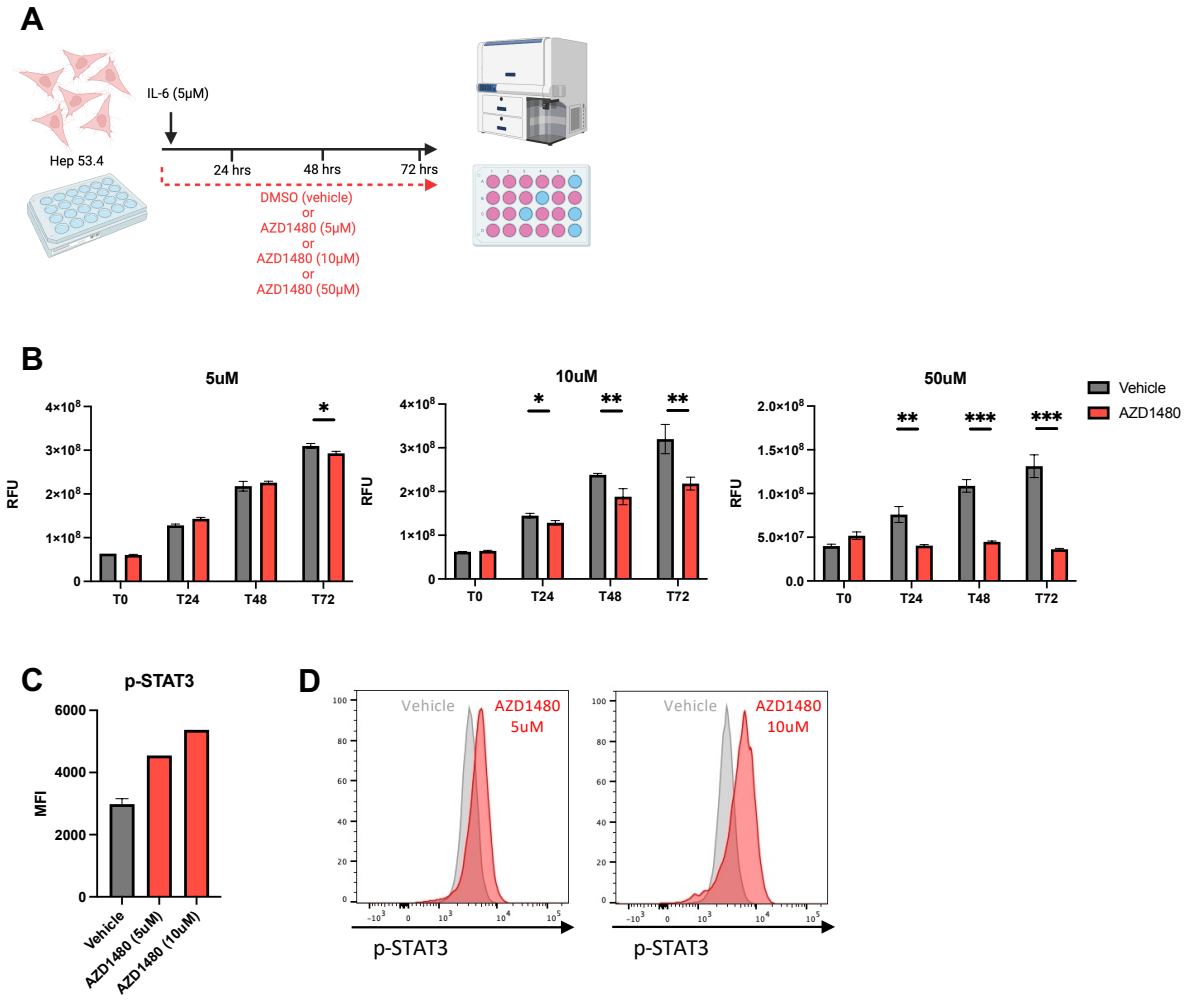



**Figure 6.4 – In vitro effect of AZD1480 on the Hep 53.4 cell line. A.** Schematic outlining in vitro culture experiment to test the effect of AZD1480 on Hep 53.4 tumour cells. **B.** Quantification of Hep 53.4 cell proliferation with AZD1480 at 5 μM, 10 μM and 50 μM as measured with a resazurin assay, units in relative florescence units (RFU), n=3 technical replicates. **C.** Quantification of Hep 53.4 p-STAT3 expression measured by flow cytometry, vehicle n=2, 5 μM and 10 μM n=1. **D.** Representative histograms demonstrating p-STAT3 expression in Hep 53.4 cells. P values calculated using an unpaired t-test *p<0.05, **p<0.01, ***p<0.001, ****p<0.0001, ns non-significant.

### 6.2.4. JAK2 inhibition in a lean HCC pre-clinical model

As an initial experiment I tested the in vivo effect of AZD1480 in HCC bearing mice fed with control diet (figure 6.5 A). These mice are lean without background liver disease or steatosis. I used a dose of 20 mg/kg twice daily. This is based on previous in vivo studies and early clinical trials using a total daily dose of between 30-60 mg/kg.[378,380,381] I decided to use twice daily dosing because the in vivo half-life of AZD1480 has been shown to be relatively short at around 2-5 hours.[381,382] AZD1480 significantly reduced tumour burden (figure 6.5 B-C). AZD1480 had no significant

effects on granulopoiesis (figure 6.5 D) or neutrophil frequency in the blood, spleen, liver or tumour (figure 6.5 E). Like the ex vivo study (figure 6.3) AZD1480 induced an increase in CD62L expression (figure 6.5 F-G) and reduction in CXCR4 expression (figure 6.5 H-I) which indicates a reduction in neutrophil ageing. Additionally, within the tumour immune microenvironment there was a trend towards an increase in intra-tumour CD8 T cell frequency in the AZD1480 treated mice (figure 6.5 J-K), this may indicate more anti-tumour immunity within tumours and a treatment effect of JAK2 inhibition.

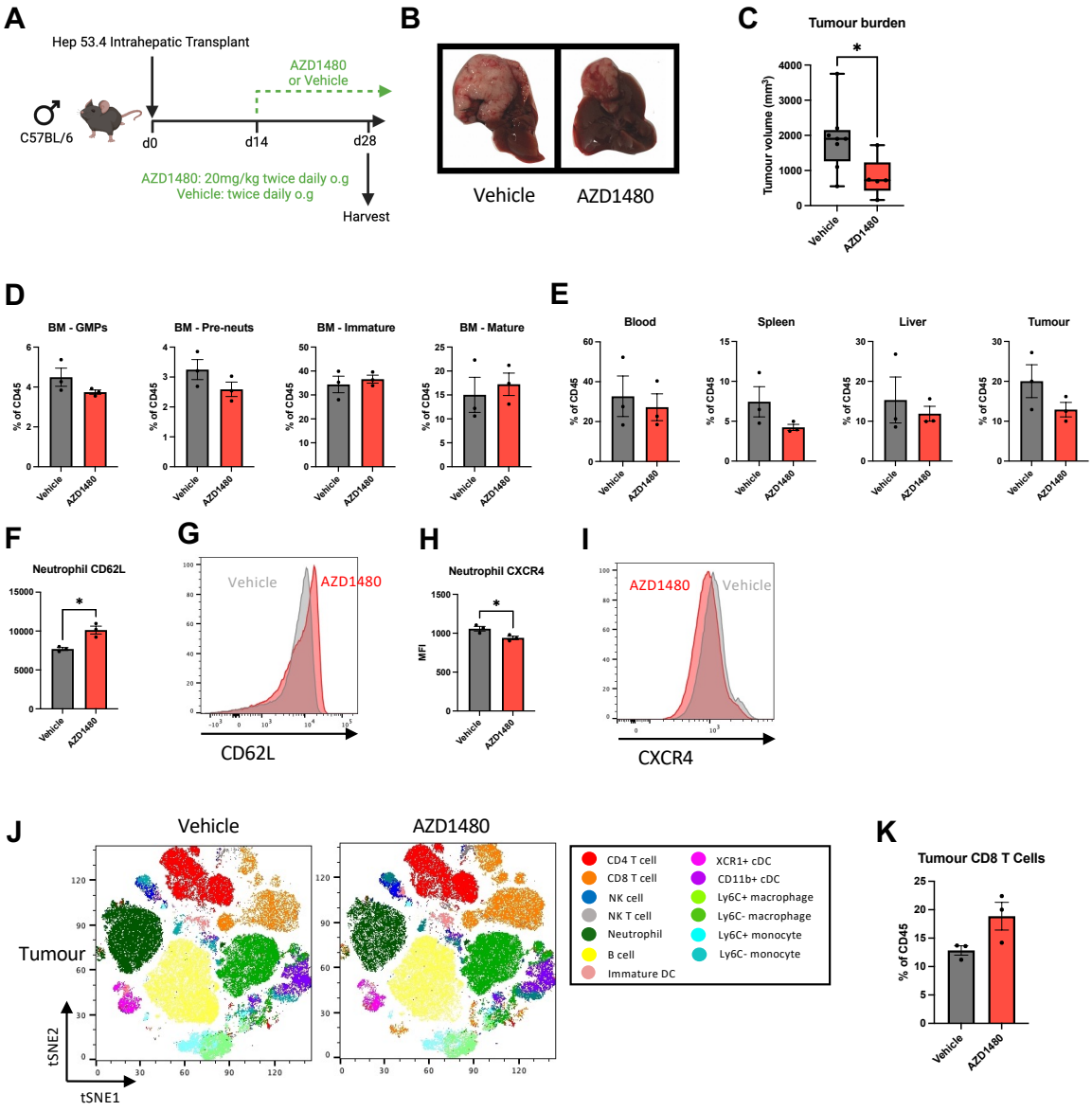



**Figure 6.5 – In vivo effect of AZD1480 in lean HCC-bearing mice. A.** Schematic outlining experiment design. To test the in vivo effect of AZD1480 in lean HCC-bearing mice. **B.** Representative images of livers/tumours in AZD1480 vs vehicle treated mice. **C.** Quantification of tumour burden in AZD1480 vs

vehicle treated mice, vehicle n=8, AZD1480 n=5. **D.** Quantification of bone marrow neutrophil and neutrophil progenitor frequencies in AZD1480 vs vehicle treated mice, n=3. **E.** Quantification of blood, spleen, liver and tumour neutrophil frequency in AZD1480 vs vehicle treated mice. **F.** Quantification of neutrophil CD62L expression in AZD1480 vs vehicle treated mice, n=3. **G.** Representative histogram demonstrating neutrophil CD62L expression in AZD1480 vs vehicle treated mice. **H.** Quantification of neutrophil CXCR4 expression in AZD1480 vs vehicle treated mice, n=3. **I.** Representative histogram demonstrating neutrophil CXCR4 expression in AZD1480 vs vehicle treated mice. **J.** tSNE plots representing the tumour immune cell populations as assessed by flow cytometry. **K.** Quantification of tumour CD8 T cells frequency in AZD1480 vs vehicle treated mice, n=3. P values calculated using an unpaired t-test *p<0.05, **p<0.01, ***p<0.001, ****p<0.0001, ns non-significant.

### 6.2.5. JAK2 inhibition in a MASH-HCC pre-clinical model

Next, I tested the in vivo efficacy of AZD1480 in a cohort of HCC bearing mice on western diet which have background liver disease/ steatosis (figure 6.6 A). This like the previous experiment demonstrated that AZD1480 significantly reduced tumour burden (figure 6.6 B-C). Interestingly AZD1480 also had the effect of increasing body weight (figure 6.6 D-E). A toxicity of AZD1480 was also noted in that a significant proportion of mice developed urinary retention towards the end of the study (data not shown). In terms of effects on neutrophils there was no difference in bone marrow, blood LD and blood ND neutrophil frequency (figure 6.6 F-H), but there was a significant increase in the frequency of tumour neutrophils in AZD1480 vs vehicle treated mice (figure 6.6 I-J). There was a trend towards reduced p-STAT3 expression in the tumour neutrophils of AZD1480 treated mice compared to vehicle treated mice (figure 6.6 K-L) demonstrating some degree of drug specific neutrophil effect in vivo.

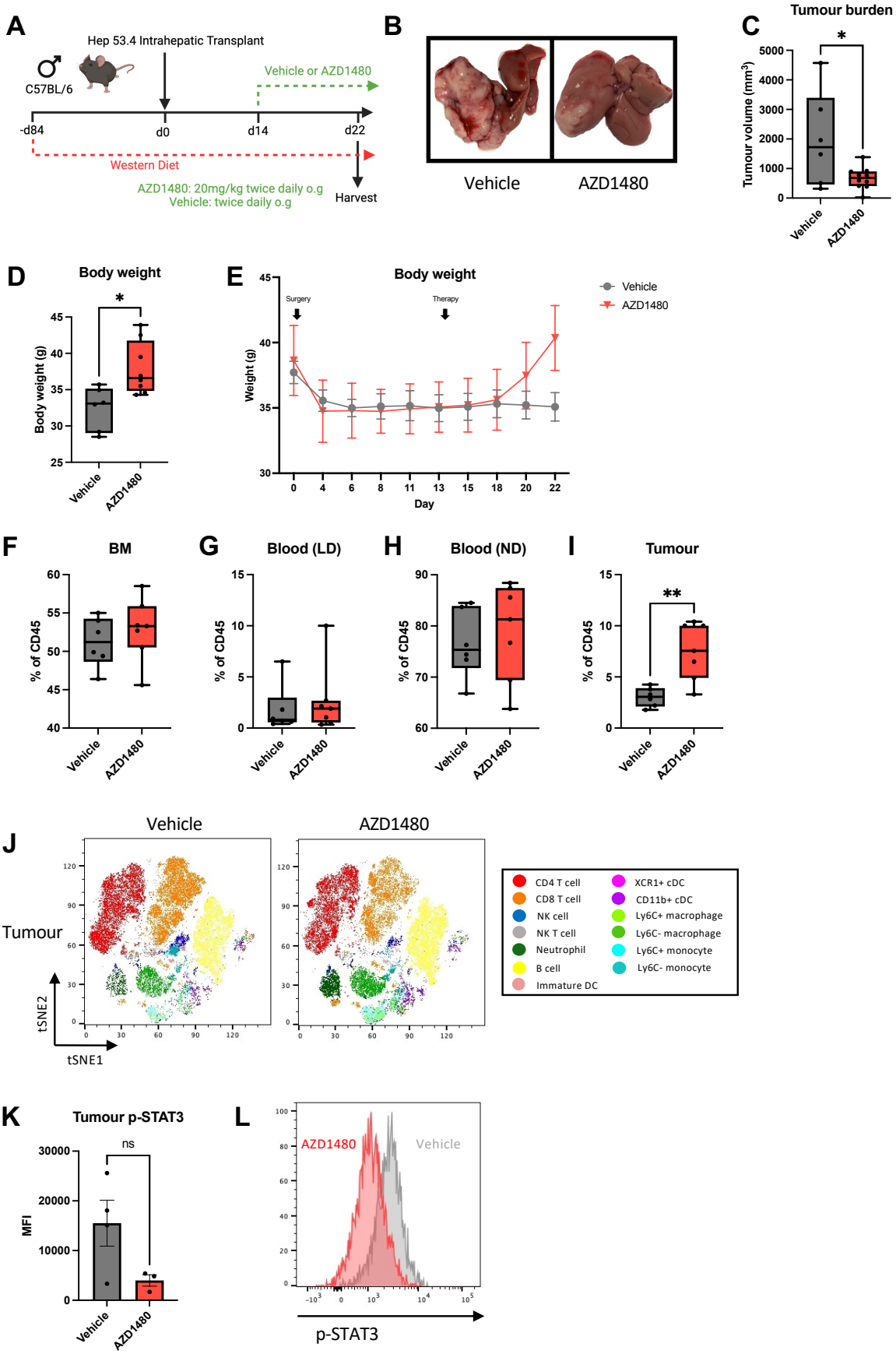



**Figure 6.6 – In vivo effect of AZD1480 in MASH HCC-bearing mice. A.** Schematic outlining experiment design. To test the in vivo effect of AZD1480 in western diet fed HCC-bearing mice. **B.**

Representative images of livers/tumours in AZD1480 vs vehicle treated mice. **C.** Quantification of tumour burden in AZD1480 vs vehicle treated mice, vehicle n=6, AZD1480 n=10. **D.** Quantification of body weight at harvest (day 22) of AZD1480 vs vehicle treated mice, vehicle n=6, AZD1480 n=10. **E.** Quantification of body weight throughout the experiment from tumour transplant (day 0) to harvest (day 22), vehicle n=6, AZD1480 n=10. **F.** Quantification of bone marrow neutrophil frequency in in AZD1480 vs vehicle treated mice, vehicle n=6, AZD1480 n=7. **G.** Quantification of LD blood neutrophil frequency in AZD1480 vs vehicle treated mice, vehicle n=6, AZD1480 n=7. **H.** Quantification of ND blood neutrophil frequency in AZD1480 vs vehicle treated mice, vehicle n=6, AZD1480 n=7. **I.** Quantification of tumour neutrophil frequency in in AZD1480 vs vehicle treated mice, vehicle n=6, AZD1480 n=7. **J.** tSNE plots representing the tumour immune cell populations as assessed by flow cytometry. **K.** Quantification of tumour neutrophil p-STAT3 expression in AZD1480 vs vehicle treated mice, vehicle n=4, AZD1480 n=3. **L.** Representative histograms demonstrating p-STAT3 expression in tumour neutrophils from AZD1480 vs vehicle treated mice. P values calculated using an unpaired t-test *p<0.05, **p<0.01, ***p<0.001, ****p<0.0001, ns non-significant.

### 6.2.6. JAK2 inhibitor study conclusion

From these in vitro, ex vivo and in vivo studies I have demonstrated that although the JAK2 small molecule inhibitor AZD1480 is not a neutrophil specific inhibitor of JAK2-STAT3 signalling, neutrophils have the highest STAT3 pathway activity of cells in the tumour microenvironment. I also demonstrated that tumour neutrophils have much higher STAT3 activity compared to neutrophils from other biological compartments both in patients and mice. Although AZD1480 did have some direct effects on tumour cell proliferation, AZD1480 also had noticeable impacts on neutrophil phenotype with alterations in activation and reduced ageing demonstrated both ex vivo and in vivo. AZD1480 reduced tumour burden in vivo both in lean and MASH-HCC models. Additionally, AZD1480 led to an enrichment in tumour neutrophils and tumour CD8 T cells suggesting and possible alteration in neutrophil phenotype to a more anti-tumour function. These results demonstrate the JAK2-STAT3 pathway to be a potential therapeutic target in neutrophils in HCC. Further studies are needed using neutrophil specific and conditional JAK2-STAT3 knockout models to further confirm the neutrophil JAK2-STAT3 contribution versus the global JAK2-STAT3 effect. Unexpected side effects/ toxicities were also noted in the in vivo studies. Mice treated with AZD1480 gained more weight compared to controls. Without doing further studies it is hard to attribute this weight gain to the reduced tumour burden versus a direct drug effect, however the JAK inhibitors such as ruxolitinib and tofacitinib have been reported to cause weight gain in patients taking them.[383,384] The main limitation of

AZD1480 in my study was the toxicity of urinary retention. This occurred in a significant proportion of animals and led to an early end to the study. Urinary retention has not been reported in any other pre-clinical study or clinical trial using AZD1480, although the initial phase I study did report a range of neurological dose-limiting toxicities.[381]

### 6.3. Targeting S100A8 and S100A9 in a HCC pre-clinical model

S100A8 and S100A9 are calcium binding proteins which have previously been shown to induce tumour neutrophil recruitment in pre-clinical models of HCC, with genetic knockout resulting in the amelioration of carcinogen induced HCCs.[23] Furthermore S100A9 is an activator of neutrophils and may preferentially recruit pro-tumour neutrophils.[224,314] Therefore to target neutrophil tumour recruitment I used anti-S100A8 and anti-S100A9 antibodies in control diet fed HCC-bearing mice with no background liver disease (figure 6.7 A). Anti-S100A8 and anti-S100A9 antibodies were developed and obtained from a collaborator who had previously shown them to inhibit S100A8/9 dependent neutrophil recruitment in response to LPS.[315] I used a dose of 200 μg IP twice weekly based on previous data and used an IgG matched control provided by the same collaborator. Anti-S100A8/9 had no effect on tumour burden (figure 6.7 B-C). Anti-S100A8/9 had the effect of significantly reducing the frequency of blood neutrophils and there was a trend towards a reduction in frequency of spleen and tumour neutrophils (figure 6.7 D). Anti-S100A8/9 caused no difference in tumour neutrophil phenotype (figure 6.7 E). There were no significant differences in tumour macrophage and monocyte frequencies (figure 6.7 F), however there was a significant reduction in the frequency of tumour CD8 T cells in mice treated with anti-S100A8/9 compared to controls (figure 6.7 F-G). CD8 T cells are not recruited via S100A8/9 so one explanation for this would be the reduced neutrophil/ myeloid recruitment and subsequent reduced CD8 T cell recruitment via chemokines released by myeloid populations.[385] Due to this negative result I did not conduct any further investigation into the use of anti-S100A8/9.

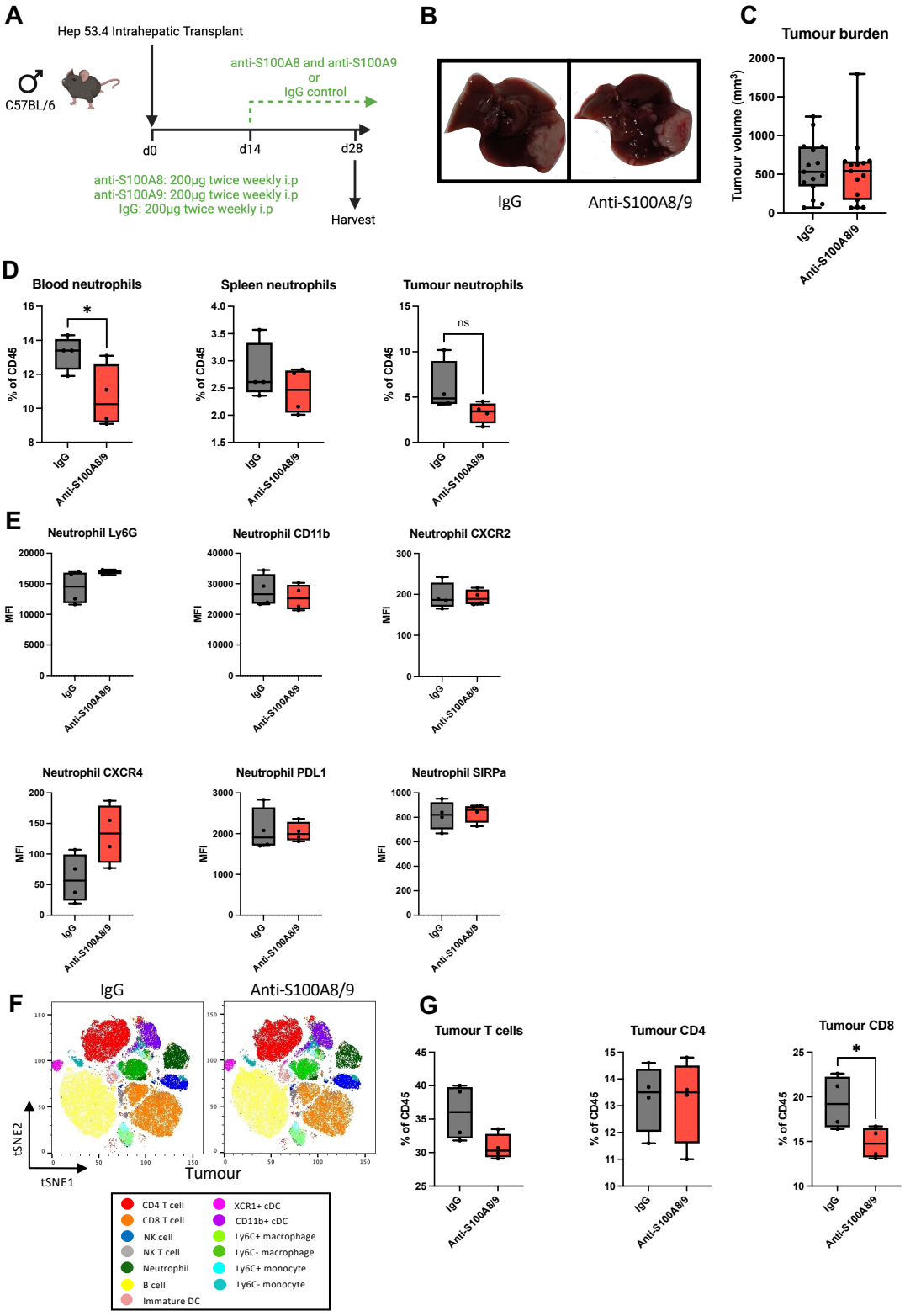



**Figure 6.7 – In vivo effect of targeting S100A8 and S100A9 in HCC-bearing mice. A.** Schematic outlining experiment design. To test the in vivo effect of anti-S100A8/9 antibodies lean HCC-bearing mice. **B.** Representative images of livers/tumours in anti-S100A8/9 vs IgG treated mice. **C.** Quantification of tumour burden in anti-S100A8/9 vs IgG treated mice, n=15. **D.** Quantification of blood, spleen and tumour neutrophil frequency in anti-S100A8/9 vs IgG treated mice, n=4. **E.** Quantification

of tumour neutrophil Ly6G, CD11b, CXCR2, CXCR4, PDL1 and SIRPα expression in anti-S100A8/9 vs IgG treated mice, n=4. **F.** tSNE plots representing the tumour immune cell populations as assessed by flow cytometry. **G.** Quantification of tumour total T cell, CD4 T cell and CD8 T cell frequency in anti-S100A8/9 vs IgG treated mice, n=4. P values calculated using an unpaired t-test *p<0.05, **p<0.01, ***p<0.001, ****p<0.0001, ns non-significant.

### 6.4. ALK5 inhibition in pre-clinical models

From my observational work I described an expansion of circulating LD neutrophils in both HCC patients and in HCC-bearing mice. Further analysis showed these neutrophils to have an aged, activated and degranulated phenotype with a poor migration ability to CXCL2 and reduced phagocytosis capacity. Based on my analysis these LD neutrophils are also likely to be the PMN-MDSC population previously described in the literature. The location in which these LD neutrophils develop was not clear from my neutrophil tracking studies however their early BrdU signal suggested that they may develop in the bone marrow. Work by others has demonstrated LD neutrophil formation to be dependent on TGF-β.[118] Activin receptor-like kinase 5 (ALK5) is the receptor for TGF-β. Therefore, I chose to use the ALK5 inhibitor AZ12601011 in my pre-clinical models as a way of targeting LD neutrophils.[386] I chose a dosing regimen of 50 mg/kg twice daily based on previous studies.[387]

#### 6.4.1. ALK5 inhibition in a lean HCC pre-clinical model

As a preliminary experiment I tested the in vivo effect of AZ12601011 in HCC bearing mice fed with control diet (figure 6.8 A). These mice are without background liver disease or steatosis. AZ12601011 had no effect on tumour burden (figure 6.8 B-C) however did have effects on neutrophils. Whilst the number of ND neutrophils was unchanged there was a significant reduction in LD neutrophil number with AZ12601011 (figure 6.8 D-F). There was also a significant increase in the frequency of tumour neutrophils with AZ12601011 (figure 6.8 G-H) with tumour neutrophils also having and increased expression of CD62L (figure 6.8 I-J) suggesting a less aged neutrophil phenotype within the tumour. The findings of reduced LD neutrophils and increased intra-tumour neutrophils are consistent with previous studies.[108,118]

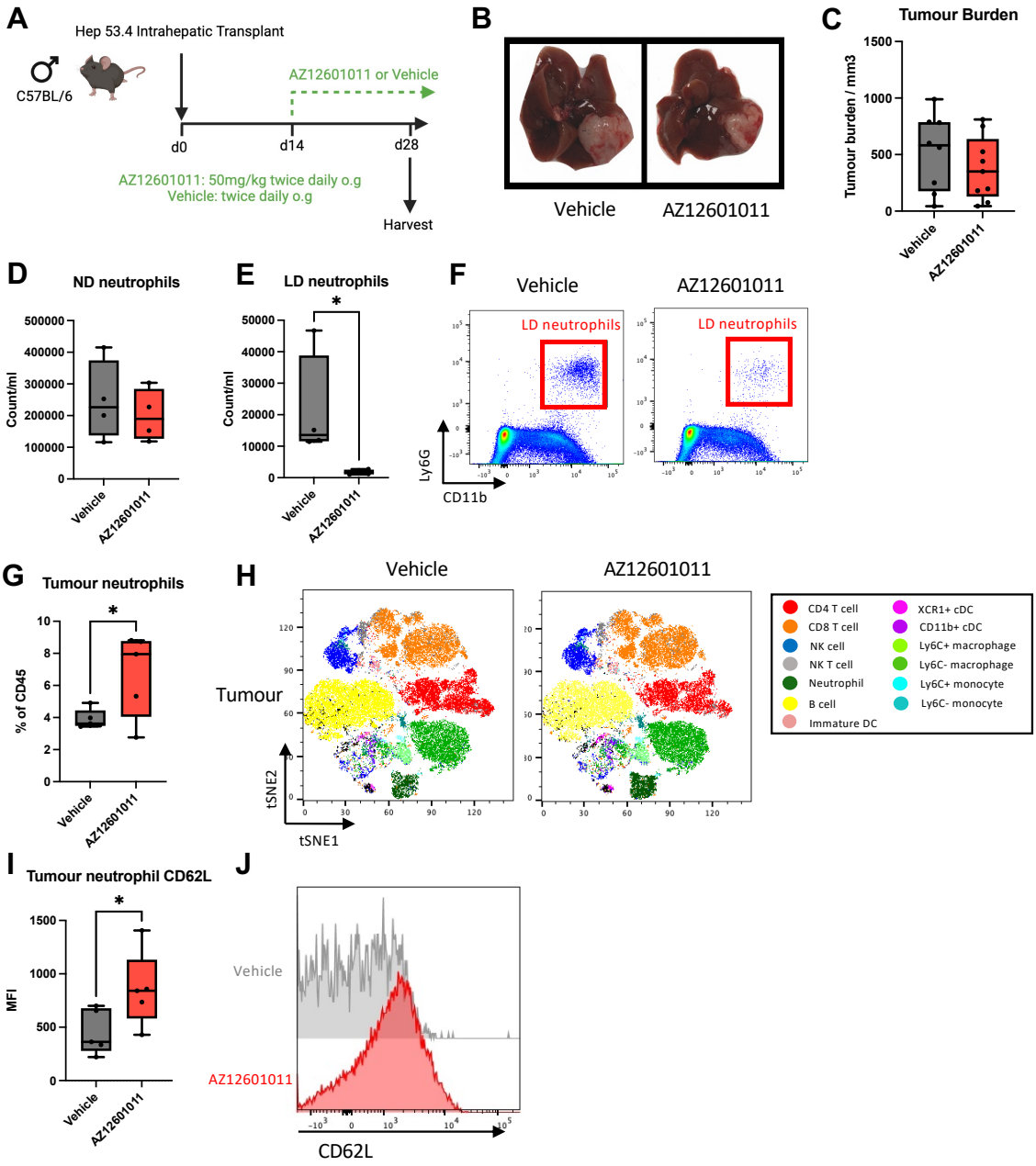



**Figure 6.8 – In vivo effect of AZ12601011 in lean HCC-bearing mice. A.** Schematic outlining experiment design. To test the in vivo effect of ALK5 inhibition using AZ12601011 in lean HCC-bearing mice. **B.** Representative images of livers/tumours in AZ12601011 vs vehicle treated mice. **C.** Quantification of tumour burden in AZ12601011 vs vehicle treated mice, vehicle n=8, AZD12601011 n=9. **D.** Quantification of ND neutrophil count in AZ12601011 vs vehicle treated mice, n=4. **E.** Quantification of LD neutrophil count in AZ12601011 vs vehicle treated mice, n=4. **F.** Representative plots of LD neutrophils in AZ12601011 vs vehicle treated mice. **G.** Quantification of tumour neutrophil frequency in AZ12601011 vs vehicle treated mice, n=5. **H.** tSNE plots representing the tumour immune cell populations as assessed by flow cytometry. **I.** Quantification of tumour neutrophil CD62L expression in AZ12601011 vs vehicle treated mice, n=5. **J.** Representative histogram demonstrating tumour

neutrophil CD62L expression in AZ12601011 vs vehicle treated mice. P values calculated using Mann-Whitney test *p<0.05, **p<0.01, ***p<0.001, ****p<0.0001, ns non-significant.

### 6.4.2. ALK5 inhibition in a MASH-HCC pre-clinical model

Next, I tested the effect of AZ12601011 in HCC bearing mice fed with western diet (figure 6.9 A). These mice have background MASH (figures 5.1 and 5.3). Like the previous experiment in lean mice there was no anti-tumour effect of AZ12601011 (figure 6.9 B-C), despite there being effects on neutrophils (figure 6.9 D-F) with a significant reduction in the number of LD neutrophils (figure 6.9 E-F). Contrary to the previous experiment there was a trend towards a reduction in tumour neutrophil frequency in AZ12601011 treated mice compared to vehicle controls (figure 6.9 G-H) and no change in tumour neutrophil CD62L expression (figure 6.9 I-J). The contrasting intra-tumour effects of AZ12601011 in lean vs MASH mice suggests that the presence of background steatosis or liver disease is altering treatment response. The fact that AZ12601011 has the same systemic effect of reducing the number of LD neutrophils (figure 6.8 D-F and figure 6.9 D-F) but has differing effects on intra-tumour neutrophils (figure 6.8 G-J, figure 6.9 G-J) in lean vs MASH mice suggests that there is something unique about the MASH intrahepatic microenvironment which alters treatment effects.

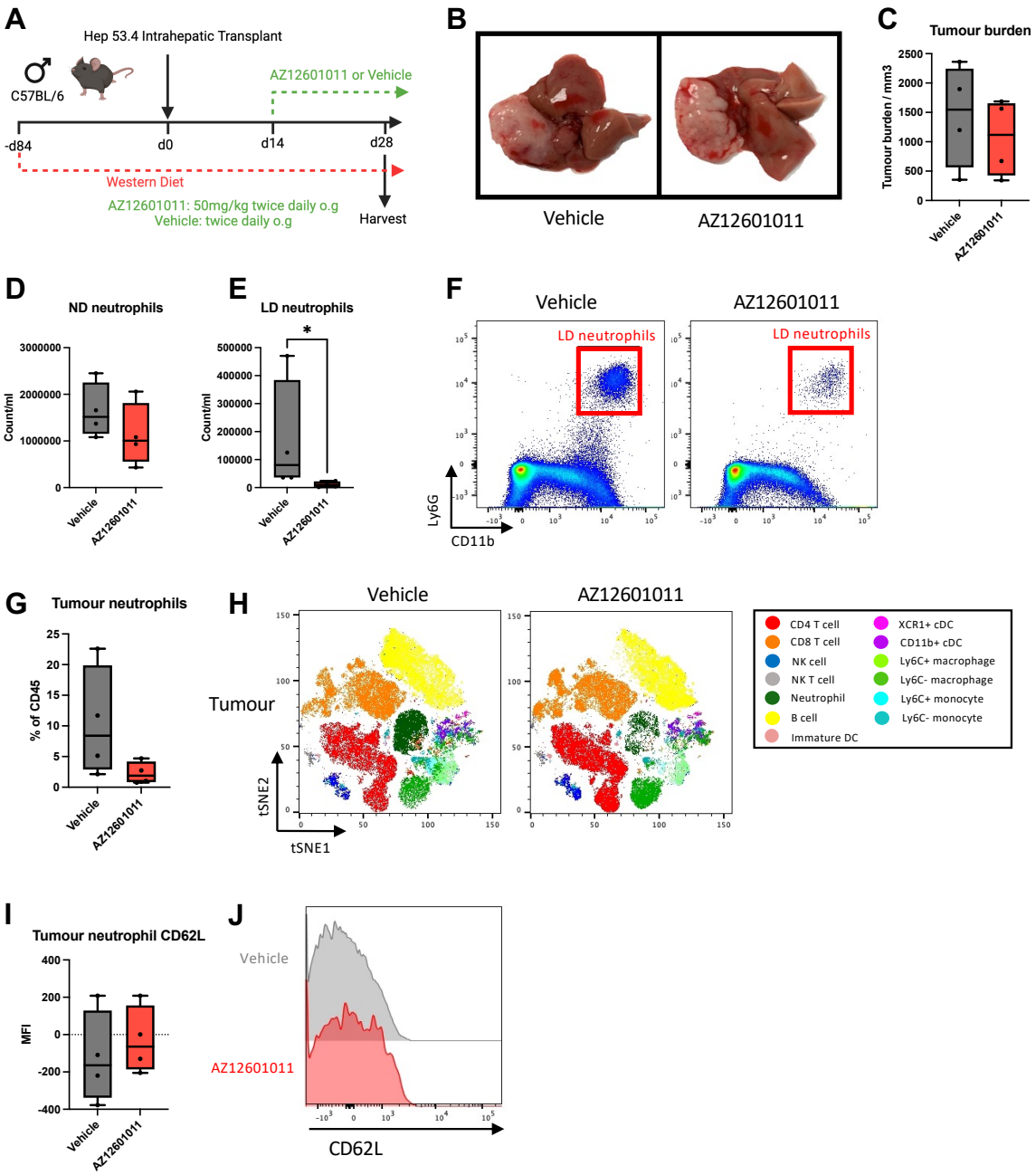



**Figure 6.9 – In vivo effect of AZ12601011 in MASH HCC-bearing mice. A.** Schematic outlining experiment design. To test the in vivo effect of AZ12601011 in MASH HCC-bearing mice. **B.** Representative images of livers/tumours in AZ12601011 vs vehicle treated mice. **C.** Quantification of tumour burden in AZ12601011 vs vehicle treated mice, n=4. **D.** Quantification of ND neutrophil count in AZ12601011 vs vehicle treated mice, n=4. **E.** Quantification of LD neutrophil count in AZ12601011 vs vehicle treated mice, n=4. **F.** Representative plots of LD neutrophils in AZ12601011 vs vehicle treated mice. **G.** Quantification of tumour neutrophil frequency in AZ12601011 vs vehicle treated mice, n=4. **H.** tSNE plots representing the tumour immune cell populations as assessed by flow cytometry. **I.** Quantification of tumour neutrophil CD62L expression in AZ12601011 vs vehicle treated mice, n=4. **J.** Representative histogram demonstrating tumour neutrophil CD62L expression in AZ12601011 vs

vehicle treated mice. P values calculated using Mann-Whitney test *p<0.05, **p<0.01, ***p<0.001, ****p<0.0001, ns non-significant.

### 6.5. Conclusion

Using pre-clinical models of HCC, I have investigated therapeutic agents which alter neutrophil pro-tumour polarisation (JAK2-STAT3 inhibition), neutrophil tumour recruitment (anti-S100A8/9) and LD neutrophil generation (ALK5 inhibition). JAK2-STAT3 inhibition was highlighted as a potential therapeutic target of interest from my patient and pre-clinical model observational studies as JAK2-STAT3 is a downstream signalling pathway to CXCR2 and IL-6, which are important factors in neutrophil activation, ageing and granulopoiesis. I demonstrated that tumour neutrophils have the highest baseline STAT3 activity of all immune cells and that both ex vivo and in vivo JAK2-STAT3 inhibition causes alterations of neutrophil phenotype resulting in a less aged phenotype. JAK2-STAT3 inhibition resulted in reduced tumour burden in both lean and MASH HCC-bearing mice. This anti-tumour effect was likely more than just a direct result of tumour cell JAK2-STAT3 inhibition as demonstrated by minimal in vitro anti-tumour effects at comparable drug concentrations. I propose that this additional anti-tumour effect seen in the in vivo experiment is due at least in part to the effects of JAK2-STAT3 inhibition in neutrophils causing a less aged and pro-tumour phenotype. Targeting neutrophil recruitment via S100A8/9 failed to demonstrate anti-tumour activity and only had small effects on tumour neutrophil recruitment with no alteration in neutrophil phenotype. One explanation for this failure in treatment is that S100A8/9 is only one mechanism of neutrophil tumour recruitment and other mechanisms such as chemokine recruitment would be unaffected. Finally, I targeted LD circulating neutrophils through blockade of TGF-β-ALK5. Although this did not show any significant anti-tumour effects it did show effects on neutrophils. ALK5 inhibition reduced the number of circulating LD neutrophils in both lean and MASH HCC-bearing mice. On the other hand, ALK5 inhibition only successfully altered tumour neutrophil frequency and phenotype in lean HCC-bearing mice but not in MASH HCC-bearing mice. This suggests that the response to therapy is in part determined by the presence of background liver disease, in this case MASH.

# 7. Exploring mechanisms behind primary immune checkpoint inhibitor resistance in MASH-HCC

## 7.1. Introduction

There is growing evidence from both clinical trials and real-world data to suggest that the aetiology of underlying liver disease in HCC is a factor in determining treatment response. In particular there is suggestion that immune checkpoint inhibitors are less effective in HCC with underlying MASLD.[47-49] Because I am using a pre-clinical model of HCC with underlying MASH I aimed to investigate the effectiveness of immune checkpoint inhibition in HCC on the background of lean vs MASH livers. Indeed, I had already seen a difference in therapeutic effect in lean vs MASH mice in my ALK5 inhibitor study, with different intrahepatic effects in MASH (figure 6.8 B-C and 6.9 B-C). My data suggest this may be underpinned by different immunological effects of treatment within the tumour microenvironment. ALK5 inhibition had the same systemic effects on neutrophils in lean and MASH HCC-bearing mice with there being a reduction in the number of circulating LD neutrophils (figure 6.8 E-F and figure 6.9 E-F). On the other hand, ALK5 inhibition had different effects on tumour neutrophils inducing an increased neutrophil frequency and increased CD62L expression in lean HCC-bearing mice with these effects not being seen in MASH HCC-bearing mice (figure 6.8 G-J and figure 6.9 G-J). The current pre-clinical studies investigating immune checkpoint inhibitor effectiveness on MASLD have used anti-PD1 monotherapy.[47,55,56] Given that the current first line systemic therapy for advanced HCC is the combination of atezolizumab (anti-PDL1) and bevacizumab (anti-VEGF) I wanted to test the effectiveness of these therapies in lean vs MASH HCC-bearing mice and investigate the underlying mechanism.

## 7.2. Therapy response to anti-PDL1/anti-VEGF in lean vs MASH intrahepatic HCC

For my initial experiment I treated lean (control diet fed) or MASH (western diet fed) HCC-bearing mice with either anti-PDL1/anti-VEGF combination or IgG control (figure 7.1 A), with a dosing regimen derived from previous studies.[56,388] From my previous experiments I know that mice on a western diet develop liver steatosis and inflammation characteristic of MASH without significant fibrosis (figure 5.1 and figure 5.3). In lean mice anti-PDL1/VEGF significantly reduced tumour burden compared to

the IgG control, whereas there was only a small and non-significant treatment effect in MASH HCC-bearing mice treated with anti-PDL1/VEGF compared to the IgG control (figure 7.1 B-C). In this experiment MASH mice were confirmed to have a greater body and liver weight compared to lean mice (figure 7.1 D-E). MASH mice also had greater liver and tumour steatosis compared to lean mice with the treatments having no effect on steatosis (figure 7.1 F-I). Therefore, similar to some of the preliminary clinical studies my data demonstrates a suboptimal treatment effect in MASH compared to lean mice.

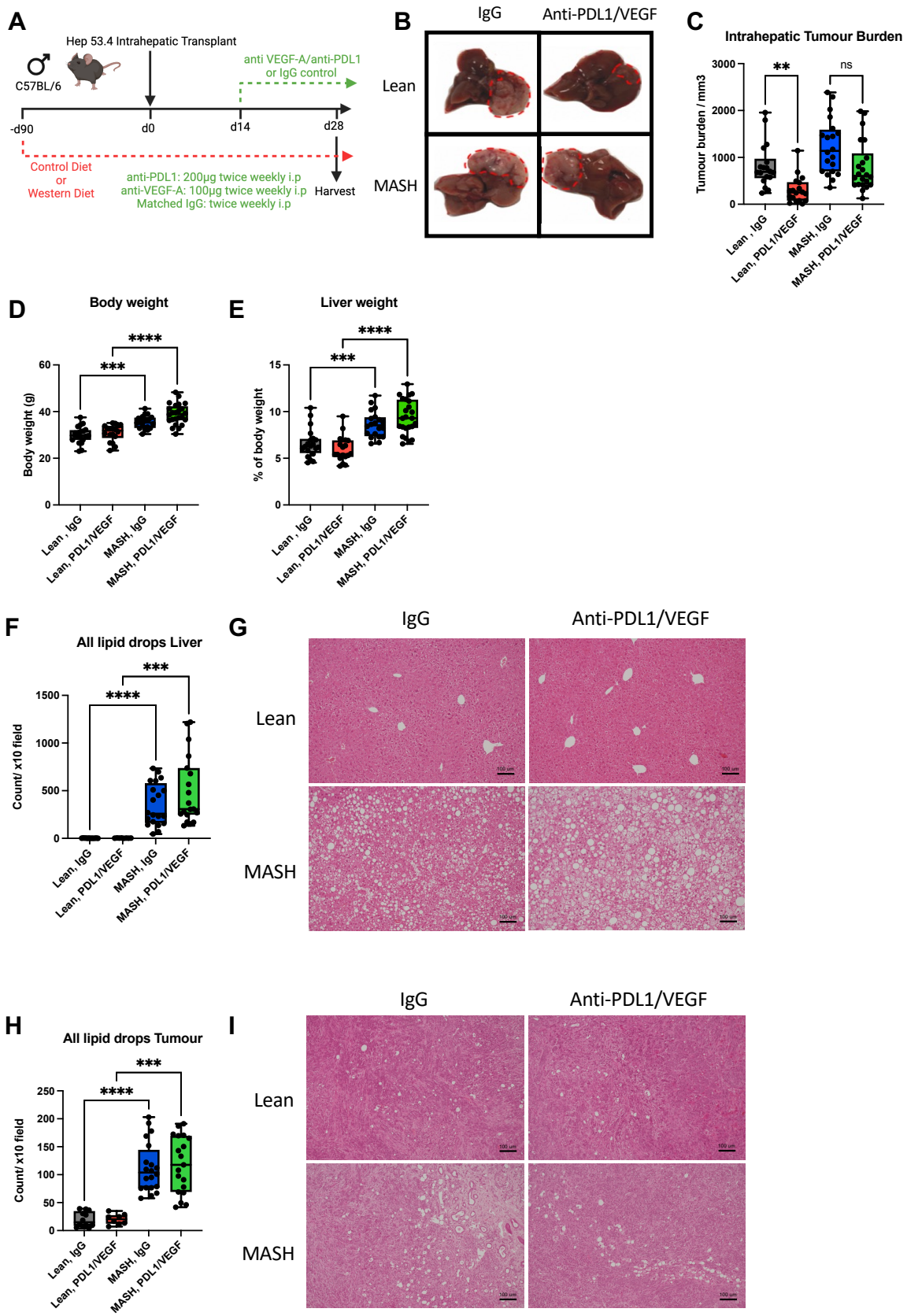



**Figure 7.1 – Therapy response to anti-PDL1/anti-VEGF in lean vs MASH intrahepatic HCC. A.** Schematic outlining experiment design to test the effectiveness of anti-PDL1/VEGF therapy in intrahepatic HCC bearing lean vs MASH mice. **B.** Representative images of livers/tumours in lean and

MASH mice treated with anti-PDL1/VEGF vs IgG control. **C.** Quantification of tumour burden in lean and MASH mice treated with anti-PDL1/VEGF vs IgG control, lean IgG n=18, lean PDL1/VEGF n=18, MASH IgG n=20, MASH PDL1/VEGF n=22. **D.** Quantification of body weight in lean and MASH mice treated with anti-PDL1/VEGF vs IgG control, lean IgG n=18, lean PDL1/VEGF n=18, MASH IgG n=20, MASH PDL1/VEGF n=22. **E**. Quantification of liver weight in lean and MASH mice treated with anti-PDL1/VEGF vs IgG control, lean IgG n=18, lean PDL1/VEGF n=18, MASH IgG n=20, MASH PDL1/VEGF n=22. **F.** Quantification of liver steatosis as assessed by lipid drop count on H&E staining in lean and MASH mice treated with anti-PDL1/VEGF vs IgG control, lean IgG n=12, lean PDL1/VEGF n=8, MASH IgG n=20, MASH PDL1/VEGF n=19. **G.** Representative liver H&E stain of lean and MASH mice treated with anti-PDL1/VEGF vs IgG control, at 100x magnification. **H.** Quantification of tumour steatosis as assessed by lipid drop count on H&E staining in lean and MASH mice treated with anti-PDL1/VEGF vs IgG control, lean IgG n=12, lean PDL1/VEGF n=8, MASH IgG n=20, MASH PDL1/VEGF n=19. **I.** Representative tumour H&E stain of lean and MASH mice treated with anti-PDL1/VEGF vs IgG control, at 100x magnification. P values calculated using a Kruskal-Wallis test with Dunn's post-hoc test. *p<0.05, **p<0.01, ***p<0.001, ****p<0.0001, ns non-significant.

### 7.3. Immunological effects of anti-PDL1/anti-VEGF therapy in lean vs MASH intrahepatic HCC

The intrahepatic tumour immune infiltrates of lean vs MASH mice treated with anti-PDL1/anti-VEGF vs IgG are summarised in figure 7.2 A. There were no significant differences in the frequencies of NK cells, NK T cells, B cells, neutrophils, cDC1s, cDC2s, $Ly6C^+$ macrophages, $Ly6C^-$ macrophages, $Ly6C^+$ monocytes and $Ly6C^-$ monocytes (figure 7.1 B-K). Anti-PDL1/anti-VEGF treatment significantly increased tumour T cell frequency in lean mice but not MASH nice (figure 7.2 L). There was no difference in CD4 frequency (figure 7.2 M) but in both lean and MASH mice there was a significant increase in tumour CD8 T cell frequency with anti-PDL1/anti-VEGF therapy (figure 7.2 N). This was confirmed on IHC staining (figure 7.2 O-P). CD8 T cell infiltration is a known effect and marker of efficacy in PDL1 blockade.[389] This is interesting since despite there being a different treatment response in terms of tumour burden, there is a similar immunological effect in terms of tumour CD8 T cell infiltration. Therefore the mechanism underlying the poor therapeutic effect of anti-PDL1/anti-VEGF in MASH must be in the functional nature of the tumour CD8 T cells rather than just their presence or infiltration.

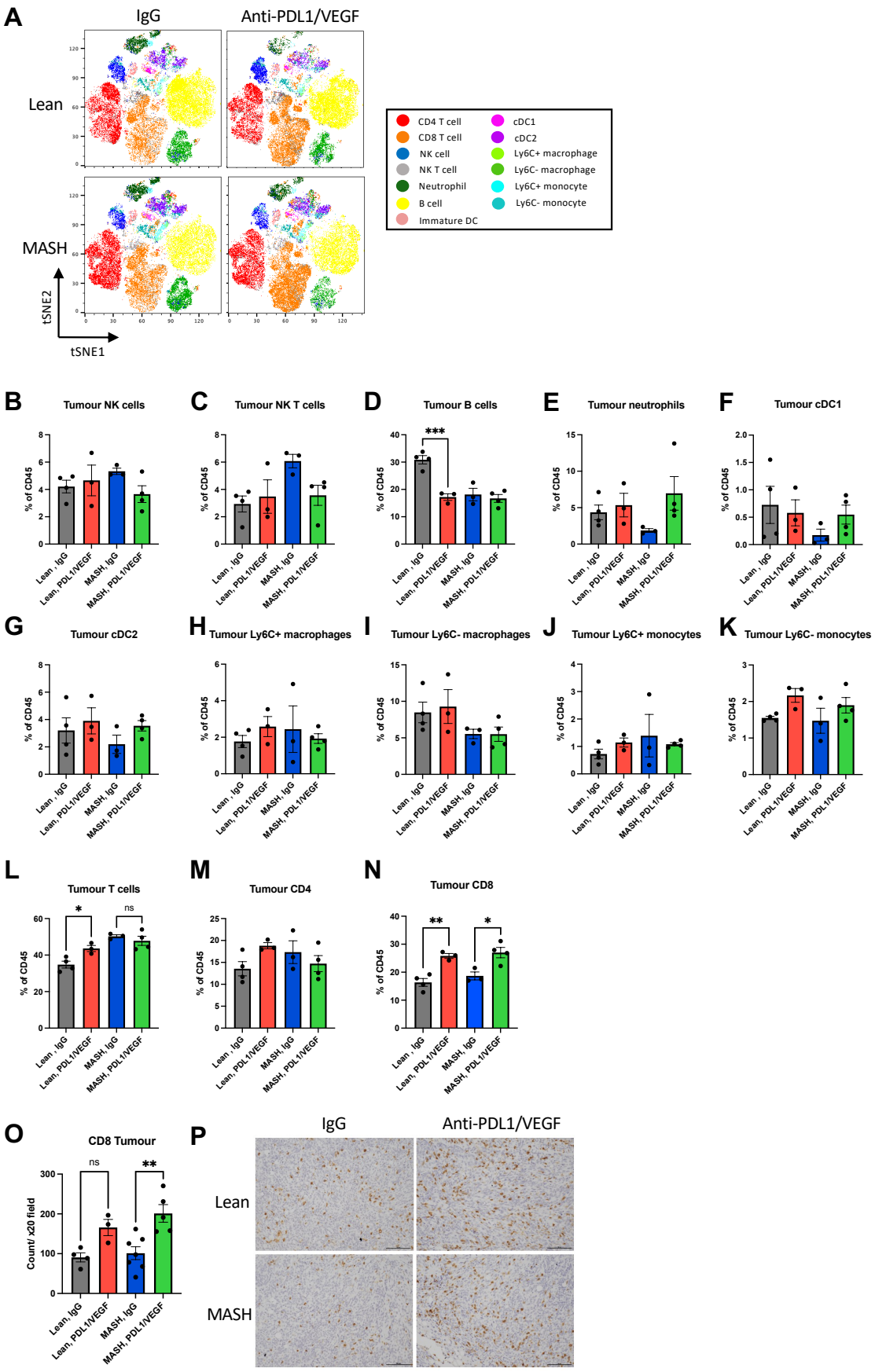



**Figure 7.2 – Immunological effects of anti-PDL1/anti-VEGF therapy in lean vs MASH intrahepatic HCC. A.** tSNE plots representing the tumour immune cell populations as assessed by flow cytometry

in lean and MASH intrahepatic HCC-bearing mice treated with anti-PDL1/anti-VEGF vs IgG control. **B-N.** Quantification of tumour NK cell, NK T cell, B cell, neutrophil, cDC1, cDC2, $Ly6C^+$ macrophage, $Ly6C^-$ macrophage, $Ly6C^+$ monocyte, $Ly6C^-$ monocyte, T cell, CD4 T cell and CD8 T cell frequency in lean and MASH intrahepatic HCC-bearing mice treated with anti-PDL1/anti-VEGF vs IgG control as assessed by flow cytometry, lean IgG n=4, lean PDL1/VEGF n=3, MASH IgG n=3, MASH PDL1/VEGF n=4. **O.** Quantification of tumour CD8 T cell count in lean and MASH intrahepatic HCC-bearing treated mice with anti-PDL1/anti-VEGF vs IgG control as assessed by IHC staining, lean IgG n=4, lean PDL1/VEGF n=3, MASH IgG n=7, MASH PDL1/VEGF n=5. **P.** Representative intrahepatic tumour CD8 stain of lean and MASH mice treated with anti-PDL1/anti-VEGF vs IgG control, at 200x magnification. P values calculated using a one-way ANOVA with Tukey post-hoc test *p<0.05, **p<0.01, ***p<0.001, ****p<0.0001, ns non-significant.

### 7.4. Effects of anti-PDL1/anti-VEGF therapy on CD8 subpopulations in lean vs MASH intrahepatic HCC

Given that anti-PDL1/anti-VEGF therapy induced tumour CD8 expansion/ infiltration in both lean and MASH mice with different treatment effects I then investigated differences in CD8 subpopulations. Previous work investigating anti-PD1 treatment resistance in MASH-HCC has demonstrated an expansion of $PD1^+EOMES^+CXCR6^+$ CD8 T cells in MASH. These have shown at least in part to be responsible for immune checkpoint inhibitor resistance given their exhausted and auto-aggressive phenotype.[47,51] PD1 expression is a known marker of T cell exhaustion, EOMES is a transcription factor and another marker of T cell exhaustion and CXCR6 indicates tissue residency.

In my experiment there was a preferential expansion of $PD1^+EOMES^+CXCR6^+$ CD8 T cells in MASH intrahepatic tumours treated with anti-PDL1/anti-VEGF (figure 7.3 A-B). This was also confirmed on IHC analysis showing a preferential expansion of $PD1^+$ staining in MASH intrahepatic tumours treated with anti-PDL1/anti-VEGF (figure 7.3 C-D). Therefore, a preferential expansion of exhausted $PD1^+EOMES^+CXCR6^+$ CD8 T cells in response to anti-PDL1/anti-VEGF therapy in MASH maybe the reason why there is a suboptimal anti-tumour response compared to that seen in lean mice, despite both groups having an expansion/ recruitment of total CD8 T cells.

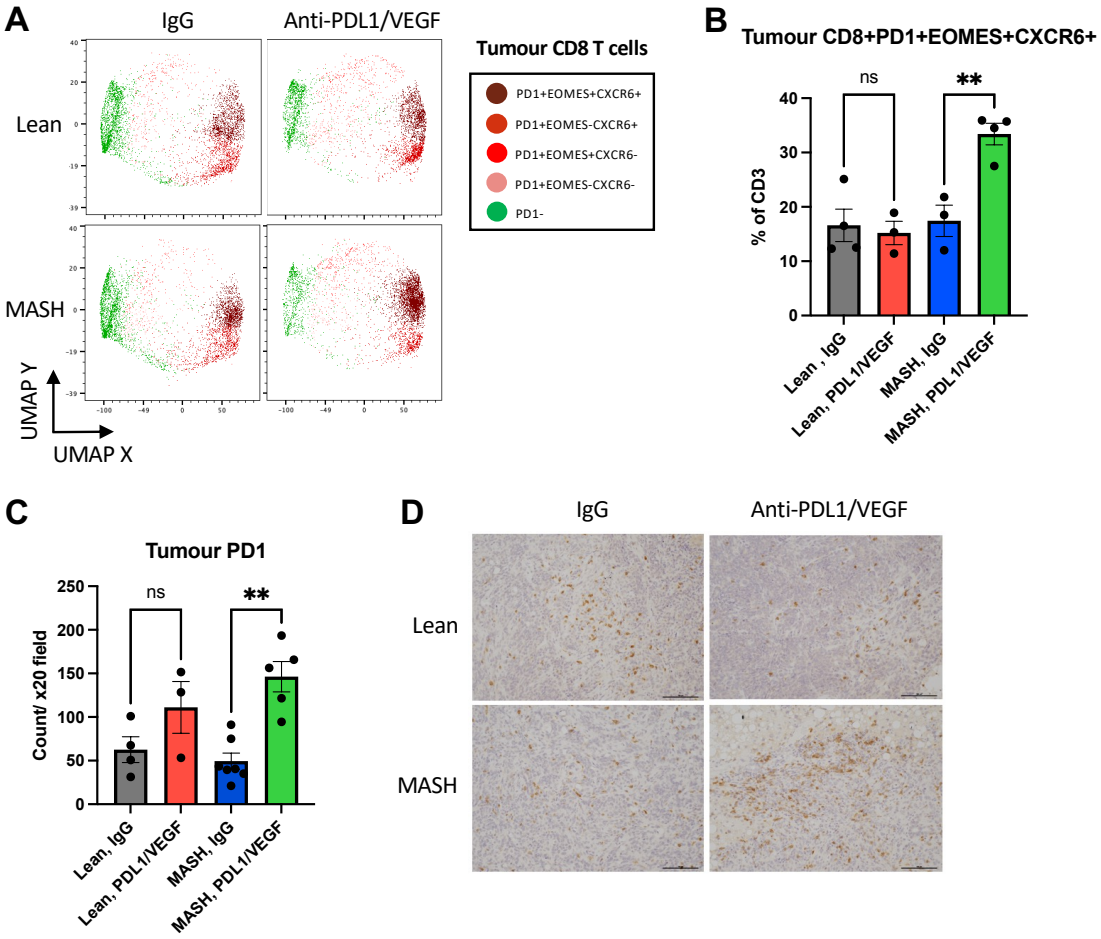



**Figure 7.3 – Effects of anti-PDL1/anti-VEGF therapy on CD8 subpopulations in lean vs MASH intrahepatic HCC. A.** High dimensional UMAP plots representing tumour CD8 subpopulations as assessed by flow cytometry in lean and MASH intrahepatic HCC-bearing mice treated with anti-PDL1/VEGF vs IgG control. **B.** Quantification of $PD1^{+}EOMES^{+}CXCR6^{+}$ CD8 T cell frequency in lean and MASH intrahepatic tumours treated with anti-PDL1/VEGF vs IgG control as assessed by flow cytometry, lean IgG n=4, lean PDL1/VEGF n=3, MASH IgG n=3, MASH PDL1/VEGF n=4. **C.** Quantification of PD1 IHC staining in lean and MASH intrahepatic HCC-bearing mice treated with anti-PDL1/VEGF vs IgG control, lean IgG n=4, lean PDL1/VEGF n=3, MASH IgG n=7, MASH PDL1/VEGF n=5. **D.** Representative tumour PD1 stain of lean and MASH mice treated with anti-PDL1/VEGF vs IgG control, at 200x magnification. P values calculated using a one-way ANOVA with Tukey post-hoc test *p<0.05, **p<0.01, ***p<0.001, ****p<0.0001, ns non-significant.

## 7.5. CD8 T cell subpopulations in the MASH

To investigate whether the expansion of $PD1^{+}EOMES^{+}CXCR6^{+}$ CD8 T cells are specific to intrahepatic tumour bearing mice or are a feature of MASH I conducted a diet only study without the introduction of the intrahepatic tumours (figure 7.4 A). This demonstrated a large expansion of $PD1^{+}EOMES^{+}CXCR6^{+}$ CD8 T cells in the livers of

MASH mice (figure 7.4 B-C). This was also confirmed on IHC analysis showing an expansion of PD1$^{+}$ staining in MASH livers compared to lean livers (figure 7.4 D-E). A small number of PD1$^{+}$EOMES$^{+}$CXCR6$^{+}$ CD8 T cells could also be found in the spleens and blood of MASH mice (figure 7.4 B-C).

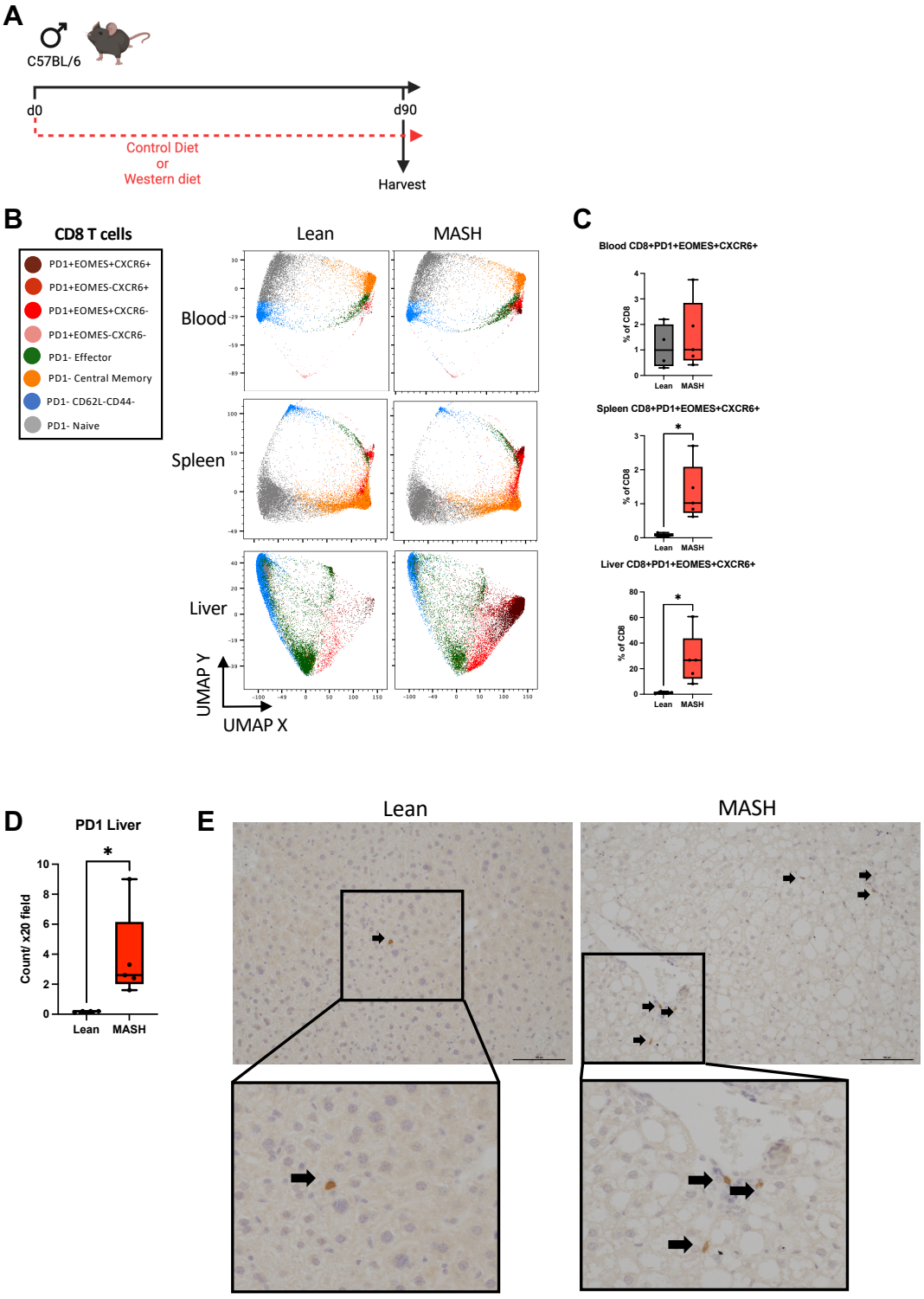


**Figure 7.4 – CD8 T cell subpopulations in MASH. A.** Schematic outlining experiment design, mice were placed on either control diet (lean) or western diet (MASH) and harvested at day 90. **B.** High dimensional UMAP plots representing blood, spleen and liver CD8 subpopulations as assessed by flow cytometry in lean and MASH mice. **C**. Quantification of $PD1^{+}EOMES^{+}CXCR6^{+}$ CD8 T cell frequency in the blood, spleen and liver of lean vs MASH mice as assessed by flow cytometry. **D.** Quantification of PD1 IHC staining in lean vs MASH livers. **E.** Representative liver PD1 stains of lean vs MASH mice, at 200x magnification. P values calculated using an unpaired t-test *p<0.05, **p<0.01, ***p<0.001, ****p<0.0001, ns non-significant. Lean n=4, MASH n=5

## 7.6. Therapy response to anti-PDL1/anti-VEGF in lean vs MASH subcutaneous HCC

In both my dietary study (figure 7.4) and intrahepatic tumour therapy study (figure 7.3) $PD1^{+}EOMES^{+}CXCR6^{+}$ CD8 T cells were almost exclusively found in the liver or intrahepatic tumours of MASH mice. This subset was preferentially expanded in the intrahepatic tumours of MASH mice treated with anti-PDL1/anti-VEGF therapy and hence may explain the suboptimal response to therapy seen in MASH mice, especially given that they have been previously described as having an exhausted and auto-aggressive phenotype in MASH.[47,51] My hypothesis was that these $PD1^{+}EOMES^{+}CXCR6^{+}$ CD8 T cells are specific to the MASH liver and that they are at least in part contributing to an immune checkpoint inhibitor resistant liver/tumour microenvironment in MASH.

Therefore, to test whether HCC immune checkpoint inhibitor resistance in MASH is driven by the hepatic microenvironment or the systemic environment of MASH I conducted an experiment in which I subcutaneously implanted the Hep 53.4 HCC cell line in MASH or lean mice then treated them with either anti-PDL1/anti-VEGF therapy or IgG control (figure 7.5 A). Unlike in intrahepatic tumours (figure 7.1 B-C) this demonstrated a significant reduction in subcutaneous tumour burden in both MASH and lean mice treated with anti-PDL1/anti-VEGF (figure 7.5 B-D), with this same treatment effect also being demonstrated in longitudinal tumour surface area measurements (figure 7.5 E). Hepatic steatosis was confirmed in the MASH mice and there was no treatment effect on steatosis (figure 7.5 F-G). There was a small increase in number of lipid drops in the subcutaneous tumours of MASH mice compared to lean mice and again the treatment had no effect on tumour lipid drop number (figure 7.5 H-I). Therefore, this experiment confirms that it is the intrahepatic microenvironment of

MASH which is driving immune checkpoint inhibitor resistance rather than the systemic environment of MASH.

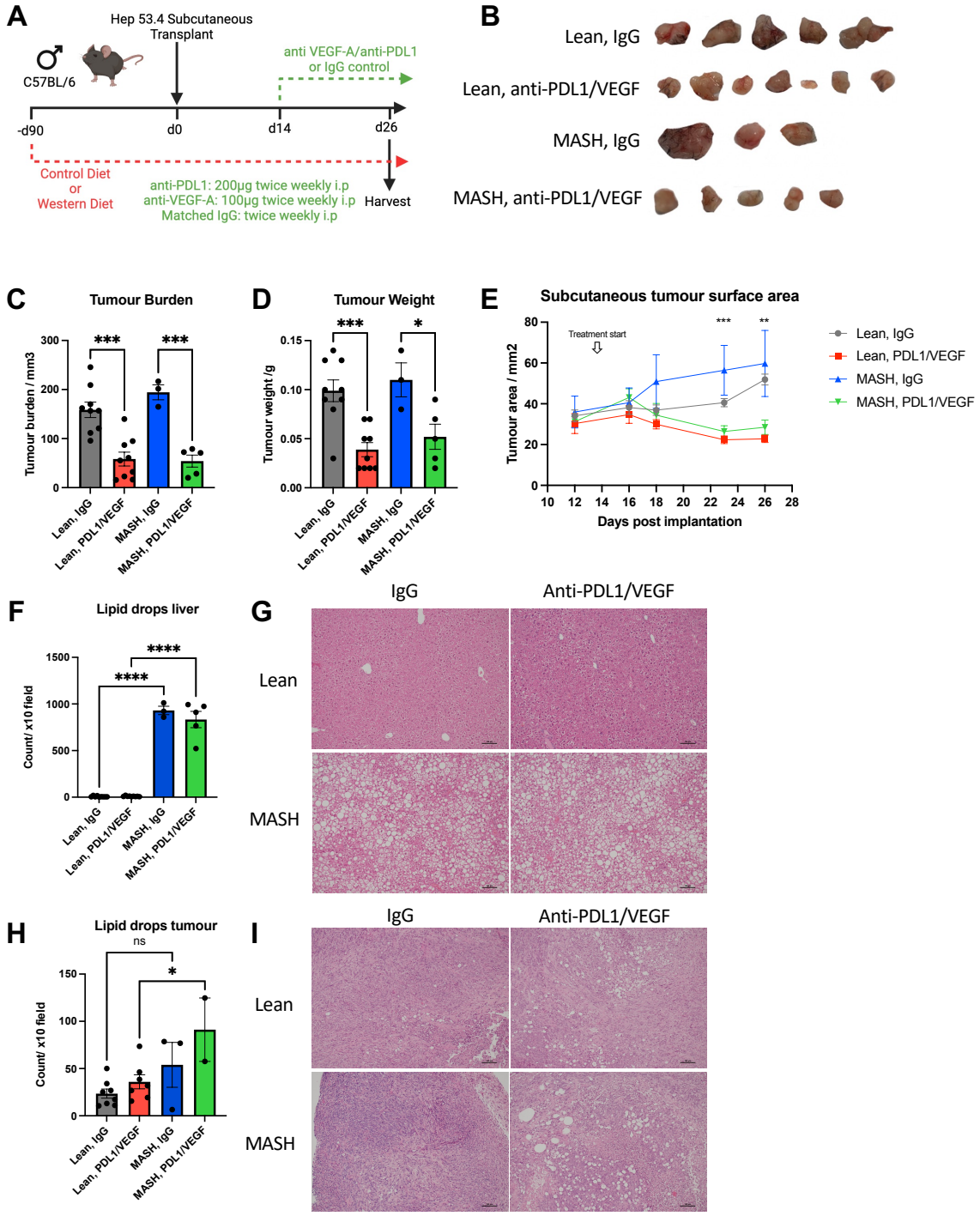



**Figure 7.5 – Therapy response to anti-PDL1/anti-VEGF in lean vs MASH subcutaneous HCC. A.** Schematic outlining experiment design to test the effectiveness of anti-PDL1/VEGF therapy in subcutaneous HCC bearing lean vs MASH mice. **B**. Representative images of dissected subcutaneous tumours following harvest. **C.** Quantification of subcutaneous tumour burden in lean and MASH mice

treated with anti-PDL1/anti-VEGF vs IgG control, lean IgG n=9, lean PDL1/VEGF n=9, MASH IgG n=3, MASH PDL1/VEGF n=5. **D.** Quantification of subcutaneous tumour weight in lean and MASH mice treated with anti-PDL1/anti-VEGF vs IgG control, lean IgG n=9, lean PDL1/VEGF n=9, MASH IgG n=3, MASH PDL1/VEGF n=5. **E.** Quantification of subcutaneous tumour surface area measured in vivo during the experiment in lean and MASH mice treated with anti-PDL1/anti-VEGF vs IgG control, lean IgG n=9, lean PDL1/VEGF n=9, MASH IgG n=3, MASH PDL1/VEGF n=5. **F.** Quantification of hepatic steatosis as assessed by H&E staining and lipid drop count in lean and MASH mice treated with anti-PDL1/anti-VEGF vs IgG control, lean IgG n=9, lean PDL1/VEGF n=9, MASH IgG n=3, MASH PDL1/VEGF n=5. **G.** Representative H&E staining of livers from lean and MASH mice treated with anti-PDL1/anti-VEGF vs IgG control, 100x magnification. **H.** Quantification of subcutaneous tumour lipid count as assessed by H&E stain in lean and MASH mice treated with anti-PDL1/anti-VEGF vs IgG control, 100x magnification, lean IgG n=8, lean PDL1/VEGF n=7, MASH IgG n=3, MASH PDL1/VEGF n=2. **I**. Representative H&E staining of subcutaneous tumours from lean and MASH mice treated with anti-PDL1/anti-VEGF vs IgG control, 100x magnification. P values calculated using a one-way ANOVA with Tukey post-hoc test *p<0.05, **p<0.01, ***p<0.001, ****p<0.0001, ns non-significant.

## 7.7. Immunological effects of anti-PDL1/anti-VEGF therapy in lean vs MASH subcutaneous HCC

The subcutaneous tumour immune infiltrates of lean vs MASH mice treated with anti-PDL1/anti-VEGF vs IgG are summarised in figure 7.6 A. There were no significant differences in the frequencies of NK cells, NK T cells, B cells, neutrophils, cDC1s, cDC2s and $Ly6C^+$ macrophages (figure 7.6 B-H). There was a reduction in the frequency of $Ly6C^-$ macrophages in lean mice treated with anti-PDL1/anti-VEGF but this was not seen in MASH mice (figure 7.6 I). There were no significant differences in $Ly6C^+$ monocytes and $Ly6C^-$ monocytes (figure 7.6 J-K). There was no difference in total T cell or CD4 T cell frequency (figure 7.6 L-M) but like in the intrahepatic tumours there was a significant increase in CD8 T cell frequency in lean mice and a trend towards increase in MASH mice with anti-PDL1/anti-VEGF treatment (figure 7.6 N). This was confirmed on IHC staining (figure 7.6 O-P). Therefore, like in the intrahepatic HCC study anti-PDL1/anti-VEGF treatment induced a recruitment or expansion of subcutaneous tumour CD8 T cells (figure 7.2), however unlike in the intrahepatic study there was an excellent treatment response in both lean and MASH mice (figure 7.1 and 7.5). Therefore, the difference in MASH treatment response in intrahepatic vs subcutaneous tumours likely lies in the functional status of these CD8 T cells.

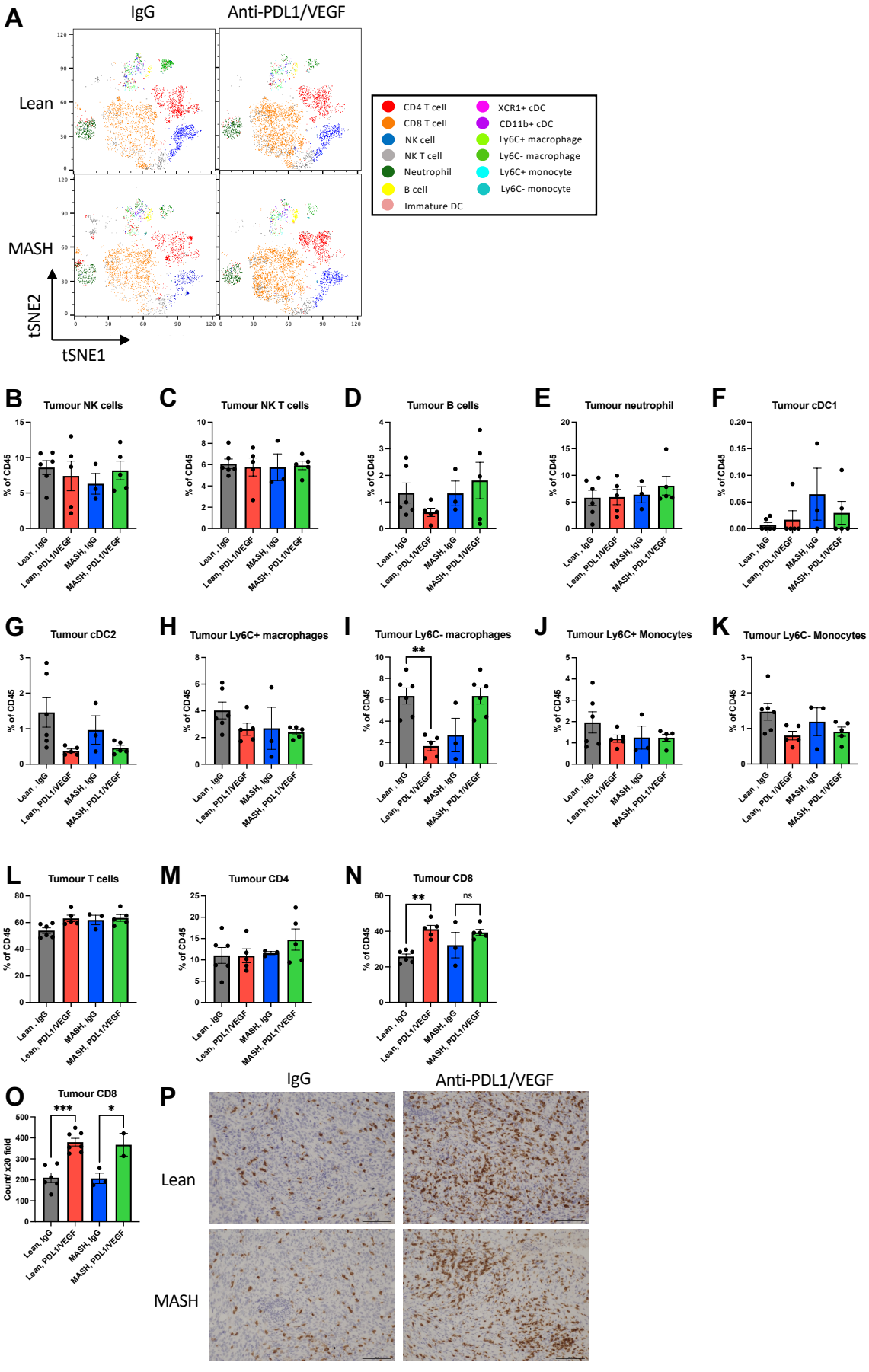

A
IgG
Anti-PDL1/VEGF
Lean
MASH
tSNE2
tSNE1
CD4 T cell
CD8 T cell
NK cell
NK T cell
Neutrophil
B cell
Immature DC
XCR1+ cDC
CD11b+ cDC
Ly6C+ macrophage
Ly6C- macrophage
Ly6C+ monocyte
Ly6C- monocyte
B Tumour NK cells
C Tumour NK T cells
D Tumour B cells
E Tumour neutrophil
F Tumour cDC1
G Tumour cDC2
H Tumour Ly6C+ macrophages
I Tumour Ly6C- macrophages
J Tumour Ly6C+ Monocytes
K Tumour Ly6C- Monocytes
L Tumour T cells
M Tumour CD4
N Tumour CD8
O Tumour CD8
P
% of CD45
Count/ x20 field
Lean , IgG
Lean, PDL1/VEGF
MASH, IgG
MASH, PDL1/VEGF
**
***
*
ns

**Figure 7.6 – Immunological effects of anti-PDL1/anti-VEGF therapy in lean vs MASH subcutaneous HCC. A.** tSNE plots representing the tumour immune cell populations as assessed by flow cytometry in lean and MASH subcutaneous HCC-bearing mice treated with anti-PDL1/anti-VEGF vs IgG control. **B-N.** Quantification of tumour NK cell, NK T cell, B cell, neutrophil, cDC1, cDC2, $Ly6C^+$ macrophage, $Ly6C^-$ macrophage, $Ly6C^+$ monocyte, $Ly6C^-$ monocyte, T cell, CD4 T cell and CD8 T cell frequency in lean and MASH subcutaneous HCC-bearing treated with anti-PDL1/anti-VEGF vs IgG control as assessed by flow cytometry, lean IgG n=6, lean PDL1/VEGF n=5, MASH IgG n=3, MASH PDL1/VEGF n=5. **O.** Quantification of tumour CD8 T cell count in lean and MASH subcutaneous HCC-bearing treated with anti-PDL1/VEGF vs IgG control as assessed by IHC staining, lean IgG n=6, lean PDL1/VEGF n=7, MASH IgG n=3, MASH PDL1/VEGF n=2. **P.** Representative subcutaneous tumour CD8 stain of lean and MASH mice treated with anti-PDL1/VEGF vs IgG control, at 200x magnification. P values calculated using a one-way ANOVA with Tukey post-hoc test *p<0.05, **p<0.01, ***p<0.001, ****p<0.0001, ns non-significant.

## 7.8. Effects of anti-PDL1/anti-VEGF therapy on T cell subpopulations in lean vs MASH subcutaneous HCC

Next, I looked at PD1 expression in CD8 and CD4 T cells within the subcutaneous tumours (figure 7.7 A). Unfortunately, due to limitations in the yield of leukocytes isolated from the subcutaneous tumours I was unable to use the full antibody panel and was therefore not able to look at EOMES and CXCR6 expression. Unlike in the intrahepatic tumours there was no difference in the frequency of $PD1^+$ CD8 T cells in MASH and lean subcutaneous tumour bearing mice treated with anti-PDL1/anti-VEGF (figure 7.7 B). This was confirmed on IHC analysis, again with no significant differences in PD1 staining (figure 7.7 C-D).

Although I have not confirmed the absence of the exhausted and auto-aggressive $PD1^+EOMES^+CXCR6^+$ CD8 T cell population in the subcutaneous tumours. I did show that this population is almost exclusively found in the livers of MASH mice with very few being found elsewhere (figure 7.4). I also demonstrated that there is not a preferential expansion of $PD1^+$ CD8 T cells in MASH subcutaneous tumours compared to lean subcutaneous tumours treated with anti-PDL1/anti-VEGF therapy like that found in the intrahepatic tumours (figure 7.3).

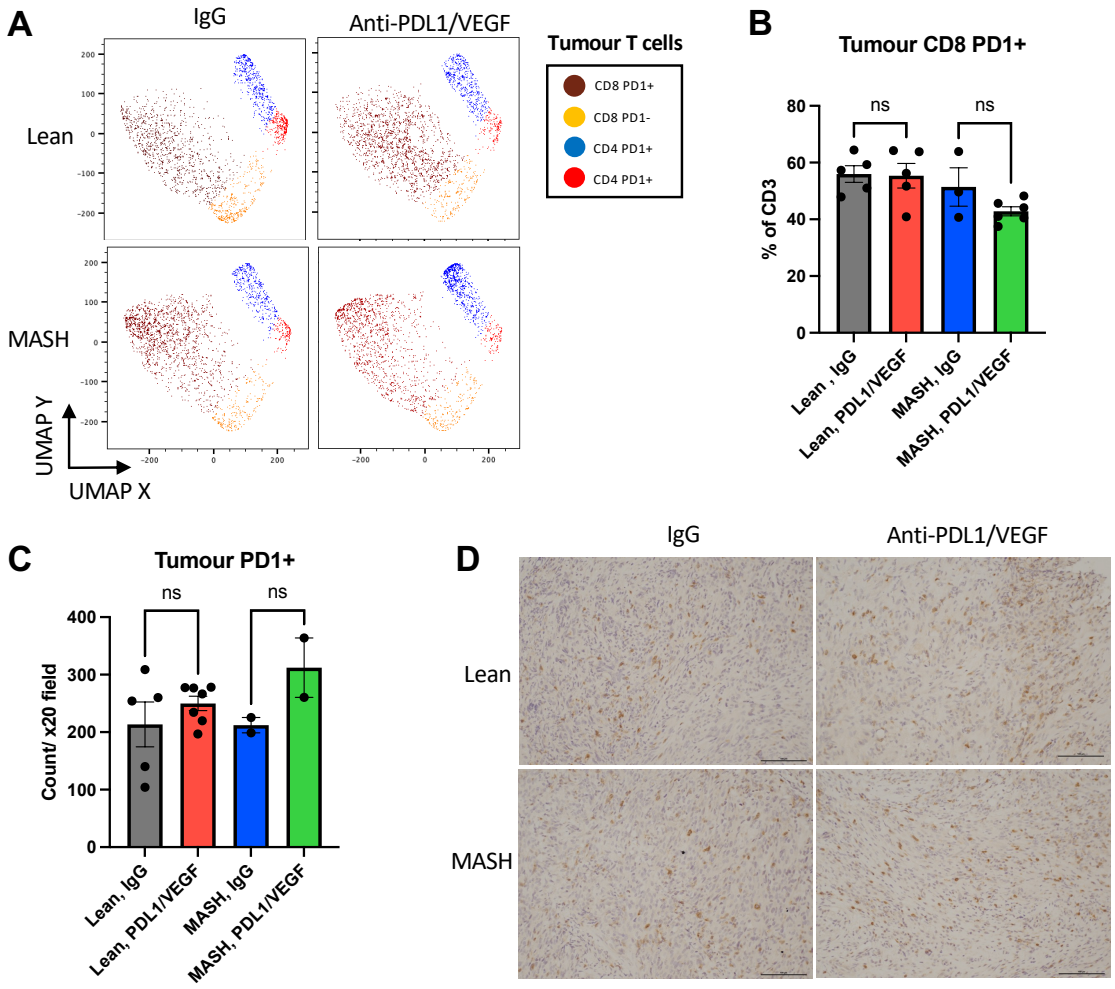



**Figure 7.7 – Effects of anti-PDL1/anti-VEGF therapy on T cell subpopulations in lean vs MASH subcutaneous HCC. A.** High dimensional UMAP plots representing tumour CD4 and CD8 PD1 expression as assessed by flow cytometry in lean and MASH subcutaneous HCC-bearing mice treated with anti-PDL1/VEGF vs IgG control. **B.** Quantification of PD1$^{+}$ CD8 T cell frequency in lean and MASH subcutaneous tumours treated with anti-PDL1/anti-VEGF vs IgG control as assessed by flow cytometry, lean IgG n=5, lean PDL1/VEGF n=5, MASH IgG n=3, MASH PDL1/VEGF n=6. **C.** Quantification of PD1 IHC staining in lean and MASH subcutaneous tumours treated with anti-PDL1/VEGF vs IgG control, lean IgG n=5, lean PDL1/VEGF n=7, MASH IgG n=2, MASH PDL1/VEGF n=2. **D.** Representative subcutaneous tumour PD1 stain of lean and MASH mice treated with anti-PDL1/VEGF vs IgG control, at 200x magnification. P values calculated using a one-way ANOVA with Tukey post-hoc test *p<0.05, **p<0.01, ***p<0.001, ****p<0.0001, ns non-significant.

## 7.9. Conclusion

Like reports from clinical trials and patient cohorts I found that anti-PDL1/anti-VEGF combination therapy has reduced anti-tumour treatment efficacy in HCC bearing mice with underlying MASH compared to lean mice. On further exploration of the underlying

intra-tumour immune response, I found that despite the treatment being less effective in MASH there was the same immunological response to therapy with an expansion or recruitment of CD8 T cells within the tumours of both MASH and lean mice. This suggested that the underlying difference in treatment response was underpinned by the functional status of these CD8 T cells. Indeed, on further characterisation of CD8 T cells I found a preferential expansion of $PD1^{+}EOMES^{+}CXCR6^{+}$ CD8 T cells in the tumours of MASH mice treated with anti-PDL1/anti-VEGF therapy. $PD1^{+}EOMES^{+}CXCR6^{+}$ CD8 T cells have previously been described as expanded in the MASH liver and as having an exhausted and auto-aggressive phenotype. Therefore, the reason for this reduced anti-PDL1/anti-VEGF treatment efficacy is likely because it is recruiting/ expanding already functionally exhausted CD8 T cells in MASH-HCC which have limited anti-tumour function. I then investigated the presence of $PD1^{+}EOMES^{+}CXCR6^{+}$ CD8 T cells in the MASH model without HCC. This confirmed that there was a large expansion of $PD1^{+}EOMES^{+}CXCR6^{+}$ CD8 T cells in MASH livers, and that this population was almost exclusively found in the liver. Finally, to test whether treatment resistance in MASH was being driven by the systemic conditions of MASH or the hepatic microenvironment of MASH I conducted a subcutaneous HCC model. Unlike in the intrahepatic HCCs, this demonstrated a good treatment response to anti-PDL1/anti-VEGF therapy in both MASH and lean mice, with no differences in CD8 $PD1^{+}$ T cell frequency.

# 8. Discussion

I set out to investigate neutrophil phenotype, function and heterogeneity in health, CLD and HCC using both patient samples and pre-clinical models. I then aimed to identify conserved alterations in neutrophil phenotypes and test the effects of therapeutically targeting these neutrophils in a pre-clinical model. Finally, I investigated immune checkpoint inhibitor effectiveness in a pre-clinical model of MASH-HCC. I will discuss my findings under these aims and provide interpretation and contextualisation in view of previous literature. I will also discuss the limitations of my work and suggest the direction of future work.

## 8.1. Neutrophil heterogeneity in health, CLD and HCC

In both HCC patients and HCC-bearing mice with background MASLD I found an expansion of circulating low density neutrophils compared to controls. These low density neutrophils had a mature, activated, aged and degranulated phenotype and were functionally distinct from normal density neutrophils.

### 8.1.1. Circulating neutrophil heterogeneity

I have demonstrated heterogeneity of circulating neutrophils in both humans and mice. In humans I found three populations of circulating neutrophils: ND, LD CD16$^{high}$ and LD CD16$^{low}$ (table 8.1). In mice I found two populations of circulating neutrophils: ND and LD (table 8.1). In humans morphological (figure 4.5), phenotypical (figure 4.6, figure 4.8 and figure 4.10) and functional analysis (figure 4.7) demonstrated these populations to be distinct. LD CD16$^{low}$ neutrophils were found to be immature, progenitor neutrophils as demonstrated by their immature morphology and lack of mature neutrophil markers such as CD16, CD10 and CXCR2. In addition their high expression of CD66b, CD15 and CD49d and lack of secondary and tertiary granules identified them as most likely being promyelocytes.[390] ND neutrophils were found to be mature resting neutrophils as demonstrated by their typical lobulated nuclear morphology, expression of mature neutrophil markers and low expression of activation markers. LD CD16$^{high}$ neutrophils were found to be activated, degranulated and aged neutrophils as demonstrated by their high expression of CXCR4, CD10, CD11b and low expression of CD62L and CXCR2. The mouse ND neutrophils and LD neutrophils corresponded to the human ND and LD CD16$^{high}$ neutrophils respectively, having

conversed patterns of CD11b, CXCR2 and CD62L expression and similar trends in terms of migratory abilities to CXCL2 and phagocytosis (figure 5.12). In my human study there was an expansion of LD CD16$^{high}$ (aged) neutrophils in both patients with CLD and HCC compared to health controls (figure 4.4), while in my pre-clinical model there was an expansion of LD neutrophils in HCC-bearing mice compared to sham controls (figure 5.9).

My findings support previous literature which reports the presence of circulating low-density and normal (or high) density neutrophils in both humans and mice.[118] Similar to Sagiv et al,[118] who first described the presence of circulating neutrophil populations with different densities, I found an immature LD population in humans (LD CD16$^{low}$) along with a mature LD population (LD CD16$^{high}$). Notably, instead of splitting them on FSC and nuclear morphology, I was able to define them based on expression of several surface markers, including CD16, CD10, CD66b, CD11b, CD62L and CXCR2.

#### 8.1.1.1. LD CD16$^{low}$ neutrophil characterisation

The circulating LD CD16$^{low}$ population, although described in previous studies has not been extensively characterised.[391-395] I am the first to further phenotype this population and identify them as neutrophil progenitors, most likely promyelocytes. I could not identify a corresponding immature LD population in mice, possibly because of the varying nomenclature and surface markers between human and mouse neutrophils. Further progenitor markers, including C-kit, CD34 and CD16/32 failed to distinguish these. Therefore, either this immature LD population was not present in my mouse model or the markers I was using to try to identify them were not relevant. In hindsight CD101 expression maybe worth investigating as a way to identify LD immature mouse neutrophils given that it has been shown to closely correlate to neutrophil maturity in the bone marrow.[371] In humans, circulating CD16$^{low}$ neutrophils have previously been described in states of acute inflammation such as trauma, infection, cardiac surgery and LPS challenge.[396-398] Their presence is thought to be a result of emergency granulopoiesis and premature release of immature neutrophils/ progenitors from the bone marrow. Interestingly, unlike in acute inflammation, they do not appear increased in states of chronic inflammation.[396] This may explain why I saw no difference in the frequency of these LD CD16$^{low}$ neutrophils between healthy controls, CLD and HCC, which are more associated with states of chronic inflammation. Functionally CD16$^{low}$

neutrophils have been described as having impaired NET formation and reduced phagocytic ability,[399] which is in keeping with my data. Because the frequency of LD CD16$^{low}$ neutrophil was not significantly changed in my patient groups I did not make further attempts to identify these in my pre-clinical model. My experimental set up did not enable me to perform morphological analysis like those employed by Sagiv et al.[118] However, a LEGENDScreen assay, as I did in patients, screening 253 different cell surface markers, may in future identify this immature LD population in mice.

#### 8.1.1.2. LD CD16$^{high}$ neutrophil characterisation

The circulating LD CD16$^{high}$ neutrophils had a mature, activated, and aged phenotype as demonstrated by them being CD62L$^{low}$, CD10$^{high}$, CD11b$^{high}$, CD66b$^{high}$ and CXCR2$^{low}$. This LD CD16$^{high}$ population has been previously reported in several studies.[118,393,400-403] In line with my data previous work has also described them as primed and activated with high ROS production and high phagocytosis capacity.[401] They have also been described as being immunosuppressive towards T cells in the context of pregnancy, G-CSF administration and advanced urological cancers.[149,404,405] Importantly I identified high LOX-1 and CD33 expression on LD CD16$^{high}$ neutrophils, which suggests that they are the PMN-MDSC population, extensively described in the literature as being expanded in cancer and states of chronic inflammation and as exerting their T cell immunosuppressive functions via ARG1, ROS and prostaglandin E2 activity.[406] This finding is important as it allows me to link the LD neutrophil and PMN-MDSC literature together. Going forward in the study of neutrophils I think there should be concerted efforts to standardise nomenclature and phenotypic definitions of neutrophil and PMN-MDSC populations in both humans and mice. This would allow greater comparison between studies and enable greater progress in this important field of cancer immunology. I cannot comment on the immunosuppressive vs inflammatory functions of LD CD16$^{high}$ neutrophils as I did not conduct T cell suppression assays, this being a limitation of my work. My work would be improved by doing some T cell suppression assays, however these are not without limitations, the main one being the phagocytosis of T cell stimulating beads causing artefactual decreases in T cell activation.[407] Although most the literature suggest these LD CD16$^{high}$ neutrophils to be immunosuppressive one study investigating neutrophils in infections suggests that neutrophils with a similar CD11b$^{high}$, CD62L$^{low}$, CXCR2$^{low}$ phenotype (density not investigated) can

behave like antigen presenting neutrophils after encountering antigen, migrating to lymph nodes to stimulate adaptive immunity.[403] This would be another novel function of neutrophils worth investigating in the context of HCC.

#### 8.1.1.3. LD CD16$^{high}$ neutrophil expansion in CLD and HCC

I found that the frequency of total neutrophils was increased in both CLD patients and HCC patients compared to healthy controls (figure 4.2) and that this was driven by an expansion of LD CD16$^{high}$ neutrophils (figure 4.4). A couple of previous studies have also described this increase in neutrophil frequency being correlated to an expansion of neutrophils in the PBMC isolations of blood, which is equivalent to the low density isolations in my experiments.[156,408] These studies also found that higher neutrophil count corresponded to a poorer overall survival. My study was different in that rather than comparing HCC patients to healthy controls, I also compared to CLD patients. This is important as patients with HCC almost always have underlying CLD, which is a state of chronic inflammation itself. Importantly I found that both CLD and HCC patients have an expansion of LD CD16$^{high}$ neutrophils compared to healthy controls. This is in keeping with the work of others which show an expansion of CD62L$^{low}$CD16$^{high}$ neutrophils in states of chronic inflammation.[396] In my pre-clinical model HCC-bearing mice with underlying MASH also had an increase in neutrophil frequency compared to MASH mice which had undergone a sham procedure (figure 5.7), which was driven by an expansion of LD neutrophils (figure 5.9). However unlike in the equivalent patient comparison, there was not an expansion of LD neutrophils in MASH mice compared to lean mice (figure 5.7). One reason for this difference could be because my pre-clinical model only modelled steatohepatitis with very minimal fibrosis (figure 5.1 and figure 5.3). In contrast, my patient cohort was mainly made up of patients with underlying cirrhosis (table 4.1). Therefore, it could be the advanced fibrosis component of the CLD, or its associated portal hypertension, driving the increase in LD neutrophils, with the presence of HCC also being a potential driver of LD neutrophils. The clinical characteristics of my patient cohort in terms of age, gender, cirrhosis stage, aetiology and performance status were reasonably well matched. The healthy control group overall had a younger age compared to the CLD and HCC groups which could be a confounder. Because of the small group sizes statistical comparisons according to cirrhosis stage and aetiology were not possible. This is a big limitation of my study. Given the chance I would recruit a larger patient

cohort and look at correlations of LD neutrophils with cirrhosis stage, aetiology as well as overall survival. I would also recruit a healthy control group with a more comparable age to the CLD and HCC groups. Given that an older 'healthy control' group would likely have more co-existing medical conditions a detailed past medical history and screening for current infection or illness could be conducted to enable a more robust control. Although I could not report on these associations in my data, there are several existing studies in HCC which correlate circulating neutrophil count with advanced disease, poor overall survival and poor response to therapy.[153-155,157-167]

#### 8.1.1.4. Technical limitations

The main technical limitations of my patient study are the time to isolation of my blood samples and use of MFI for phenotyping. There was variability of between 1 and 2 hours between obtaining blood samples and starting the isolation protocol. I know from my longitudinal isolation study that time between sample collection and neutrophil isolation corresponds to the frequency of LD neutrophils as well as changes in phenotype (figure 4.12). Because of this observation I always made sure to start the isolation process within 1-2 hours of collection. Although there was no significant increase in LD neutrophil frequency at the 4 hour timepoint of my longitudinal study (figure 4.12), there was a trend supporting this. Because I collected healthy control samples in a location nearer to the laboratory than the CLD and HCC patient samples there was a risk that the overall time to isolation would be different between the groups. Therefore, for healthy control samples I made sure to leave them at room temperature for a minimum of 1 hour before starting the isolation protocol, enabling the isolation times between groups to be comparable. To minimise the effects of circadian rhythm I collected all my blood samples in morning. The other limitation to my patient study was phenotyping neutrophils based on MFI. Technically despite maintaining the same experimental set up in terms of acquisition mode and laser voltages on the flow cytometer, over time there is a risk of the laser power drifting and affecting MFI values. To try to avoid this I applied set cytometer settings at each acquisition. This enabled variation of laser power to be measured by running standardisation beads which could then be adjusted for at the time of acquisition.[409,410] Despite this there is still a degree of error in this correction. I do not think this would have impacted my neutrophil phenotyping MFI data greatly as the HCC, CLD and healthy control groups were collected throughout the project and often run alongside each other. Therefore, this

small error would not have affected the comparison between groups but may have increased the variability of each group and consequently the sensitivity of the assay. There was a large range of expression of markers such as CXCR4 (figure 4.13) and small differences in marker expression between groups could have been lost. I considered running all samples together by cryopreserving samples, however the recovery and viability of cryopreserved and defrosted neutrophils was poor. In my patient study I only collected immune cell frequency data rather than absolute counts. This is a limitation as the increase in frequency of a population maybe because of the reduction in another population. For example, the increase in neutrophil frequency could have been because of the reduction in T cells. In future I would also collect absolute counts. In my mouse study however, I did collect absolute counts and these corresponded to the frequency data.

#### 8.1.1.5. Differences between mouse and human LD neutrophils

Human LD $CD16^{high}$ and mouse LD neutrophils had conserved patterns of CD11b, CXCR2, CXCR4 and CD62L suggesting equivalence. The main difference however between human and mouse ND and LD populations were in their functional characteristics. Whereas human LD $CD16^{high}$ neutrophils had a low basal ROS and high PMA stimulated ROS compared to ND neutrophils, mouse LD neutrophils had a high basal ROS and low PMA stimulated ROS compared to ND neutrophils. This is a stark difference and may suggest that the mouse LD neutrophils are functionally exhausted whereas the human LD $CD16^{high}$ neutrophils are functionally primed. Given that ROS production is a known mechanism of neutrophil T cell suppression, human and mouse LD neutrophil may have very different functions in terms of T cell suppression. In future I would also include an N-formylmethionine-leucyl-phenylalanine (fMLP) condition in my ROS assay as this is a more biologically relevant route of neutrophil stimulation as opposed to PMA which stimulates neutrophils intracellularly and is an artificial method of neutrophil activation. In future I would also like to do T cell suppression assays to investigate if this difference in ROS production between mouse and human LD neutrophils translates to differences in T cell suppression.

#### 8.1.1.6. Disease specific changes in neutrophil phenotype

In addition to an expansion of circulating LD neutrophil frequency I also found some disease related changes in neutrophil phenotype. In both CLD and HCC patients I found a reduction in CXCR2 expression of ND and LD CD16$^{high}$ neutrophils compared to healthy controls (figure 4.13). This was also functionally demonstrated with a reduced ND neutrophil migration to CXCL2 in HCC patients (figure 4.14). The only HCC specific change in neutrophil phenotype was an increase in CD15 expression in ND neutrophils (figure 4.13). The reduced CXCR2 expression may suggest an increased degree of activation and ageing in CLD and HCC neutrophils compared to healthy controls.[61] This is supported by my data, showing a reduction in neutrophil CXCR2 expression with both PMA stimulation (figure 4.11) and time (figure 4.12). There is evidence both in vitro and in patients following coronary artery bypass surgery that neutrophil CXCR2 expression negatively correlates to serum IL-8 concentration.[411] IL-8 levels are reported to be raised in both HCC and chronic liver disease and may explain this phenotypic change.[412-415] In future I would like to quantify the serum levels of IL-8 in my patient cohort, especially as I have collected and stored serum samples. The increase in neutrophil CD15 I observed in HCC patients compared to CLD patients and healthy controls has not been previous reported in the literature. It maybe because of increased neutrophil activation in HCC as supported by my PMA stimulation data (figure 4.11). I do not think this CD15 increase is a result of ageing as CD15 reduced in my time course experiment (figure 4.12). In the literature neutrophil CD15 expression is generally reported to be reduced in infection and there are no reports of its expression being altered in cancer.[416,417]

In my pre-clinical model, I showed that neutrophils from HCC-bearing mice had reduced expression of Ly6G compared to sham controls, across biological compartments (figure 5.20). Reduced neutrophil Ly6G expression is usually attributed to a more immature phenotype.[418,419] However my data has also shown a reduction in Ly6G expression following PMA stimulation (figure 5.20). In addition, aged neutrophils as well as neutrophils from aged mice have reduced Ly6G expression.[67,373] Therefore HCC-bearing mice either have a more immature phenotype or a more activated/ aged phenotype. A more aged/ activated phenotype would be in keeping with my human data and as well as my data showing accelerated granulopoiesis and ageing of neutrophils in the bone marrow of HCC-bearing mice (figure 5.17). To further

investigate this, I would do some bulk RNA sequencing on purified mouse neutrophils from HCC-bearing and sham control mice and compare maturation according to the neutrotime.[100]

### 8.1.1.7. Role of neutrophil ageing in MASH and HCC

Neutrophil ageing has also been linked to metabolic alterations and disease progression in pre-clinical models of MASH.[75] This study used neutrophil specific conditional CXCR2 (constitutionally fresh) or CXCR4 (constitutionally aged) knockouts to show that aged neutrophils drive increased body weight, reduced glucose tolerance, and increased steatosis and liver fibrosis in mice on a high fat diet.[75] Interestingly they showed that high fat diet primes aged neutrophils, but not fresh neutrophils, to infiltrate the liver and promote inflammation. This study highlights the importance of aged neutrophils being preferentially recruited to the liver and driving disease progression in MASH. My observation of an accumulation of neutrophils across biological compartments with reduced Ly6G expression in MASH-HCC vs MASH-Sham mice mirrors the observations of this study. Therefore, I speculate that HCC is a further driver of neutrophil ageing on top of MASH. To further investigate the role of neutrophil ageing in my pre-clinical model I plan to use the CXCR2 specific knockout mice in my HCC model and explore the effects on neutrophil frequency and phenotype, granulopoiesis and tumour progression.

| Species | Neutrophil population | Morphology | Phenotype | Function |
|---|---|---|---|---|
| Human | LD CD16$^{low}$ |  | CD16$^{low}$,CD11b$^{low}$,CD66b$^{high}$CD15$^{high}$ CD10$^{low}$,CXCR2$^{low}$, CXCR4$^{high}$,CD62L$^{-}$ CD49$^{+}$ | Intermediate basal ROS, low PMA ROS, Low phagocytosis, low migration to CXCL2 |
| | LD CD16$^{high}$ |  | CD16$^{high}$,CD11b$^{high}$,CD66b$^{high}$,CD15$^{high}$ CD10$^{high}$,CXCR2$^{low}$,CD62L$^{low}$,LOX1$^{+}$,CD33$^{+}$ CD41$^{+}$,CD36$^{+}$ | Low basal ROS, high PMA ROS, High phagocytosis, intermediate migration to CXCL2 |
| | ND |  | CD16$^{high}$CD11b$^{low}$,CD66b$^{low}$, CD15$^{low}$, CD10$^{low}$,CXCR2$^{high}$,CD62L$^{high}$ | Intermediate basal ROS, intermediate PMA ROS, high phagocytosis, high migration CXCL2 |
| Mouse | LD |  | Ly6G$^{high}$,CD11b$^{high}$,CXCR2$^{low}$,CXCR4$^{high}$ CD62L$^{low}$,CD41$^{+}$,CD36$^{+}$ | High basal ROS, low PMA ROS, low phagocytosis, low migration to CXCL2 |
| | ND |  | Ly6G$^{int}$,CD11b$^{low}$,CXCR2$^{high}$,CXCR4$^{low}$ CD62L$^{high}$ | Low basal ROS, high PMA ROS, high phagocytosis, high migration to CXCL2 |

**Table 8.1 – Circulating neutrophil heterogeneity in humans and mice.** Three populations of circulating neutrophils were identified in humans. LD CD16$^{low}$ neutrophils had an immature phenotype and nuclear morphology. ND neutrophils had a mature and resting phenotype and nuclear morphology.

LD CD16$^{high}$ neutrophils had a mature, activated, degranulated and aged phenotype with a hypersegmented nuclear morphology. LD CD16$^{high}$ neutrophils were expanded in patients with CLD and HCC compared to healthy controls. Two populations of circulating neutrophils were identified in mice. ND neutrophils had a mature resting phenotype whereas LD neutrophils had a mature, activated, degranulated and aged phenotype.

### 8.1.2. Origins of low density circulating neutrophils

My data raises important questions over the origin of LD circulating neutrophils. In vitro experiments on human whole blood showed that both time (figure 4.12) and PMA activation (figure 4.11) could transform ND neutrophils into LD CD16$^{high}$ neutrophils. However, with time although there was a change in density, the generated LD CD16$^{high}$ neutrophils did not completely match those of freshly isolated in vivo LD CD16$^{high}$ neutrophils. There was not an increase in the activation markers CD11b and CD10 as seen in LD CD16$^{high}$ neutrophils in vivo (figure 4.12). In contrast, the phenotype of LD CD16$^{high}$ neutrophils generated by PMA stimulation (rather than time) more closely matched those in vivo (figure 4.12). This suggests LD CD16$^{high}$ neutrophils are more than just aged ND neutrophils and that some activation is also required. This is supported by my neutrophil specific CXCR2 knock out experiment, in which CXCR2 knock out mice (*Cxcr2*$^{DNeut}$) had the same frequency of LD neutrophils as wild type mice (figure 5.13). Given that CXCR2 is central to neutrophil ageing this suggests that LD neutrophils are not just aged neutrophils.[61] I also demonstrated that inhibition of TGFβ type 1 receptor (ALK5) in my pre-clinical model of HCC significantly reduced the frequency of circulating LD neutrophils (figure 6.8 and 6.9). This supports the importance of TGFβ in the formation of LD neutrophils as previously described.[118] This again emphasises LD neutrophils as being activated and polarised, rather than simply aged neutrophils. The work of others has also shown stimulation with fMLP, LPS and TNF can transform ND neutrophils into LD neutrophils.[420] In future I would like to do more in vitro stimulation studies on human whole blood to further explore neutrophil activation and density. Given that LD neutrophils are degranulated and aged they could also be pre-apoptotic. In future I could look at this by incorporating annexin V staining into my experiments.

My BrdU tracking experiment showed that LD neutrophils maybe emerging directly from the bone marrow (figure 5.15). Supporting this, I found an accelerated rate of

granulopoiesis with neutrophils of a more degranulated phenotype in HCC-bearing mice compared to sham controls (figure 5.17). An altered state of granulopoiesis in the presence of HCC may explain the increased frequency of neutrophils seen in all biological compartments in HCC-bearing mice (figure 5.16), alongside the increased frequency of circulating LD neutrophils (figure 5.9). Cancer induced alterations in granulopoiesis have been previously reported and are thought to contribute to the pro-tumour functions of neutrophils.[418,421] My data suggests this maybe through the increased production of circulating LD neutrophils which may have pro-tumour functions.

One possible confounder in the BrdU tracking experiment and my assumptions, is that I could not identify the immature LD neutrophil population in mice. This means the early BrdU signal seen in the LD neutrophils could be from the immature precursor neutrophils equivalent to the LD $CD16^{low}$ population I observed in humans. To clarify whether this is the case I could collect cytospins of ND and LD neutrophils and do dual BrdU and nuclear immunofluorescence staining to correlate nuclear morphology with BrdU staining.

Another possible origin of LD neutrophils maybe neutrophils which have undergone reverse migration from tissues back into the circulation.[236] I noted that both LD $CD16^{high}$ neutrophils from HCC patients and LD neutrophils from HCC-bearing mice had a similar phenotype to liver and tumour neutrophils (figure 4.16 and figure 5.18). In humans both LD $CD16^{high}$ and tumour neutrophils had high expression of the activation markers CD66b, CD11b and CD10 and low expression of CD62L. In mice both LD neutrophils and tumour neutrophils had high expression of Ly6G and CD11b and low expression of CD62L. In the BrdU tracking experiment there was a general accumulation of BrdU positive LD neutrophils at the later time point, with higher BrdU positivity compared to liver and tumour neutrophils (figure 5.14 and figure 5.15). To better investigate whether reverse migration of neutrophils out of the tumour or liver is a source of LD neutrophils I would conduct some in vivo intravital imaging studies. The possible origins of the different circulating neutrophil populations are summarised in figure 8.1.

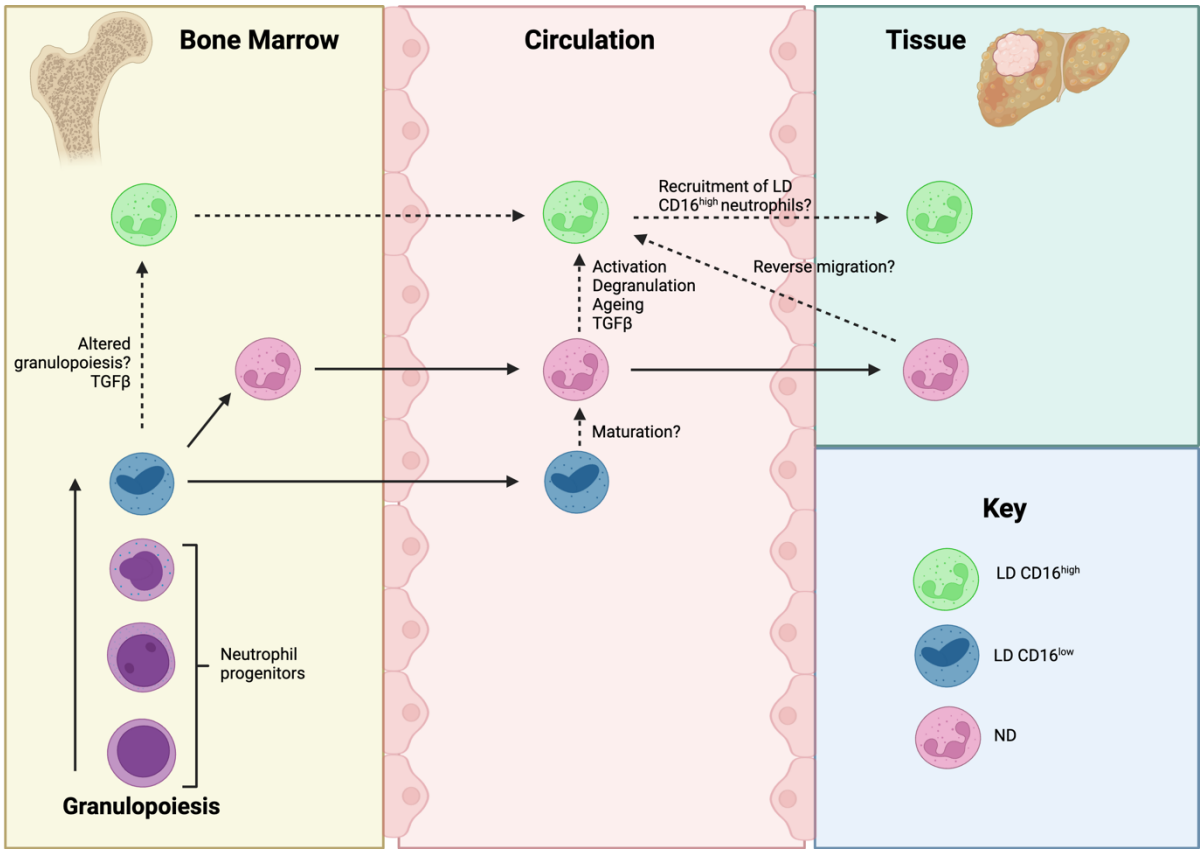



**Figure 8.1 – Possible origins of circulating LD neutrophil populations.** LD CD16$^{low}$ neutrophils are neutrophil precursors which have been prematurely released from the bone marrow. The frequency of LD CD16$^{low}$ neutrophils is not changed in CLD and HCC. Circulating LD CD16$^{high}$ neutrophils have an aged, degranulated and activated phenotype and are increased in CLD and HCC. The origin of LD CD16$^{high}$ neutrophils is uncertain. They may arise in the bone marrow as result of altered granulopoiesis and exposure to TGFβ. They could also arise from circulating ND neutrophils as a result of ageing, activation, degranulation and TGFβ exposure. Another possibility is that LD CD16$^{high}$ neutrophils are neutrophils which have undergone reverse migration out of tissues such as liver and tumour. This is supported by data showing that circulating LD CD16$^{high}$ neutrophils and tissue neutrophils have a similar phenotype. Created with https://BioRender.com.

### 8.1.3. Low density neutrophil-platelet aggregates

I found that in both humans and mice a significant proportion of LD neutrophils had positive expression of platelet makers. On further investigation these were found to be due to the presence of neutrophil platelets aggregates (NPAs) (figure 4.9). Neutrophils are well known to interact with platelets in states of inflammation, thrombosis, tissue injury and repair.[422] NPAs are observed in a wide range of inflammatory conditions such as psoriasis, rheumatological disease, inflammatory bowel disease and atherosclerosis.[423-426] In the context of cancer NPAs are associated with a poor prognosis and have been shown mechanistically to promote tumour thrombosis and

angiogenesis as well as tumour metastasis.[427,428] Neutrophils are known to interact with platelets through a number of direct and indirect interactions.[429] Platelet P-selectin, glycoprotein Ibα (GPIbα), CD40L, ICAM2 and TREM-1L bind to neutrophil P-selectin glycoprotein ligand-1 (PSGL-1), neutrophil macrophage-1 antigen (Mac-1), CD40, lymphocyte function-associated antigen 1 (LFA-1) and TREM-1 respectively.[95,430-433] These direct interactions can promote neutrophil NET formation, activation and tissue recruitment. Platelets secreted CCL5 and high mobility group box 1 (HMGB1) that promotes neutrophil activation and extravasation via CCR5 and RAGE signalling respectively,[434,435] and platelet derived serotonin promotes neutrophil CD11b expression, ROS production and degranulation.[436] These interactions are summarised in figure 8.2. In the context of MASLD, platelets have been shown to be critical in mediating immune recruitment to the liver, driving disease progression and development of HCC.[437] Furthermore there is evidence that anti platelet drugs such as aspirin and ticagrelor can reduce liver steatosis and inflammation.[437] This suggests that platelets and platelet-leukocyte interactions maybe critical in the pathogenesis of MASLD and maybe an important therapeutic target. A couple of previous studies have described neutrophil platelet interactions in LD neutrophils,[394,395] with one describing an enrichment of platelet markers in LD neutrophils.[438] I am however the first to confirm these as NPAs using imaging flow cytometry.

Outstanding questions remain. Is it neutrophil activation which drives NPA formation or NPA formation driving neutrophil activation? Are these NPAs then recruited to the liver and tumour? How does portal hypertension induced thrombocytopenia in cirrhosis affect the presence of NPAs and LD neutrophils? Does targeting neutrophil platelet interactions affect the development of LD neutrophils? Does targeting platelets or neutrophil platelet interactions affect disease progression of MASH and HCC? In the future I would like to conduct in vitro and in vivo studies using platelet inhibitors such as aspirin and ticagrelor as well as selective targeting of p-selectin and mac-1 to answer some of these questions. Intravital imaging and transendothelial migration assays would also be an interesting line of experimentation. I would also like to repeat the image stream experiment in mice to visually confirm the presence of NPAs.

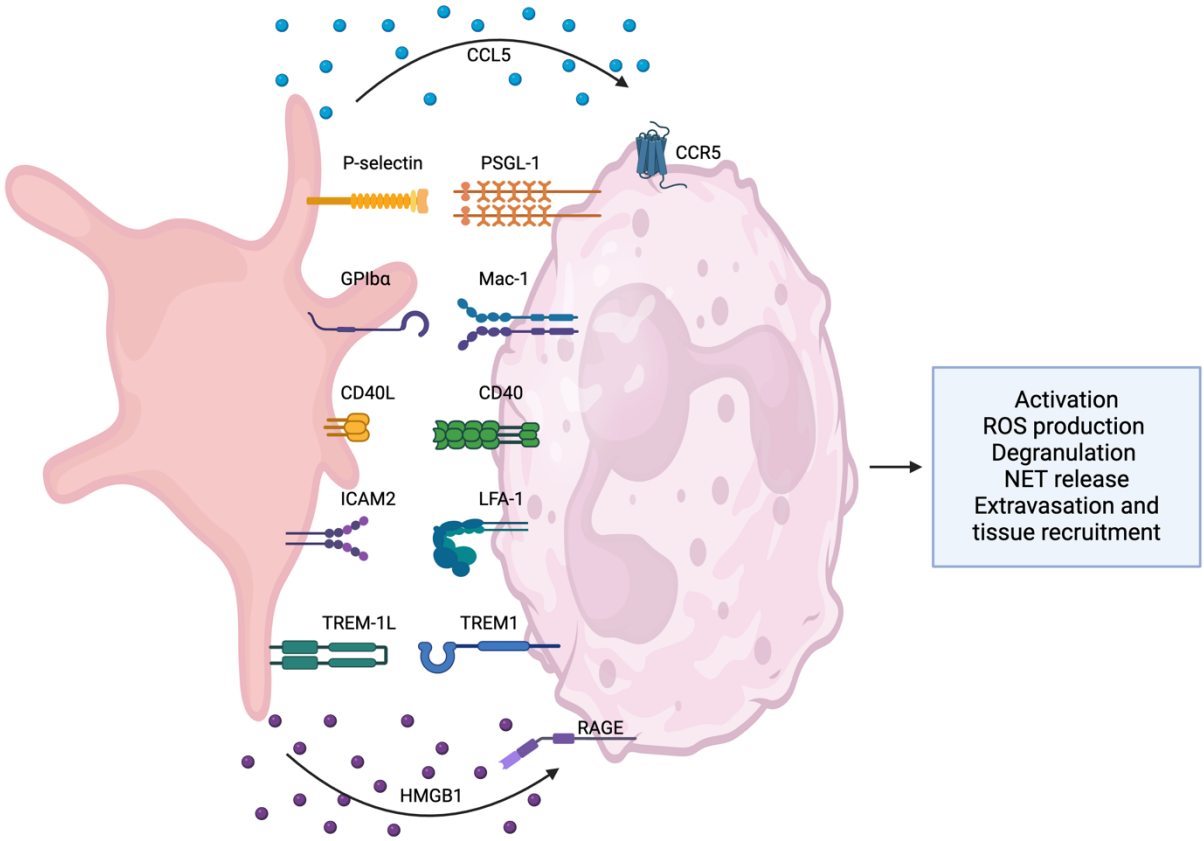



**Figure 8.2 – Neutrophil platelet interactions.** Summary of direct and indirect neutrophil platelet interactions and effect on neutrophils. Created with https://BioRender.com.

### 8.1.4. Neutrophil heterogeneity across biological compartments

I found that in both humans and mice neutrophils from different biological compartments had unique phenotypes (figure 4.16 and figure 5.18). This is in line with previous work which has shown that neutrophil phenotype is determined by tissue of residence as well as maturation and local inflammatory signals.[88,100] I found that neutrophils from the tumour and liver had an activated, degranulated and aged phenotype as demonstrated by their high expression of CD11b, CD10, CD66b and CXCR4 and low expression of CXCR2 and CD62L (figure 4.16 and figure 5.18). Tumour and liver neutrophils also tended to have a higher expression of PDL1. There were also differences in neutrophil function between the biological compartments (figure 5.19). Tumour neutrophils had both a high basal and stimulated ROS. This suggests that the activated, degranulated and aged neutrophils found in tumours maybe highly immunosuppressive due to their high PDL1 expression and high ROS production, as both are known mechanisms of T cell suppression within the tumour microenvironment.[114,250] In future I would like to confirm this by carrying out T cell

suppression assays on neutrophils isolated from these different biological compartments.

One limitation of my comparison of neutrophils between the different biological compartments is the different isolation methods used. Neutrophils isolated from tumour and liver where exposed to a combination of enzymatic and mechanical digestion at 37°C, whereas neutrophils isolated from bone marrow, blood or spleen were not. These are factors that could have artificially activated neutrophils during the isolation protocol. An alternative would be to phenotype the tissue neutrophils in situ using multiplex imaging technologies.[439,440]

### 8.2. Experimental neutrophil therapeutics

From my patient and pre-clinical studies, I observed that a circulating LD population of neutrophils with an activated, aged and degranulated phenotype was expanded in HCC and CLD. Furthermore, I noted that tumour and liver isolated neutrophils also had this activated, aged and degranulated phenotype. Therefore, this highlighted LD neutrophils as well as activated or aged neutrophils as possible therapeutic targets. I targeted neutrophil activation and LD neutrophils with ALK5 inhibition. ALK5 is the receptor for TGFβ, a known inducer of LD neutrophils.[118] I targeted neutrophil recruitment with anti-S100A8/A9 antibodies.[315] S100A8/A9 are also known activators of neutrophils making it a therapeutic target of interest for me.[314] I also targeted neutrophil activation with AZD1480, a JAK2 inhibitor. The JAK2-STAT3 signalling pathway is downstream to both IL-6 and CXCR2,[209,375] and has been shown to be central to neutrophil recruitment and activation to pro-tumour phenotypes.[209,230,231] Furthermore CXCR2 is central to both neutrophil recruitment and ageing, making the JAK2-STAT3 pathway a very attractive therapeutic target in neutrophils.[61,183]

#### 8.2.1. ALK5 inhibition

ALK5 inhibition with AZ12601011 successfully reduced the frequency of circulating LD neutrophils in lean and MASH HCC-bearing mice (figure 6.8 and figure 6.9). In lean HCC-bearing mice ALK5 inhibition induced an increase in tumour neutrophils with an altered phenotype, having increased CD62L expression (figure 6.8). This may indicate a less aged and degranulated phenotype. In MASH HCC-bearing mice however there

was no effect on tumour neutrophils (figure 6.9). In both lean and MASH HCC-bearing mice there was no significant effect of ALK5 inhibition on tumour burden (figure 6.8 and figure 6.9).

TGFβ inhibition has previously been shown to reduce the frequency of LD neutrophils both in vitro and in vivo.[118] Therefore my data supports TGFβ as being an important driver of LD neutrophils. The site at which LD neutrophils develop remains unclear and in future I plan to do density separation and phenotyping on the bone marrow with and without ALK5 inhibition/TGFβ stimulation to ascertain if LD neutrophils are present in the bone marrow. TGFβ inhibition has been shown to increase the number of tumour associated neutrophils, in line with my data in lean HCC bearing mice.[108] A previous study found a reduction in tumour burden in tumour bearing mice treated with SM16, an ALK5/ALK4 inhibitor.[108] This study was different to mine as it used subcutaneously implanted mouse lung cancer cell lines as well as a different ALK5 inhibitor. My study used intrahepatic tumours which have a different microenvironment and response to systemic therapies (as discussed in section 8.3). It is interesting that although ALK5 inhibition has the same systemic effects in lean and MASH mice of reducing circulating LD neutrophils, it had different intratumor effects. This suggests that there are unique features of the MASH intrahepatic tumour microenvironment which may influence responses to systemic therapies. The fact that ALK5 inhibition reduced LD neutrophil frequency but not tumour burden, suggests that LD neutrophils may not be crucial in tumour progression and brings into question their relevance. Likewise, the fact that there was a treatment associated influx of tumour associated neutrophils in lean mice, which has previously been shown to be the mechanism of efficacy in subcutaneous tumours,[108] suggests there is something inherently different about intrahepatic tumours. Changing neutrophil frequency or phenotype in intrahepatic tumours may not be enough to elicit changes in tumour burden and there may be other more important targets.

Of note, the ALK5 inhibitor I used was not specific to neutrophils. Also, TGFβ has important direct effects on HCC tumour cells. In early disease TGFβ can act as a tumour suppressor but in late stage disease contributes to disease progression partly by promoting Epithelial-Mesenchymal Transition (EMT).[441-443] Additionally TGFβ signalling also promotes the immunosuppressive and pro-tumour functions of other

cell types in the tumour microenvironment such as HSCs, CAFs, macrophages, CD8 T cells, CD4 T cells, NK cells and DCs.[442] Indeed high TGFβ expression is a key feature of immune exhausted HCCs which have a poor response to immune checkpoint inhibition.[27] In vitro culture experiments would be a way of investigating the direct effects of ALK5 inhibition on the Hep 53.4 cell line. In the future I would also repeat the in vivo ALK5 inhibition experiment using higher drug doses to investigate whether an anti-tumour effect can be obtained, although this would increase the non-neutrophil specific effects. Ways to investigate the neutrophil specific effects of TGFβ inhibition could include conducting a neutrophil transfer experiment of ALK5 inhibited or knockout neutrophils into HCC bearing mice or using a neutrophil specific conditional genetic knockout model.

### 8.2.2. S100A8/9 inhibition

The S100A8/9 antibodies failed to reduced tumour burden in lean HCC bearing mice (figure 6.7). Anti-S100A8/9 treatment significantly reduced the frequency of total circulating neutrophils and caused a non-statistically significant reduction in tumour neutrophils (figure 6.7). Interestingly anti-S100A8/9 treatment caused a reduction in tumour CD8 T cell frequency. Perhaps critically, there were no significant changes in neutrophil phenotype.

A previous study used a genetic S100A9 knockout in the DEN model of HCC to show that S100A9 knockout protected from DEN induced HCC and was associated with reduced liver neutrophil recruitment.[23] My findings are similar in that there was a trend towards a reduction in tumour neutrophils indicating some disruption of neutrophil recruitment, however I failed to show a reduction in tumour burden. My study was trying to treat already established tumours whereas the previous study was looking at prevention of HCC development following DEN injury. Therefore, disrupting neutrophil recruitment and activation through S100A8/9 may be effective at preventing hepatocarcinogenesis or treating early stage HCCs rather than treating late-stage disease. The finding of anti-S100A8/9 treatment causing a reduction in circulating neutrophil frequency is in keeping with other studies demonstrating that S100A8/9 is a mediator of bone marrow neutrophil release.[315] The reason anti-S100A8/9 caused a reduction in tumour CD8 T cell frequency is not understood, however I speculate it may be due to a reduction of innate immune cell recruitment and subsequent

generation of T cell chemokines. Another reason for the poor therapeutic effect in vivo could be the use of a rabbit IgG antibody. Over the 2 week experiment an anti-rabbit IgG immune response could have developed in the mice leading to inhibition and clearance of the S100A8/9 antibodies.

Although I demonstrated some effects on neutrophils, I did not demonstrate an effect on tumour burden. In future I would like to repeat the in vivo anti-S100A8/9 study with increasing doses and with a rat antibody. Then if an anti-tumour effect is found, conduct separate anti-S100A8 and anti-S100A9 treatment arms to further interrogate mechanisms. It would also be useful to confirm the inhibition of S100A8/9 by conducting in vitro neutrophil migration and activation studies with S100A8/9 proteins. In future studies I would also look at granulopoiesis and ND/LD circulating neutrophils.

### 8.2.3. JAK2-STAT3 inhibition

Neutrophils had the highest expression of p-STAT3 compared to other immune cells as well as compared to the Hep 53.4 HCC cell line (figure 6.2). Within neutrophil populations p-STAT3 expression correlated with activation. Tumour neutrophils expressed the highest p-STAT3 in both HCC patients and HCC bearing mice (figure 6.2). This identified the JAK2-STAT3 pathway as being an important neutrophil therapeutic target as it may alter neutrophil activation and pro-tumour polarisation. Treatment of neutrophils ex vivo with the JAK2 inhibitor AZD1480 (leading to inhibition of JAK/STAT signalling) led to a reduction in neutrophil ageing and degranulation as demonstrated by reduced CXCR4 and increased CD62L expression (figure 6.3). In vivo AZD1480 treatment significantly reduced tumour burden in both lean and MASH HCC bearing mice and was again associated with a reduction in neutrophil ageing and degranulation as well as an increase in tumour neutrophil frequency (figure 6.5 and 6.6). There was no change in neutrophil PDL1 expression and no changes in granulopoiesis.

There are no other studies comparing STAT3 activity between immune cells and cancer cells. One study has reported increased p-STAT3 expression in primed versus naïve neutrophils in the context of fungal infection.[444] The effects of JAK and STAT3 inhibition on neutrophils are better described. JAK inhibitors have been described as reducing neutrophil activation as well as subsequent IL-8, MMP-9 and ROS

release.[445,446] STAT3 inhibition is reported to impair neutrophil mobilisation from the bone marrow as well as reduce CXCR2 mediated chemotaxis.[376,447] I am the first to demonstrate effects on neutrophil ageing and degranulation with JAK2 inhibition. In terms of the anti-tumour effects of JAK2 inhibition a previous study, similar to mine, showed that JAK2 inhibition can reduce the viability and invasive capacity of HCC cells lines in vitro.[448] Results are similar to in vitro studies using STAT3 inhibitors.[449] Similarly in vivo studies using subcutaneous xenograft models of HCC have demonstrated reduced tumour burden with both JAK2 and STAT3 inhibitors.[449-452] I am the first to investigate the effects of JAK2 inhibition on neutrophils as well as tumour growth in vivo using an orthotopic model. This more closely replicates the immune microenvironment of HCC on the background of chronic liver disease compared to subcutaneous xenograft models.

It should be pointed out that AZD1480 is a general JAK2 inhibitor and not specific to neutrophils. JAK-STAT3 signalling directly promotes HCC tumour cell growth, invasiveness and metastasis as well as having immunosuppressive effects on other immune cell in the HCC microenvironment including DCs and CD8 T cells.[453,454] Therefore the mechanism underlying the anti-tumour effect I observed is likely due to a combination effect on various cell types. This is not necessarily a limitation for the development of clinical therapies, as more broad activity may improve efficacy.

Of note, although I observed similar alterations of neutrophil phenotype in vivo as I had in vitro (figure 6.3 and figure 6.5), these were not consistent between the lean and MASH HCC bearing mice. This could be due to several reasons; 1. The difference in microenvironment and therapy response (as discussed in 8.3). 2. The effect of neutrophil tissue isolation and further alteration of phenotype. 3. Difference in drug concentration in vitro versus in tissue. A way to truly test the effect of JAK2-STAT3 inhibition in neutrophils would be to use a neutrophil specific conditional knockout model. An alternative would be to do an experiment in which neutrophils are isolated from a matched control, treated in vitro with AZD1480, then transfused into an HCC bearing mouse to assess for the specific effect of JAK2 inhibition in neutrophils. This has previously been done with LPS treated neutrophils.[56]

I demonstrated that AZD1480 had some direct anti-proliferative and cytotoxic effects on the Hep 53.4 cell line in vitro (figure 6.4). The 5 μM dose, which induced significant changes in neutrophil phenotype in vitro (figure 6.3), had only a very minor effect on Hep 53.4 cell growth at the late time point. Higher concentrations did have both cytostatic and cytotoxic activity. Interestingly when I measured p-STAT3 activity in Hep 53.4 cells using flow cytometry there was a trend to increased expression of p-STAT3 with AZD1480. I cannot fully explain this observation but I speculate that it may be due to compensatory upregulation of alternative pathways such as JAK1-STAT3.[374] A further way of investigating this would be to confirm expression of the different JAK and STAT proteins using a western blot or proteomics. Additionally, I could analyse downstream transcriptome changes using reverse transcription polymerase chain reaction (RT-PCR).

Another interesting finding was that AZD1480 increased the frequency of intra-tumour neutrophils (figure 6.6). A similar effect has been observed with CXCR2 inhibition and was linked to an expansion of immature neutrophils within the tumour.[56] As JAK2-STAT3 is one of the downstream pathways of CXCR2 this maybe a conserved effect. This may identify JAK2-STAT3 signalling as the intracellular mechanism underlying this response, and is supported by the fact that STAT3 is also a regulator of emergency granulopoiesis.[376] I could confirm this in my study by doing laser capture RNA sequencing on my embedded samples.

A major limitation of AZD1480 was that I observed significant drug associated toxicities. A significant number of AZD1480 treated mice developed urinary retention resulting in them having to be culled before the study end date. This would explain why AZD1480 treated mice had a greater body weight compared to vehicle controls (figure 6.6). As far as I am aware this toxicity has not previously been described with AZD1480 or JAK inhibitors in general. One reason for this maybe because I used a research grade drug which could have contained impurities. In future I could try using a clinical grade drug or other JAK2/STAT3 inhibitors which hopefully will have less toxicities. A further limitation of targeting the JAK-STAT3 pathway in HCC is that all the clinical trials targeting this pathway have failed to show significant efficacy.[453] A future focus could be combining JAK-STAT3 inhibition with immune checkpoint blockade. The rationale behind this approach being JAK-STAT3 would help block the

immunosuppressive elements of the HCC microenvironment hopefully improving the efficacy of immune checkpoint inhibitors. A major limitation to my work is that for each drug therapy I only used one dose so am unable to demonstrate dose responses. A way to do this in future would be to use an ex vivo tumour/liver slice model. This would allow the investigation of multiple drug doses per biological replicate.

### 8.3. The hepatic microenvironment of MASH makes HCC resistant to immune checkpoint inhibition

I found that MASH intrahepatic tumour bearing mice had a poor response to combination anti-PDL1/anti-VEGF treatment compared to lean mice (figure 7.1). On the other hand, MASH subcutaneous tumour bearing mice had a good response to anti-PDL1/anti-VEGF treatment, with a similar treatment response to lean mice (figure 7.5). This suggests that the aetiology of background liver disease is an important determinant of immune checkpoint inhibitor response, and that anti-PDL1/anti-VEGF treatment may have a poorer efficacy in MASH-HCC. This also suggests that anti-PDL1/anti-VEGF treatment resistance in MASH is driven by the hepatic microenvironment of MASH rather than the systemic environment of MASH. Further analysis showed that anti-PDL1/anti-VEGF treatment induced an expansion of CD8 T cells in the intrahepatic tumours of both MASH and lean mice (figure 7.2), however in MASH mice there was a preferential expansion of $PD1^{+}EOMES+CXCR6^{+}$ CD8 T cells (figure 7.3). These $PD1^{+}EOMES^{+}CXCR6^{+}$ CD8 T cells have previously been shown to have an exhausted and auto-aggressive phenotype and were present almost exclusively in the livers of MASH mice without HCC, but not in the livers of lean mice (figure 7.4). In subcutaneous tumours there was again an expansion of CD8 T cells in both MASH and lean mice in response to treatment (figure 7.6), but without a preferential increase in $PD1^{+}$ CD8 T cells in MASH mice (figure 7.7). Therefore, it is likely the presence and/or expansion of $PD1^{+}EOMES^{+}CXCR6^{+}$ CD8 T cells which are almost exclusively found in the MASH liver, which contributes to poorer immune checkpoint inhibitor responses in MASH/MASLD HCC models.

My data is in line with other pre-clinical studies demonstrating poor response to anti-PD1 monotherapy in MASH-HCC models.[47,55,56] Given that anti-PDL1/anti-VEGF combination therapy is now the first line systemic therapy for HCC,[34] the clinical relevance of these studies is limited. I am the first to study therapy response to anti-

PDL1/anti-VEGF. Preliminary clinical data from both clinical trials and real world experience suggests that anti-PDL1/anti-VEGF therapy may be less effective in HCC on the background of MASLD/MASH compared to other aetiologies.[47,49] These studies however need to be interpreted with caution given their post hoc nature and small sample sizes. Further larger prospective studies are still awaited. Another study has reported resistance to anti-PD1 monotherapy in intrahepatic MASH tumours but not in subcutaneous tumours.[55] This again confirms the importance of the unique hepatic microenvironment of MASH rather than the systemic environment.

Previous work has described the role of $PD1^{+}EOMES^{+}CXCR6^{+}$ CD8 T cells in MASH. In the MASH liver they have a tissue resident ($CXCR6^{+}$), effector (Granzyme $B^{+}$) and exhausted ($EOMES^{+}$ and $PD1^{+}$) phenotype.[47,51] They are thought to be induced through metabolic stimuli such as acetate and extracellular ATP. Functionally they have been shown to be both exhausted and auto-aggressive and promote the development of HCC in MASH. Given that they are exhausted it is understandable that they do not respond to anti-PD1/PDL1 treatment. Interestingly another pre-clinical study of MASH-HCC immune checkpoint inhibitor responses found similar proportions of $PD1^{+}CXCR6^{+}GrmzB^{+}$ CD8 T cells in MASH and lean intrahepatic tumours despite a showing a difference in anti-PD1 treatment response.[55] Instead the authors found functional differences in CD8 T cells with those in MASH displaying impaired motility and altered metabolism. This study however, unlike mine, did not look at EOMES expression. Reductions in CD4 T cells in MASH have been described by others, although I did not see this.[52,53]

A limitation of my work is that I have not definitively proved the absence of $PD1^{+}EOMES^{+}CXCR6^{+}$ CD8 T cells within the subcutaneous tumours of MASH mice. This was due to the small subcutaneous tumour size and subsequent small leukocyte isolation yield, meaning that I could not apply both my general and T cell flow cytometry panels. A future aspect of my work will be proving this by repeating the experiment, as well as applying multiplex imaging techniques to my paraffin embedded samples. The previous study which examined both intrahepatic and subcutaneous HCC tumours in MASH found CD8 T cells in MASH subcutaneous tumours had reduced motility compared to those of lean mice, however the motility was not as impaired as those found in the MASH intrahepatic tumours.[55] This suggests

there may be some systemic CD8 T cells changes in MASH extrahepatic tumours, although not to the degree found in the MASH liver. Given that these $PD1^{+}EOMES^{+}CXCR6^{+}$ CD8 T cells have a tissue resident phenotype and are activated in an MHC independent manner,[51] it would also be worthwhile phenotyping innate lymphoid cells in this model.

There are also limitations to the pre-clinical model I used. The background livers have a high degree of steatosis and inflammation but very little fibrosis (figure 5.1 and 5.3). Therefore, this models MASH without significant fibrosis/cirrhosis which only accounts for around a quarter of MASLD-HCC cases.[455,456] In addition, the orthotopic tumour models give rise to rapidly growing, aggressive tumours which are only in vivo for 4-6 weeks. Therefore, immune changes related to the chronicity of in situ hepatocarcinogenesis and slowly progressive tumours may be lost. Future elements of my work would be to repeat my experiments in an additional model of MASH-HCC. I could use a longer model with in-situ hepatocarcinogenesis such as the DEN/ American lifestyle-induced obesity syndrome (ALIOS) model or a spontaneous dietary model.[47,56] These however have their own limitations. The DEN/ALIOS model relies on DEN induced carcinogenesis for which the mutational landscape poorly resembles that of human HCCs.[355] Spontaneous dietary models, although they most closely resemble the natural history of human HCCs, are expensive, time consuming and have a highly variable clinical phenotype meaning complex imaging modalities are required to monitor for tumour development.[457]

Another limitation to my work is that I did not have anti-PDL1 and anti-VEGF monotherapy groups. Therefore, I cannot determine whether the immunological effects observed where specifically due to the anti-PDL1 or anti-VEGF therapy or a combination. I would like to repeat this work including these groups to allow me to determine the effect of each monotherapy, but I suspect the increase in tumour CD8 T cells seen is due to anti-PDL1, given that anti-PD1 does the same.[55] I would like to translate these findings into patients by conducting multiplex imaging on biopsy samples of patients undergoing treatment with atezolizumab/bevacizumab. This would allow me to identify $PD1^{+}EOMES^{+}CXCR6^{+}$ CD8 T cells in tumours and livers and investigate whether they are more frequent in MASLD and whether their frequency correlates with treatment response.

A major question raised by my work is can these MASH related PD1$^{+}$EOMES$^{+}$CXCR6$^{+}$ CD8 T cells be therapeutically targeted? Further, what effect will this have on anti-PDL1/anti-VEGF treatment response? To directly target this population, I could use a CXCR6 antibody, although this would not be CD8 T cell specific. To target the metabolic environment, I could use drugs such as metformin or glucagon-like peptide 1 (GLP-1) analogues. A previous study has already investigated the use of metformin and found that metformin metabolically reprogrammed CD8 T cells in MASH, restoring their impaired motility and sensitised intrahepatic MASH tumours to anti-PD1 monotherapy.[55] Semaglutide a GLP-1 analogue has entered clinical trials in MASLD with evidence showing its use can cause MASH resolution.[458] In pre-clinical studies semaglutide has a rapid effect on reducing body weight within 2 weeks of treatment initiation.[459] In future it would be interesting to test whether semaglutide can sensitise intrahepatic tumours to anti-PDL1/anti-VEGF in my model. The acuity of the model may prevent it from being effective, however given that semaglutide has rapid effects on body weight, it may also have rapid effects of hepatic steatosis and hence may be able to address the metabolic factors that are driving immune checkpoint inhibitor resistance in MASH. Indeed, semaglutide on its own has been shown to reduce HCC burden in a spontaneous dietary model of MASH-HCC.[460]

### 8.4. Conclusion

Neutrophils are highly heterogeneous, displaying a diverse range of phenotypes and functions depending on their maturity, age, tissue of residence and local inflammatory signals. In the context of both CLD and HCC there is an increase in circulating LD neutrophils with an activated, degranulated and aged phenotype. The origin of these LD neutrophils remains unclear, however TGFβ, activation and ageing are likely key processes underpinning their development. Tumour neutrophils are similar in that they also have an activated, aged and degranulated phenotype, highly express PDL1 and have high ROS production, implying an immunosuppressive nature. Targeting these neutrophil processes with JAK2-STAT3 inhibition results in both an alteration of neutrophil phenotype as well as reduced tumour burden in a pre-clinical model of MASLD-HCC and opens up JAK2-STAT3 inhibition as a potential neutrophil therapy in HCC. MASLD is becoming the most common aetiology of HCC, however, there is growing evidence to suggest that anti-PDL1/anti-VEGF combination therapy is less

effective in MASLD-HCC compared to other aetiologies. The unique intrahepatic microenvironment of MASLD is likely a driving factor in immune checkpoint inhibitor resistance, due to a population of $PD1^{+}EOMES^{+}CXCR6^{+}$ CD8 T cells which arise in the precancerous MASLD liver and have an exhausted and auto-aggressive phenotype. Therefore, improvements in systemic therapy for MASLD-HCC maybe achieved by targeting this CD8 T cell population or the underlying metabolic drivers in conjunction with immune checkpoint blockade. In summary I have identified both neutrophils and $PD1^{+}EOMES^{+}CXCR6^{+}$ CD8 T cells as important determinants of disease progression and response to systemic therapy in MASLD-HCC models and I propose future research should be aimed at targeting these populations and determining their relevance in human disease.

# 9. Bibliography


1 Sung, H. *et al.* Global Cancer Statistics 2020: GLOBOCAN Estimates of Incidence and Mortality Worldwide for 36 Cancers in 185 Countries. *CA Cancer J Clin* **71**, 209-249, doi:10.3322/caac.21660 (2021).

2 Feng, M., Pan, Y., Kong, R. & Shu, S. Therapy of Primary Liver Cancer. *Innovation (Camb)* **1**, 100032, doi:10.1016/j.xinn.2020.100032 (2020).

3 Gigante, E. *et al.* New insights into the pathophysiology and clinical care of rare primary liver cancers. *JHEP Reports* **3**, 100174, doi:10.1016/j.jhepr.2020.100174 (2021).

4 Lim, I., Bondoc, A., Geller, J. & Tiao, G. Hepatoblastoma—The Evolution of Biology, Surgery, and Transplantation. *Children* **6**, 1, doi:10.3390/children6010001 (2018).

5 Yang, D. *et al.* Impact of sex on the survival of patients with hepatocellular carcinoma: a Surveillance, Epidemiology, and End Results analysis. *Cancer* **120**, 3707-3716, doi:10.1002/cncr.28912 (2014).

6 Anstee, Q. M., Reeves, H. L., Kotsiliti, E., Govaere, O. & Heikenwalder, M. From NASH to HCC: current concepts and future challenges. *Nat Rev Gastroenterol Hepatol* **16**, 411-428, doi:10.1038/s41575-019-0145-7 (2019).

7 Llovet, J. M. *et al.* Hepatocellular carcinoma. *Nat Rev Dis Primers***7**, doi:10.1038/s41572-020-00240-3 (2021).

8 Rahib, L. *et al.* Projecting cancer incidence and deaths to 2030: the unexpected burden of thyroid, liver, and pancreas cancers in the United States. *Cancer Res* **74**, 2913-2921, doi:10.1158/0008-5472.Can-14-0155 (2014).

9 World Health Organisation. Cancer Factsheets*. Cancer Today.* https://gco.iarc.fr/today/en (2024)

10 Pellicoro, A., Ramachandran, P., Iredale, J. P. & Fallowfield, J. A. Liver fibrosis and repair: immune regulation of wound healing in a solid organ. *Nat Rev Immunol* **14**, 181-194, doi:10.1038/nri3623 (2014).

11 Nusrat, S., Khan, M. S., Fazili, J. & Madhoun, M. F. Cirrhosis and its complications: evidence based treatment. *World J Gastroenterol* **20**, 5442-5460, doi:10.3748/wjg.v20.i18.5442 (2014).

12 Ginès, P. *et al.* Liver cirrhosis. *Lancet* **398**, 1359-1376, doi:10.1016/s0140-6736(21)01374-x (2021).

13 Cheemerla, S. & Balakrishnan, M. Global Epidemiology of Chronic Liver Disease. *Clin Liver Dis (Hoboken)* **17**, 365-370, doi:10.1002/cld.1061 (2021).

14 Dyson, J. *et al.* Hepatocellular cancer: the impact of obesity, type 2 diabetes and a multidisciplinary team. *J Hepatol* **60**, 110-117, doi:10.1016/j.jhep.2013.08.011 (2014).

15 Rinella, M. E. *et al.* A multisociety Delphi consensus statement on new fatty liver disease nomenclature. *Hepatology* **78**, 1966-1986, doi:10.1097/hep.0000000000000520 (2023).

16 Kumar, R., Priyadarshi, R. N. & Anand, U. Non-alcoholic Fatty Liver Disease: Growing Burden, Adverse Outcomes and Associations. *J Clin Transl Hepatol* **8**, 76-86, doi:10.14218/jcth.2019.00051 (2020).

17 Williams, R. *et al.* Addressing liver disease in the UK: a blueprint for attaining excellence in health care and reducing premature mortality from lifestyle issues of

excess consumption of alcohol, obesity, and viral hepatitis. *Lancet* **384**, 1953-1997, doi:10.1016/s0140-6736(14)61838-9 (2014).
18 Bedossa, P. & Poynard, T. An algorithm for the grading of activity in chronic hepatitis C. The METAVIR Cooperative Study Group. *Hepatology* **24**, 289-293, doi:10.1002/hep.510240201 (1996).
19 Kisseleva, T. & Brenner, D. Molecular and cellular mechanisms of liver fibrosis and its regression. *Nat Rev Gastroenterol Hepatol* **18**, 151-166, doi:10.1038/s41575-020-00372-7 (2021).
20 Llovet, J. M. *et al.* Hepatocellular carcinoma. *Nat Rev Dis Primers* **2**, 16018, doi:10.1038/nrdp.2016.18 (2016).
21 Ringelhan, M., Pfister, D., O'Connor, T., Pikarsky, E. & Heikenwalder, M. The immunology of hepatocellular carcinoma. *Nat Immunol* **19**, 222-232, doi:10.1038/s41590-018-0044-z (2018).
22 Lagnado, A. *et al.* Neutrophils induce paracrine telomere dysfunction and senescence in ROS-dependent manner. *EMBO J* **40**, e106048, doi:10.15252/embj.2020106048 (2021).
23 Wilson, C. L. *et al.* NFκB1 is a suppressor of neutrophil-driven hepatocellular carcinoma. *Nat Commun* **6**, 6818, doi:10.1038/ncomms7818 (2015).
24 Wang, J., Chenivesse, X., Henglein, B. & Bréchot, C. Hepatitis B virus integration in a cyclin A gene in a hepatocellular carcinoma. *Nature* **343**, 555-557, doi:10.1038/343555a0 (1990).
25 Hsu, I. C. *et al.* Mutational hotspot in the p53 gene in human hepatocellular carcinomas. *Nature* **350**, 427-428, doi:10.1038/350427a0 (1991).
26 Montironi, C. *et al.* Inflamed and non-inflamed classes of HCC: a revised immunogenomic classification. *Gut* **72**, doi:10.1136/gutjnl-2021-325918 (2022).
27 Sia, D. *et al.* Identification of an Immune-specific Class of Hepatocellular Carcinoma, Based on Molecular Features. *Gastroenterology* **153**, 812-826, doi:10.1053/j.gastro.2017.06.007 (2017).
28 EASL Clinical Practice Guidelines: Management of hepatocellular carcinoma. *J Hepatol* **69**, 182-236, doi:10.1016/j.jhep.2018.03.019 (2018).
29 Heimbach, J. K. *et al.* AASLD guidelines for the treatment of hepatocellular carcinoma. *Hepatology* **67**, 358-380, doi:10.1002/hep.29086 (2018).
30 Omata, M. *et al.* Asia-Pacific clinical practice guidelines on the management of hepatocellular carcinoma: a 2017 update. *Hepatol Int* **11**, 317-370, doi:10.1007/s12072-017-9799-9 (2017).
31 Vogel, A. *et al.* Hepatocellular carcinoma: ESMO Clinical Practice Guidelines for diagnosis, treatment and follow-up. *Ann Oncol* **30**, 871-873, doi:10.1093/annonc/mdy510 (2019).
32 Geh, D., Rana, F. A. & Reeves, H. L. Weighing the benefits of hepatocellular carcinoma surveillance against potential harms. *J Hepatocell Carcinoma* **6**, 23-30, doi:10.2147/jhc.S159581 (2019).
33 Reig, M. *et al.* BCLC strategy for prognosis prediction and treatment recommendation: The 2022 update. *J Hepatol* **76**, 681-693, doi:10.1016/j.jhep.2021.11.018 (2022).
34 Suddle, A. *et al.* British Society of Gastroenterology guidelines for the management of hepatocellular carcinoma in adults. *Gut* **73**, doi:10.1136/gutjnl-2023-331695 (2024).

35 da Fonseca, L. G. *et al.* Safety and efficacy of cytotoxic chemotherapy in hepatocellular carcinoma after first-line treatment with sorafenib. *BMC Cancer* **18**, 1250, doi:10.1186/s12885-018-5173-0 (2018).
36 Llovet, J. M. *et al.* Sorafenib in advanced hepatocellular carcinoma. *N Engl J Med* **359**, 378-390, doi:10.1056/NEJMoa0708857 (2008).
37 Kudo, M. *et al.* Lenvatinib versus sorafenib in first-line treatment of patients with unresectable hepatocellular carcinoma: a randomised phase 3 non-inferiority trial. *Lancet* **391**, 1163-1173, doi:10.1016/s0140-6736(18)30207-1 (2018).
38 Abou-Alfa, G. K. *et al.* Cabozantinib in Patients with Advanced and Progressing Hepatocellular Carcinoma. *N Engl J Med* **379**, 54-63, doi:10.1056/nejmoa1717002 (2018).
39 Bruix, J. *et al.* Regorafenib for patients with hepatocellular carcinoma who progressed on sorafenib treatment (RESORCE): a randomised, double-blind, placebo-controlled, phase 3 trial. *Lancet* **389**, 56-66, doi:10.1016/s0140-6736(16)32453-9 (2017).
40 Zhu, A. X. *et al.* Ramucirumab after sorafenib in patients with advanced hepatocellular carcinoma and increased α-fetoprotein concentrations (REACH-2): a randomised, double-blind, placebo-controlled, phase 3 trial. *Lancet Oncol* **20**, 282-296, doi:10.1016/s1470-2045(18)30937-9 (2019).
41 Finn, R. S. *et al.* Atezolizumab plus Bevacizumab in Unresectable Hepatocellular Carcinoma. *N Engl J Med* **382**, 1894-1905, doi:10.1056/NEJMoa1915745 (2020).
42 El-Khoueiry, A. B. *et al.* Nivolumab in patients with advanced hepatocellular carcinoma (CheckMate 040): an open-label, non-comparative, phase 1/2 dose escalation and expansion trial. *Lancet* **389**, 2492-2502, doi:10.1016/s0140-6736(17)31046-2 (2017).
43 Finn, R. S. *et al.* Pembrolizumab As Second-Line Therapy in Patients With Advanced Hepatocellular Carcinoma in KEYNOTE-240: A Randomized, Double-Blind, Phase III Trial. *J Clin Oncol* **38**, 193-202, doi:10.1200/jco.19.01307 (2020).
44 Cheng, A.-L. *et al.* Updated efficacy and safety data from IMbrave150: Atezolizumab plus bevacizumab vs. sorafenib for unresectable hepatocellular carcinoma. *J Hepatol* **76**, 862-873, doi:10.1016/j.jhep.2021.11.030 (2022).
45 Abou-Alfa, G. K. *et al.* Phase 3 randomized, open-label, multicenter study of tremelimumab (T) and durvalumab (D) as first-line therapy in patients (pts) with unresectable hepatocellular carcinoma (uHCC): HIMALAYA. *JCO* **40**, 379-379, doi:10.1200/JCO.2022.40.4_suppl.379 (2022).
46 Qin, S. *et al.* Atezolizumab plus bevacizumab versus active surveillance in patients with resected or ablated high-risk hepatocellular carcinoma (IMbrave050): a randomised, open-label, multicentre, phase 3 trial. *Lancet* **402**, 1835-1847, doi:10.1016/s0140-6736(23)01796-8 (2023).
47 Pfister, D. *et al.* NASH limits anti-tumour surveillance in immunotherapy-treated HCC. *Nature* **592**, 450-456, doi:10.1038/s41586-021-03362-0 (2021).
48 Pinter, M., Pinato, D. J., Ramadori, P. & Heikenwalder, M. NASH and Hepatocellular Carcinoma: Immunology and Immunotherapy. *Clin Cancer Res* **29**, 513-520, doi:10.1158/1078-0432.Ccr-21-1258 (2023).
49 Rimini, M. *et al.* Atezolizumab plus bevacizumab versus lenvatinib or sorafenib in non-viral unresectable hepatocellular carcinoma: an international propensity score

matching analysis. *ESMO Open* **7**, 100591, doi:10.1016/j.esmoop.2022.100591 (2022).
50 Wang, Z. *et al.* Paradoxical effects of obesity on T cell function during tumor progression and PD-1 checkpoint blockade. *Nat Med* **25**, 141-151, doi:10.1038/s41591-018-0221-5 (2019).
51 Dudek, M. *et al.* Auto-aggressive CXCR6(+) CD8 T cells cause liver immune pathology in NASH. *Nature* **592**, 444-449, doi:10.1038/s41586-021-03233-8 (2021).
52 Heinrich, B. *et al.* Steatohepatitis Impairs T-cell-Directed Immunotherapies Against Liver Tumors in Mice. *Gastroenterology* **160**, 331-345.e336, doi:10.1053/j.gastro.2020.09.031 (2021).
53 Ma, C. *et al.* NAFLD causes selective CD4(+) T lymphocyte loss and promotes hepatocarcinogenesis. *Nature* **531**, 253-257, doi:10.1038/nature16969 (2016).
54 McVey, J. C. *et al.* NAFLD indirectly impairs antigen-specific CD8(+) T cell immunity against liver cancer in mice. *iScience* **25**, 103847, doi:10.1016/j.isci.2022.103847 (2022).
55 Wabitsch, S. *et al.* Metformin treatment rescues CD8(+) T-cell response to immune checkpoint inhibitor therapy in mice with NAFLD. *J Hepatol* **77**, 748-760, doi:10.1016/j.jhep.2022.03.010 (2022).
56 Leslie, J. *et al.* CXCR2 inhibition enables NASH-HCC immunotherapy. *Gut* **71**, doi:10.1136/gutjnl-2021-326259 (2022).
57 Espinoza, M. *et al.* Disease Etiology and Outcomes After Atezolizumab Plus Bevacizumab in Hepatocellular Carcinoma: Post-Hoc Analysis of IMbrave150. *Gastroenterology* **165**, doi:10.1053/j.gastro.2023.02.042 (2023).
58 Borregaard, N. Neutrophils, from marrow to microbes. *Immunity* **33**, 657-670, doi:10.1016/j.immuni.2010.11.011 (2010).
59 Dancey, J. T., Deubelbeiss, K. A., Harker, L. A. & Finch, C. A. Neutrophil kinetics in man. *J Clin Invest* **58**, 705-715, doi:10.1172/jci108517 (1976).
60 von Vietinghoff, S. & Ley, K. Homeostatic regulation of blood neutrophil counts. *J Immunol* **181**, 5183-5188, doi:10.4049/jimmunol.181.8.5183 (2008).
61 Adrover, J. M. *et al.* A Neutrophil Timer Coordinates Immune Defense and Vascular Protection. *Immunity* **50**, 390-402.e310, doi:10.1016/j.immuni.2019.01.002 (2019).
62 Aroca-Crevillén, A., Adrover, J. M. & Hidalgo, A. Circadian Features of Neutrophil Biology. *Front Immunol* **11**, 576, doi:10.3389/fimmu.2020.00576 (2020).
63 Zhang, D. *et al.* Neutrophil ageing is regulated by the microbiome. *Nature* **525**, 528-532, doi:10.1038/nature15367 (2015).
64 Casanova-Acebes, M. *et al.* Rhythmic modulation of the hematopoietic niche through neutrophil clearance. *Cell* **153**, 1025-1035, doi:10.1016/j.cell.2013.04.040 (2013).
65 Kuhns, D. B., Long Priel, D. A. & Gallin, J. I. Loss of L-selectin (CD62L) on human neutrophils following exudation in vivo. *Cell Immunol* **164**, 306-310, doi:10.1006/cimm.1995.1174 (1995).
66 Jaiswal, S. *et al.* CD47 is upregulated on circulating hematopoietic stem cells and leukemia cells to avoid phagocytosis. *Cell* **138**, 271-285, doi:10.1016/j.cell.2009.05.046 (2009).
67 Rosales, C. Neutrophil: A Cell with Many Roles in Inflammation or Several Cell Types? *Front Physiol* **9**, 113, doi:10.3389/fphys.2018.00113 (2018).

68 Wigerblad, G. & Kaplan, M. J. Neutrophil extracellular traps in systemic autoimmune and autoinflammatory diseases. *Nat Rev Immunol* **23**, 1-15, doi:10.1038/s41577-022-00787-0 (2022).
69 Casanova-Acebes, M. *et al.* Neutrophils instruct homeostatic and pathological states in naive tissues. *J Exp Med* **215**, 2778-2795, doi:10.1084/jem.20181468 (2018).
70 Ella, K., Csépányi-Kömi, R. & Káldi, K. Circadian regulation of human peripheral neutrophils. *Brain Behav Immun* **57**, 209-221, doi:10.1016/j.bbi.2016.04.016 (2016).
71 Adrover, J. M. *et al.* Programmed 'disarming' of the neutrophil proteome reduces the magnitude of inflammation. *Nat Immunol* **21**, 135-144, doi:10.1038/s41590-019-0571-2 (2020).
72 Mittmann, L. A. *et al.* Uncoupled biological and chronological aging of neutrophils in cancer promotes tumor progression. *J Immunother Cancer* **9**, e003495, doi:10.1136/jitc-2021-003495 (2021).
73 Peng, Z. *et al.* Tumors exploit CXCR4hiCD62Llo aged neutrophils to facilitate metastatic spread. *OncoImmunology* **10**, 1870811, doi:10.1080/2162402x.2020.1870811 (2021).
74 Wang, Z. *et al.* CD62L(dim) Neutrophils Specifically Migrate to the Lung and Participate in the Formation of the Pre-Metastatic Niche of Breast Cancer. *Front Oncol* **10**, 540484, doi:10.3389/fonc.2020.540484 (2020).
75 Baragetti, A. *et al.* Neutrophil aging exacerbates high fat diet induced metabolic alterations. *Metabolism* **144**, 155576, doi:10.1016/j.metabol.2023.155576 (2023).
76 Mittmann, L. A. *et al.* Uncoupled biological and chronological aging of neutrophils in cancer promotes tumor progression. *J Immunother Cancer* **9**, doi:10.1136/jitc-2021-003495 (2021).
77 Yang, C. *et al.* Aged neutrophils form mitochondria-dependent vital NETs to promote breast cancer lung metastasis. *J Immunother Cancer* **9**, doi:10.1136/jitc-2021-002875 (2021).
78 Eash, K. J., Means, J. M., White, D. W. & Link, D. C. CXCR4 is a key regulator of neutrophil release from the bone marrow under basal and stress granulopoiesis conditions. *Blood* **113**, 4711-4719, doi:10.1182/blood-2008-09-177287 (2009).
79 Köhler, A. *et al.* G-CSF-mediated thrombopoietin release triggers neutrophil motility and mobilization from bone marrow via induction of Cxcr2 ligands. *Blood* **117**, 4349-4357, doi:10.1182/blood-2010-09-308387 (2011).
80 Petit, I. *et al.* G-CSF induces stem cell mobilization by decreasing bone marrow SDF-1 and up-regulating CXCR4. *Nat Immunol* **3**, 687-694, doi:10.1038/ni813 (2002).
81 Semerad, C. L. *et al.* G-CSF potently inhibits osteoblast activity and CXCL12 mRNA expression in the bone marrow. *Blood* **106**, 3020-3027, doi:10.1182/blood-2004-01-0272 (2005).
82 Summers, C. *et al.* Neutrophil kinetics in health and disease. *Trends Immunol* **31**, 318-324, doi:10.1016/j.it.2010.05.006 (2010).
83 Ley, K., Laudanna, C., Cybulsky, M. I. & Nourshargh, S. Getting to the site of inflammation: the leukocyte adhesion cascade updated. *Nat Rev Immunol* **7**, 678-689, doi:10.1038/nri2156 (2007).
84 Kolaczkowska, E. & Kubes, P. Neutrophil recruitment and function in health and inflammation. *Nat Rev Immunol* **13**, 159-175, doi:10.1038/nri3399 (2013).
85 Scheiermann, C., Kunisaki, Y. & Frenette, P. S. Circadian control of the immune system. *Nat Rev Immunol* **13**, 190-198, doi:10.1038/nri3386 (2013).

86 Scheiermann, C. *et al.* Adrenergic nerves govern circadian leukocyte recruitment to tissues. *Immunity* **37**, 290-301, doi:10.1016/j.immuni.2012.05.021 (2012).
87 Colotta, F., Re, F., Polentarutti, N., Sozzani, S. & Mantovani, A. Modulation of granulocyte survival and programmed cell death by cytokines and bacterial products. *Blood* **80**, 2012-2020 (1992).
88 Ballesteros, I. *et al.* Co-option of Neutrophil Fates by Tissue Environments. *Cell* **183**, doi:10.1016/j.cell.2020.10.003 (2020).
89 Martin, C. *et al.* Chemokines acting via CXCR2 and CXCR4 control the release of neutrophils from the bone marrow and their return following senescence. *Immunity* **19**, 583-593, doi:10.1016/s1074-7613(03)00263-2 (2003).
90 Li, Y. *et al.* The regulatory roles of neutrophils in adaptive immunity. *Cell Commun Signal* **17**, doi:10.1186/s12964-019-0471-y (2019).
91 Mayadas, T. N., Cullere, X. & Lowell, C. A. The multifaceted functions of neutrophils. *Annu Rev Pathol* **9**, 181-218, doi:10.1146/annurev-pathol-020712-164023 (2014).
92 Segal, A. W., Dorling, J. & Coade, S. Kinetics of fusion of the cytoplasmic granules with phagocytic vacuoles in human polymorphonuclear leukocytes. Biochemical and morphological studies. *J Cell Biol* **85**, 42-59, doi:10.1083/jcb.85.1.42 (1980).
93 Sheppard, F. R. *et al.* Structural organization of the neutrophil NADPH oxidase: phosphorylation and translocation during priming and activation. *J Leukoc Biol* **78**, 1025-1042, doi:10.1189/jlb.0804442 (2005).
94 Evans, T. J. *et al.* Cytokine-treated human neutrophils contain inducible nitric oxide synthase that produces nitration of ingested bacteria. *Proc Natl Acad Sci U S A* **93**, 9553-9558, doi:10.1073/pnas.93.18.9553 (1996).
95 Papayannopoulos, V. Neutrophil extracellular traps in immunity and disease. *Nat Rev Immunol* **18**, 134-147, doi:10.1038/nri.2017.105 (2018).
96 Clark, S. R. *et al.* Platelet TLR4 activates neutrophil extracellular traps to ensnare bacteria in septic blood. *Nat Med* **13**, 463-469, doi:10.1038/nm1565 (2007).
97 Kwok, I. *et al.* Combinatorial Single-Cell Analyses of Granulocyte-Monocyte Progenitor Heterogeneity Reveals an Early Uni-potent Neutrophil Progenitor. *Immunity* **53**, 303-318.e305, doi:10.1016/j.immuni.2020.06.005 (2020).
98 Muench, D. E. *et al.* Mouse models of neutropenia reveal progenitor-stage-specific defects. *Nature* **582**, 109-114, doi:10.1038/s41586-020-2227-7 (2020).
99 Xie, X. *et al.* Single-cell transcriptome profiling reveals neutrophil heterogeneity in homeostasis and infection. *Nat Immunol* **21**, 1119-1133, doi:10.1038/s41590-020-0736-z (2020).
100 Grieshaber-Bouyer, R. *et al.* The neutrotime transcriptional signature defines a single continuum of neutrophils across biological compartments. *Nat Commun* **12**, 2856, doi:10.1038/s41467-021-22973-9 (2021).
101 Chee, D. O., Townsend, C. M., Jr., Galbraith, M. A., Eilber, F. R. & Morton, D. L. Selective reduction of human tumor cell populations by human granulocytes in vitro. *Cancer Res* **38**, 4534-4539 (1978).
102 Shaul, M. E. & Fridlender, Z. G. Tumour-associated neutrophils in patients with cancer. *Nat Rev Clin Oncol* **16**, 601-620, doi:10.1038/s41571-019-0222-4 (2019).
103 Dvorak, A. M., Connell, A. B., Proppe, K. & Dvorak, H. F. Immunologic rejection of mammary adenocarcinoma (TA3-St) in C57BL/6 mice: participation of neutrophils and activated macrophages with fibrin formation. *J Immunol* **120**, 1240-1248 (1978).

104 Carvalho, L. O., Aquino, E. N., Neves, A. C. & Fontes, W. The Neutrophil Nucleus and Its Role in Neutrophilic Function. *J Cell Biochem* **116**, 1831-1836, doi:10.1002/jcb.25124 (2015).
105 Daley, J. M., Thomay, A. A., Connolly, M. D., Reichner, J. S. & Albina, J. E. Use of Ly6G-specific monoclonal antibody to deplete neutrophils in mice. *J Leukoc Biol* **83**, 64-70, doi:10.1189/jlb.0407247 (2008).
106 Dumitru, C. A., Moses, K., Trellakis, S., Lang, S. & Brandau, S. Neutrophils and granulocytic myeloid-derived suppressor cells: immunophenotyping, cell biology and clinical relevance in human oncology. *Cancer Immunol Immunother* **61**, 1155-1167, doi:10.1007/s00262-012-1294-5 (2012).
107 Mantovani, A., Marchesi, F., Malesci, A., Laghi, L. & Allavena, P. Tumour-associated macrophages as treatment targets in oncology. *Nat Rev Clin Oncol* **14**, 399-416, doi:10.1038/nrclinonc.2016.217 (2017).
108 Fridlender, Z. G. *et al.* Polarization of tumor-associated neutrophil phenotype by TGF-beta: "N1" versus "N2" TAN. *Cancer Cell* **16**, 183-194, doi:10.1016/j.ccr.2009.06.017 (2009).
109 Blattner, C. *et al.* CCR5(+) Myeloid-Derived Suppressor Cells Are Enriched and Activated in Melanoma Lesions. *Cancer Res* **78**, 157-167, doi:10.1158/0008-5472.Can-17-0348 (2018).
110 Dumitru, C. A., Fechner, M. K., Hoffmann, T. K., Lang, S. & Brandau, S. A novel p38-MAPK signaling axis modulates neutrophil biology in head and neck cancer. *J Leukoc Biol* **91**, 591-598, doi:10.1189/jlb.0411193 (2012).
111 Eruslanov, E. B. *et al.* Tumor-associated neutrophils stimulate T cell responses in early-stage human lung cancer. *J Clin Invest* **124**, 5466-5480, doi:10.1172/jci77053 (2014).
112 Fridlender, Z. G. *et al.* Transcriptomic analysis comparing tumor-associated neutrophils with granulocytic myeloid-derived suppressor cells and normal neutrophils. *PLoS One* **7**, e31524, doi:10.1371/journal.pone.0031524 (2012).
113 Haqqani, A. S., Sandhu, J. K. & Birnboim, H. C. Expression of interleukin-8 promotes neutrophil infiltration and genetic instability in mutatect tumors. *Neoplasia* **2**, 561-568, doi:10.1038/sj.neo.7900110 (2000).
114 He, G. *et al.* Peritumoural neutrophils negatively regulate adaptive immunity via the PD-L1/PD-1 signalling pathway in hepatocellular carcinoma. *J Exp Clin Cancer Res* **34**, 141, doi:10.1186/s13046-015-0256-0 (2015).
115 Kuang, D. M. *et al.* Peritumoral neutrophils link inflammatory response to disease progression by fostering angiogenesis in hepatocellular carcinoma. *J Hepatol* **54**, 948-955, doi:10.1016/j.jhep.2010.08.041 (2011).
116 Mishalian, I. *et al.* Neutrophils recruit regulatory T-cells into tumors via secretion of CCL17--a new mechanism of impaired antitumor immunity. *Int J Cancer* **135**, 1178-1186, doi:10.1002/ijc.28770 (2014).
117 Munder, M. *et al.* Suppression of T-cell functions by human granulocyte arginase. *Blood* **108**, 1627-1634, doi:10.1182/blood-2006-11-010389 (2006).
118 Sagiv, J. Y. *et al.* Phenotypic diversity and plasticity in circulating neutrophil subpopulations in cancer. *Cell Rep* **10**, 562-573, doi:10.1016/j.celrep.2014.12.039 (2015).

119 Shaul, M. E. *et al.* Tumor-associated neutrophils display a distinct N1 profile following TGFβ modulation: A transcriptomics analysis of pro- vs. antitumor TANs. *Oncoimmunology* **5**, e1232221, doi:10.1080/2162402x.2016.1232221 (2016).
120 Toor, S. M. & Elkord, E. Comparison of Myeloid Cells in Circulation and in the Tumor Microenvironment of Patients with Colorectal and Breast Cancers. *J Immunol Res* **2017**, 7989020, doi:10.1155/2017/7989020 (2017).
121 Wu, P. *et al.* γδT17 cells promote the accumulation and expansion of myeloid-derived suppressor cells in human colorectal cancer. *Immunity* **40**, 785-800, doi:10.1016/j.immuni.2014.03.013 (2014).
122 Zhou, S. L. *et al.* Tumor-Associated Neutrophils Recruit Macrophages and T-Regulatory Cells to Promote Progression of Hepatocellular Carcinoma and Resistance to Sorafenib. *Gastroenterology* **150**, 1646-1658.e1617, doi:10.1053/j.gastro.2016.02.040 (2016).
123 Takeshima, T. *et al.* Key role for neutrophils in radiation-induced antitumor immune responses: Potentiation with G-CSF. *Proc Natl Acad Sci U S A* **113**, 11300-11305, doi:10.1073/pnas.1613187113 (2016).
124 Rice, C. M. *et al.* Tumour-elicited neutrophils engage mitochondrial metabolism to circumvent nutrient limitations and maintain immune suppression. *Nat Commun* **9**, 5099, doi:10.1038/s41467-018-07505-2 (2018).
125 Ramachandran, P., Matchett, K. P., Dobie, R., Wilson-Kanamori, J. R. & Henderson, N. C. Single-cell technologies in hepatology: new insights into liver biology and disease pathogenesis. *Nat Rev Gastroenterol Hepatol* **17**, 457-472, doi:10.1038/s41575-020-0304-x (2020).
126 Brunner, A. D. *et al.* Ultra-high sensitivity mass spectrometry quantifies single-cell proteome changes upon perturbation. *Mol Syst Biol* **18**, e10798, doi:10.15252/msb.202110798 (2022).
127 Böyum, A. Isolation of mononuclear cells and granulocytes from human blood. Isolation of monuclear cells by one centrifugation, and of granulocytes by combining centrifugation and sedimentation at 1 g. *Scand J Clin Lab Invest Suppl* **97**, 77-89 (1968).
128 Mishalian, I., Granot, Z. & Fridlender, Z. G. The diversity of circulating neutrophils in cancer. *Immunobiology* **222**, 82-88, doi:10.1016/j.imbio.2016.02.001 (2017).
129 Hacbarth, E. & Kajdacsy-Balla, A. Low density neutrophils in patients with systemic lupus erythematosus, rheumatoid arthritis, and acute rheumatic fever. *Arthritis Rheum* **29**, 1334-1342, doi:10.1002/art.1780291105 (1986).
130 Lin, A. M. *et al.* Mast cells and neutrophils release IL-17 through extracellular trap formation in psoriasis. *J Immunol* **187**, 490-500, doi:10.4049/jimmunol.1100123 (2011).
131 Grayson, P. C. *et al.* Neutrophil-Related Gene Expression and Low-Density Granulocytes Associated With Disease Activity and Response to Treatment in Antineutrophil Cytoplasmic Antibody-Associated Vasculitis. *Arthritis Rheumatol* **67**, 1922-1932, doi:10.1002/art.39153 (2015).
132 Cloke, T., Munder, M., Taylor, G., Müller, I. & Kropf, P. Characterization of a novel population of low-density granulocytes associated with disease severity in HIV-1 infection. *PLoS One* **7**, e48939, doi:10.1371/journal.pone.0048939 (2012).

133 Morisaki, T., Goya, T., Ishimitsu, T. & Torisu, M. The increase of low density subpopulations and CD10 (CALLA) negative neutrophils in severely infected patients. *Surg Today* **22**, 322-327, doi:10.1007/bf00308740 (1992).
134 Rocha, B. C. *et al.* Type I Interferon Transcriptional Signature in Neutrophils and Low-Density Granulocytes Are Associated with Tissue Damage in Malaria. *Cell Rep* **13**, 2829-2841, doi:10.1016/j.celrep.2015.11.055 (2015).
135 Sanchez-Pino, M. D. *et al.* Increased inflammatory low-density neutrophils in severe obesity and effect of bariatric surgery: Results from case-control and prospective cohort studies. *eBioMedicine* **77**, 103910, doi:10.1016/j.ebiom.2022.103910 (2022).
136 Matthews, N. C., Burton, C. S. & Alfred, A. Low-density neutrophils in chronic graft versus host disease (cGVHD) are primarily immature CD10(-) and enhance T cell activation. *Clin Exp Immunol* **205**, 257-273, doi:10.1111/cei.13612 (2021).
137 Cho, Y. *et al.* Neutrophil extracellular traps contribute to liver damage and increase defective low-density neutrophils in alcohol-associated hepatitis. *J Hepatol* **78**, 28-44, doi:10.1016/j.jhep.2022.08.029 (2023).
138 Ssemaganda, A. *et al.* Characterization of neutrophil subsets in healthy human pregnancies. *PLoS One* **9**, e85696, doi:10.1371/journal.pone.0085696 (2014).
139 Carmona-Rivera, C. & Kaplan, M. J. Low-density granulocytes: a distinct class of neutrophils in systemic autoimmunity. *Semin Immunopathol* **35**, 455-463, doi:10.1007/s00281-013-0375-7 (2013).
140 Denny, M. F. *et al.* A distinct subset of proinflammatory neutrophils isolated from patients with systemic lupus erythematosus induces vascular damage and synthesizes type I IFNs. *J Immunol* **184**, 3284-3297, doi:10.4049/jimmunol.0902199 (2010).
141 Youn, J. I., Nagaraj, S., Collazo, M. & Gabrilovich, D. I. Subsets of myeloid-derived suppressor cells in tumor-bearing mice. *J Immunol* **181**, 5791-5802, doi:10.4049/jimmunol.181.8.5791 (2008).
142 Garcia-Romo, G. S. *et al.* Netting neutrophils are major inducers of type I IFN production in pediatric systemic lupus erythematosus. *Sci Transl Med* **3**, 73ra20, doi:10.1126/scitranslmed.3001201 (2011).
143 Villanueva, E. *et al.* Netting neutrophils induce endothelial damage, infiltrate tissues, and expose immunostimulatory molecules in systemic lupus erythematosus. *J Immunol* **187**, 538-552, doi:10.4049/jimmunol.1100450 (2011).
144 Gabrilovich, D. I. & Nagaraj, S. Myeloid-derived suppressor cells as regulators of the immune system. *Nat Rev Immunol* **9**, 162-174, doi:10.1038/nri2506 (2009).
145 Young, M. R., Newby, M. & Wepsic, H. T. Hematopoiesis and suppressor bone marrow cells in mice bearing large metastatic Lewis lung carcinoma tumors. *Cancer Res* **47**, 100-105 (1987).
146 Gabrilovich, D. I. Myeloid-Derived Suppressor Cells. *Cancer Immunol Res* **5**, 3-8, doi:10.1158/2326-6066.Cir-16-0297 (2017).
147 Medina, E. & Hartl, D. Myeloid-Derived Suppressor Cells in Infection: A General Overview. *J Innate Immun* **10**, 407-413, doi:10.1159/000489830 (2018).
148 Condamine, T. *et al.* Lectin-type oxidized LDL receptor-1 distinguishes population of human polymorphonuclear myeloid-derived suppressor cells in cancer patients. *Sci Immunol* **1**, doi:10.1126/sciimmunol.aaf8943 (2016).

149 Lang, S. *et al.* Clinical Relevance and Suppressive Capacity of Human Myeloid-Derived Suppressor Cell Subsets. *Clin Cancer Res* **24**, 4834-4844, doi:10.1158/1078-0432.Ccr-17-3726 (2018).
150 Liu, C. Y. *et al.* Population alterations of L-arginase- and inducible nitric oxide synthase-expressed CD11b+/CD14$^{-}$/CD15+/CD33+ myeloid-derived suppressor cells and CD8+ T lymphocytes in patients with advanced-stage non-small cell lung cancer. *J Cancer Res Clin Oncol* **136**, 35-45, doi:10.1007/s00432-009-0634-0 (2010).
151 Zea, A. H. *et al.* Arginase-producing myeloid suppressor cells in renal cell carcinoma patients: a mechanism of tumor evasion. *Cancer Res* **65**, 3044-3048, doi:10.1158/0008-5472.Can-04-4505 (2005).
152 Geh, D. *et al.* Neutrophils as potential therapeutic targets in hepatocellular carcinoma. *Nat Rev Gastroenterol Hepatol* **19**, doi:10.1038/s41575-021-00568-5 (2022).
153 Guo, L. *et al.* The prognostic value of inflammation factors in hepatocellular carcinoma patients with hepatic artery interventional treatments: A retrospective study. *Cancer Manag Res* **12**, 7173-7188 (2020).
154 Hu, X. G. *et al.* Blood neutrophil-to-lymphocyte ratio predicts tumor recurrence in patients with hepatocellular carcinoma within milan criteria after hepatectomy. *Yonsei Medical Journal* **57**, 1115-1123 (2016).
155 Kong, W. *et al.* The prognostic role of a combined fibrinogen and neutrophil-to-lymphocyte ratio score in patients with resectable hepatocellular carcinoma: A retrospective study. *Med Sci Monit* **26,** (2020).
156 Li, X. *et al.* Neutrophil count is associated with myeloid derived suppressor cell level and presents prognostic value of for hepatocellular carcinoma patients. *Oncotarget* **8**, 24380-24388, doi:10.18632/oncotarget.15456 (2017).
157 Limaye, A. R. *et al.* Neutrophil-lymphocyte ratio predicts overall and recurrence-free survival after liver transplantation for hepatocellular carcinoma. *Hepatol Res* **43**, 757-764 (2013).
158 Lu, S. D. *et al.* Preoperative ratio of neutrophils to lymphocytes predicts postresection survival in selected patients with early or intermediate stage hepatocellular carcinoma. *Medicine (United States)* **95** (2016).
159 Margetts, J. *et al.* Neutrophils: driving progression and poor prognosis in hepatocellular carcinoma? *Br J Cancer* **118**, 248-257, doi:10.1038/bjc.2017.386 (2018).
160 McVey, J. C. *et al.* Prognostication of inflammatory cells in liver transplantation: Is the waitlist neutrophil-to-lymphocyte ratio really predictive of tumor biology? *Clin Transplant* **33** (2019).
161 Okamura, Y. *et al.* Neutrophil to lymphocyte ratio as an indicator of the malignant behaviour of hepatocellular carcinoma. *Br J Surg* **103**, 891-898, doi:10.1002/bjs.10123 (2016).
162 Schobert, I. T. *et al.* Neutrophil-to-lymphocyte and platelet-to-lymphocyte ratios as predictors of tumor response in hepatocellular carcinoma after DEB-TACE. *Eur Radiol* **30**, 5663-5673, doi:10.1007/s00330-020-06931-5 (2020).
163 Wang, Y. *et al.* Circulating Neutrophils Predict Poor Survival for HCC and Promote HCC Progression Through p53 and STAT3 Signaling Pathway. *J Cancer* **11**, 3736-3744, doi:10.7150/jca.42953 (2020).

164 Wu, X. L. *et al.* Correlation between postoperative neutrophil to lymphocyte ratio and recurrence and prognosis of hepatocellular carcinoma after radical liver resection. [Chinese]. *Zhonghua zhong liu za zhi [Chinese journal of oncology]* **40**, 365-371 (2018).
165 Yuan, J. *et al.* Peripheral blood neutrophil count as a prognostic factor for patients with hepatocellular carcinoma treated with sorafenib. *Mol Clin Oncol* **7**, 837-842 (2017).
166 Terashima, T. *et al.* Blood neutrophil to lymphocyte ratio as a predictor in patients with advanced hepatocellular carcinoma treated with hepatic arterial infusion chemotherapy. *Hepatol Res* **45**, 949-959, doi:10.1111/hepr.12436 (2015).
167 Dharmapuri, S. *et al.* Predictive value of neutrophil to lymphocyte ratio and platelet to lymphocyte ratio in advanced hepatocellular carcinoma patients treated with anti–PD-1 therapy. *Cancer Med* **9**, 4962-4970, doi:10.1002/cam4.3135 (2020).
168 Shi, K. *et al.* Neutrophil-lymphocyte ratio and the risk of hepatocellular carcinoma in patients with hepatitis B-caused cirrhosis. *Eur J Gastroenterol Hepatol* **33**, e686-e692, doi:10.1097/meg.0000000000002217 (2021).
169 Thomas, C. E. *et al.* Neutrophil-lymphocyte ratio in relation to risk of hepatocellular carcinoma in patients with non-alcoholic fatty liver disease. *Cancer Med* **12**, 3589-3600, doi:10.1002/cam4.5185 (2023).
170 Biyik, M. *et al.* Blood neutrophil-to-lymphocyte ratio independently predicts survival in patients with liver cirrhosis. *Eur J Gastroenterol Hepatol* **25**, 435-441, doi:10.1097/MEG.0b013e32835c2af3 (2013).
171 Leithead, J. A., Rajoriya, N., Gunson, B. K. & Ferguson, J. W. Neutrophil-to-lymphocyte ratio predicts mortality in patients listed for liver transplantation. *Liver Int* **35**, 502-509, doi:10.1111/liv.12688 (2015).
172 Li, S. C., Xu, Z., Deng, Y. L., Wang, Y. N. & Jia, Y. M. Higher neutrophil-lymphocyte ratio is associated with better prognosis of hepatocellular carcinoma. *Medicine (Baltimore)* **99**, e20919, doi:10.1097/md.0000000000020919 (2020).
173 Grenader, T. *et al.* Derived neutrophil lymphocyte ratio is predictive of survival from intermittent therapy in advanced colorectal cancer: a post hoc analysis of the MRC COIN study. *Br J Cancer* **114**, 612-615, doi:10.1038/bjc.2016.23 (2016).
174 Gu, X. *et al.* Prognostic significance of neutrophil-to-lymphocyte ratio in prostate cancer: evidence from 16,266 patients. *Sci Rep* **6**, 22089, doi:10.1038/srep22089 (2016).
175 Lin, G. *et al.* Elevated neutrophil-to-lymphocyte ratio is an independent poor prognostic factor in patients with intrahepatic cholangiocarcinoma. *Oncotarget* **7**, 50963-50971, doi:10.18632/oncotarget.7680 (2016).
176 Peng, B., Wang, Y. H., Liu, Y. M. & Ma, L. X. Prognostic significance of the neutrophil to lymphocyte ratio in patients with non-small cell lung cancer: a systemic review and meta-analysis. *Int J Clin Exp Med* **8**, 3098-3106 (2015).
177 Schmidt, H. *et al.* Elevated neutrophil and monocyte counts in peripheral blood are associated with poor survival in patients with metastatic melanoma: a prognostic model. *Br J Cancer* **93**, 273-278, doi:10.1038/sj.bjc.6602702 (2005).
178 Kemal, Y. *et al.* Elevated serum neutrophil to lymphocyte and platelet to lymphocyte ratios could be useful in lung cancer diagnosis. *Asian Pac J Cancer Prev* **15**, 2651-2654, doi:10.7314/apjcp.2014.15.6.2651 (2014).

179 Sun, H. L. *et al.* Prognostic performance of lymphocyte-to-monocyte ratio in diffuse large B-cell lymphoma: an updated meta-analysis of eleven reports. *Onco Targets Ther* **9**, 3017-3023, doi:10.2147/ott.S96910 (2016).
180 Hu, K., Lou, L., Ye, J. & Zhang, S. Prognostic role of the neutrophil-lymphocyte ratio in renal cell carcinoma: a meta-analysis. *BMJ Open* **5**, e006404, doi:10.1136/bmjopen-2014-006404 (2015).
181 Chen, W., Chen, X., Li, S. & Ren, B. Expression, immune infiltration and clinical significance of SPAG5 in hepatocellular carcinoma: A gene expression-based study. *J Gene Med* **22** (2020).
182 Gao, Q. *et al.* CXCR6 upregulation contributes to a proinflammatory tumor microenvironment that drives metastasis and poor patient outcomes in hepatocellular carcinoma. *Cancer Res* **72**, 3546-3556, doi:10.1158/0008-5472.Can-11-4032 (2012).
183 Li, L. *et al.* CXCR2-CXCL1 axis is correlated with neutrophil infiltration and predicts a poor prognosis in hepatocellular carcinoma. *J Exp Clin Cancer Res* **34**, 129, doi:10.1186/s13046-015-0247-1 (2015).
184 Li, W., Xu, L., Han, J., Yuan, K. & Wu, H. Identification and Validation of Tumor Stromal Immunotype in Patients With Hepatocellular Carcinoma. *Front Oncol* **9**, 664, doi:10.3389/fonc.2019.00664 (2019).
185 Li, Y. W. *et al.* Intratumoral neutrophils: a poor prognostic factor for hepatocellular carcinoma following resection. *J Hepatol* **54**, 497-505, doi:10.1016/j.jhep.2010.07.044 (2011).
186 Liu, T., Wu, H., Qi, J., Qin, C. & Zhu, Q. Seven immune-related genes prognostic power and correlation with tumor-infiltrating immune cells in hepatocellular carcinoma. *Cancer Med* **9**, doi:10.1002/cam4.3406 (2020).
187 Liu, Y. *et al.* Prognostic potential of PRPF3 in hepatocellular carcinoma. *Aging (Albany NY)* **12**, 912-930, doi:10.18632/aging.102665 (2020).
188 Song, D. *et al.* DCK is a promising prognostic biomarker and correlated with immune infiltrates in hepatocellular carcinoma. *World J Surg Oncol* **18** (2020).
189 Wang, Y. *et al.* IDO and intra-tumoral neutrophils were independent prognostic factors for overall survival for hepatocellular carcinoma. *J Clin Lab Anal* **33**, e22872, doi:10.1002/jcla.22872 (2019).
190 Zhou, S. L. *et al.* Overexpression of CXCL5 mediates neutrophil infiltration and indicates poor prognosis for hepatocellular carcinoma. *Hepatology* **56**, 2242-2254, doi:10.1002/hep.25907 (2012).
191 Fossati, G. *et al.* Neutrophil infiltration into human gliomas. *Acta Neuropathol* **98**, 349-354, doi:10.1007/s004010051093 (1999).
192 Ino, Y. *et al.* Immune cell infiltration as an indicator of the immune microenvironment of pancreatic cancer. *Br J Cancer* **108**, 914-923, doi:10.1038/bjc.2013.32 (2013).
193 Jensen, H. K. *et al.* Presence of intratumoral neutrophils is an independent prognostic factor in localized renal cell carcinoma. *J Clin Oncol* **27**, 4709-4717, doi:10.1200/jco.2008.18.9498 (2009).
194 Jensen, T. O. *et al.* Intratumoral neutrophils and plasmacytoid dendritic cells indicate poor prognosis and are associated with pSTAT3 expression in AJCC stage I/II melanoma. *Cancer* **118**, 2476-2485, doi:10.1002/cncr.26511 (2012).

195 Krabbe, J. *et al.* Blood collection technique, anticoagulants and storing temperature have minor effects on the isolation of polymorphonuclear neutrophils. *Sci Rep* **10**, 14646, doi:10.1038/s41598-020-71500-1 (2020).
196 Trellakis, S. *et al.* Polymorphonuclear granulocytes in human head and neck cancer: enhanced inflammatory activity, modulation by cancer cells and expansion in advanced disease. *Int J Cancer* **129**, 2183-2193, doi:10.1002/ijc.25892 (2011).
197 Zhao, J. J. *et al.* The prognostic value of tumor-infiltrating neutrophils in gastric adenocarcinoma after resection. *PLoS One* **7**, e33655, doi:10.1371/journal.pone.0033655 (2012).
198 He, M. *et al.* Peritumoral stromal neutrophils are essential for c-Met-elicited metastasis in human hepatocellular carcinoma. *Oncoimmunology* **5**, e1219828, doi:10.1080/2162402x.2016.1219828 (2016).
199 Wu, Y. *et al.* Neutrophils promote motility of cancer cells via a hyaluronan-mediated TLR4/PI3K activation loop. *J Pathol* **225**, 438-447, doi:10.1002/path.2947 (2011).
200 Deng, Y. *et al.* Hepatic carcinoma-associated fibroblasts enhance immune suppression by facilitating the generation of myeloid-derived suppressor cells. *Oncogene* **36**, 1090-1101, doi:10.1038/onc.2016.273 (2017).
201 Alvarez, M. *et al.* Human liver single nucleus and single cell RNA sequencing identify a hepatocellular carcinoma-associated cell-type affecting survival. *Genome Med* **14**, 50, doi:10.1186/s13073-022-01055-5 (2022).
202 Ho, D. W. *et al.* Single-cell RNA sequencing shows the immunosuppressive landscape and tumor heterogeneity of HBV-associated hepatocellular carcinoma. *Nat Commun* **12**, 3684, doi:10.1038/s41467-021-24010-1 (2021).
203 Lu, Y. *et al.* A single-cell atlas of the multicellular ecosystem of primary and metastatic hepatocellular carcinoma. *Nat Commun* **13**, 4594, doi:10.1038/s41467-022-32283-3 (2022).
204 Sun, Y. *et al.* Single-cell landscape of the ecosystem in early-relapse hepatocellular carcinoma. *Cell* **184**, 404-421.e416, doi:10.1016/j.cell.2020.11.041 (2021).
205 Xue, R. *et al.* Liver tumour immune microenvironment subtypes and neutrophil heterogeneity. *Nature* **612**, 141-147, doi:10.1038/s41586-022-05400-x (2022).
206 Liu, Y., Beyer, A. & Aebersold, R. On the Dependency of Cellular Protein Levels on mRNA Abundance. *Cell* **165**, 535-550, doi:10.1016/j.cell.2016.03.014 (2016).
207 Eash, K. J., Greenbaum, A. M., Gopalan, P. K. & Link, D. C. CXCR2 and CXCR4 antagonistically regulate neutrophil trafficking from murine bone marrow. *J Clin Invest* **120**, 2423-2431, doi:10.1172/jci41649 (2010).
208 Metzemaekers, M., Gouwy, M. & Proost, P. Neutrophil chemoattractant receptors in health and disease: double-edged swords. *Cell Mol Immunol* **17**, 433-450, doi:10.1038/s41423-020-0412-0 (2020).
209 Cheng, Y. *et al.* Cancer-associated fibroblasts induce PDL1+ neutrophils through the IL6-STAT3 pathway that foster immune suppression in hepatocellular carcinoma. *Cell Death Dis* **9**, 422, doi:10.1038/s41419-018-0458-4 (2018).
210 Chiu, D. K. *et al.* Hypoxia induces myeloid-derived suppressor cell recruitment to hepatocellular carcinoma through chemokine (C-C motif) ligand 26. *Hepatology* **64**, 797-813, doi:10.1002/hep.28655 (2016).
211 Mohs, A. *et al.* Functional role of CCL5/RANTES for HCC progression during chronic liver disease. *J Hepatol* **66**, 743-753, doi:10.1016/j.jhep.2016.12.011 (2017).

212 Xu, Y. *et al.* Activated hepatic stellate cells regulate MDSC migration through the SDF-1/CXCR4 axis in an orthotopic mouse model of hepatocellular carcinoma. *Cancer Immunol Immunother* **68**, 1959-1969, doi:10.1007/s00262-019-02414-9 (2019).
213 Zhang, H. *et al.* Tumour-activated liver stromal cells regulate myeloid-derived suppressor cells accumulation in the liver. *Clin Exp Immunol* **188**, 96-108, doi:10.1111/cei.12917 (2017).
214 Haider, C. *et al.* Transforming Growth Factor-β and Axl Induce CXCL5 and Neutrophil Recruitment in Hepatocellular Carcinoma. *Hepatology* **69**, 222-236, doi:10.1002/hep.30166 (2019).
215 Li, Y. M. *et al.* Receptor-Interacting Protein Kinase 3 Deficiency Recruits Myeloid-Derived Suppressor Cells to Hepatocellular Carcinoma Through the Chemokine (C-X-C Motif) Ligand 1-Chemokine (C-X-C Motif) Receptor 2 Axis. *Hepatology* **70**, 1564-1581, doi:10.1002/hep.30676 (2019).
216 Liu, W. R. *et al.* PKM2 promotes metastasis by recruiting myeloid-derived suppressor cells and indicates poor prognosis for hepatocellular carcinoma. *Oncotarget* **6**, 846-861, doi:10.18632/oncotarget.2749 (2015).
217 Peng, Z. P. *et al.* Glycolytic activation of monocytes regulates the accumulation and function of neutrophils in human hepatocellular carcinoma. *J Hepatol* **73**, doi:10.1016/j.jhep.2020.05.004 (2020).
218 Zhou, S. L. *et al.* A Positive Feedback Loop Between Cancer Stem-Like Cells and Tumor-Associated Neutrophils Controls Hepatocellular Carcinoma Progression. *Hepatology* **70**, 1214-1230, doi:10.1002/hep.30630 (2019).
219 Wang, S. *et al.* S100A8/A9 in Inflammation. *Front Immunol* **9**, doi:10.3389/fimmu.2018.01298 (2018).
220 Wiechert, L. *et al.* Hepatocyte-specific S100a8 and S100a9 transgene expression in mice causes Cxcl1 induction and systemic neutrophil enrichment. *Cell Commun Signal* **10**, 40, doi:10.1186/1478-811x-10-40 (2012).
221 Németh, J. *et al.* S100A8 and S100A9 are novel nuclear factor kappa B target genes during malignant progression of murine and human liver carcinogenesis. *Hepatology* **50**, 1251-1262, doi:10.1002/hep.23099 (2009).
222 Huang, M. *et al.* S100A9 Regulates MDSCs-Mediated Immune Suppression via the RAGE and TLR4 Signaling Pathways in Colorectal Carcinoma. *Front Immunol* **10**, doi:10.3389/fimmu.2019.02243 (2019).
223 Ryckman, C., Vandal, K., Rouleau, P., Talbot, M. & Tessier, P. A. Proinflammatory activities of S100: proteins S100A8, S100A9, and S100A8/A9 induce neutrophil chemotaxis and adhesion. *J Immunol* **170**, 3233-3242, doi:10.4049/jimmunol.170.6.3233 (2003).
224 Cheng, P. *et al.* Inhibition of dendritic cell differentiation and accumulation of myeloid-derived suppressor cells in cancer is regulated by S100A9 protein. *J Exp Med* **205**, 2235-2249, doi:10.1084/jem.20080132 (2008).
225 Tan, W. *et al.* TNF-α is a potential therapeutic target to overcome sorafenib resistance in hepatocellular carcinoma. *EBioMedicine* **40**, 446-456, doi:10.1016/j.ebiom.2018.12.047 (2019).
226 Vieira, S. M. *et al.* A crucial role for TNF-alpha in mediating neutrophil influx induced by endogenously generated or exogenous chemokines, KC/CXCL1 and LIX/CXCL5. *Br J Pharmacol* **158**, 779-789, doi:10.1111/j.1476-5381.2009.00367.x (2009).

227 Massena, S. *et al.* Identification and characterization of VEGF-A–responsive neutrophils expressing CD49d, VEGFR1, and CXCR4 in mice and humans. *Blood* **126**, 2016-2026, doi:10.1182/blood-2015-03-631572 (2015).
228 Yamaguchi, R. *et al.* Expression of vascular endothelial growth factor in human hepatocellular carcinoma. *Hepatology* **28**, 68-77, doi:10.1002/hep.510280111 (1998).
229 Chiu, D. K. *et al.* Hypoxia inducible factor HIF-1 promotes myeloid-derived suppressor cells accumulation through ENTPD2/CD39L1 in hepatocellular carcinoma. *Nat Commun* **8**, 517, doi:10.1038/s41467-017-00530-7 (2017).
230 Hsieh, C. C., Hung, C. H., Chiang, M., Tsai, Y. C. & He, J. T. Hepatic Stellate Cells Enhance Liver Cancer Progression by Inducing Myeloid-Derived Suppressor Cells through Interleukin-6 Signaling. *Int J Mol Sci* **20**, doi:10.3390/ijms20205079 (2019).
231 Xu, M. *et al.* Interactions between interleukin-6 and myeloid-derived suppressor cells drive the chemoresistant phenotype of hepatocellular cancer. *Exp Cell Res* **351**, 142-149, doi:10.1016/j.yexcr.2017.01.008 (2017).
232 Xu, Y. *et al.* Activated hepatic stellate cells promote liver cancer by induction of myeloid-derived suppressor cells through cyclooxygenase-2. *Oncotarget* **7**, 8866-8878, doi:10.18632/oncotarget.6839 (2016).
233 Zhou, J. *et al.* Hepatoma-intrinsic CCRK inhibition diminishes myeloid-derived suppressor cell immunosuppression and enhances immune-checkpoint blockade efficacy. *Gut* **67**, 931-944, doi:10.1136/gutjnl-2017-314032 (2018).
234 Elwan, N. *et al.* High numbers of myeloid derived suppressor cells in peripheral blood and ascitic fluid of cirrhotic and HCC patients. *Immunol Invest* **47**, 169-180, doi:10.1080/08820139.2017.1407787 (2018).
235 Shen, P., Wang, A., He, M., Wang, Q. & Zheng, S. Increased circulating Lin(-/low) CD33(+) HLA-DR(-) myeloid-derived suppressor cells in hepatocellular carcinoma patients. *Hepatol Res* **44**, 639-650, doi:10.1111/hepr.12167 (2014).
236 Nourshargh, S., Renshaw, S. A. & Imhof, B. A. Reverse Migration of Neutrophils: Where, When, How, and Why? *Trends Immunol* **37**, 273-286, doi:10.1016/j.it.2016.03.006 (2016).
237 van der Windt, D. J. *et al.* Neutrophil extracellular traps promote inflammation and development of hepatocellular carcinoma in nonalcoholic steatohepatitis. *Hepatology* **68**, 1347-1360, doi:10.1002/hep.29914 (2018).
238 Wang, H. *et al.* Regulatory T cell and neutrophil extracellular trap interaction contributes to carcinogenesis in non-alcoholic steatohepatitis. *J Hepatol* **75**, doi:10.1016/j.jhep.2021.07.032 (2021).
239 Yan, C., Huo, X., Wang, S., Feng, Y. & Gong, Z. Stimulation of hepatocarcinogenesis by neutrophils upon induction of oncogenic kras expression in transgenic zebrafish. *J Hepatol* **63**, 420-428, doi:10.1016/j.jhep.2015.03.024 (2015).
240 Liu, K., Wang, F.-S. & Xu, R. Neutrophils in liver diseases: pathogenesis and therapeutic targets. *Cell Mol Immunol* **18**, 38-44, doi:10.1038/s41423-020-00560-0 (2021).
241 Chang, C. J. *et al.* Targeting tumor-infiltrating Ly6G(+) myeloid cells improves sorafenib efficacy in mouse orthotopic hepatocellular carcinoma. *Int J Cancer* **142**, 1878-1889, doi:10.1002/ijc.31216 (2018).

242 Hoechst, B. *et al.* Myeloid derived suppressor cells inhibit natural killer cells in patients with hepatocellular carcinoma via the NKp30 receptor. *Hepatology* **50**, 799-807, doi:10.1002/hep.23054 (2009).
243 Imai, Y. *et al.* Neutrophils enhance invasion activity of human cholangiocellular carcinoma and hepatocellular carcinoma cells: an in vitro study. *J Gastroenterol Hepatol* **20**, 287-293, doi:10.1111/j.1440-1746.2004.03575.x (2005).
244 Lacotte, S. *et al.* Impact of myeloid-derived suppressor cell on Kupffer cells from mouse livers with hepatocellular carcinoma. *Oncoimmunology* **5**, e1234565, doi:10.1080/2162402x.2016.1234565 (2016).
245 Li, H., Han, Y., Guo, Q., Zhang, M. & Cao, X. Cancer-expanded myeloid-derived suppressor cells induce anergy of NK cells through membrane-bound TGF-beta 1. *J Immunol* **182**, 240-249, doi:10.4049/jimmunol.182.1.240 (2009).
246 Li, X. F. *et al.* Increased autophagy sustains the survival and pro-tumourigenic effects of neutrophils in human hepatocellular carcinoma. *J Hepatol* **62**, 131-139, doi:10.1016/j.jhep.2014.08.023 (2015).
247 Yu, S. J. *et al.* Targeting the crosstalk between cytokine-induced killer cells and myeloid-derived suppressor cells in hepatocellular carcinoma. *J Hepatol* **70**, 449-457, doi:10.1016/j.jhep.2018.10.040 (2019).
248 Riley, J. L. PD-1 signaling in primary T cells. *Immunol Rev* **229**, 114-125, doi:10.1111/j.1600-065X.2009.00767.x (2009).
249 Bronte, V. & Zanovello, P. Regulation of immune responses by L-arginine metabolism. *Nat Rev Immunol* **5**, 641-654, doi:10.1038/nri1668 (2005).
250 Kusmartsev, S., Nefedova, Y., Yoder, D. & Gabrilovich, D. I. Antigen-specific inhibition of CD8+ T cell response by immature myeloid cells in cancer is mediated by reactive oxygen species. *J Immunol* **172**, 989-999, doi:10.4049/jimmunol.172.2.989 (2004).
251 Mazzoni, A. *et al.* Myeloid suppressor lines inhibit T cell responses by an NO-dependent mechanism. *J Immunol* **168**, 689-695, doi:10.4049/jimmunol.168.2.689 (2002).
252 Couper, K. N., Blount, D. G. & Riley, E. M. IL-10: The Master Regulator of Immunity to Infection. *J Immunol* **180**, 5771-5777, doi:10.4049/jimmunol.180.9.5771 (2008).
253 Batlle, E. & Massagué, J. Transforming Growth Factor-β Signaling in Immunity and Cancer. *Immunity* **50**, 924-940, doi:10.1016/j.immuni.2019.03.024 (2019).
254 Yamashita, T. & Wang, X. W. Cancer stem cells in the development of liver cancer. *J Clin Invest* **123**, 1911-1918, doi:10.1172/jci66024 (2013).
255 Wang, C. Q. *et al.* Interleukin-6 enhances cancer stemness and promotes metastasis of hepatocellular carcinoma via up-regulating osteopontin expression. *Am J Cancer Res* **6**, 1873-1889 (2016).
256 Yu, Q. & Stamenkovic, I. Cell surface-localized matrix metalloproteinase-9 proteolytically activates TGF-beta and promotes tumor invasion and angiogenesis. *Genes Dev* **14**, 163-176 (2000).
257 Feng, X. X. *et al.* β3 integrin promotes TGF-β1/H2O2/HOCl-mediated induction of metastatic phenotype of hepatocellular carcinoma cells by enhancing TGF-β1 signaling. *PLoS One* **8**, e79857, doi:10.1371/journal.pone.0079857 (2013).
258 Yang, L. Y. *et al.* Increased neutrophil extracellular traps promote metastasis potential of hepatocellular carcinoma via provoking tumorous inflammatory response. *J Hematol Oncol* **13**, 3, doi:10.1186/s13045-019-0836-0 (2020).

259 Gregory, A. D. & Houghton, A. M. Tumor-associated neutrophils: new targets for cancer therapy. *Cancer Res* **71**, 2411-2416, doi:10.1158/0008-5472.Can-10-2583 (2011).
260 Gershkovitz, M. *et al.* TRPM2 Mediates Neutrophil Killing of Disseminated Tumor Cells. *Cancer Res* **78**, 2680-2690, doi:10.1158/0008-5472.Can-17-3614 (2018).
261 Finisguerra, V. *et al.* MET is required for the recruitment of anti-tumoural neutrophils. *Nature* **522**, 349-353, doi:10.1038/nature14407 (2015).
262 Singhal, S. *et al.* Origin and Role of a Subset of Tumor-Associated Neutrophils with Antigen-Presenting Cell Features in Early-Stage Human Lung Cancer. *Cancer Cell* **30**, 120-135, doi:10.1016/j.ccell.2016.06.001 (2016).
263 van Egmond, M. & Bakema, J. E. Neutrophils as effector cells for antibody-based immunotherapy of cancer. *Semin Cancer Biol* **23**, 190-199, doi:10.1016/j.semcancer.2012.12.002 (2013).
264 Matlung, H. L. *et al.* Neutrophils Kill Antibody-Opsonized Cancer Cells by Trogoptosis. *Cell Rep* **23**, 3946-3959.e3946, doi:10.1016/j.celrep.2018.05.082 (2018).
265 Huertas, A. *et al.* Stereotactic body radiation therapy as an ablative treatment for inoperable hepatocellular carcinoma. *Radiother Oncol* **115**, 211-216, doi:10.1016/j.radonc.2015.04.006 (2015).
266 Chen, J. *et al.* Hypofractionated Irradiation Suppressed the Off-Target Mouse Hepatocarcinoma Growth by Inhibiting Myeloid-Derived Suppressor Cell-Mediated Immune Suppression. *Front Oncol* **10**, 4, doi:10.3389/fonc.2020.00004 (2020).
267 Stadtmann, A. & Zarbock, A. CXCR2: From Bench to Bedside. *Front Immunol* **3**, 263, doi:10.3389/fimmu.2012.00263 (2012).
268 BMC*. ISRCTN registry,* https://doi.org/10.1186/ISRCTN12669009 (2023)
269 US National Library of Medicine*. ClinicalTrials.gov*, https://clinicaltrials.gov/ct2/show/NCT02583477 (2015).
270 Xu, J. M. *et al.* Blockade of the CXCR6 signaling inhibits growth and invasion of hepatocellular carcinoma cells through inhibition of the VEGF expression. *Int J Immunopathol Pharmacol* **27**, 553-561, doi:10.1177/039463201402700411 (2014).
271 Peddibhotla, S. *et al.* Discovery of small molecule antagonists of chemokine receptor CXCR6 that arrest tumor growth in SK-HEP-1 mouse xenografts as a model of hepatocellular carcinoma. *Bioorg Med Chem Lett* **30**, 126899, doi:10.1016/j.bmcl.2019.126899 (2020).
272 Hawila, E. *et al.* CCR5 Directs the Mobilization of CD11b(+)Gr1(+)Ly6C(low) Polymorphonuclear Myeloid Cells from the Bone Marrow to the Blood to Support Tumor Development. *Cell Rep* **21**, 2212-2222, doi:10.1016/j.celrep.2017.10.104 (2017).
273 Chen, Y. *et al.* CXCR4 inhibition in tumor microenvironment facilitates anti-programmed death receptor-1 immunotherapy in sorafenib-treated hepatocellular carcinoma in mice. *Hepatology* **61**, 1591-1602, doi:10.1002/hep.27665 (2015).
274 Song, J.-S. *et al.* A highly selective and potent CXCR4 antagonist for hepatocellular carcinoma treatment. *Proc Natl Acad Sci U S A* **118**, e2015433118, doi:10.1073/pnas.2015433118 (2021).
275 Biasci, D. *et al.* CXCR4 inhibition in human pancreatic and colorectal cancers induces an integrated immune response. *Proc Natl Acad Sci U S A* **117**, 28960-28970, doi:10.1073/pnas.2013644117 (2020).

276 Zhou, J., Nefedova, Y., Lei, A. & Gabrilovich, D. Neutrophils and PMN-MDSC: Their biological role and interaction with stromal cells. *Semin Immunol* **35**, 19-28, doi:10.1016/j.smim.2017.12.004 (2018).
277 Liu, H., Shen, J. & Lu, K. IL-6 and PD-L1 blockade combination inhibits hepatocellular carcinoma cancer development in mouse model. *Biochem Biophys Res Commun* **486**, 239-244, doi:10.1016/j.bbrc.2017.02.128 (2017).
278 Fan, Y. *et al.* First-in-class immune-modulating small molecule Icaritin in advanced hepatocellular carcinoma: preliminary results of safety, durable survival and immune biomarkers. *BMC Cancer* **19**, 279, doi:10.1186/s12885-019-5471-1 (2019).
279 Zhao, H. *et al.* A novel anti-cancer agent Icaritin suppresses hepatocellular carcinoma initiation and malignant growth through the IL-6/Jak2/Stat3 pathway. *Oncotarget* **6**, 31927-31943, doi:10.18632/oncotarget.5578 (2015).
280 Zhou, J. *et al.* Icariin and its derivative, ICT, exert anti-inflammatory, anti-tumor effects, and modulate myeloid derived suppressive cells (MDSCs) functions. *Int Immunopharmacol* **11**, 890-898, doi:10.1016/j.intimp.2011.01.007 (2011).
281 Ikeda, M. *et al.* A phase 1b study of transforming growth factor-beta receptor I inhibitor galunisertib in combination with sorafenib in Japanese patients with unresectable hepatocellular carcinoma. *Invest New Drugs* **37**, 118-126, doi:10.1007/s10637-018-0636-3 (2019).
282 Kelley, R. K. *et al.* A Phase 2 Study of Galunisertib (TGF-β1 Receptor Type I Inhibitor) and Sorafenib in Patients With Advanced Hepatocellular Carcinoma. *Clin Transl Gastroenterol* **10**, e00056, doi:10.14309/ctg.0000000000000056 (2019).
283 US National Library of Medicine. *ClinicalTrials.gov*, https://clinicaltrials.gov/ct2/show/NCT02423343 (2015).
284 Radomska, H. S. *et al.* CCAAT/enhancer binding protein alpha is a regulatory switch sufficient for induction of granulocytic development from bipotential myeloid progenitors. *Mol Cell Biol* **18**, 4301-4314, doi:10.1128/mcb.18.7.4301 (1998).
285 Voutila, J. *et al.* Development and Mechanism of Small Activating RNA Targeting CEBPA, a Novel Therapeutic in Clinical Trials for Liver Cancer. *Mol Ther* **25**, 2705-2714, doi:10.1016/j.ymthe.2017.07.018 (2017).
286 Mackert, J. R. *et al.* Dual negative roles of C/EBPα in the expansion and pro-tumor functions of MDSCs. *Sci Rep* **7**, 14048, doi:10.1038/s41598-017-12968-2 (2017).
287 Reebye, V. *et al.* Gene activation of CEBPA using saRNA: preclinical studies of the first in human saRNA drug candidate for liver cancer. *Oncogene* **37**, 3216-3228, doi:10.1038/s41388-018-0126-2 (2018).
288 Sarker, D. *et al.* MTL-CEBPA, a Small Activating RNA Therapeutic Upregulating C/EBP-α, in Patients with Advanced Liver Cancer: A First-in-Human, Multicenter, Open-Label, Phase I Trial. *Clin Cancer Res* **26**, 3936-3946, doi:10.1158/1078-0432.Ccr-20-0414 (2020).
289 Rohaan, M. W., Wilgenhof, S. & Haanen, J. B. A. G. Adoptive cellular therapies: the current landscape. *Virchows Archiv* **474**, 449-461, doi:10.1007/s00428-018-2484-0 (2019).
290 Lee, J. H. *et al.* Adjuvant immunotherapy with autologous cytokine-induced killer cells for hepatocellular carcinoma. *Gastroenterology* **148**, 1383-1391.e1386, doi:10.1053/j.gastro.2015.02.055 (2015).

291 Yoon, J. S. *et al.* Adjuvant cytokine-induced killer cell immunotherapy for hepatocellular carcinoma: a propensity score-matched analysis of real-world data. *BMC Cancer* **19**, 523, doi:10.1186/s12885-019-5740-z (2019).
292 US National Library of Medicine. *ClinicalTrials.gov*, https://clinicaltrials.gov/ct2/show/NCT03785210 (2018).
293 Mann, D. A. Epigenetics in liver disease. *Hepatology* **60**, 1418-1425, doi:10.1002/hep.27131 (2014).
294 Orillion, A. *et al.* Entinostat Neutralizes Myeloid-Derived Suppressor Cells and Enhances the Antitumor Effect of PD-1 Inhibition in Murine Models of Lung and Renal Cell Carcinoma. *Clin Cancer Res* **23**, 5187-5201, doi:10.1158/1078-0432.Ccr-17-0741 (2017).
295 Bitzer, M. *et al.* Resminostat plus sorafenib as second-line therapy of advanced hepatocellular carcinoma - The SHELTER study. *J Hepatol* **65**, 280-288, doi:10.1016/j.jhep.2016.02.043 (2016).
296 Yeo, W. *et al.* Epigenetic therapy using belinostat for patients with unresectable hepatocellular carcinoma: a multicenter phase I/II study with biomarker and pharmacokinetic analysis of tumors from patients in the Mayo Phase II Consortium and the Cancer Therapeutics Research Group. *J Clin Oncol* **30**, 3361-3367, doi:10.1200/jco.2011.41.2395 (2012).
297 Su, Y. L., Banerjee, S., White, S. V. & Kortylewski, M. STAT3 in Tumor-Associated Myeloid Cells: Multitasking to Disrupt Immunity. *Int J Mol Sci* **19**, doi:10.3390/ijms19061803 (2018).
298 Bu, L. L. *et al.* Targeting STAT3 signaling reduces immunosuppressive myeloid cells in head and neck squamous cell carcinoma. *Oncoimmunology* **5**, e1130206, doi:10.1080/2162402x.2015.1130206 (2016).
299 US National Library of Medicine*. ClinicalTrials.gov*, https://clinicaltrials.gov/ct2/show/NCT01839604 (2017).
300 US National Library of Medicine. *ClinicalTrials.gov*, https://clinicaltrials.gov/ct2/show/NCT02279719 (2014).
301 US National Library of Medicine. *ClinicalTrials.gov*, https://clinicaltrials.gov/ct2/show/NCT03195699 (2017).
302 Matlung, H. L., Szilagyi, K., Barclay, N. A. & van den Berg, T. K. The CD47-SIRPα signaling axis as an innate immune checkpoint in cancer. *Immunol Rev* **276**, 145-164, doi:10.1111/imr.12527 (2017).
303 Lee, T. K. *et al.* Blockade of CD47-mediated cathepsin S/protease-activated receptor 2 signaling provides a therapeutic target for hepatocellular carcinoma. *Hepatology* **60**, 179-191, doi:10.1002/hep.27070 (2014).
304 Jalil, A. R., Andrechak, J. C. & Discher, D. E. Macrophage checkpoint blockade: results from initial clinical trials, binding analyses, and CD47-SIRPα structure-function. *Antib Ther* **3**, 80-94, doi:10.1093/abt/tbaa006 (2020).
305 Lo, J. *et al.* Nuclear factor kappa B-mediated CD47 up-regulation promotes sorafenib resistance and its blockade synergizes the effect of sorafenib in hepatocellular carcinoma in mice. *Hepatology* **62**, 534-545, doi:10.1002/hep.27859 (2015).
306 Xiao, Z. *et al.* Antibody mediated therapy targeting CD47 inhibits tumor progression of hepatocellular carcinoma. *Cancer Lett* **360**, 302-309, doi:10.1016/j.canlet.2015.02.036 (2015).

307 Condamine, T. *et al.* ER stress regulates myeloid-derived suppressor cell fate through TRAIL-R-mediated apoptosis. *J Clin Invest* **124**, 2626-2639, doi:10.1172/jci74056 (2014).
308 Dominguez, G. A. *et al.* Selective Targeting of Myeloid-Derived Suppressor Cells in Cancer Patients Using DS-8273a, an Agonistic TRAIL-R2 Antibody. *Clin Cancer Res* **23**, 2942-2950, doi:10.1158/1078-0432.Ccr-16-1784 (2017).
309 Renshaw, S. A. *et al.* Acceleration of human neutrophil apoptosis by TRAIL. *J Immunol* **170**, 1027-1033, doi:10.4049/jimmunol.170.2.1027 (2003).
310 Thorburn, A. Tumor Necrosis Factor-Related Apoptosis-Inducing Ligand (TRAIL) Pathway Signaling. *J Thorac Oncol* **2**, 461-465, doi:10.1097/jto.0b013e31805fea64 (2007).
311 Cheng, A. L. *et al.* Safety and efficacy of tigatuzumab plus sorafenib as first-line therapy in subjects with advanced hepatocellular carcinoma: A phase 2 randomized study. *J Hepatol* **63**, 896-904, doi:10.1016/j.jhep.2015.06.001 (2015).
312 Wang, S. *et al.* S100A8/A9 in Inflammation. *Front Immunol* **9**, 1298, doi:10.3389/fimmu.2018.01298 (2018).
313 Markowitz, J. & Carson, W. E. Review of S100A9 biology and its role in cancer. *Biochim Biophys Acta* **1835**, 100-109, doi:10.1016/j.bbcan.2012.10.003 (2013).
314 Sprenkeler, E. G. G. *et al.* S100A8/A9 Is a Marker for the Release of Neutrophil Extracellular Traps and Induces Neutrophil Activation. *Cells* **11**, doi:10.3390/cells11020236 (2022).
315 Vandal, K. *et al.* Blockade of S100A8 and S100A9 suppresses neutrophil migration in response to lipopolysaccharide. *J Immunol* **171**, 2602-2609, doi:10.4049/jimmunol.171.5.2602 (2003).
316 Björk, P. *et al.* Identification of human S100A9 as a novel target for treatment of autoimmune disease via binding to quinoline-3-carboxamides. *PLoS Biol* **7**, e97, doi:10.1371/journal.pbio.1000097 (2009).
317 Shen, L. *et al.* Tasquinimod modulates suppressive myeloid cells and enhances cancer immunotherapies in murine models. *Cancer Immunol Res* **3**, 136-148, doi:10.1158/2326-6066.Cir-14-0036 (2015).
318 Jennbacken, K. *et al.* Inhibition of metastasis in a castration resistant prostate cancer model by the quinoline-3-carboxamide tasquinimod (ABR-215050). *Prostate* **72**, 913-924, doi:10.1002/pros.21495 (2012).
319 Deronic, A., Tahvili, S., Leanderson, T. & Ivars, F. The anti-tumor effect of the quinoline-3-carboxamide tasquinimod: blockade of recruitment of CD11b+ Ly6Chi cells to tumor tissue reduces tumor growth. *BMC Cancer* **16**, doi:10.1186/s12885-016-2481-0 (2016).
320 Fransén Pettersson, N. *et al.* The immunomodulatory quinoline-3-carboxamide paquinimod reverses established fibrosis in a novel mouse model for liver fibrosis. *PLoS One* **13**, e0203228, doi:10.1371/journal.pone.0203228 (2018).
321 Linde, I. L. *et al.* Neutrophil-activating therapy for the treatment of cancer. *Cancer Cell* **41**, 356-372.e310, doi:10.1016/j.ccell.2023.01.002 (2023).
322 Patel, U. *et al.* CAR T cell therapy in solid tumors: A review of current clinical trials. *EJHaem* **3**, 24-31, doi:10.1002/jha2.356 (2022).
323 Sterner, R. C. & Sterner, R. M. CAR-T cell therapy: current limitations and potential strategies. *Blood Cancer J* **11**, 69, doi:10.1038/s41408-021-00459-7 (2021).

324 US National Library of Medicine. *ClinicalTrials.gov*, https://clinicaltrials.gov/study/NCT05003895 (2021).
325 Salmon, H. *et al.* Matrix architecture defines the preferential localization and migration of T cells into the stroma of human lung tumors. *J Clin Invest* **122**, 899-910, doi:10.1172/jci45817 (2012).
326 Chang, Y. *et al.* Engineering chimeric antigen receptor neutrophils from human pluripotent stem cells for targeted cancer immunotherapy. *Cell Rep* **40**, 111128, doi:10.1016/j.celrep.2022.111128 (2022).
327 Chang, Y. *et al.* CAR-neutrophil mediated delivery of tumor-microenvironment responsive nanodrugs for glioblastoma chemo-immunotherapy. *Nat Commun* **14**, doi:10.1038/s41467-023-37872-4 (2023).
328 Steele, C. W. *et al.* CXCR2 Inhibition Profoundly Suppresses Metastases and Augments Immunotherapy in Pancreatic Ductal Adenocarcinoma. *Cancer Cell* **29**, 832-845, doi:10.1016/j.ccell.2016.04.014 (2016).
329 US National Library of Medicine ClinicalTrials.gov, https://clinicaltrials.gov/ct2/show/NCT02423343 (2015).
330 US National Library of Medicine. *ClinicalTrials.gov*, https://clinicaltrials.gov/ct2/show/NCT01972672 (2013).
331 US National Library of Medicine. *ClinicalTrials.gov*, https://clinicaltrials.gov/ct2/show/NCT03236636 (2017).
332 US National Library of Medicine. *ClinicalTrials.gov*, https://clinicaltrials.gov/ct2/show/NCT03236649 (2017).
333 US National Library of Medicine. *ClinicalTrials.gov*, https://clinicaltrials.gov/ct2/show/NCT03177187 (2017).
334 US National Library of Medicine. *ClinicalTrials.gov*, https://clinicaltrials.gov/ct2/show/NCT02499328 (2015).
335 US National Library of Medicine. *ClinicalTrials.gov*, https://clinicaltrials.gov/ct2/show/NCT04477343 (2020).
336 US National Library of Medicine. *ClinicalTrials.gov*, https://clinicaltrials.gov/ct2/show/NCT04245397 (2020).
337 US National Library of Medicine. *ClinicalTrials.gov*, https://clinicaltrials.gov/ct2/show/NCT02370238 (2015).
338 US National Library of Medicine. *ClinicalTrials.gov*, https://clinicaltrials.gov/ct2/show/NCT02001974 (2013).
339 US National Library of Medicine. *ClinicalTrials.gov*, https://clinicaltrials.gov/ct2/show/NCT03274804 (2017).
340 Halama, N. *et al.* Tumoral Immune Cell Exploitation in Colorectal Cancer Metastases Can Be Targeted Effectively by Anti-CCR5 Therapy in Cancer Patients. *Cancer Cell* **29**, 587-601, doi:10.1016/j.ccell.2016.03.005 (2016).
341 US National Library of Medicine. *ClinicalTrials.gov*, https://clinicaltrials.gov/ct2/show/NCT02734160 (2016).
342 US National Library of Medicine. *ClinicalTrials.gov*, https://clinicaltrials.gov/ct2/show/NCT01682187 (2012).
343 US National Library of Medicine. *ClinicalTrials.gov*, https://clinicaltrials.gov/ct2/show/NCT02452008 (2015).
344 Weed, D. T. *et al.* The Reversal of Immune Exclusion Mediated by Tadalafil and an Anti-tumor Vaccine Also Induces PDL1 Upregulation in Recurrent Head and Neck

Squamous Cell Carcinoma: Interim Analysis of a Phase I Clinical Trial. *Front Immunol* **10**, 1206, doi:10.3389/fimmu.2019.01206 (2019).
345 US National Library of Medicine. *ClinicalTrials.gov*, https://clinicaltrials.gov/ct2/show/NCT00752115 (2011).
346 US National Library of Medicine. *ClinicalTrials.gov*, https://clinicaltrials.gov/ct2/show/NCT02953782 (2016).
347 US National Library of Medicine. *ClinicalTrials.gov*, https://clinicaltrials.gov/ct2/show/NCT02890368 (2016).
348 US National Library of Medicine. *ClinicalTrials.gov*, https://clinicaltrials.gov/ct2/show/NCT03834948 (2019).
349 US National Library of Medicine*. ClinicalTrials.gov*, https://clinicaltrials.gov/ct2/show/NCT03990233 (2019).
350 US National Library of Medicine. *ClinicalTrials.gov*, https://clinicaltrials.gov/ct2/show/NCT02991196 (2019).
351 US National Library of Medicine. *ClinicalTrials.gov*, https://clinicaltrials.gov/ct2/show/NCT02983006 (2016).
352 Armstrong, A. J. *et al.* Long-term Survival and Biomarker Correlates of Tasquinimod Efficacy in a Multicenter Randomized Study of Men with Minimally Symptomatic Metastatic Castration-Resistant Prostate Cancer. *Clin Cancer Res* **19**, 6891-6901, doi:10.1158/1078-0432.ccr-13-1581 (2013).
353 Pili, R. *et al.* Phase II Randomized, Double-Blind, Placebo-Controlled Study of Tasquinimod in Men With Minimally Symptomatic Metastatic Castrate-Resistant Prostate Cancer. *JCO* **29**, 4022-4028, doi:10.1200/jco.2011.35.6295 (2011).
354 Brown, Z. J., Heinrich, B. & Greten, T. F. Mouse models of hepatocellular carcinoma: an overview and highlights for immunotherapy research. *Nat Rev Gastroenterol Hepatol* **15**, 536-554, doi:10.1038/s41575-018-0033-6 (2018).
355 Connor, F. *et al.* Mutational landscape of a chemically-induced mouse model of liver cancer. *J Hepatol* **69**, 840-850, doi:10.1016/j.jhep.2018.06.009 (2018).
356 Tian, H., Lyu, Y., Yang, Y. G. & Hu, Z. Humanized Rodent Models for Cancer Research. *Front Oncol* **10**, 1696, doi:10.3389/fonc.2020.01696 (2020).
357 Skelton, J. K., Ortega-Prieto, A. M. & Dorner, M. A Hitchhiker's guide to humanized mice: new pathways to studying viral infections. *Immunology* **154**, 50-61, doi:10.1111/imm.12906 (2018).
358 Stackowicz, J., Jönsson, F. & Reber, L. L. Mouse Models and Tools for the in vivo Study of Neutrophils. *Front Immunol* **10**, 3130, doi:10.3389/fimmu.2019.03130 (2019).
359 Faget, J. *et al.* Efficient and specific Ly6G+cell depletion: A change in the current practices toward more relevant functional analyses of neutrophils. bioRxiv 498881; doi:hhts:doi.org/10.1101/498881 (2018).
360 Boivin, G. *et al.* Durable and controlled depletion of neutrophils in mice. *Nat Commun* **11**, doi:10.1038/s41467-020-16596-9 (2020).
361 Liu, K., Wang, F. S. & Xu, R. Neutrophils in liver diseases: pathogenesis and therapeutic targets. *Cell Mol Immunol* **18**, doi:10.1038/s41423-020-00560-0 (2020).
362 Friedman, S. L., Neuschwander-Tetri, B. A., Rinella, M. & Sanyal, A. J. Mechanisms of NAFLD development and therapeutic strategies. *Nat Med* **24**, 908-922, doi:10.1038/s41591-018-0104-9 (2018).

363 Pulli, B. *et al.* Myeloperoxidase-Hepatocyte-Stellate Cell Cross Talk Promotes Hepatocyte Injury and Fibrosis in Experimental Nonalcoholic Steatohepatitis. *Antioxid Redox Signal* **23**, 1255-1269, doi:10.1089/ars.2014.6108 (2015).
364 Harty, M. W. *et al.* Neutrophil depletion blocks early collagen degradation in repairing cholestatic rat livers. *Am J Pathol* **176**, 1271-1281, doi:10.2353/ajpath.2010.090527 (2010).
365 Taïeb, J. *et al.* Polymorphonuclear neutrophils are a source of hepatocyte growth factor in patients with severe alcoholic hepatitis. *J Hepatol* **36**, 342-348, doi:10.1016/s0168-8278(01)00276-8 (2002).
366 Xie, Z. *et al.* Gene Set Knowledge Discovery with Enrichr. *Curr Protoc* **1**, e90, doi:10.1002/cpz1.90 (2021).
367 Lacy, P. Mechanisms of degranulation in neutrophils. *Allergy Asthma Clin Immunol* **2**, 98-108, doi:10.1186/1710-1492-2-3-98 (2006).
368 Finsterbusch, M., Schrottmaier, W. C., Kral-Pointner, J. B., Salzmann, M. & Assinger, A. Measuring and interpreting platelet-leukocyte aggregates. *Platelets* **29**, 677-685, doi:10.1080/09537104.2018.1430358 (2018).
369 Torrens, L. *et al.* Immunomodulatory effects of lenvatinib plus anti-PD1 in mice and rationale for patient enrichment in hepatocellular carcinoma. *Hepatology* **74**, doi:10.1002/hep.32023 (2021).
370 Huby, T. & Gautier, E. L. Immune cell-mediated features of non-alcoholic steatohepatitis. *Nat Rev Immunol* **22**, 429-443, doi:10.1038/s41577-021-00639-3 (2022).
371 Evrard, M. *et al.* Developmental Analysis of Bone Marrow Neutrophils Reveals Populations Specialized in Expansion, Trafficking, and Effector Functions. *Immunity* **48**, 364-379.e368, doi:10.1016/j.immuni.2018.02.002 (2018).
372 Boussiotis, V. A. Molecular and Biochemical Aspects of the PD-1 Checkpoint Pathway. *N Engl J Med* **375**, 1767-1778, doi:10.1056/NEJMra1514296 (2016).
373 Saito, S. *et al.* Lymphocyte antigen 6 complex locus G6D downregulation is a novel parameter for functional impairment of neutrophils in aged mice. *Front Immunol* **13**, 1001179, doi:10.3389/fimmu.2022.1001179 (2022).
374 Hu, X., Li, J., Fu, M., Zhao, X. & Wang, W. The JAK/STAT signaling pathway: from bench to clinic. *Signal Transduct Target Ther* **6**, doi:10.1038/s41392-021-00791-1 (2021).
375 Nguyen-Jackson, H., Panopoulos, A. D., Zhang, H., Li, H. S. & Watowich, S. S. STAT3 controls the neutrophil migratory response to CXCR2 ligands by direct activation of G-CSF–induced CXCR2 expression and via modulation of CXCR2 signal transduction. *Blood* **115**, 3354-3363, doi:10.1182/blood-2009-08-240317 (2010).
376 Panopoulos, A. D. *et al.* STAT3 governs distinct pathways in emergency granulopoiesis and mature neutrophils. *Blood* **108**, 3682-3690, doi:10.1182/blood-2006-02-003012 (2006).
377 Yu, H., Lee, H., Herrmann, A., Buettner, R. & Jove, R. Revisiting STAT3 signalling in cancer: new and unexpected biological functions. *Nat Rev Cancer* **14**, 736-746, doi:10.1038/nrc3818 (2014).
378 Hedvat, M. *et al.* The JAK2 inhibitor AZD1480 potently blocks Stat3 signaling and oncogenesis in solid tumors. *Cancer Cell* **16**, 487-497, doi:10.1016/j.ccr.2009.10.015 (2009).

379 Derenzini, E. *et al.* The JAK inhibitor AZD1480 regulates proliferation and immunity in Hodgkin lymphoma. *Blood Cancer J* **1**, e46, doi:10.1038/bcj.2011.46 (2011).
380 Houghton, P. J. *et al.* Initial solid tumor testing (stage 1) of AZD1480, an inhibitor of Janus kinases 1 and 2 by the pediatric preclinical testing program. *Pediatr Blood Cancer* **61**, 1972-1979, doi:10.1002/pbc.25175 (2014).
381 Plimack, E. R. *et al.* AZD1480: a phase I study of a novel JAK2 inhibitor in solid tumors. *Oncologist* **18**, 819-820, doi:10.1634/theoncologist.2013-0198 (2013).
382 Ioannidis, S. *et al.* Discovery of 5-chloro-N2-[(1S)-1-(5-fluoropyrimidin-2-yl)ethyl]-N4-(5-methyl-1H-pyrazol-3-yl)pyrimidine-2,4-diamine (AZD1480) as a novel inhibitor of the Jak/Stat pathway. *J Med Chem* **54**, 262-276, doi:10.1021/jm1011319 (2011).
383 Sapre, M. *et al.* Metabolic Effects of JAK1/2 Inhibition in Patients with Myeloproliferative Neoplasms. *Sci Rep* **9**, 16609, doi:10.1038/s41598-019-53056-x (2019).
384 Shah, K., Shukla, D., Patel, M. & Malhotra, S. A case series on tofacitinib-induced weight gain. *Indian J Pharmacol* **55**, 263-265, doi:10.4103/ijp.ijp_158_23 (2023).
385 Maimela, N. R., Liu, S. & Zhang, Y. Fates of CD8+ T cells in Tumor Microenvironment. *Comput Struct Biotechnol J* **17**, 1-13, doi:10.1016/j.csbj.2018.11.004 (2019).
386 Derynck, R., Turley, S. J. & Akhurst, R. J. TGFβ biology in cancer progression and immunotherapy. *Nat Rev Clin Oncol* **18**, 9-34, doi:10.1038/s41571-020-0403-1 (2021).
387 Flanagan, D. J. *et al.* Epithelial TGFβ engages growth-factor signalling to circumvent apoptosis and drive intestinal tumourigenesis with aggressive features. *Nat Commun* **13**, 7551, doi:10.1038/s41467-022-35134-3 (2022).
388 Lu, R., Kujawski, M., Pan, H. & Shively, J. E. Tumor angiogenesis mediated by myeloid cells is negatively regulated by CEACAM1. *Cancer Res* **72**, 2239-2250, doi:10.1158/0008-5472.Can-11-3016 (2012).
389 Raskov, H., Orhan, A., Christensen, J. P. & Gögenur, I. Cytotoxic CD8+ T cells in cancer and cancer immunotherapy. *Br J Cancer* **124**, 359-367, doi:10.1038/s41416-020-01048-4 (2021).
390 McKenna, E. *et al.* Neutrophils: Need for Standardized Nomenclature. *Front Immunol* **12**, doi:10.3389/fimmu.2021.602963 (2021).
391 Brandau, S. *et al.* Myeloid-derived suppressor cells in the peripheral blood of cancer patients contain a subset of immature neutrophils with impaired migratory properties. *J Leukoc Biol* **89**, 311-317, doi:10.1189/jlb.0310162 (2010).
392 Morrissey, S. M. *et al.* A specific low-density neutrophil population correlates with hypercoagulation and disease severity in hospitalized COVID-19 patients. *JCI Insight* **6**, doi:10.1172/jci.insight.148435 (2021).
393 Pillay, J. *et al.* A subset of neutrophils in human systemic inflammation inhibits T cell responses through Mac-1. *J Clin Invest* **122**, 327-336, doi:10.1172/jci57990 (2012).
394 Dean, L. S. *et al.* Phenotypic alteration of low-density granulocytes in people with pulmonary post-acute sequalae of SARS-CoV-2 infection. *Front Immunol* **13**, 1076724, doi:10.3389/fimmu.2022.1076724 (2022).
395 Morrissey, S. M. *et al.* A specific low-density neutrophil population correlates with hypercoagulation and disease severity in hospitalized COVID-19 patients. *JCI Insight* **6**, doi:10.1172/jci.insight.148435 (2021).
396 Bongers, S. H. *et al.* Kinetics of Neutrophil Subsets in Acute, Subacute, and Chronic Inflammation. *Front Immunol* **12**, 674079, doi:10.3389/fimmu.2021.674079 (2021).

397 Orr, Y., Taylor, J. M., Bannon, P. G., Geczy, C. & Kritharides, L. Circulating CD10-/CD16low neutrophils provide a quantitative index of active bone marrow neutrophil release. *Br J Haematol* **131**, 508-519, doi:10.1111/j.1365-2141.2005.05794.x (2005).
398 van Grinsven, E. *et al.* Immature Neutrophils Released in Acute Inflammation Exhibit Efficient Migration despite Incomplete Segmentation of the Nucleus. *J Immunol* **202**, 207-217, doi:10.4049/jimmunol.1801255 (2019).
399 Weinhage, T. *et al.* Cord Blood Low-Density Granulocytes Correspond to an Immature Granulocytic Subset with Low Expression of S100A12. *J Immunol* **205**, 56-66, doi:10.4049/jimmunol.1901308 (2020).
400 Arebro, J. *et al.* A possible role for neutrophils in allergic rhinitis revealed after cellular subclassification. *Sci Rep* **7**, 43568, doi:10.1038/srep43568 (2017).
401 Blanco-Camarillo, C., Alemán, O. R. & Rosales, C. Low-Density Neutrophils in Healthy Individuals Display a Mature Primed Phenotype. *Front Immunol* **12**, 672520, doi:10.3389/fimmu.2021.672520 (2021).
402 Cortjens, B. *et al.* Neutrophil subset responses in infants with severe viral respiratory infection. *Clin Immunol* **176**, 100-106, doi:10.1016/j.clim.2016.12.012 (2017).
403 Hampton, H. R., Bailey, J., Tomura, M., Brink, R. & Chtanova, T. Microbe-dependent lymphatic migration of neutrophils modulates lymphocyte proliferation in lymph nodes. *Nat Commun* **6**, 7139, doi:10.1038/ncomms8139 (2015).
404 Marini, O. *et al.* Mature CD10(+) and immature CD10(-) neutrophils present in G-CSF-treated donors display opposite effects on T cells. *Blood* **129**, 1343-1356, doi:10.1182/blood-2016-04-713206 (2017).
405 Scapini, P., Marini, O., Tecchio, C. & Cassatella, M. A. Human neutrophils in the saga of cellular heterogeneity: insights and open questions. *Immunol Rev* **273**, 48-60, doi:10.1111/imr.12448 (2016).
406 Veglia, F., Sanseviero, E. & Gabrilovich, D. I. Myeloid-derived suppressor cells in the era of increasing myeloid cell diversity. *Nat Rev Immunol* **21**, 485-498, doi:10.1038/s41577-020-00490-y (2021).
407 Negorev, D. *et al.* Human neutrophils can mimic myeloid-derived suppressor cells (PMN-MDSC) and suppress microbead or lectin-induced T cell proliferation through artefactual mechanisms. *Sci Rep* **8**, 3135, doi:10.1038/s41598-018-21450-6 (2018).
408 Nan, J. *et al.* Endoplasmic reticulum stress induced LOX-1(+ ) CD15(+) polymorphonuclear myeloid-derived suppressor cells in hepatocellular carcinoma. *Immunology* **154**, 144-155, doi:10.1111/imm.12876 (2018).
409 Cossarizza, A. *et al.* Guidelines for the use of flow cytometry and cell sorting in immunological studies (second edition). *Eur J Immunol* **49**, 1457-1973, doi:10.1002/eji.201970107 (2019).
410 Perfetto, S. P., Ambrozak, D., Nguyen, R., Chattopadhyay, P. K. & Roederer, M. Quality assurance for polychromatic flow cytometry using a suite of calibration beads. *Nat Protoc* **7**, 2067-2079, doi:10.1038/nprot.2012.126 (2012).
411 Chishti, A. D. *et al.* Expression of chemokine receptors CXCR1 and CXCR2 during cardiopulmonary bypass. *J Thorac Cardiovasc Surg* **122**, 1162-1166, doi:10.1067/mtc.2001.116559 (2001).
412 Huang, Y. S. *et al.* Serum levels of interleukin-8 in alcoholic liver disease: relationship with disease stage, biochemical parameters and survival. *J Hepatol* **24**, 377-384, doi:10.1016/s0168-8278(96)80156-5 (1996).

413 Ren, Y. *et al.* Interleukin-8 serum levels in patients with hepatocellular carcinoma: correlations with clinicopathological features and prognosis. *Clin Cancer Res* **9**, 5996-6001 (2003).
414 Zhang, J. *et al.* Changes in Serum Interleukin-8 Levels Predict Response to Immune Checkpoint Inhibitors Immunotherapy in Unresectable Hepatocellular Carcinoma Patients. *J Inflamm Res* **17**, 3397-3406, doi:10.2147/jir.S460931 (2024).
415 Zimmermann, H. W. *et al.* Interleukin-8 is activated in patients with chronic liver diseases and associated with hepatic macrophage accumulation in human liver fibrosis. *PLoS One* **6**, e21381, doi:10.1371/journal.pone.0021381 (2011).
416 Karawajczyk, M. *et al.* High expression of neutrophil and monocyte CD64 with simultaneous lack of upregulation of adhesion receptors CD11b, CD162, CD15, CD65 on neutrophils in severe COVID-19. *Ther Adv Infect Dis* **8**, 20499361211034065, doi:10.1177/20499361211034065 (2021).
417 Ndlovu, L. N. *et al.* Increased Neutrophil Count and Decreased Neutrophil CD15 Expression Correlate With TB Disease Severity and Treatment Response Irrespective of HIV Co-infection. *Front Immunol* **11**, 1872, doi:10.3389/fimmu.2020.01872 (2020).
418 Mackey, J. B. G., Coffelt, S. B. & Carlin, L. M. Neutrophil Maturity in Cancer. *Front Immunol* **10**, 1912, doi:10.3389/fimmu.2019.01912 (2019).
419 Mackey, J. B. G. *et al.* Maturation, developmental site, and pathology dictate murine neutrophil function. *bioRxiv*, 2021.2007.2021.453108, doi:10.1101/2021.07.21.453108 (2021).
420 Hardisty, G. R. *et al.* High Purity Isolation of Low Density Neutrophils Casts Doubt on Their Exceptionality in Health and Disease. *Front Immunol* **12**, 625922, doi:10.3389/fimmu.2021.625922 (2021).
421 Kalafati, L. *et al.* Innate Immune Training of Granulopoiesis Promotes Anti-tumor Activity. *Cell* **183**, 771-785.e712, doi:10.1016/j.cell.2020.09.058 (2020).
422 Lisman, T. Platelet-neutrophil interactions as drivers of inflammatory and thrombotic disease. *Cell Tissue Res* **371**, 567-576, doi:10.1007/s00441-017-2727-4 (2018).
423 Ott, I., Neumann, F. J., Gawaz, M., Schmitt, M. & Schömig, A. Increased neutrophil-platelet adhesion in patients with unstable angina. *Circulation* **94**, 1239-1246, doi:10.1161/01.cir.94.6.1239 (1996).
424 Herster, F. *et al.* Platelets Aggregate With Neutrophils and Promote Skin Pathology in Psoriasis. *Front Immunol* **10**, 1867, doi:10.3389/fimmu.2019.01867 (2019).
425 Łukasik, Z. M., Makowski, M. & Makowska, J. S. From blood coagulation to innate and adaptive immunity: the role of platelets in the physiology and pathology of autoimmune disorders. *Rheumatol Int* **38**, 959-974, doi:10.1007/s00296-018-4001-9 (2018).
426 Pamuk, G. E. *et al.* Increased circulating platelet-neutrophil, platelet-monocyte complexes, and platelet activation in patients with ulcerative colitis: a comparative study. *Am J Hematol* **81**, 753-759, doi:10.1002/ajh.20655 (2006).
427 Li, Y. *et al.* Effects of the interactions between platelets with other cells in tumor growth and progression. *Front Immunol* **14**, 1165989, doi:10.3389/fimmu.2023.1165989 (2023).
428 Lecot, P. *et al.* Gene signature of circulating platelet-bound neutrophils is associated with poor prognosis in cancer patients. *Int J Cancer* **151**, 138-152, doi:10.1002/ijc.33991 (2022).

429 Kaiser, R., Escaig, R., Erber, J. & Nicolai, L. Neutrophil-Platelet Interactions as Novel Treatment Targets in Cardiovascular Disease. *Front Cardiovasc Med* **8**, 824112, doi:10.3389/fcvm.2021.824112 (2021).
430 Gerdes, N. *et al.* Platelet CD40 Exacerbates Atherosclerosis by Transcellular Activation of Endothelial Cells and Leukocytes. *Arterioscler Thromb Vasc Biol* **36**, 482-490, doi:10.1161/atvbaha.115.307074 (2016).
431 Haselmayer, P., Grosse-Hovest, L., von Landenberg, P., Schild, H. & Radsak, M. P. TREM-1 ligand expression on platelets enhances neutrophil activation. *Blood* **110**, 1029-1035, doi:10.1182/blood-2007-01-069195 (2007).
432 Nicolai, L., Gaertner, F. & Massberg, S. Platelets in Host Defense: Experimental and Clinical Insights. *Trends Immunol* **40**, 922-938, doi:10.1016/j.it.2019.08.004 (2019).
433 Wang, Y. *et al.* Leukocyte integrin Mac-1 regulates thrombosis via interaction with platelet GPIbα. *Nat Commun* **8**, 15559, doi:10.1038/ncomms15559 (2017).
434 Stark, K. *et al.* Disulfide HMGB1 derived from platelets coordinates venous thrombosis in mice. *Blood* **128**, 2435-2449, doi:10.1182/blood-2016-04-710632 (2016).
435 Vajen, T. *et al.* Blocking CCL5-CXCL4 heteromerization preserves heart function after myocardial infarction by attenuating leukocyte recruitment and NETosis. *Sci Rep* **8**, 10647, doi:10.1038/s41598-018-29026-0 (2018).
436 Wang, W. Letter by Wang Regarding Article, "Platelet Serotonin Aggravates Myocardial Ischemia/Reperfusion Injury via Neutrophil Degranulation. *Circulation* **140**, e290-e291, doi:10.1161/circulationaha.119.040803 (2019).
437 Malehmir, M. *et al.* Platelet GPIbα is a mediator and potential interventional target for NASH and subsequent liver cancer. *Nat Med* **25**, 641-655, doi:10.1038/s41591-019-0379-5 (2019).
438 Valadez-Cosmes, P. *et al.* Identification of Novel Low-Density Neutrophil Markers Through Unbiased High-Dimensional Flow Cytometry Screening in Non-Small Cell Lung Cancer Patients. *Front Immunol* **12**, 703846, doi:10.3389/fimmu.2021.703846 (2021).
439 Scheuermann, S. *et al.* Unveiling spatial complexity in solid tumor immune microenvironments through multiplexed imaging. *Front Immunol* **15**, 1383932, doi:10.3389/fimmu.2024.1383932 (2024).
440 Zhang, J., Song, J., Sheng, J., Bai, X. & Liang, T. Multiplex imaging reveals the architecture of the tumor immune microenvironment. *Cancer Biol Med* **18**, 949-954, doi:10.20892/j.issn.2095-3941.2021.0494 (2021).
441 Giannelli, G., Bergamini, C., Fransvea, E., Sgarra, C. & Antonaci, S. Laminin-5 with transforming growth factor-beta1 induces epithelial to mesenchymal transition in hepatocellular carcinoma. *Gastroenterology* **129**, 1375-1383, doi:10.1053/j.gastro.2005.09.055 (2005).
442 Gonzalez-Sanchez, E. *et al.* The TGF-β Pathway: A Pharmacological Target in Hepatocellular Carcinoma? *Cancers (Basel)* **13**, doi:10.3390/cancers13133248 (2021).
443 Russell, W. E., Coffey, R. J., Jr., Ouellette, A. J. & Moses, H. L. Type beta transforming growth factor reversibly inhibits the early proliferative response to partial hepatectomy in the rat. *Proc Natl Acad Sci U S A* **85**, 5126-5130, doi:10.1073/pnas.85.14.5126 (1988).

444 Taylor, P. R. *et al.* JAK/STAT regulation of Aspergillus fumigatus corneal infections and IL-6/23-stimulated neutrophil, IL-17, elastase, and MMP9 activity. *J Leukoc Biol* **100**, 213-222, doi:10.1189/jlb.4A1015-483R (2016).
445 Milara, J. *et al.* The pan-JAK inhibitor LAS194046 reduces neutrophil activation from severe asthma and COPD patients in vitro. *Sci Rep* **12**, 5132, doi:10.1038/s41598-022-09241-6 (2022).
446 Mitchell, T. S., Moots, R. J. & Wright, H. L. Janus kinase inhibitors prevent migration of rheumatoid arthritis neutrophils towards interleukin-8, but do not inhibit priming of the respiratory burst or reactive oxygen species production. *Clin Exp Immunol* **189**, 250-258, doi:10.1111/cei.12970 (2017).
447 Zhang, S., Hwaiz, R., Luo, L., Herwald, H. & Thorlacius, H. STAT3-dependent CXC chemokine formation and neutrophil migration in streptococcal M1 protein-induced acute lung inflammation. *Am J Physiol Lung Cell Mol Physiol* **308**, L1159-1167, doi:10.1152/ajplung.00324.2014 (2015).
448 Cherng, Y. G. *et al.* Induced Mitochondrial Alteration and DNA Damage via IFNGR-JAK2-STAT1-PARP1 Pathway Facilitates Viral Hepatitis Associated Hepatocellular Carcinoma Aggressiveness and Stemness. *Cancers (Basel)* **13**, doi:10.3390/cancers13112755 (2021).
449 Li, Y., Han, Q., Zhao, H., Guo, Q. & Zhang, J. Napabucasin Reduces Cancer Stem Cell Characteristics in Hepatocellular Carcinoma. *Front Pharmacol* **11**, 597520, doi:10.3389/fphar.2020.597520 (2020).
450 Hayakawa, F. *et al.* A novel STAT inhibitor, OPB-31121, has a significant antitumor effect on leukemia with STAT-addictive oncokinases. *Blood Cancer J* **3**, e166, doi:10.1038/bcj.2013.63 (2013).
451 Li, C. L. *et al.* The Natural Compound Dehydrocrenatidine Attenuates Nicotine-Induced Stemness and Epithelial-Mesenchymal Transition in Hepatocellular Carcinoma by Regulating a7nAChR-Jak2 Signaling Pathways. *Dis Markers* **2022**, 8316335, doi:10.1155/2022/8316335 (2022).
452 Xu, J. *et al.* Etomidate elicits anti-tumor capacity by disrupting the JAK2/STAT3 signaling pathway in hepatocellular carcinoma. *Cancer Lett* **552**, 215970, doi:10.1016/j.canlet.2022.215970 (2023).
453 Park, H., Lee, S., Lee, J., Moon, H. & Ro, S. W. Exploring the JAK/STAT Signaling Pathway in Hepatocellular Carcinoma: Unraveling Signaling Complexity and Therapeutic Implications. *Int J Mol Sci* **24**, doi:10.3390/ijms241813764 (2023).
454 Xu, J., Lin, H., Wu, G., Zhu, M. & Li, M. IL-6/STAT3 Is a Promising Therapeutic Target for Hepatocellular Carcinoma. *Front Oncol* **11**, 760971, doi:10.3389/fonc.2021.760971 (2021).
455 Geh, D., Anstee, Q. M. & Reeves, H. L. NAFLD-Associated HCC: Progress and Opportunities. *J Hepatocell Carcinoma* **8**, 223-239, doi:10.2147/jhc.S272213 (2021).
456 Geh, D., Manas, D. M. & Reeves, H. L. Hepatocellular carcinoma in non-alcoholic fatty liver disease—a review of an emerging challenge facing clinicians. *Hepatobiliary Surg Nutr* **10**, 59-75. doi: 10.21037/hbsn.2019.08.08. (2019).
457 Febbraio, M. A. *et al.* Preclinical Models for Studying NASH-Driven HCC: How Useful Are They? *Cell Metab* **29**, 18-26, doi:10.1016/j.cmet.2018.10.012 (2019).
458 Newsome, P. N. *et al.* A Placebo-Controlled Trial of Subcutaneous Semaglutide in Nonalcoholic Steatohepatitis. *N Engl J Med* **384**, 1113-1124, doi:10.1056/NEJMoa2028395 (2021).

459 Inia, J. A. *et al.* Semaglutide Has Beneficial Effects on Non-Alcoholic Steatohepatitis in Ldlr-/-.Leiden Mice. *Int J Mol Sci* **24**, 8494, doi:10.3390/ijms24108494 (2023).
460 Hansen, H. H. *et al.* Semaglutide reduces tumor burden in the GAN diet-induced obese and biopsy-confirmed mouse model of NASH-HCC with advanced fibrosis. *Sci Rep* **13**, doi:10.1038/s41598-023-50328-5 (2023).